



<https://theses.gla.ac.uk/>

Theses Digitisation:

<https://www.gla.ac.uk/myglasgow/research/enlighten/theses/digitisation/>

This is a digitised version of the original print thesis.

Copyright and moral rights for this work are retained by the author

A copy can be downloaded for personal non-commercial research or study, without prior permission or charge

This work cannot be reproduced or quoted extensively from without first obtaining permission in writing from the author

The content must not be changed in any way or sold commercially in any format or medium without the formal permission of the author

When referring to this work, full bibliographic details including the author, title, awarding institution and date of the thesis must be given

Enlighten: Theses

<https://theses.gla.ac.uk/>  
[research-enlighten@glasgow.ac.uk](mailto:research-enlighten@glasgow.ac.uk)

**A STUDY OF FACTORS DETERMINING THE CROSSBRIDGE KINETICS,  
WORK AND POWER OF CARDIAC MUSCLE ANALYSED WITH  
SINUSOIDAL OSCILLATION AND OTHER TECHNIQUES**

Jamie J Varghese  
University of Glasgow, UK

*March 2002*

ProQuest Number: 10391023

All rights reserved

INFORMATION TO ALL USERS

The quality of this reproduction is dependent upon the quality of the copy submitted.

In the unlikely event that the author did not send a complete manuscript and there are missing pages, these will be noted. Also, if material had to be removed, a note will indicate the deletion.



ProQuest 10391023

Published by ProQuest LLC (2017). Copyright of the Dissertation is held by the Author.

All rights reserved.

This work is protected against unauthorized copying under Title 17, United States Code  
Microform Edition © ProQuest LLC.

ProQuest LLC.  
789 East Eisenhower Parkway  
P.O. Box 1346  
Ann Arbor, MI 48106 – 1346

GLASGOW  
UNIVERSITY  
LIBRARY:

13097

copy 2.

## ACKNOWLEDGEMENTS

In the years that I have worked on the projects that ultimately resulted in this thesis, many people have supported me both academically and personally. I wish to thank all of you for your cooperation, without which both this thesis and I would not be the same.

First I want to thank my Supervisor, Dr. D.J. Miller for his expert guidance in the scientific research process. Thank you for letting me come and do research with you. You were always patient and understanding in helping a nurse think like a scientist. Our many debates, scientific or not, were always stimulating. Most of all thank you for believing in me.

Next I want to thank Dr. R.J. Solaro, for the opportunity he gave me to come home to Chicago and use that time to be involved in such an interesting project. I was so lucky to be there and learn so much. We certainly made the most of it, thanks to your expert supervision. You challenged me both in science and in life, and I will never forget all your fatherly advice. I will also never forget your willingness to keep an eye out for me for a 'nice' Indian boy!

I wish to thank everyone in the Physiology Department in NBLs at the University of Glasgow, UK, for your warm welcome to Scotland and to the world of research, and for always being around to answer any of my questions. I want to thank Professor G.L. Smith for the many times you calmed me down when I was frustrated. Alex and Sarah, you girls made homesickness go away. I will never forget Mexico! Niall, thank you for the countless times you helped me out with my experiments and for exposure to a serious Scottish accent! Gayle, thank you for your shoulder, you helped me get through some really tough spots. You also inspired me to go after what I want and never settle.

I want to send many thanks everyone at the Biophysics and Physiology Labs at the University of Illinois, Chicago. You made my summer fun and created such an amazing atmosphere for both work time and breaks. Murali, our many talks about India as well as science were always interesting. But most of all, thank you for all the time you spend helping me find my way around the lab and with the computer. David, thanks for always being there to give me a hand and for having such an interesting middle name.

I want to thanks all my family and friends for your constant prayers and support through these last four years. Thank you for always going out of you way to keep in touch, and even visiting me wherever I was on the blue marble. Suma, thanks for always keeping me informed about important and less important events at the homefront. Arvind, thanks for always making me laugh no matter how down I was and helping me on all the problems that I had with this thesis. Dina, thank you for always showing me how to enjoy life with such passion. Mathew, Sam, Lisa, and Becka, thank you for missing me so much, I miss you and love you very much. Kunjamol Auntie, Benny Achachen, and Roy Achachen, thank you for your constant encouragement. Most of all, I want to thank my Dad, Mom, and brother Jayson for everything. I am who I am because of you. I love you very much. Mom, Thank you for all your sacrifices, they are too numerous to mention. But most of all, thank you for the endless nights of comforting me, and encouraging me over the phone. And for all the tears you shed on your knees for me. You are the reason I am here today.

## TABLE OF CONTENTS - TEXT

<i>Sections</i>	<i>Page</i>
Declaration	1
Summary of Thesis	3
Chapter 1: Introduction to Thesis	8
Preamble	9
Molecular Structure of Muscle Fibers	10
Excitation-Contraction Coupling	25
Muscle Contraction and Force	28
Crossbridges	36
General Features of Congestive Heart Failure	45
Chapter 2: Methods and Materials	47
Isolated Ventricular Trabeculae Experiments	48
Solution Composition	54
The Oscillation Protocol	61
Chapter 3: Effects of pH on Crossbridge Kinetics	71
Introduction	72
Methods	78
Results	79
Discussion	117
Chapter 4: Effect of Phosphate on Crossbridge Kinetics	124
Introduction	125
Methods	128
Results	129
Discussion	152

Chapter 5:	Relaxation Kinetics of Rat Cardiac Trabeculae Using an 'EGTA-jump' Protocol	157
	Introduction	158
	Methods	164
	Results	167
	Discussion	174
Chapter 6:	Effects of Caffeine on Relaxation Rates and Muscle Work and Power	178
	Introduction	179
	Methods	181
	Results	182
	Discussion	193
Chapter 7:	Effects of TnC Isoform Changes on Crossbridge Kinetics	196
	Introduction	197
	Methods	199
	Results	201
	Discussion	214
Chapter 8:	Effects of TnT mutation Arg <sup>92</sup> Gln on Ca <sup>2+</sup> Sensitivity and Crossbridge Kinetics	222
	Introduction	223
	Methods	228
	Results	235
	Discussion	241
Chapter 9:	Conclusion	246
Chapter 10:	References	253

## TABLE OF CONTENTS - FIGURES

<i>Figures</i>	<i>Page</i>
1.1 Striated Muscle	11
1.2 Thick Filament and Thin Filament	12
1.3 Thin Filament	16
1.4 Action Potential	26
1.5 Length Dependence	32
1.6 Crossbridge Cycle	33
2.1 Transducer Set-Up	50
2.2 Experimental Trace of Control - Activation and Oscillation	60
2.3 Work Loops - Control	67
3.1 Activation vs. Time	80
3.2 Phase Shift for Muscle at Rest	81
3.3 Work Loops at Rest	82
3.4 Trace of Rigor Experiment	83
3.5 Stiffness Plot in Rigor	84
3.6 Stiffness Plot at Control	89
3.7 Stiffness Alkaline pHs - Combined Data	90
3.8 Gradual Change in Stiffness from Control to pH 7.8	91
3.9 Stiffness Acidic pHs - Combined Data	96
3.10 Gradual Change in Stiffness from Control to pH 6.2	97
3.11 Dextran vs. Control	98
3.12 Phase Plot - Control	102
3.13 Phase Plot - 7.2	103
3.14 Phase Plot - 7.5	104
3.15 Phase Plot - 7.8	105
3.16 Phase Plot - 6.75	109
3.17 Phase Plot - 6.5	110
3.18 Work Loops vs. Frequency	111
3.19 Change in Stiffness During Sinusoidal Oscillation	112
3.20 Work Loop - pH 6.5, Control, and pH 7.5	113-14
3.21 Determining an Unclear $f_{min}$	115
3.22 Maximum Stiffness vs. Maximum Tension	116

4.1 Experimental Trace – Control, 2mM, 5mM, and 10mM Phosphate	130
4.2 [Pi] vs. Maximum Tension	131
4.3 Stiffness [Pi] vs. pH7 - Combined Data	135
4.4 Stiffness [Pi] vs. pH7 - Single Experiment	136
4.5 Phase Plot - 2mM Phosphate	139
4.6 Phase Plot - 5mM Phosphate	140
4.7 Phase Plot - 10mM Phosphate	141
4.8 Stiffness-frequency plot pH 6.5 and 10mM phosphate combined	146
4.9 Phase Plot - pH 6.5 + 10mM Phosphate	147
4.10 Schematic of the Three-State Model	148
4.11 Work Loops - Control, 2mM, and 10mM Phosphate	149-50
4.12 Maximum Stiffness vs. Maximum Tension	151
5.1 Relaxation Transients with Curve Fitting	170
5.2 Relaxation Rate Constants Obtained from the Exponential Curve Fitting	171
5.3 Semi-Log Plot of the Rates of Relaxation at Different [EGTA]-Steps	172
5.4 Experimental Traces -100mM, 5mM, and 2mM EGTA	173
6.1 Experimental Trace – 10mM Caffeine	183
6.2 Stiffness Plot - Caffeine vs. pH 7 – Combined Data	184
6.3 Stiffness [Pi] vs. Caffeine - Single Experiment	185
6.4 Phase Plot - 10mM Caffeine	191
6.5 Maximum Stiffness vs. Maximum Tension	192
7.1 Stiffness Plot After Extraction (11.8.98)	203
7.2 Stiffness Plot - After Reconstitution with Human Cardiac TnC – Combined Data	204
7.3 Stiffness Plot After Reconstitution with Rabbit Skeletal TnC – Combined Data	205
7.4 Phase Plot - After Reconstitution with Rabbit Skeletal TnC	210
7.5 Phase Plot - After Reconstitution with Human Cardiac TnC	211
7.6 Stiffness Plots - Double Extraction	212-13
8.1 Figure of TnT Subregions with Region CB2	225
8.2 Transducer Set-Up	226
8.3 Typical Experimental Trace	227
8.4 pCa vs. pH, - Wildtype vs. Mutant	237
8.5 pCa50 Data	238
8.6 Hill Coefficient vs. pH	239
8.7 Maximum Force vs. pH - Wildtype vs. Mutant	240

## TABLE OF CONTENTS – TABLES

<i>Tables</i>	<i>Page</i>
2.1 Solution components	55
2.2 Solution ratios	56
2.3 Rigor Solution components	57
3.1 Change in Maximum Ca-activated force vs. pH	87
3.2 Average change in $f_{min}$ vs. pHs	93
3.3 Change in Maximum Dynamic Stiffness vs. pH	94
3.4 Phase Shift in Frequencies (Hz) from pH 7 to pH 7.5	105
3.5 Phase Shift in Frequencies (Hz) from pH 6.5 to pH 7	106
4.1 Change in Maximum Ca-activated force vs. [Pi]	131
4.2 Change in Dynamic Stiffness at $f_{min}$ vs. [Pi]	133
4.3 Phase Shift in Frequencies (Hz) from control to 2mM added Phosphate	141
4.4 Phase Shift in Frequencies (Hz) from 2 to 10mM added Phosphate	141
4.5 pH and Pi combined vs pH or Pi alone	144
5.1 [EGTA] of relaxing and activating solutions	164
5.2 Theoretical vs Actual Relaxation Rates at Various [EGTA]s	168
6.1 Change in Maximum Ca-activated force vs. [Caffeine]	181
6.2 Change in Dynamic Stiffness at $f_{min}$ vs. [Caffeine]	186
8.1 Solution composition for TnT experiments	230
8.2 Solution ratios for TnT experiments	231

## ABBREVIATIONS / TERMS IN TEXT

The following are fairly new concepts and terms introduced in this thesis.  
(In alphabetical order)

<i>Abbreviations / Terms</i>	<i>Page</i>
Crossbridge (XB)	14
Dynamic Stiffness	41
Familial Hypertrophic Cardiomyopathy (FHC)	222
Frequency of Minimum Stiffness ( $f_{\min}$ )	41
Human Cardiac Troponin C (cTnC)	6
Left Ventricular (LV)	45
Maximal Shortening Velocity ( $V_{\max}$ )	29
Phase Angle ( $\Phi$ )	64
phaseDown	67
phaseUp	67
Phase Lead	64
Phase Lag	64
Power Stroke	29
Rabbit Skeletal Troponin C (sTnC)	6

## DECLARATION

All the experimental work described in this thesis was done by me, unless specifically stated otherwise. Preliminary results of some of the work have been published, as detailed below. None of the work reported here has been previously submitted for a higher degree.

In this thesis I have studied the effects of the changes in intracellular pH, and phosphate, caffeine, as well as changes in TnT and TnC isoforms, on myofibrillar kinetics of cardiac muscle. All the work reported in this thesis is based upon my own experimental findings. The genetic manipulation (transgenic mice) to produce tissue for the experiments described in Chapter 8 was done by researchers in A.J. Marian's lab in Texas (Baylor University). The transgenic experiments were done in R.J. Solaro's labs in Chicago where I worked for 2 months during my work for this thesis.

## PUBLICATIONS

### Abstracts

VARGHESE, J.J., MILLER, D.J. (1999) Spreading of crossbridge rates at acid pH revealed by sinusoidal analysis in chemically 'skinned' rat heart. *Journal of Physiology*, (Presented at London Meeting, Physiological Society, University College, April, 1999) **518P**, 53P.

MILLER, D.J., VARGHESE, J.J., WILSON, G. (1999) Myofilament relaxation is slowed in chemically 'skinned' ventricle trabeculae from an infarction model of heart failure in rabbits. *Journal of Physiology*, (Presented at Glasgow Meeting, Physiological Society, September, 1999) **521P**, 36P.

VARGHESE, J.J., MILLER, D.J. (2000) Effects of pH and phosphate on rat myocardium crossbridge kinetics studied by sinusoidal analysis. *Biophysical Journal*, (Presented at Biophysical Meeting, New Orleans, February, 2000), **78** (1), no. 694, 117A.

VARGHESE, J.J., CHANDRA, M., MARIAN, A.J., SOLARO, R.J., (2000) Differential effects of pH on  $\text{Ca}^{2+}$ -activation of myofilaments from transgenic mouse hearts expressing normal (Arg<sup>92</sup>) and mutant (Gln<sup>92</sup>) human troponin T. *Biophysical Journal*, (Presented at Biophysical Meeting, New Orleans, February, 2000).

VARGHESE, J.J., MILLER, D.J. (2000) Effects of phosphate on rat myocardium crossbridge kinetics, work and power, studied by sinusoidal analysis. *Journal of Physiology*, (Presented at Joint British and Hungarian Physiologic Society Meeting, Budapest, May 2000) **526P**, 86P.

## SUMMARY

The pumping action of the heart is the driving force of the cardiovascular system that supplies all the organs and tissue with blood. The mechanical basis behind generation of sufficient pressure for the task lies in the ability of the cardiac cell to shorten. Shortening of the cardiac cells is accomplished by the interaction of two sets of proteins divided up into thick and thin filaments. Together these protein filaments form the backbone of the contractile protein matrix. The interaction between the myosin, of the thick filament, and actin, of the thin filament, also known as crossbridge cycling, is the basic process that can generate the force that is needed for the myocytes to shorten against a certain load. Regulation of the kinetics of crossbridge cycling is therefore a crucial element in myocardial contraction. This thesis focuses on studying how changes in muscle pH and [Pi], as well as variations in certain muscle protein isoforms, affect crossbridge kinetics. These studies were done using sinusoidal oscillation and other methods on rat and mouse cardiac muscle.

Ischaemia of cardiac muscle is seen in a high percentage of heart failure cases. It is known that during acute ischaemic episodes, the intracellular pH within the cardiac muscle can drop as low as 6.2 and the intracellular [Pi] rises from a value of 1-3 mM to 20 mM or more. (In the present work, the intracellular space of the cardiac cells was brought under direct control by chemically skinning the rat myocardial muscle preparations to destroy the membranes.) The experiments in this thesis examined the effects on force and the frequency-dependence of dynamic stiffness over a range of pH and [Pi] when rapid, small length changes are imposed on the rat cardiac muscle trabeculae using a sinusoidal oscillation method.

A primary finding of this study was that, at maximal  $\text{Ca}^{2+}$  activation, stiffness (at all frequencies) reduced progressively as pH was lowered, in agreement with previous

studies (see Chapter 3). It is generally assumed that stiffness provides a measure of the number (or more strictly the proportion) of attached crossbridges. Therefore, it can be concluded that a decrease in pH reduces crossbridge attachment. The rate at which the crossbridges cycle is also pH-sensitive, as this method reveals. The stiffness-frequency relationship is reversibly displaced to higher frequencies the lower the pH. The increase in  $[H^+]$  may be inhibiting the individual crossbridges from moving forward in the crossbridge cycle into the attachment phase or speeding detachment. This can be by increasing detachment rate, or relative speeding in any or all parts of the cycle so that the 'attached' time becomes a smaller fraction of the total.

There is not only a change in the crossbridge cycling rate, but also a spreading of the stiffness vs. frequency characteristic in part of the frequency range that implies the rates of individual crossbridges spread over a wider range of frequencies under acidic conditions. Studies have shown that the myofilament lattice is disrupted at low pH, notably the regularity of the actin hexagonal array. Myofilament shrinkage alone does not account for the discrepancy in muscle function at low pH. This was confirmed by studying the effects of Dextran polymers. These alter lattice spacing, like acidity, but evidently without affecting the kinetic features examined here. The results using phase shift analysis show the muscle is doing less work in acidic conditions. This change in crossbridge kinetics and the disarray in the myofilament lattice, rather than shrinkage, during acidosis can thus lead to the decrease in force, but also in work and power, as shown by the present results.

Many studies have shown that maximal force and stiffness decrease in skinned fibres at increased  $[Pi]$ . The present results reveal decreases in both maximum tension and stiffness (Chapter 4, Figure 4.2-3) and the overall decreases in stiffness at all frequencies in the stiffness-frequency plots. This supports the theory that raised  $[Pi]$  inhibits the crossbridge from entering the 'power-stroke state' where muscle movement actually

occurs. The results also show that crossbridge kinetics relating to the crossbridge cycling rate actually speed up with increased [Pi]. For the reduced population of attached bridges at high Pi, the ability to generate work is actually greater. Since the optimum frequency at which this achieved is also higher, greater power per bridge is possible.

The results for the combined effects of these chemical factors associated with ischaemia and hypoxia on cardiac muscle kinetics show how the average force under ischaemic conditions is not significantly different from the product of the relative reductions in force of increased [Pi] or decreased pH separately. However, the present results differ with these previous reports. I found that a decrease in acidity and Pi separately yield more than a 50 to 60% reduction in force, but the combined effect of acidity and Pi yielded around a 30% decrease in force. However, the stiffness and work results for acidity and Pi together, differed compared to those of force. The combined stiffness and work values were found to be between the individual acidity and Pi values.

Previous studies suggest that caffeine acts by a completely different mechanism from Pi and acidosis and could as a useful check because of its ability to alter crossbridge kinetics (Chapter 6). The effects of 10mM caffeine were studied on fully activated as well as relaxing myocardial muscle. Although there is evidence showing a decrease in relaxation rates, this effect was re-examined using the [EGTA]-step protocol developed in this lab. This protocol is further described in Chapter 5. The results show that caffeine reduces maximal force production in cardiac muscle. This effect is similar to the effect of acidity and Pi. In addition, the results show that the fall of tension is greater than the fall of stiffness with added caffeine. This is similar to the phosphate results obtain for this thesis, and implies a decreased mean force per crossbridge. It has been suggested that caffeine may be working through direct interaction on the crossbridge. The compiled  $f_{min}$  and stiffness data (terms explained on page 41) in this thesis show a small but significant difference attributable to caffeine and thus does support this idea. pH and Pi cause

significant changes in both work and power. Unlike the pH and Pi findings, phase analysis shows that there is no change in the positive or negative work or power output. The combination of these results suggests that caffeine does not affect the myofilament at the pre-power stroke steps where pH or Pi is released in the crossbridge cycle.

This thesis also reports on the consequences of the extraction of rat cardiac TnC and replacing it with human cardiac (cTnC) or rabbit skeletal TnCs (sTnC) (Chapter 7). However, before the effect of the TnC isoform could be tested, the efficiency of the extraction and replacement protocol needed to be determined. With the present results of over 85% loss of maximum tension in fully activated fibres, it can be speculated that over 30% of the native TnCs were removed by the extraction protocol. A maximum of about 60-70% of original tension and 70% of the original stiffness returned after TnC replacement. Therefore, some of the observed slowing of muscle kinetics can be attributed to non-uptake of TnC due to time rather than lack of native TnC removal during the extraction phase. The results show that there was no significant difference in maximum tension, stiffness, work or power produced between TnC isoforms although relatively few experiments were completed. One explanation for this is that the difference between the two isoforms lies in the trigger speed due to the additional Ca<sup>2+</sup> binding site on skeletal TnC isoforms. However, the additional binding site does not increase the number of crossbridges attached at one time and therefore will not alter production of force, work or power in fully activated muscle preparations.

Last, the effects of the genetically created isoform of TnT (one having the Arg<sup>92</sup>Gln mutation) were studied (Chapter 8). The Arg<sup>92</sup>Gln mutation is one of the eight mutants found in the TnT in cases of familial hypertrophic cardiomyopathy (FHC). Heart failure is seen in the most severe FHC cases. Ischaemia of the cardiac muscle itself is seen in a high percentage of heart failure cases. It is mentioned above that during acute ischaemic episodes, the pH within the cardiac muscle can drop. Therefore, the effect of pH changes

on the Ca sensitivity of mouse cardiac was studied in tissue expressing the Arg<sup>92</sup>Gln mutation. The results indicate that muscle fibres with the Arg<sup>92</sup>Gln mutation activate at higher pCas. This leads to longer Ca<sup>2+</sup>-activation of the muscle fibres. These results agree with the established fact that hearts of patients with FHC are known to hypercontract and are less compliant.

The general conclusion from these studies is that intracellular chemical conditions, which are known to affect the crossbridges directly, influence the kinetic properties of the crossbridge. The latter effects modify the ability of crossbridges to do work and develop power, but not always in a way obvious from the effects on isometric force generation.

## **CHAPTER 1 INTRODUCTION TO THESIS**

## **PREAMBLE**

The work to be reported in this thesis describes experiments on cardiac muscle. The experimental approach is focused at the subcellular level. It seeks to elucidate some features of the heart's contractile mechanisms at the level of myofilament function. The aim of the project was to investigate the influence that some physiologically- and pathophysiologically-relevant factors might have on the ability of heart muscle to produce mechanical work and power by the contraction process. The Introduction therefore reviews relevant detail of the myofilament protein structure in heart and elements of sarcomere structure and function and the process of force production and movement by the crossbridges. The experiments mostly concern events 'downstream' of the cellular processes of excitation-contraction coupling, the provision of ATP and the control of intracellular ionic conditions. However, some introduction to this important background is also given here.

## MOLECULAR STRUCTURE OF MUSCLE FIBERS

Skeletal and cardiac muscle are referred to as striated muscle due to the appearance of lighter and darker bands when viewed under a suitable microscope. These bands, referred to as the A and I bands, arise from the interdigitation of the two types of highly organised and regular structures, the thick and thin filaments. The A band contains the hexagonal lattices of both the thin and thick filaments overlapped, while the I band contains only the thin filaments and Z disks. The Z disks are structures at right angles to the filaments from which thin filaments extend to run between the thick filaments.

### **Myosin- the thick filament**

More than 130 units of the 470 kDa protein myosin form each thick filament. In summary, it contains two heavy polypeptide chains and two sets of light polypeptide chains. The heavy chain has the shape of a long 'tail' in addition to two globular tertiary structures, known as the 'heads'. The heads project out from the surface of thick filament sufficiently far for it to be able to attach to the thin filament as discussed later. The light chains are located under the base of the head and are involved in regulating the 'rowing' motion of the head during a 'crossbridge cycle' (*e.g.*, Irving & Piazzesi 1997), which will also be explained later.

Myosin is the main protein found in the thick filament. It is an ATPase that converts the chemical energy of ATP into directed movement. In muscle it is referred to as the 'motor' behind contraction. Myosin is a hexamer molecule about 160 nm in length. Its structure involves the two globular heads and two heavy chains intertwined to form an  $\alpha$ -helical, coiled-coil myosin tail. Each of the heavy chains has a molecular weight of 220 kDa. Its COOH-terminal (carboxyl) is located at the helical region while the NH<sub>2</sub>-terminal (amino) is at the globular head region of the heavy chain. The myosin head, 130 kDa, corresponds to the motor domain; it contains the

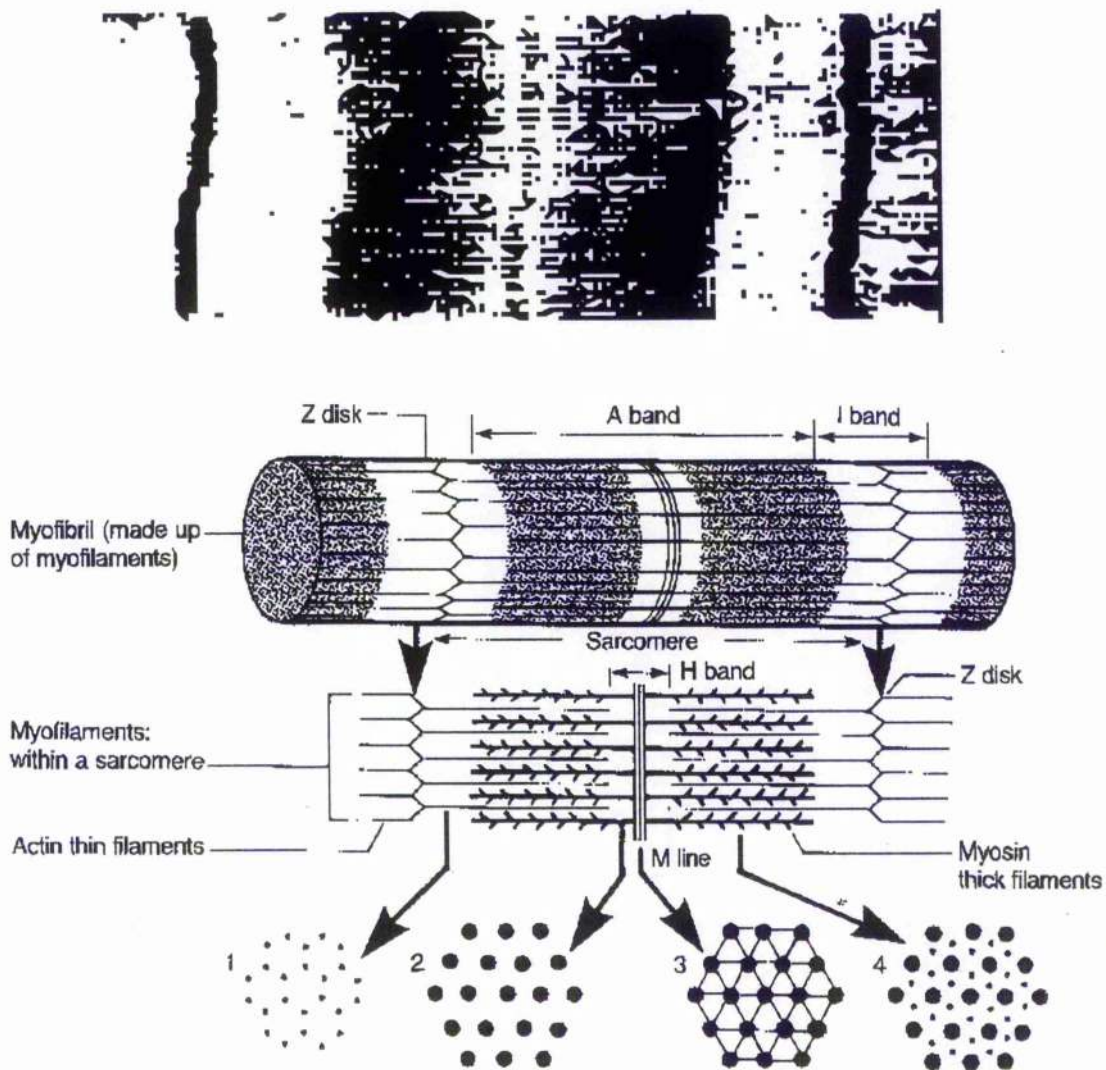


**Figure 1.1.** Upper Panel) This figure shows how striated muscle looks at high magnification by light microscopy. It shows the alternating dark and light transverse bands that are created by the overlap of two myofilament arrays. Lower Panel) Two major structures form the striated muscle sarcomere pattern: the thick filaments are located in the central portion of the sarcomere. The thin filaments, mainly constructed by two strands of actin molecules, protrude from the Z-lines at either end, towards the centre of the sarcomere. (Web source: <http://www.mednote.co.kr/BOKnote/muscle.html#red>, <http://www.ultranet.com/~jkimball/BiologyPages/M/Muscles.html#Anatomy of Skeletal Muscle>)

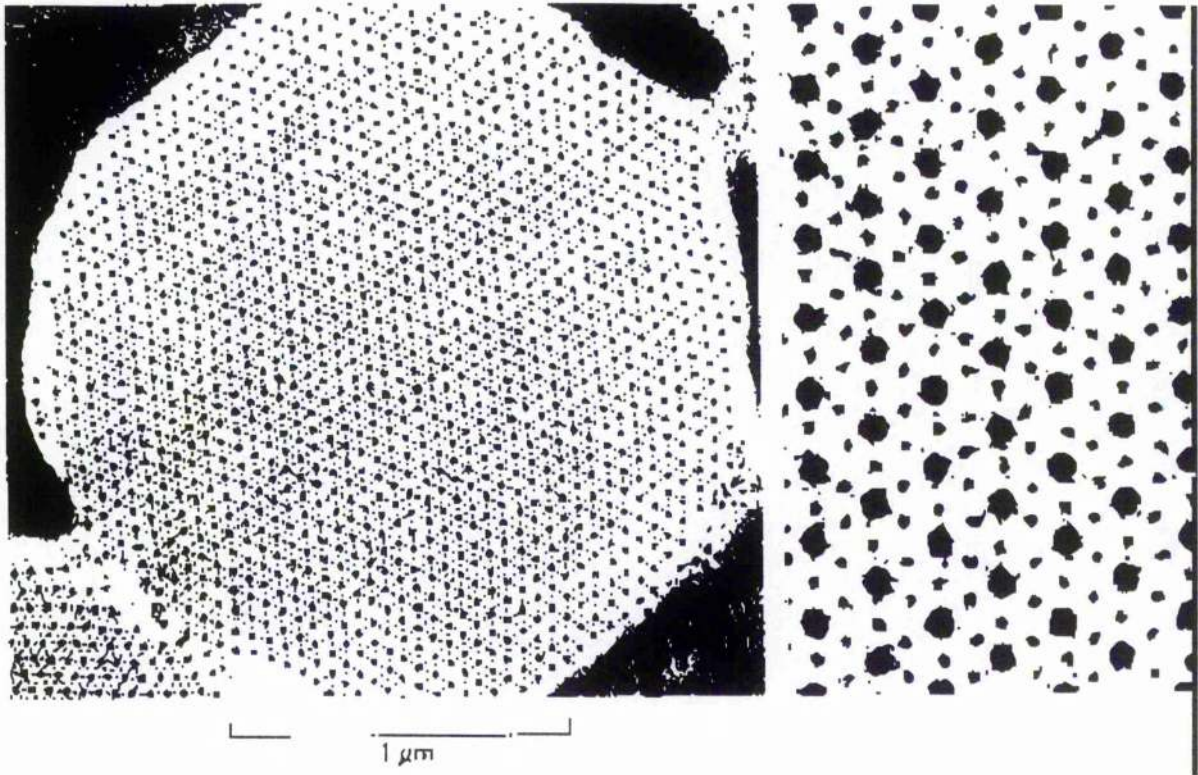


**Figure 1.2.** The lattice structure of striated muscle can be seen clearly in this figure. Each myosin filament is surrounded by six actin filaments to create a symmetrical lattice. The geometry of this lattice is sensitive to pH, chemical composition and ionic strength. (Web Source: <http://anatomy.med.unsw.edu.au/cbl/cbl.htm>)

ATP- and actin-binding sites. This domain is connected to the long myosin backbone by a neck region. The long  $\alpha$ -helical tails of the myosin heavy chains form the main axis of the thick filament from which the globular heads of the myosin heavy chains protrude.

The light chains are found at the neck region. Each of the heavy chains has a pair of light chains. The first of the two light chains is the 'essential' or 'alkali' light chain (MLC<sub>1</sub>), which lies close to the motor domain of the myosin and is non-phosphorylatable. The second is the 'regulatory' or 'phosphorylatable' light chain (MLC<sub>2</sub>), and lies close to the head-myosin rod junction (Schaub *et al* 1998). MLC<sub>1</sub> is termed 'essential' because it was originally thought to be essential for the hydrolytic activity of myosin, though now that has been proved by various labs to be true. MLC<sub>2</sub> is termed 'regulatory' because in vertebrate smooth muscle and non-muscle cells, contractile activity is triggered by phosphorylation of this myosin light chain. Though neither isoform has shown to affect ATPase activity, it has become evident that the MLCs are involved in the fine-tuning of contractile activity in both cardiac and non-cardiac muscle (Schaub *et al* 1998).

The head region, subfragment 1 (S1), can dissociate from the tail when subjected to proteolytic treatment. The S1 head connects to the backbone via subfragment 2 (S2). The heavy meromyosin (HMM) fragment comprises of S1 and S2, the rest of the molecule is light meromyosin (LMM).

Cardiac muscle myosin heavy chains exist in two different isoforms,  $\alpha$  and  $\beta$ -myosin. The two myosin heavy chains can thus form three different dimers (V<sub>1</sub> ( $\alpha$ - $\alpha$ ), V<sub>2</sub> ( $\alpha$ - $\beta$ ) and V<sub>3</sub> ( $\beta$ - $\beta$ )) whose expression can be modulated *in vivo* (Swynghedauw, 1986; Morkin, 1987). The MHC <sub>$\alpha$</sub>  isoform is predominantly found in the atria, with the exception of mouse and rat myocardium where it is the predominant form throughout the myocardium (Hoh *et al*, 1978). In the rabbit and larger mammals, however, the predominant isoform found in the ventricles is the MHC <sub>$\beta$</sub>  (Lompre *et al*, 1984; Swynghedauw, 1986). The V<sub>1</sub>

isoform has a much higher actin-activated MgATPase rate, but lower affinity, than the  $V_3$  isoform (Dillman, 1980; Lompre *et al.*, 1979; Mercadier *et al.*, 1981).

Myocardial hypertrophy is a basic adaptive response to increased cardiac loading conditions. Immunofluorescence studies of hypertrophic rabbit myocytes indicate that  $V_1$  and  $V_3$  myosin isoforms are simultaneously expressed within a single cell (Samuels *et al.*, 1983). Biochemical alterations, such as the shift in myosin isoform from  $V_1$  to  $V_3$  occurs during myocardial hypertrophy and permits the affected myocardium to compensate to some degree for its reduced contractility. Compared with  $V_1$ , the reduced ATPase catalytic activity of  $V_3$  results in an improved thermo-mechanical efficiency of cardiac work.

### **Actin- The Thin Filament**

The thin filament contains several protein types directly relevant to muscle contraction. These are actin, tropomyosin, and the troponin complex of troponins C, I, and T (TnC, TnI, and TnT, respectively). Actin, the largest of these molecules, 42 kDa, is the protein to which the myosin head attaches during contraction to form the 'crossbridge' (XB) (Bagshaw & Trentham, 1974). XB formation can be described using the simplified, convention steric-block model of Ca-regulation of XB function. According to this model, the myosin binding site on actin is sterically blocked by tropomyosin before contraction. Tropomyosin is also attached to the troponin complex, which interacts with  $Ca^{2+}$  ions to initiate the muscle contraction process. Upon binding  $Ca^{2+}$ , the troponin complex changes its shape, thereby interacts with tropomyosin, causing it to move away from the myosin binding site on actin. Once this binding site is free, myosin, due to its high affinity for actin, binds to create the actomyosin complex. However, in light of recent reviews, it has been shown that many complex interactions between protein subunits are essential to bring about the protein interactions described above (Solaro & Rarick 1998). Some of these properties are brought to light in the following sections that describe the

muscle-regulatory proteins. Actin is reportedly the most abundant protein in cytoplasm in mammalian cells. The crystal structure of the globular actin monomer, known as G-actin, was first obtained by Holmes and co-workers (Kabsch *et al*, 1990). It is a spherical monomer that contains a high affinity binding site for the myosin head. There are two types of G-actin expressed in striated muscle, skeletal and cardiac isoforms. The amount of each isoform present, and their respective mRNAs, vary with species, muscle type, development and age.

The G-actin monomer polymerises to form the double-helical actin filament F-actin. It is F-actin that comprises the filament structure associated with the sliding myofilament mechanism of muscle. The actin monomer comprises four subdomains with a tightly bound nucleotide inserted into a central cleft in the molecule. In the filament model, subdomains 3 and 4 form the core of the filament, while subdomains 1 and 2 project toward the periphery. Subdomain 1 has been shown to contain sites for the interaction with the myosin heads (Miller *et al*, 1995) as determined by cross-linking and site-directed mutagenesis. The inner two subdomains are connected to the outer two by only two polypeptide strands. Actin is usually considered a 'passive' partner in the contraction process. However, conformational changes within the actin filament play a role in the generation of force (Schutt *et al*, 1993). Studies using spectroscopic probes (dos Remedios & Moens, 1995) show that there are changes in the structure of actin upon interaction with myosin.

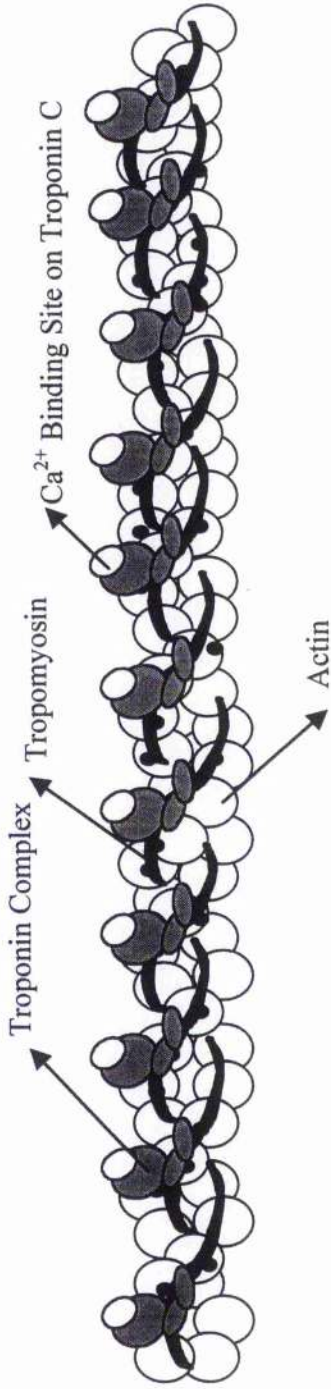


**Figure 1.3.** The major components of the thin filament include actin, troponin, and tropomyosin. Two intertwined helical chains of actin molecules form the primary structure of the thin filaments. Each molecule of troponin is bound to a molecule of tropomyosin. Troponin and tropomyosin are the two proteins that regulate the crossbridge binding sites on actin.

## Regulatory Proteins

Vertebrate skeletal and cardiac muscle contain the regulatory protein troponin in the thin filament. Troponin is found in the muscle at a ratio of one troponin to one tropomyosin and seven actin monomers. The troponin complex is a trimer containing, Troponin C (TnC), Troponin I (TnI), and Troponin T (TnT). Each subunit has a different role in muscle contraction and relaxation. TnC is the  $\text{Ca}^{2+}$  binding subunit of the troponin complex. Therefore, it is the first protein on the myofilaments to be involved in the sequence that leads to Ca-activated tension. It has been shown that when TnC is removed, Ca regulated tension is decreased in proportion to the amount of TnC removed (Babu *et al*, 1987).

### *Troponin C*

TnC (MW 18 kDa) has the crystal structure of a dumb-bell shaped protein with two globular domains connected by a long central helix. Each of these domains contain two  $\text{Ca}^{2+}$  binding sites numbered I-IV [Sites I-III in cardiac muscle]. Sites III and IV are located in the COOH-terminal and have a high  $\text{Ca}^{2+}$  binding affinity (affinity constant  $\sim 10^3 \text{ M}^{-1}$ ). Sites I and II are located in the  $\text{NH}_2$ -terminal and bind two  $\text{Ca}^{2+}$  with relatively lower affinity (affinity constant  $10^5 \text{ M}^{-1}$ ). The kinetics of  $\text{Ca}^{2+}$  binding to the empty, low affinity  $\text{NH}_2$ -terminal domain site are fast, unlike the slow kinetics of the COOH-terminal. This is because the COOH-terminal is limited by  $\text{Mg}^{2+} / \text{Ca}^{2+}$  exchange (Farah & Reinach, 1995). Thus, TnC can be divided into a regulatory  $\text{NH}_2$ -terminal domain that binds  $\text{Ca}^{2+}$  specifically and a structural COOH-terminal domain that binds  $\text{Ca}^{2+}$  or  $\text{Mg}^{2+}$ .

The structure of TnC in the relaxed muscle shows the two COOH-terminals occupied by the  $\text{Ca}^{2+}$  while the  $\text{NH}_2$ -terminal specific sites are empty. Studies show that TnC molecules whose COOH-terminal  $\text{Ca}^{2+}$  binding site has been inactivated by site-directed mutagenesis can restore  $\text{Ca}^{2+}$ -dependent muscle contraction to TnC-depleted skinned muscle fibres. However, TnC mutants in which sites I or II have been disrupted fail to restore  $\text{Ca}^{2+}$ -dependent contraction to TnC-depleted fibres (Sorenson *et al*, 1995, Sheng *et al*, 1990). Therefore, this suggests that  $\text{Ca}^{2+}$  binding to Sites I and II is the initial event in the removal of inhibition of the actomyosin reaction.

The signal of  $\text{Ca}^{2+}$  binding to TnC is transmitted through the thin filament by changes in the TnC molecule's interaction with the other subunits of troponin. This causes the inhibition of contraction by TnI to be removed. However, the exact mechanisms by which these events occur have not yet been fully understood. The main observation by Slupsky and Sykes (1995) studies, relative to the crystal structure, is that  $\text{Ca}^{2+}$  saturation of the N-terminal domain results in the exposure of a hydrophobic pocket that is likely to bind to part of TnI, resulting in removal of inhibition for contraction.

Because TnC is bound strongly to TnI but weakly to TnT, the effects of its removal from the thin filament have been the central theme of many muscle contraction studies. It has been shown that in TnC mutants with disrupted Sites III and IV, the COOH-terminal  $\text{Ca}^{2+}$  /  $\text{Mg}^{2+}$  sites, which are occupied by  $\text{Mg}^{2+}$  in the relaxed state, can be easily removed by washing the fibres with very low  $[\text{Mg}^{2+}]$  media (Negele *et al*, 1992, Sorenson *et al*, 1995). This suggests that the  $\text{Mg}^{2+}$  occupation of the COOH-terminal plays a structural role in TnC binding to the thin filament. The extraction of TnC from muscle fibres *in vitro*, along with replacing it with different TnC isoforms, have been accomplished by many different groups, mainly using selective TnC extraction, employing low-ionic strength EDTA-containing buffers. Selective extraction of TnC from myofibrils was shown to decrease Ca-dependent ATPase activity (Zot & Potter, 1982), whereas extraction from

skinned fibres resulted in a decrease of maximum force (Brandt *et al*, 1987; Moss *et al*; 1985). TnC extraction also shifted the tension-pCa relationship to higher Ca concentrations and decreased its slope (Brandt *et al*, 1987; Moss *et al*; 1985). This apparently is the result of reduced cooperativity. These studies by Brandt and by Moss and their colleagues conclude that there must be some mechanism of inter-unit cooperativity transmitted by TnC.

Selective TnC extraction from myofibrils has allowed many studies in which different types of TnC could be incorporated into the native thin filament. Early studies substituted cardiac TnC into skeletal fibres (Moss *et al*, 1986, Kerrick *et al*, 1991) or skeletal TnC into cardiac trabecula (Babu *et al*, 1987, 1988), leading to insights into how the difference in the number of regulatory Ca binding sites influence the tension-pCa relationship. The studies by Babu *et al* have shown that, with the extraction of TnC, tension produced during activation is only 5 to 10% that of the original contraction. This shows that TnC has a vital role in Ca<sup>2+</sup>-regulated muscle contraction. This group was able to retrieve up to 69% of the original Ca-activated tension with the replacement on the fast skeletal TnC isoform into cardiac trabecula.

### *Troponin I*

TnI, part of the troponin complex, is located on the thin filament. Using various biochemical methods, specific TnI domains have been identified which interact with actin-Tm and/or TnC. These domains are responsible for controlling the 'on-off' states. As a result, TnI is responsible for determining the maximum Ca-dependent actomyosin ATPase activity as well as the Ca-sensitivity of the thin filament (Solaro & Van Eyk, 1996). On its own, purified TnI inhibits actomyosin ATPase in a Ca<sup>2+</sup>-independent manner (Greaser & Gergely, 1971). This actin-binding and inhibitory activity of TnI is enhanced in the presence of Tm (Perry *et al*, 1972; Potter & Gergely, 1974). One region

of cTnI involved in the inhibition is a stretch of basic amino acids that bind either to actin or Ca-TnC, but not to both simultaneously (Talbot & Hodges, 1981; Van Eyk & Hodges, 1988). A region of the C-terminal of TnI is also essential for inhibitory activity. In both diastole and systole, the N-terminus of cardiac TnI (cTnI) anchors cardiac TnC (cTnC) to the thin filament by binding tightly to its C-terminus (Solaro & Van Eyk, 1996).

Cardiac TnI contains an N-terminal extension making it a bigger and possibly longer protein than the skeletal counterpart (Tobacman, 1996, Solaro & Rarick, 1998). This N-terminus extension contains both PKA- and PKC-dependent phosphorylation sites, at serine residues 22 and 23, that modulate  $Ca^{2+}$ -activation (Cole & Perry, 1975, Swiderek *et al*, 1988, Wattanapermpool *et al*, 1995) as well as maximum ATPase rate (Noland *et al*, 1995) respectively. This is accomplished by affecting the interaction of TnI with TnC (Dong *et al*, 1997), the co-operative binding of TnI to actin-Tm (which is unique to the cardiac variant: Al-Hillawi *et al*, 1995), the structure of TnI, and the binding of  $Ca^{2+}$  to TnC (Robertson *et al*, 1982). Studies using mutant cTnI lacking the amino-terminal extension demonstrated that phosphorylation of TnI is both necessary and sufficient to induce the reduction in the  $Ca^{2+}$  sensitivity of myofilament activity (Guo *et al*, 1994, Wattanapermpool *et al*, 1995).

The near amino-terminal domain binds to the carboxy-terminus of cTnC in a  $Ca^{2+}$ -independent manner, anchoring cTnC to actin and, therefore, maintaining the TnI-TnC complex in its antiparallel arrangement (Krudy *et al*, 1994). This region also contains phosphorylatable serine residues (at position 41 and 43) which when phosphorylated by PKC causes a reduction in the maximal activity of the actomyosin ATPase.

The changes in muscle function associated with heart failure point to the effects of cTnI phosphorylation, especially the phosphorylation of the cTnI-specific N-terminal that decreases myofilament sensitivity to Ca (Wattanapermpool *et al*, 1995). Studies have

shown that PKA treatment eliminates the Ca sensitivity difference between failing and control heart preparations (Wolff *et al*, 1996). This suggests that the decrease in phosphorylation of the cTnI terminal extension causes the heart failure associated increase in myofibril sensitivity to Ca (Bodor *et al*, 1997). It has been found, in human and canine hearts, that cTnI phosphorylation occurs at a greater extent in normal heart, occurring near the N-terminal extension of cTnI (Bodor *et al*, 1996).

### ***Troponin T***

Troponin T (TnT), a component of the troponin complex, is a structurally asymmetric protein, containing a globular carboxyl-terminus and an extended amino-terminal 'tail' region and has a molecular weight in the 31-36 kDa range (Perry, 1998). Its carboxy terminus mediates its interactions with TnC and TnI, whereas its amino-terminus binds tropomyosin (Tanokura *et al*, 1983). TnI can be split into two functional domains, TnT<sub>1</sub> and TnT<sub>2</sub>. TnT<sub>1</sub>, makes up the N-terminal and interacts, in a Ca<sup>2+</sup>-independent manner, with the region of Tropomyosin (Tm) extending of the end to end overlap regions of adjacent Tm molecules. TnT<sub>2</sub> makes up the C-terminal region and is involved in the major Ca<sup>2+</sup>-sensitive conformational changes in TnT (Palmiter & Solaro 1997).

The three main isoforms of TnT that exist are fast skeletal, slow skeletal and cardiac. Of the cardiac TnTs, there are several forms that are widely present in vertebrates. In mouse, there are four protein isoforms differing in two variable regions (Jin *et al*, 1996). Five different isoforms exist in rabbit (Anderson & Oakeley, 1988). Four isoforms have also been identified in human cardiac muscle as well as seven isoforms in human skeletal muscle (Perry 1998). Alteration in relative content of these isoforms and the functional consequences have sparked interest in the last few years because of reports of altered isoform content in human myocardium with end-stage heart failure (Anderson *et al*,

1992, 1995). Also, 15% of all cases of familial hypertrophic cardiomyopathy (FHC) involve mutations to TnT (Watkins *et al*, 1995, Forissier *et al*, 1996).

TnT has a marked affinity for tropomyosin. Previous experiments have shown that it forms a stable complex with tropomyosin that is independent of the presence of Ca (Yamamoto & Maruyama, 1973, Van Eerd & Kawasaki, 1973) and Mg (Kawasaki & Van Eerd, 1972). Studies on TnI of rabbit skeletal muscle have identified two regions of the molecule that are involved with the C-terminal region of tropomyosin (Jackson *et al*, 1975; Perry, 1998). Research has shown that the binding of the C-terminal fragment, TnT<sub>159-259</sub> to tropomyosin is strengthened in the presence of TnI, and the components form a ternary complex. This suggests that TnI strengthens this TnT site 2 interaction with tropomyosin but the mechanism is still unclear (Perry, 1998). The major binding site for TnC appears to be located in the C-terminal part of the TnT molecule (Tanokura *et al*, 1983). The possibility that TnT may directly interact with actin does exist, but has not been widely investigated. Evidence shows that TnT is probably close to and possibly in contact with three to four actin monomers of the seven present (Perry, 1998). Early investigations suggested the interaction between TnT and F-actin was only a weak one (Potter & Gergely, 1974, Hitchcock, 1975). There is evidence that both the N- and C-terminal regions of TnT increase the affinity of tropomyosin for actin, but it is not clear whether this is from direct interaction between TnT and actin (Perry, 1998).

TnT is essential in the regulation of Ca sensitivity in muscle. The regulatory function of TnT depends on its ability to convert the TnI-TnC complex to a Ca-sensitive inhibitor of the myofibrillar actomyosin MgATPase. Previous experiments with calmodulin, a Ca binding protein, suggested that a direct effect of TnT alone on TnC lowered its affinity for TnI, promoting Ca sensitivity (Amphlett *et al*, 1976). Studies with mutant forms of TnI support this hypothesis (Potter *et al*, 1995). Evidence is now accumulating that the tension response of permeabilised rabbit fast muscle fibres to Ca depends on the isoforms

of TnT and tropomyosin present (Perry, 1998). But the relationship between isoform composition, force and  $pCa_{50}$  is not restricted to the TnT of skeletal muscle as similar observations have been reported from bovine and rabbit hearts (Tobacman & Lee, 1987, Tobacman, 1998, Nassar *et al*, 1991).

## **Other Proteins in the Myofibrils**

### ***Tropomyosin***

Tropomyosin (Tm) is a highly extended  $\alpha$ -helical coiled coil protein of ~40 nm in length. Tm molecules are assembled in a head-to-tail fashion forming a filament that lies in each of the grooves of the actin double helix. The continuous Tm strand spans seven actin monomers and forms an indirect connection between the troponins. The troponins have the ability to control the position of the Tms along the actin filament and therefore regulate muscle activation (Solaro & Rarick, 1998).

### ***Titin***

Titin, a giant polypeptide, is an integral part of the myofibril found in vertebrate skeletal and cardiac muscle. It makes up a third sarcomeric filament system after the thick and thin filaments (Labeit *et al*, 1997). Titin acts as a scaffold for the formation of thick filaments (Maruyama, 1994, Trinick, 1996). It is responsible for the elasticity of relaxed muscle and bears most of the resting tension in both skeletal (Granzier & Wang, 1993) and cardiac (Linke *et al*, 1994) muscle. The stiffness of the relaxed muscle decreased when titin was removed (Maruyama, 1994).

### *C-protein*

C-protein is a substantial component of the muscle thick filaments. It is composed of a single polypeptide chain with a molecular weight of 137 kDa. It is located in the middle one-third of each half of an A-band and binds to the tail region of myosin. The three types of C-protein that exists are fast and slow skeletal and cardiac (Schaub *et al*, 1998).

## EXCITATION-CONTRACTION COUPLING

The experiments in this thesis employ a method which destroys all membranes in the cardiac myocytes so that the myofilaments alone can be studied. (Described in the Methods Section). The excitation-contraction coupling phenomena do not play a role in this analysis of cardiac muscle. However, a brief outline of the process leading to and initiating muscle contraction *in vivo* is needed to complete the picture.

The action potential, originating from the pacemaker region of the heart *in vivo*, propagates throughout the cardiac tissue and begins the sequence of events that ultimately leads to cardiac muscle contraction. Depolarisation causes permeability changes in the cardiac cell membrane, that is membrane channels open allowing the increased influx of  $\text{Na}^{2+}$  and  $\text{Ca}^{2+}$  ions and the efflux of  $\text{K}^+$  ions. The influx of calcium triggers a release of additional calcium ions from the intracellular  $\text{Ca}^{2+}$  storage system, the sarcoplasmic reticulum (SR). The free cytoplasmic  $\text{Ca}^{2+}$  then acts as a trigger by binding to Troponin C, which initiates the series of protein structural changes throughout the thin filament (described in the next section) and allows the formation of the crossbridges.

Excitation-contraction coupling (E-C coupling) encompasses the process by which an action potential causes the myocyte to contract. Although a number of morphological differences exist between myocardial and skeletal cells, processes involved in activation-contraction coupling have some similarities. E-C coupling begins when an action potential depolarises the plasma membrane of the myocyte. This action potential consists of five phases. The flow of certain ion currents ( $\text{Na}^+$ ,  $\text{K}^+$ , and  $\text{Ca}^{2+}$ ) across the sarcolemma determines each phase. In phase 0, a rapid depolarisation occurs when the diastolic membrane potential has reduced from the resting potential (by about +20mV for cardiac cells and +30 mV for skeletal cells) which provokes an increasing conductance for sodium ions. This rapid depolarisation leads to phase 1 where the rapid sodium

# Ventricular Muscle Action Potential

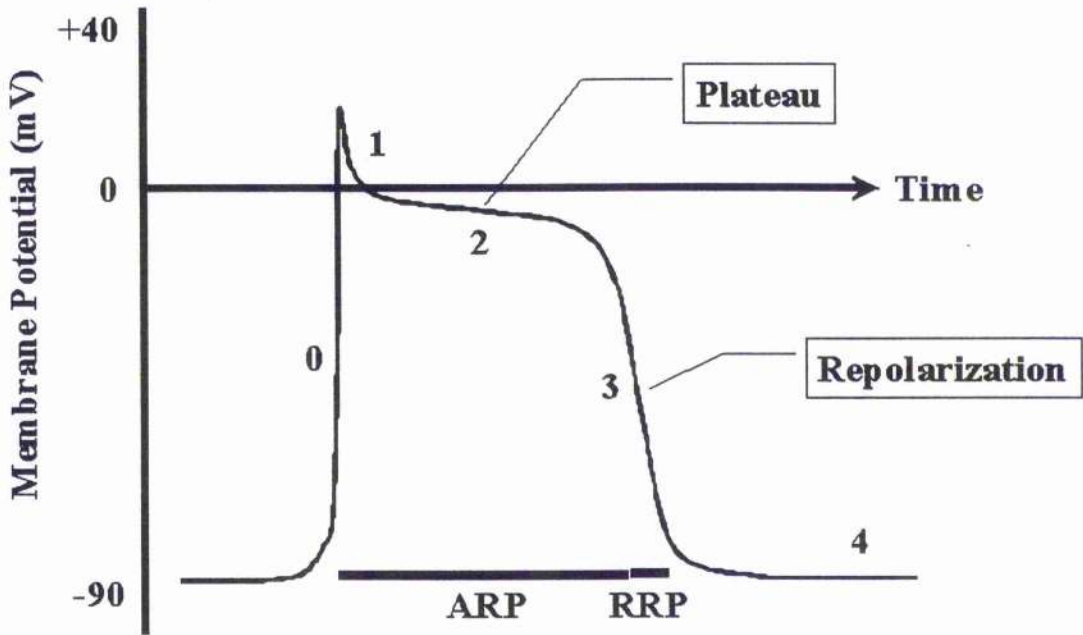


**Figure 1.4.** Changes in membrane permeability to certain cations such as sodium potassium and calcium cause a change in the net electrical charge across the membrane. This change in electrical potential is the action potential and involves a depolarisation and repolarisation period as explained in the text. The firing of the action potential ultimately leads to muscle contraction.

(Web source: <http://plpk04.plpk.uq.edu.au/GMC/Physiology/ECG99/sld014.htm>)

inward current concludes but the outward potassium current continues. The combination of these events causes a small repolarisation in some cardiac cells. The initial rapid depolarisation activates a slow inward current that continues through the first three phases and is responsible for the plateau in phase 2. In phase 3, the inward Ca current partially inactivates and outward potassium current develops leading to a rapid phase of repolarisation. Phase 4 is the resting potential.

The changes in intracellular  $[Ca^{2+}]$  that are triggered by the action potential and their relationship to the contraction process are detailed in the next section.

## MUSCLE CONTRACTION AND FORCE

The muscle contraction process is powered by the hydrolysis of adenosine triphosphate (ATP), principally in the form  $MgATP^{2-}$ . This is widely understood as a cyclic process of crossbridge formation and detachment associated with ATP hydrolysis. We can start the cycle where ATP binds to the myosin head, causing it to detach from actin. This occurs because the myosin-ATP complex has a low affinity for actin. Myosin then acts as an ATPase, hydrolysing it to ADP,  $P_i$  and  $H^+$ . The  $P_i$  is released allowing the complex to be stable and increasing myosin's affinity for actin. A series of structural changes in the myosin allow it to perform a rowing action by which it attaches to an actin, detaches and then attaches again to another actin molecule. Finally, ADP is released, allowing ATP to bind in its place and causing the crossbridge to detach once again. This process will be explained further in this Chapter.

Two types of 'contraction' processes that occur in heart muscle are where muscle length changes (shortens or lengthens) and where muscle lengths remain constant. When muscle shortens (or lengthens), the thick and thin filament move past each other, typically by a few nm or tens of nm in each sarcomere. In shortening, this distance moved is determined by the myosin step size and is based on the muscle model where the myosin head works as a "thermal ratchet" (Irving & Piazzesi 1997). If relative sliding of the filaments has occurred, the site of myosin re-attachment can be farther along the thin filament. This 'cycling' of the crossbridges causes the filaments to slide past each other, thus allowing the muscle to shorten. This process is the sliding filament mechanism, as proposed by HE Huxley with J Hanson (1954) and by AF Huxley with R Niedergerke (1954). The force developed in shortening muscle is derived from the myosin head rotating through its step size against a certain load (Irving & Piazzesi 1997). The load also affects the velocity at which the muscle shortens. If the load is higher, up to maximum isometric force, the tension development is higher but the velocity of shortening is

decreased. If there is zero load, the muscle will not generate force but can shorten at the  $V_{\max}$  (maximal shortening velocity) for the muscle.

Although crossbridges may be cycling, it is not necessary for muscle to shorten. If ATP is present, the myosin head does not remain attached to an actin monomer but repeatedly attaches and detaches from the actin filament. In isometric contraction, the myosin head detaches from an actin molecule and continues to reattach to the same actin molecule or to another actin molecule in the same vicinity. Therefore the filaments do not slide past each other and muscle shortening does not occur. The generation of force in an isometric muscle, and to some extent in muscle shortening or lengthening under load, involves the elasticity of myosin crossbridges (and, strictly speaking, all other components of the sarcomere structure in mechanical series with the active crossbridges). Myosin head rotation during the power stroke occurs in isometric contraction just as in shortening muscle. However, a large-enough load prevents the rotation of the myosin head from producing any significant relative sliding in the filaments. Instead, it is proposed that the elastic region of either the myosin head or neck is thereby stretched sufficiently to permit the head rotation of the power stroke. Here the elasticity converts conformational changes in the proteins into force changes (Irving & Piazzesi 1997).

### **Calcium Concentrations in Muscle**

The Ca available in the intracellular Ca pool arises from different sources. All sources together determine the concentration of intercellular Ca available for the contractile proteins to initiate contraction. During the first phase of E-C coupling, the rapid increase in [Ca] arises after depolarisation, when  $\text{Ca}^{2+}$  ions enter the cell through Ca channels. However, the main source of Ca responsible for the fast increase in the intracellular Ca concentration following stimulation of the myocardium is the SR (Fabiato, 1983). The

SR releases more Ca into the intercellular Ca pool through a process known as the Ca-induced Ca-release (CICR) (Bianchi, 1968, Endo *et al*, 1970, Podolsky, 1970).

Binding of calcium to the contractile proteins mainly consists of the binding of  $\text{Ca}^{2+}$  ions of the Troponin-C (TnC) subunit on the thin filament. This is potentially a large Ca sink because the concentration of TnC in the cardiac cell is about  $70 \mu\text{mol/L}$  (Solaro *et al*, 1974). Although this  $[\text{Ca}]$  detaches from the TnCs later during the twitch, it potentially decreases the intracellular concentration in the first part of the contraction. Later in the same twitch,  $\text{Ca}^{2+}$  comes off the TnC and is then either sequestered by the SR or leaves the cell by various sarcolemmal Ca transport systems.

Under normal physiological conditions, a very large Ca concentration gradient exists across the sarcolemma. The resting Ca concentration inside the cell is in the submicromolar range, around  $0.2 \mu\text{M/L}$ . Outside the cell, the Ca concentration is in the mM range. Thus, a more than 1000-fold  $\text{Ca}^{2+}$  concentration gradient exists across the sarcolemma. Active pumping out of Ca that enters the cell during the action potential is therefore a necessity for the cardiac cell to maintain adequate homeostasis and prevent Ca overload. The sarcolemmal  $\text{Na}^+/\text{Ca}^{2+}$  exchange is one of the main pathway through which Ca homeostasis is maintained.

### **Ca Regulated Tension**

As stated before,  $\text{Ca}^{2+}$  binding to TnC is the trigger for the contraction process. The extent of Ca-regulated tension produced by the filaments is affected in three main ways:  $\text{Ca}^{2+}$  concentration,  $\text{Ca}^{2+}$  sensitivity, and TnC availability. Higher concentrations of  $\text{Ca}^{2+}$  make more  $\text{Ca}^{2+}$  available to bind to TnC and initiate contraction up to the point where the maximum number of TnC sites is occupied to result in full activation (Moss 1992).

$\text{Ca}^{2+}$  sensitivity refers to the range of  $[\text{Ca}^{2+}]$  over which contraction is triggered. Normal cardiac muscle sensitivity ranges between pCa7 and pCa5 with full activation around pCa4.8. These values are strongly dependent on conditions such as pH,  $[\text{Mg}^{2+}]$ ,  $[\text{Pi}]$ , temperature, ionic strength and sarcomere length, some of which may be physiologically relevant variables. By altering these different variables, the  $\text{Ca}^{2+}$  sensitivity at which the muscle operates can thus be changed (Moss 1992).

The third aspect of  $\text{Ca}^{2+}$  regulated tension is the TnC itself. The removal of TnC takes away the only relevant sites for  $\text{Ca}^{2+}$  binding, and therefore prevents  $\text{Ca}^{2+}$  from initiating contraction (Zhao, Gangadhara, Humphries, & Kawai 1996). However, the relationship between the tension produced and the amount of TnC available is not linear but a complex sigmoidal or 'saturation' function. This is due to a cooperativity phenomenon (described later) in the regulatory system, which occurs in both  $\text{Ca}^{2+}$ -regulated tension and rigor tension.

### **Length Dependence (Frank-Starling Mechanism)**

Cardiac muscle normally functions on the ascending limb of its force-length curve, with sarcomere length falling in the range of 1.7 to 2.3  $\mu\text{M}$ . Because each actin projects  $\sim 1$   $\mu\text{m}$  from each side of the Z disk, and the myosin heads only pull in one direction (towards the Z-line nearer the end of that myosin (thick) filament), active force will decline when the sarcomere length is less than the sum of the lengths of the individual actin filaments, around 2.0-2.2  $\mu\text{m}$ . Under physiological conditions of activation, this decline in force over this sarcomere length range is much steeper in cardiac muscle than in skeletal. Crossbridges, under physiological conditions, exert a positive feedback on the TnC  $\text{Ca}^{2+}$  binding sites, more pronounced in cardiac than skeletal muscle. These length-dependent changes in TnC Ca-affinity may require the existence of force-generating crossbridge interactions with actin. This positive feedback makes an important contribution to the steep relationship between active force and muscle fibre

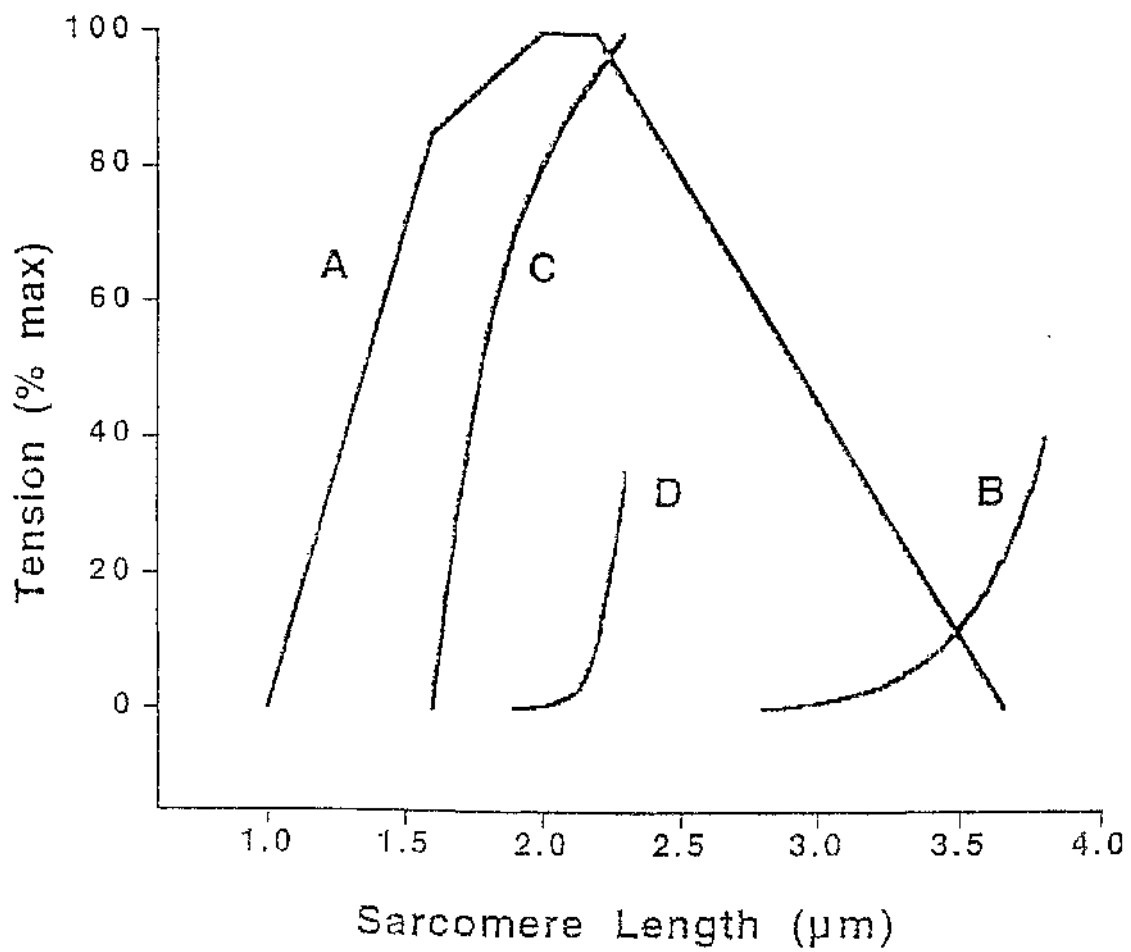


**Figure 1.5.** This figure shows the length-tension relation of striated muscle tissue. In this graph the length-tension relationships of both skeletal and cardiac muscle are shown. A: active skeletal, B: passive skeletal, C: active cardiac, and D: passive cardiac, respectively. (Figure from Janssen, 1997)

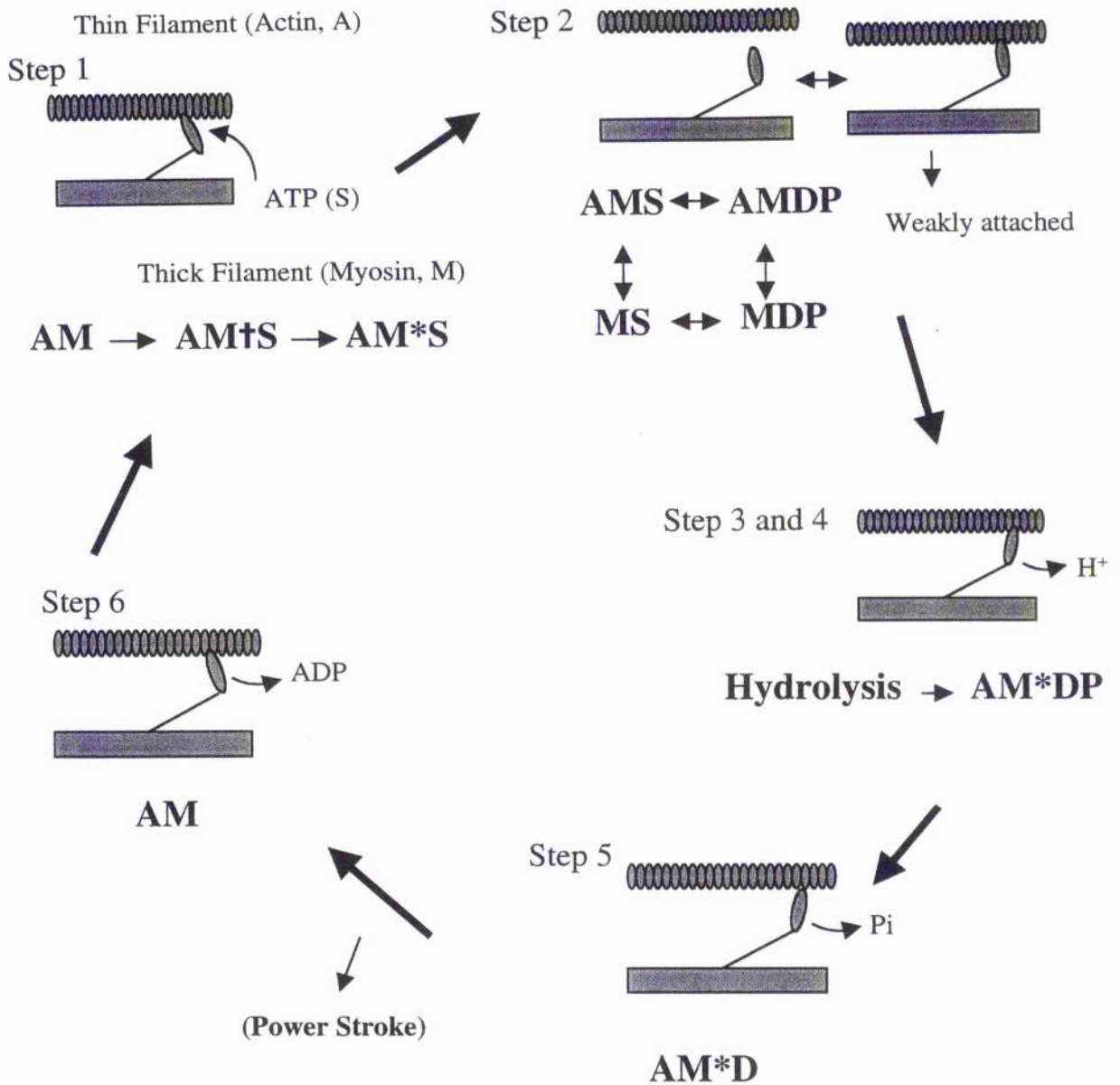


**Figure 1.6.** Chemical and mechanical changes during the various stages of the crossbridge cycle. In the resting muscle fiber, contraction begins with binding of a crossbridge to actin in a thin filament. Once the myosin head binds to the thin filament, it undergoes a conformational change that propels the thin filament toward the center of the sarcomere.

length in the heart. It appears very likely that the activation process in cardiac muscle is length dependent, and does not rely solely on the size of the  $\text{Ca}^{2+}$  transient (Fuchs 1995). A study by Hibberd and Jewell in 1982, for example, showed that trabeculae at sarcomere lengths of 2.3-2.5  $\mu\text{m}$  required significantly less Ca for half-maximal force development concentration than for those at a sarcomere length of 1.9 to 2.0  $\mu\text{m}$ .

### **Cooperativity and Rigor Tension**

Just as TnC regulates  $\text{Ca}^{2+}$  to create tension from one direction, the direction of the TnC complex to the crossbridges, the rigor tension and cooperativity phenomenon begins at the crossbridge level. Many studies involve experimental evaluation of rigor tension and cooperativity to further understand the pathways of muscle activation. The parallel effects of various physiological conditions *e.g.* pH, Pi, and TnC extraction on  $\text{Ca}^{2+}$  activation, rigor activation and cooperativity suggest that each of these processes may have steps in common.

Rigor tension develops in response to the absence of ATP. Very low MgATP concentrations and low ionic strengths favour a strong actin-myosin binding affinity, thus leading to the attachment of the rigor bridges (Fuchs, 1995). These rigor crossbridges form normally but stay strongly attached because there is no ATP to allow it to break. Thus, they are referred to as "semi-permanent." As soon as ATP is introduced, the crossbridge cycle will continue as normal. Once some bridges are in rigor they will prevent any 'internal' shortening, perhaps resulting in the filaments being maximally stiffened. Extra bridges forming as [ATP] falls cannot therefore result in greater tension at the filament ends (and therefore the preparation/fibre ends). The tension produced is only around one third that of  $\text{Ca}^{2+}$  activated tension. However, since the crossbridges are not cycling, but rather permanently attached at once, the stiffness of the muscle in rigor, which will be discussed later, is far greater than active stiffness.

The term 'cooperativity' in this context is the notion that the attachment of one crossbridge influences other crossbridges nearby (on the same thin filament) favouring their attachment to actin (Brandt & Schachat 1997). This phenomenon occurs throughout the thin filament. In  $\text{Ca}^{2+}$  activated contraction, only a fraction of crossbridges is attached at any one time (discussed further in the 'crossbridge' section). Obviously then, not all the crossbridges are attached at the time that ATP is locally consumed or removed by diffusion. During the development of rigor tension, it may be cooperativity that leads to the larger number of crossbridges attaching compared with numbers during active stiffness, where only a third of the crossbridges are attached at any one time (Fuchs, 1995). A modest motion of the lever arm on ADP release can serve to regulate the fraction of myosin bound to the thin filament, in order to recruit more heads at higher loads. Also, if the lever swings through a large angle when phosphate is released, the chemical cycles of the myosin molecules can be synchronised at high loads (Duke 2000).

## CROSSBRIDGES

### Biochemistry

The term 'crossbridge' in muscle physiology refers to the bridge formed between the thick and thin filaments. We have already discussed both  $\text{Ca}^{2+}$ -activated and rigor crossbridge formation in the previous sections. Now we will discuss the biochemistry of muscle movement.

X-ray crystallography shows that the myosin head is roughly pear-shaped. The fatter end of the head binds to the actin filament, and also contains the ATP-binding active site in the enzyme (Irving & Piazzesi, 1997). The thinner end, often called the neck region, consists of a long alpha helix. It is stabilised by the two myosin light chains that wrap around it. These myosin light chains are known as the essential and regulatory light chains (described earlier).

Muscle contraction is thought to be driven by a conformational change in the myosin head while it is bound to actin. To produce sliding between the filaments, the head would have to tilt or swivel with respect to the filament axis. Since the link between the myosin head and the myosin filament is known to be flexible, it would presumably accommodate the tilting, and transmit the resulting motion to the myosin filament. The structure of the myosin head fits neatly with this hypothesis for the motor mechanism. The elongated neck region of the head could act a lever, amplifying small structural changes around the ATP binding site to produce substantial movement between the filaments (Rayment *et al.*, 1993).

There are two distinct types of tilting motion. One is an elastic distortion. This is where the neck region bends slightly when the muscle is under tension. Elasticity in the motor would allow it to produce force as well as displacement between the filaments. A

conformational change in the myosin heads attached to actin could generate force in an isometric muscle by stretching the elastic element. The other type of tilting motion is related to the force-generated conformational change itself. The tilt angle depends on the presence or absence of ATP or its hydrolysis products at the active site. In the absence of ATP the muscle is in rigor *i.e.* where myosin is strongly bound to actin (Irving, 1997).

### **Crossbridge Cycling Rate**

The frequency at which these crossbridges attach and re-attach is the crossbridge cycling rate. The time a crossbridge spends attached to an actin molecule is brief compared with the time it is detached. The time detached is spent hydrolysing ATP and 'thermally locating' a binding site on actin. Crossbridges do not normally attach and detach simultaneously. Instead, even when fully Ca-activated, only perhaps 5% of the crossbridges on a filament are bound to actin at one time (Howard, 1997). This follows from the essentially random, independent cycling of a large number (hundreds per filament) of crossbridges. It prevents muscle contraction or relaxation from being a series of jerky motions, but rather allows it to progress smoothly. It also allows for the development of isometric and isotonic tension in a muscle where force can remain at a certain level for a period of time, whilst the individual crossbridges continue to attach and detach, converting ATP to ADP and Pi.

### **ATPase and Crossbridge Cycle**

The cyclic interaction of myosin crossbridges with actin on thin filaments is responsible for force generation and shortening in muscle. This interaction is driven by the free energy of ATP hydrolysis (Huxley *et al*, 1957, Scheuer & Bhan, 1979) and the cellular system's ability to absorb the products of hydrolysis, which are MgADP, inorganic phosphate [Pi], H<sup>+</sup>, and work output (Kawai *et al*, 1993). Since the proposal of the

'crossbridge cycle' theory, many groups have sought to discover and describe its elementary steps. This interactive cycle between actin, myosin, ATP and its hydrolysis products have been studied extensively using biochemical techniques on isolated muscle proteins, and both intact and chemically-skinned muscle fibres. More recently, biochemical techniques such as *in vitro* motility assays, involving purified actin and myosin and also other proteins such as kinesin as well as 'solution studies' have been developed (Yanagida *et al*, 1985). Studies using these techniques have paved the way for the current model for the crossbridge cycle that involves numerous intermediate states (Eisenberg *et al*, 1980, Taylor, 1979, Tonomura *et al*, 1969, Geeves *et al*, 1984). However, since these techniques cannot provide any information on the force generation of the muscle (with exception to the recent development of the 'optical tweezers' technique in motility assays) these methods have been severely limited in the amount of information they can give on contractility. Mechanical perturbation techniques such as sinusoidal analysis (Kawai & Brandt, 1980), pseudo-random binary noise (Rossmannith, 1986) and step-length changes (White & Thorson, 1973) on both intact and chemically-skinned preparations have been used to characterise the steps of the crossbridge cycle that the biochemical methods could not (discussed further in the next section). It has been shown that the process of chemically skinning the muscle preparation did not affect the validity of the kinetic data when comparing the results using intact preparations.

The crossbridge cycle scheme developed by these mechanical perturbation techniques has seven crossbridge states, and is characterised by seven rate constants and three association constants, called kinetic constants, that govern transitions between the states. Figure 1.6 illustrates this scheme and use the following abbreviations: A, actin; M, myosin head; S, MgATP; D, MgADP; and Pi, inorganic phosphate. An asterisk (\*) and a cross (☒) identify the second and third conformational states, respectively. In step 1a, MgATP binds to the rigor-like AM state to form a complex AM☒, which in turn isomerises in step 1b to form the AM\*S state. Crossbridges then detach in step 2 to form

the detached state. The detached state includes both detached states, MS and MDP, and both weakly-attached states (AMS and AMDP). In the weakly-attached states, myosin is bound to actin but not producing any force. Hydrolysis occurs in step 3. Because several states are included in the attached state, the kinetic constants within the detached state may influence  $k_4$ . In step 4, the detached crossbridges attach to form the AM\*DP state, which in turn is followed by Pi release in step 5 to form the AM\*D state. Step 6 is the isomerisation step, in which AMDP isomerises to form AMD, followed by the loss of MgADP in step 0 to form the AM state. The cycle then begins again if sufficient ATP is present. Otherwise, the myosin remains bound to actin and enters a rigor state (described earlier).

There are many methods used to study the crossbridge cycling kinetics. One method is by measuring the ATP consumption rate of the crossbridges, for example using the enzyme-coupled system. One of many variations of this technique allows the simultaneous measurement of ATPase rate and tension development and is described by Guth and Wojciechowski (1984). Another is the  $f_{\min}$  method involving mechanical oscillation of the muscle preparation (reviewed next).

### **Measuring the Kinetic Aspects of Crossbridge Cycling**

It has been, and still is, the focus of many studies to determine whether crossbridge cycling rate remains constant throughout different muscle types, and among species. The effect of disease states has been examined as a factor that changes the crossbridge cycling rate. Crossbridges have the ultimate role determining the contractile status of the heart. Therefore, any alterations in their kinetics will profoundly affect the pump function of the heart.

Research at cellular levels of analysis had tended to focus on revealing any reduced isometric force production related with heart failure as well as the slowing of isometric

tension development or relaxation. However, there is no external work involved in isometric contraction. Studies with isolated single cells, by contrast, have generally employed unrestrained shortening as an index of contractility. Here again there is no appreciable external work involved. The complexities and shortcomings of multicellular preparations have minimised the number of useful studies on muscle biophysical parameters such as the force velocity relationship that can show work and power characteristics. There is then a lack of knowledge about the mechanical work and power abilities of the failing myocardium, particularly at the level of the myofilaments.

Sinusoidal analysis has proved to be a useful technique for investigating crossbridge properties originally in skeletal muscle. The first step to developing this type of analysis was to devise a way to measure a muscle crossbridge cycling rate in relationship to mechanical events. First thoroughly described by Kawai and Brandt in 1980, sinusoidal analysis is being used by many researchers to investigate crossbridge properties. It was a technique specially used to observe oscillatory work performed in insect flight muscle (Machin & Pringle, 1959, White & Thorson, 1973). It works on the principle of the resistance tension produced by the individual crossbridges against the force applied to the muscle being measured. The muscle is subjected to small-amplitude sinusoidal oscillations of length at several different frequencies. These length changes amount to less than 1% of the muscle length. (In the present study, length changes were typically  $\pm 0.25\%$  or less and the length oscillation frequencies ranged from 0.125 to 20 Hz. When the muscle is stretched by the length change, the attached crossbridges exert an opposing force. This force quantifies the resistance to detachment of the crossbridges. Unlike the length trace, the shape of the resulting tension trace is often not a perfect sine-wave sinusoid. However, the force does take a sinusoidal form in response to the true sinus length change. The amplitude of the sinusoidal tension wave, which quantifies the muscle stiffness, varies with frequency. The amplitudes at the higher frequencies are large, at an intermediate frequency are progressively smaller until they reach a minimum,

but are slightly higher at the lowest frequencies. These amplitudes can be graphed to show a dynamic stiffness curve for the muscle, where a clear amplitude minimum can generally be observed. This minimum, the frequency of minimum stiffness ( $f_{\min}$ ), reports the frequency at which the crossbridges produce the least resistance to stretch and release.

### $f_{\min}$

$f_{\min}$ , as stated above, is the frequency on the stiffness-frequency plot where stiffness comes to a minimum. In terms of crossbridge kinetics,  $f_{\min}$  is the frequency at which least resistance force is exerted by the crossbridge(s) against the sarcomere length change imposed by the mechanical puller arm. It has been suggested by various groups (Kawai & Brandt, 1986, Rossmannith, 1998, Solaro *et al*, 1995) that the reason for this decrease in stiffness is because the oscillation frequency of the imposed length changes corresponds with the mean frequency at which the crossbridges are cycling. Thus, because this rate of the length change, or frequency, is closest to the rate of key steps in the crossbridge cycle, the crossbridges come to exert least resistance against being pulled in the opposite direction, or to sustain least tension when allowed to move in the same direction, as the myosin head movement. It can be considered that a type of 'resonance' phenomenon is generated between the imposed length change and the ability of the bridges to develop tension and resist the displacement as they cycle actively during the sinusoidal length change. At other frequencies, the timing of the length change sinus does not match that of the force generation cycle of a significant proportion of the bridges. As a result, a higher stiffness will be measured at frequencies away from  $f_{\min}$ .

Various labs used sinusoidal analysis (Rack *et al*, 1966, Steiger & Rüegg, 1969, Kawai, 1979) for sometime before Kawai and Brandt published the first detailed description in 1980. Applying this technique to chemically skinned trabeculae can give information about the dynamic properties of muscle filaments, such as crossbridge cycling rate (using  $f_{\min}$  as an index as described in the Methods section). Previously, Edman's slack test had

been used to examine the velocity ( $V_{max}$ ) at which preparation takes up the slack induced by a length change under zero load. However, the information provided by the two techniques is different in terms of the steps in the crossbridge cycle.

In 1998, Rossmannith and Tjokorda studied the interrelationship of various measurements of muscle kinetics, such as  $f_{min}$ ,  $V_{max}$ , and  $k_{tr}$ . They discussed the interpretation of their results using a simple, strain-dependent three-state model based on that formulated by Julian *et al* (1974, see also Figure 4.10). The model shows two attached states (weakly and strongly bound) the detached state, as well as the forward and reverse reaction rates involved at each step. The small amplitude mechanics are influenced by rate constants  $k_{12}$ ,  $k_{21}$ , and  $g_2$  ( $X>0$ ), which govern the dynamics of attached crossbridges. ( $X$  is the distance of actin site from the mid-position of the Brownian motion range of the myosin head when unattached.)  $f_{min}$  is most sensitive to changes in  $k_{12}$  and  $g_2$  ( $X>0$ ), supporting the link between time and frequency-domain representations of small-amplitude mechanics.  $k_{12}$  is associated with the power stroke and with the isometric rate constant  $g_2$  ( $X>0$ ), which regulates crossbridge detachment.

Unlike  $f_{min}$ ,  $k_{tr}$  is also sensitive to changes in the rate constant for attachment,  $f$ , but shares the sensitivity of the small-amplitude mechanics to the rate constant for detachment,  $g_2$  (for  $X>0$ ). The large amplitude isometric parameter ( $k_{tr}$ ) is uncoupled from the small-amplitude isometric parameters by virtue of its dependence on the rate constant for attachment  $f$ . This means that even isometric measurements are not always comparable.

$V_{max}$ , on the other hand, is affected by changes in the magnitudes of the rate constant for detachment,  $g_2$  (for  $X<0$ ), which is encountered during large range shortening. The isotonic parameter,  $V_{max}$ , is uncoupled from the small-amplitude isometric parameter,  $f_{min}$ , because of its sensitivities to changes in the magnitudes of the rate constants  $f$  and  $g_2$  ( $X<0$ ). It is also uncoupled from the large amplitude parameter  $k_{tr}$  by virtue of its response to changes in  $g_2$  ( $X<0$ ).

Although many kinetic parameters have been used to determine crossbridge kinetics and crossbridge cycling rate, ATP measurements have been commonly used to determine crossbridge cycling rates. In this enzyme-coupled system, the ADP formed by the muscle is converted back to ATP using chemical reactions involving ATP, ADP, Phosphoenolpyruvate, Pyruvate, NADH, and  $H^+$ . During these reactions, one mole of NADH is converted to NAD, for every mole of ATP converted to ADP. NADH, but not NAD, fluoresces under UV radiation. Thus, the rate of ATP consumption by the muscle is determined by measuring the fluorescence decay upon crossbridge activation (Ebus *et al.*, 1994).

Studies by Rossmanith *et al.*, (1986) found that  $f_{min}$  values compared favourably to ATPase results by Pope *et al.* (1980). However, this is not always the case. Comparison of our  $f_{min}$  results to ATPase values, found in Ebus *et al.* (1994), show some differences. This is further discussed in the conclusion section of this thesis. It should be noted that ATPase measurements, as described here, only look at the product of a chemical reaction that takes place during muscle activity, and it too is only an indirect method. In addition, recent studies have shown the more than one crossbridge cycle may occur using a single ATP molecule (Yanagida, 1999). In light of this result, conclusions drawn from ATP measurements alone can be very misleading in terms of crossbridge kinetics. Finally, because of the strain dependence of key kinetics in the crossbridge cycle, turnover rates and thus movements are slower the higher the tension (the Fenn effect). We cannot directly relate the small-amplitude, near isometric  $f_{min}$  to the actual speed of the crossbridges when undergoing large-amplitude motion under varying load (as in the ejection phase).

### **Creatine Phosphate and Creatine Kinase**

Creatine phosphate is an important biochemical component of the normal fuelling of the muscle contraction process. One of the first biochemical consequences of cardiac

hypoxia or ischaemia is the net hydrolysis of most of the creatine phosphate in the myoplasm to creatine and Pi (Dawson, 1983). This occurs because of the net effect of the continuous hydrolysis of ATP to ADP and Pi by actomyosin and other cellular ATPases and the re-phosphorylation of ADP to ATP. This last reaction takes place via the Lohmann reaction:



In the absence of oxidative rephosphorylation of creatine (at the mitochondria) under ischaemic/hypoxic conditions, the net breakdown of CrP and hydrolysis of ATP can cause the myoplasmic concentration of Pi to rise from 2-5 mM to as much as 15-20 mM (Dawson, 1983, Allen, 1985).

The enzyme catalysing the Lohmann reaction is creatine phosphokinase (CPK). CPK is present in high activity in muscle cells. CPK isoenzymes are compartmentalised within the cell where they fulfil functional and structural roles. CPK is either free in the cytosol or bound to the myofilaments and the sarcoplasmic reticulum, close to the ATPases (Ventura-Clapier, 1998). In oxidative slow and cardiac muscle, mitochondrial, cytosolic and protein bound CPKs ensure the efficiency of energy and signal transfer between the sites of energy production and the sites of energy utilisation as well as their cellular integration (Ventura-Clapier, 1998). In mitochondria, CPK is present on the outer face of the inner mitochondrial membrane and functionally coupled to oxidative phosphorylation. A high concentration of CPK is found within the M-line of the sarcomere. In fast skeletal muscle fibres, it mainly ensures efficient buffering of ATP and high metabolic energy reserve quickly mobilisable for contraction.

## GENERAL FEATURES OF CONGESTIVE HEART FAILURE

The syndrome of congestive heart failure (CHF) is an entity of ever increasing clinical significance. CHF is a long-term outcome of a number of cardiovascular diseases, such as ischaemic heart disease, hypertension, valvular diseases, and idiopathic cardiomyopathy (Smith WM 1985, Francis & Cohn 1990). Over 10 years ago (Consensus, 1987) it was stated that 'in its advanced stages, CHF has a poor prognosis despite its modern clinical management'. Unfortunately this statement remains true.

During the development of CHF there is a continuous decline in cardiac pump function (Francis & Cohn 1990, Alpert, 1983). Several potential mechanisms lead to CHF including loss of myocytes, ventricular chamber remodelling, extracellular matrix hyperplasia, and decreased myocyte function. The decrease in myocyte function is due to a combination of altered Ca handling, altered cytoskeleton, and altered myofilament function (de Tombe, 1998). These processes lead to a gradual increase in end-diastolic left ventricular pressure (LVEDP) and a decrease in end-systolic LV pressure (LVESP). Eventually, the decline in cardiac pump function results in the clinical syndrome of CHF. It is not known how, or to what degree, these alterations in cellular processes contribute to the decline of *in vivo* cardiac pump function seen in CHF.

Myocardial ischaemia is the state of insufficient blood supply globally or regionally to the heart. A lack of oxygen is the most acutely damaging of the resultant deficiencies. This lack of oxygen supply to the tissue is termed hypoxia. The primary determinants of myocardial oxygen demand are heart rate, blood pressure (myocardial wall stress), and myocardial contractile state (Buja 1995).

It is known that ventricular hypertrophy and failure create a state of increased oxygen demand by the influence on these parameters. Increased myocardial oxygen demand in inadequately perfused myocardium can induce a state of myocardial low-flow ischaemia.

Survivors of acute ischaemic damage may develop significant chronic ischaemic heart disease.

During hypoxia or ischaemia there is a decrease in force development in cardiac muscle, leading to a significant fall in tension over the next several minutes. There are many metabolic alterations responsible for this reduction in contractile performance. They include intracellular acidosis (Gibbs, 1978, Kentish 1991, Ebus, 1994), as well as changes in myoplasmic concentrations of creatine phosphate (CrP), creatine and inorganic phosphate (Pi) (Gibbs, 1978, Kentish 1991, Ebus, 1994).

Heart failure is also associated with changes in the distribution and content of myocardial proteins in human CHF (Schwartz *et al* 1992, Nadal-Ginard *et al* 1989), in animal ventricular hypertrophy (VH) (Schwartz *et al* 1992, Nadal-Ginard *et al* 1989) and in animal CHF (Li *et al*, 1997). It appears that these changes are of functional significance, since decreases myocardial myofibrillar ATPase activity has been demonstrated in the failing human heart (Pagani *et al*, 1988) and in the hearts of animal models of VH (Alpert, 1983).

## CHAPTER 2 METHODS AND MATERIALS

## ISOLATED VENTRICULAR TRABECULAE EXPERIMENTS

### Trabecular Preparations

Male Wistar rats were killed by stunning, cervical dislocation, and exsanguination. The heart, still beating, was removed immediately and placed in Ringer's solution (composition: 150 mM NaCl, 5 mM KCl, 1 mM MgCl<sub>2</sub>, 2 mM CaCl<sub>2</sub>, 5 mM HEPES, at pH 7). Once in the beaker, the heart was gently massaged to push out most remaining blood. 20mM 2,3-butanedione monoxime (BDM) was also included in the composition of the Ringer's solution as a muscle contraction inhibitor. BDM has been found to inhibit the force generation of skeletal and cardiac muscle (Fryer *et al.*, 1988, Gwathmey *et al.*, 1991, Backx *et al.*, 1994). By inhibiting force generation, BDM allowed the muscle to remain in a relaxed state. This made the muscle easier to handle without causing any damage to it during dissection and mounting.

The heart was placed in a Petri dish with the dorsal surface uppermost and then restrained by pinning it with a few fine pins. The atria were removed. The blood was cleaned out of the right ventricle by inserting a plastic syringe into the lumen through the tricuspid valve and gently flushing Ringer's solution through it. The right ventricle was then opened by cutting from the tricuspid valve to the apex and from the tricuspid valve to the pulmonary artery, both along the line of the ventricular septum.

Experiments were performed on free-running trabeculae. Most were dissected from the right ventricle where there is a higher population. The majority of trabeculae used were found at the base of the right ventricle just below the tricuspid valve. However, occasionally, trabeculae from the left ventricle were used. Experiments have shown that the myofilament make-up of rat cardiac muscle is uniform throughout both ventricles (*e.g.* Unpublished data, Varghese, 1993). The dimensions of the trabeculae are important. They must be approximately cylindrical. This was to ensure that force would be

generated uniformly throughout the preparation during contraction. Chemical diffusion rates do not change. With an increase in preparation diameter, the distance that the chemicals must travel to reach, or leave, the centre of the preparation increases. Mean diffusion time is proportional to the square of distance. As a result, the time to reach full  $\text{Ca}^{2+}$  activated force would also increase steeply the larger the preparation diameter. Preparations used were from 1-2.5 mm in length and 100-240 $\mu\text{m}$  in diameter (mean length  $\pm$  SEM:  $1.43 \pm 0.04\text{mm}$ ) Preparations were dissected with extra tissue at each end to aid in mounting and un-mounting the preparation into and from the equipment.

### **Preparation Mounting for Force Measurement**

The preparation was suspended between an Akers AE 875 force transducer and a mechanical puller arm (Cambridge Technology Inc., Watertown, Mass. USA, Series 300B Lever System). Both transducer and puller arm had four hollow stainless steel tubes (Goodfellows Metals Ltd, Cambridge; outside diameter 200 $\mu\text{m}$ , internal diameter 100 $\mu\text{m}$ ) attached in a parallel manner using 'superglue'. These steel tubes provided additional rigidity to the system in the longitudinal axis of the trabeculae to reduce the effect of the compliance of the tubing. Each piece of tubing was 3-4cm in length with one of the tubes on each set ending about 0.5cm lower than the rest. These each had a single nylon monofilament (25 $\mu\text{m}$  diameter) running through the tube in a doubled manner to create a loop at the bottom end. These loops formed the snares used to hold the muscle preparation at each end. During mounting, the preparation was fed into both loops. Once in place, the loops were tightened by pulling the free ends of the monofilament at the top ends of the steel tube. The snares were tight enough to hold the muscle in place without allowing it to slip out. Each encircled the outer diameter of the preparation without grossly distorting the preparation's natural shape. The entire mounting process was completed while the preparation remains fully immersed in Ringer's solution in the Petri dish.

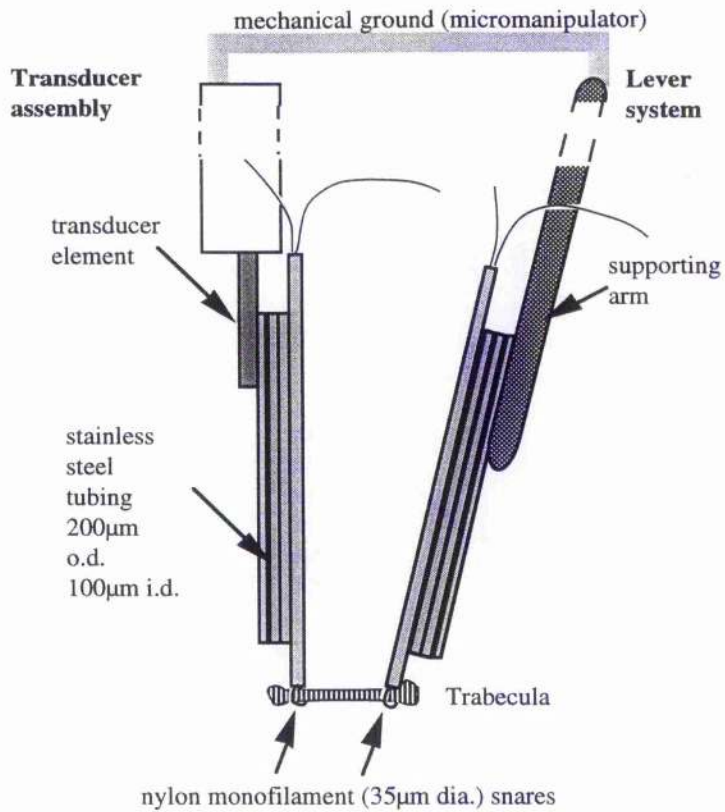


**Figure 2.1.** Experimental transducer set-up for the sinusoidal oscillation protocol.

Exact alignment of the transducer pins between the glass slides of the solution chamber in the microscope was vital due to the extreme fragile nature of the transducer element to which the hollow pins were glued. Once placed in the solution chamber, the micromanipulator holding the transducer clamp could be used to further adjust the relative positions of the pins.

The compliance of the transducer and the puller arm were measured by hanging weights on the ends of the attached steel tubes in the plane of use. The displacement was measured using a microscope with a calibrated eyepiece. At least two weights (under 1 g.wt.) were used to check the linearity of compliance and at least two smaller weights (less than 150mg wt) linearity of output voltage to applied force. The compliance of the system was found to correspond to a length change of less than  $0.1 \pm 0.02\%$  at a typical maximum Ca-activated force. In all experiments the output of the force transducer was recorded after being pre-amplified and filtered at 50Hz. (The roll-off characteristic of the active filter was 18 dB per frequency decade. Thus filter-dependent signal distortions are at frequencies comfortably above any wave components relevant to the present experiments). In some cases, the digitised record was digitally smoothed to remove high-frequency 'noise' for the purposes of phase analysis. The amplified trace was digitised using MacLab software (version 3.5.6) and hardware (version 8). The experiments in this thesis recorded the force signal from the transducer and the length signal from the automated length changing system.

The puller and lever arm system was mounted on a Narashige MM3 micromanipulator. This apparatus allowed the preparation to be moved with fine precision in three planes. This permitted the mounted trabecula to be positioned correctly. Each plane had its own graduated rule. An independent micromanipulator mounted on the MM3 supported the force transducer. This allowed the separation between the lever arm and transducer to be changed, therefore permitting the adjustment of overall muscle length and hence sarcomere length. It also allowed the transducer pin to be lowered or raised to ensure that the trabecula was horizontal. The entire transducer and lever arm system was mounted on a solid steel bar and held by a magnetic based on a metal base plate. The magnet could be turn on and off allowing the apparatus to be moved between the dissection and DIC microscopes and the bath changer, as required.

## Measurement of Sarcomere Length

As reported previously by many groups, the length-tension relationship should be considered in any muscle manipulation experiment. Sarcomere length, as explained by the Frank-Starling Mechanism (outlined in the Introduction) affects many physiological parameters of force generation, including Ca sensitivity. Therefore, it is important to measure sarcomere length accurately and consistently. The experiments described in this thesis all depend on the force generated and require the Ca sensitivity to remain constant for all the preparations used. In preference to the laser diffraction system used in some laboratories, a modified Vickers M-16 microscope with Differential Interference Contrast (DIC) optics (Smith, 1969) was used to examine the preparation and adjust sarcomere length to the optimum value (*i.e.* 2.1-2.2 $\mu\text{m}$ ) for force production in cardiac muscle. The microscope was arranged to lie horizontally ('supine'). The microscope stage was replaced with a mounting base for the transducer assembly and an observation chamber. This chamber allowed the preparation to be viewed in the optical path of the microscope. (Figure 2.1). The trabecula was viewed on a television monitor via a video camera that further enhanced the contrast of the DIC image. A calibrated graticule placed in the video camera mounting tube allowed the accurate measurement of the preparation from the monitor. The distance between the major divisions on the graticule was calibrated (by viewing a diffraction grating) at 123.7  $\mu\text{m}$  using the 5X objective lens and 21.8  $\mu\text{m}$  using the 40X lens. Therefore, since the optimum length of a sarcomere was to be 2.1-2.2  $\mu\text{m}$ , the length of the preparation was adjusted so that 10 sarcomeres could be counted across one major division on the graticule (or 20 across two). This measurement was repeated at various parts of the trabecula (between the preparation ends) to ensure that the sarcomere length was consistent across the preparation. There was only a small region of sarcomere pattern distortion, amounting to less than 1% of the preparation length, indicating relatively little damage. The distortion usually appeared as a hypercontracture of the region found immediately adjacent to the snares, but with the sarcomere structure still

evident. (The lack of significant 'end-damage' with the mounting system used in this laboratory was first reported in detail by Harrison *et al*, 1988).

### **Measurement of Preparation Dimensions**

Preparation dimensions were measured in the same microscope. Once the sarcomere length had been adjusted to 2.1-2.2  $\mu\text{m}$ , the diameter (in both vertical and depth (Z) planes) and length of the preparation was measured. All measurements in the DIC microscope, excluding the depth diameter, were done using the calibrated graticule displayed from the TV monitor. The length of the preparation was determined from the distance measured between the two snares by means of the Vernier scale on the MM3 as the preparation was translated from one end to the other whilst viewed on the monitor image (40x objective). The depth diameter was measured using a graduated focusing dial on the microscope (precision 1  $\mu\text{m}$ ). The image was first adjusted to focus on the nearer, outer rim of the trabecula at its widest point (using the 40X objective lens). Then, it was refocused to the far surface of the trabecula. The trabeculae were mostly elliptical in cross section. Thus, cross-sectional area can be calculated from the formula for the area of an ellipse *i.e.*:

$$\text{area} = (\pi \times D_h \times D_v)/4 \text{ (Equation 2.1)}$$

where  $D_h$  and  $D_v$  equal the horizontal and vertical diameters respectively.

## SOLUTION COMPOSITION

The rationale for composition of the main experimental solutions, the method for calculating free ion levels and ionic strength, the choice of ion binding constants for the various ligands, precautions for EGTA purity, Ca contamination determinations, the measurement of pH and other details of the experimental solutions are described in detail elsewhere (*e.g.* Harrison, Lamont & Miller, 1988, Miller & Smith, 1984). However, a short description of the composition of the solutions used the experiments of this thesis is given below.

The components and their respective concentrations in experimental solutions are given in detail in Table 2.1. These solutions were made by mixing the appropriate volume of the following stock solutions, which were made on a regular basis: 1M KCl, 1M MgCl<sub>2</sub>, 100 mM EGTA, 100 mM CaEGTA, and 500 mM HEPES. EGTA was dissolved by adding twice the molar amounts of KOH before finally adding distilled water to bring to the desired volume. CaEGTA was prepared in a similar way except that CaCO<sub>3</sub> was added to the EGTA and KOH and heated gently. During this process, the CO<sub>2</sub> was driven off leaving CaEGTA. ATP, creatine phosphate (CrP), and dithiothreitol (DTT) were used in solid form, as di-sodium salts. DTT was used to scavenge free radicals in the media. ATP, CrP and all other chemicals were obtained from the Sigma Chemical Company, Poole, Dorset, UK., unless otherwise stated.

When making the solutions in Table 2.1, all liquid stock solutions were mixed first and titrated to pH 7 before added the solid components. This was done to minimise spontaneous hydrolysis of ATP. The solution was then titrated again to the approximate desired pH and brought to desired volume using distilled water before a final pH check. Solutions with different Ca concentrations were obtained by mixing solutions B and C (Table 2.2). Approximately 0.05mM CaCl<sub>2</sub> was added to aliquots of solution C (Table

2.1) to achieve pCa 4.00 that, under our standard conditions, ensures maximal activation of the preparation. To make the Ca-activation as rapid and uniform as usual as possible, the 'Ca-jump' method was employed. This method produced a rapid increase in  $[Ca^{2+}]$  by increasing the  $Ca^{2+}$  buffer concentration at the same time as the free  $Ca^{2+}$  concentration (Miller, 1975, Moiescu, 1976, Ashley & Moiescu, 1977) i.e. the preparation is moved to the test pCa solution after prior equilibration in solution A (Table 2.1). Solution A has its ionic balance (0.2M) maintained by addition of KCl.

<b>Table 2.1</b>			
<b>Solution components</b>	<b>Solution A (0.2r)</b>	<b>Solution B (10r)</b>	<b>Solution C (10a)</b>
<b>EGTA</b>	0.2 mM	10 mM	-
<b>CaEGTA</b>	-	-	10 mM
<b>KCl</b>	100 mM	100 mM	100 mM
<b>MgCl<sub>2</sub></b>	7 mM	7 mM	7 mM
<b>HEPES</b>	25 mM	25 mM	25 mM
<b>Na<sub>2</sub>ATP</b>	5 mM	5 mM	5 mM
<b>Na<sub>2</sub>CrP</b>	15 mM	15 mM	15 mM
<b>DTT</b>	10 mM	10 mM	10 mM

<b>Table 2.2</b>					
<b>Solution Ratio 10a:10r</b>	<b>ml of 10a in 5 ml</b>	<b>ml of 10r in 5 ml</b>	<b>[Ca<sup>2+</sup>] total mM</b>	<b>control free [Ca<sup>2+</sup>]</b>	<b>control pCa</b>
<b>Of 1:1</b>	2.50	2.50	5.000	0.47 $\mu$ M	6.3234
<b>Of 2:1</b>	3.33	1.67	6.666	0.95 $\mu$ M	6.0219
<b>Of 5:1</b>	4.17	0.83	8.333	2.38 $\mu$ M	5.6240
<b>Of 8:1</b>	4.45	0.55	8.888	3.79 $\mu$ M	5.4212
<b>Of 15:1</b>	4.69	0.31	9.375	7.01 $\mu$ M	5.1542
<b>Of 10a</b>	5.00	0.00	10.000	51.56 $\mu$ M	4.2877
<b>Of 10a full</b>	5.00 (+50 $\mu$ l 10m M CaCl <sub>2</sub> )	0.00	10.000	87.29 $\mu$ M	4.0590
<b>Of 10r</b>	0.00	5.00	0.005	0.24 nM	9.6265
<b>Of 0.2r</b>	0.00	0.00	0.005	12.20 nM	7.9138

**\*Note that solutions A-C at pH 7 with no added phosphate was used as the controls in this thesis. This is further explained in the results section of Chapter 3.**

<b>Table 2.3</b> <b>Rigor solution</b>	EGTA	HEPES	KCl	MgCl <sub>2</sub>	DTT
mM	10	25	165	7	10

### **pH Measurements and Buffering**

The effect of pH on the various physiological properties of the cardiac myofilaments was central to the experiments of this thesis. Therefore, it was crucial that the solution pH was accurately measured and strongly buffered. Within our laboratory, separate reference and pH electrodes are generally used (Ciba Corning Diagnostics Ltd., Essex, England) to give a reliable measure of pH (Illingworth, 1981, Smith & Miller, 1985). The pH of experimental solutions was adjusted using a null point method. The electrodes were allowed to equilibrate in a standard solution (6.08mM KOH, 197mM KCl and 25mM HEPES) calculated to have the same  $pH_a$  (7.00) and ionic strength as the experimental solution (Harrison, Lamont & Miller, 1998).  $pH_a$  is the pH of the solution based on the activity of the Hydrogen ions in the media. With  $pH_a$  and ionic strength known, the value  $pH_c$ , the pH based on the hydrogen ion concentration can be calculated; it is the basis for calculating the chemical interactions within the solutions used. 25 mM HEPES was present in all experiment solution to minimise any changes in pH that may occur within the preparation during contraction.

### **Calculation of Free Metal Concentration and Ionic Strength**

It is important to take account of the concentration of other ionic species and other experimental variables, such as  $pH_c$  and temperature, in order to calculate free  $[Ca^{2+}]$ . This is because EGTA, the Ca chelator used for this thesis, binds metals ions other than Ca. The affinity constants of EGTA and other ligands in these experimental solutions,

such as ATP, CrP, and HEPES, were taken from published compilations (Pettit, & Powell, (1993), Sillén, Martell, Hogfeldt, & Smith, (1974)).

The REACT computer program, written by Professor Godfrey Smith, was used to calculate the free ion concentration of the experimental solutions (Smith, 1983, Miller & Smith, 1984). The free metal concentration of the various commonly used mixtures of solutions A and B are given in Table 2.1. Ionic strength was defined according to the following equation:

$$I_c = 0.5 \times \sum c_j z_j \text{ (Equation 2.2)}$$

where  $I_c$  is ionic strength, defined as the total of the ionic equivalents,  $c_j$  is the concentration of the  $j$ th ionic species and  $z_j$  is its valency (Smith & Miller, 1985). This expression is found empirically to be a more consistent description of ionic strength for the present media, with several species of polyvalent anions present, than the more conventional formal ionic strength *i.e.*

$$I_f = 0.5 \times \sum cz^2 \text{ (Equation 2.3)}$$

### **Chemical Skinning**

The mounted preparation was exposed to solution B containing 1% Triton X-100 (Pierce Chemicals, Rockford, Illinois, USA.) for 30-45 minutes, depending on its size. Triton X-100 disrupts all membrane diffusion barriers so that only the myofilaments remain functional (*e.g.* Miller, Elder & Smith, 1985). Therefore, any intervention that influences the contractile response of a Triton-treated preparation can be solely attributed to a direct action on the myofilaments.

## Automated Solution Bath System

A computer-controlled solution change system was used in all the experiments presented in this thesis (Miller, Sinclair, Smith & Smith, 1982). The solutions were contained within a series of wells cut into a Perspex block. Each well could hold about 5ml of solution, though actual bath volume employed was 4.65ml. A motorised rack and pinion system allowed for the controlled movement of the wells in the horizontal plane via a stepper motor. A second, similar system was employed in the vertical plane to raise and lower the assembly during a solution change. Both motors were controlled by a 486 PC using in-house software to programme and time solution changes. A solution change was thus made by lowering the Perspex block, moving it horizontally under the preparation and then raising it to immerse the preparation in the required solution. The speed of the stepper motors was such that a solution change between adjacent baths could be made in 200ms, though generally about 1-2sec was adopted as a suitable time. The software accompanying the system allowed the programming of a large number of accurately timed solution changes. The brief exposure to air did not affect the muscle.

The preparation was immersed 2mm below the meniscus. This depth eliminated the stretch effect that could be caused by the trabecula being too close to the meniscus. One of the many advantages of this system is a reduction in 'carry-over' of the solution from one bath to the next. Previous checks performed in this laboratory (*e.g.* Harrison *et al*, 1988) have shown that the emergence of the trabecula through the meniscus of the solution, as the Perspex block is lowered, removes any significant adhering droplets and therefore minimises subsequent contamination of the new experimental solution. For example, contamination of the 'rigor-inducing' solutions by even very small amounts of ATP could otherwise have a pronounced effect on force development. The solution in use was continuously stirred by a small stainless steel paddle driven by an electric motor.

Protocol: Rat ventricle trabecula (dia.130 $\mu$ m, length 1.6mm)

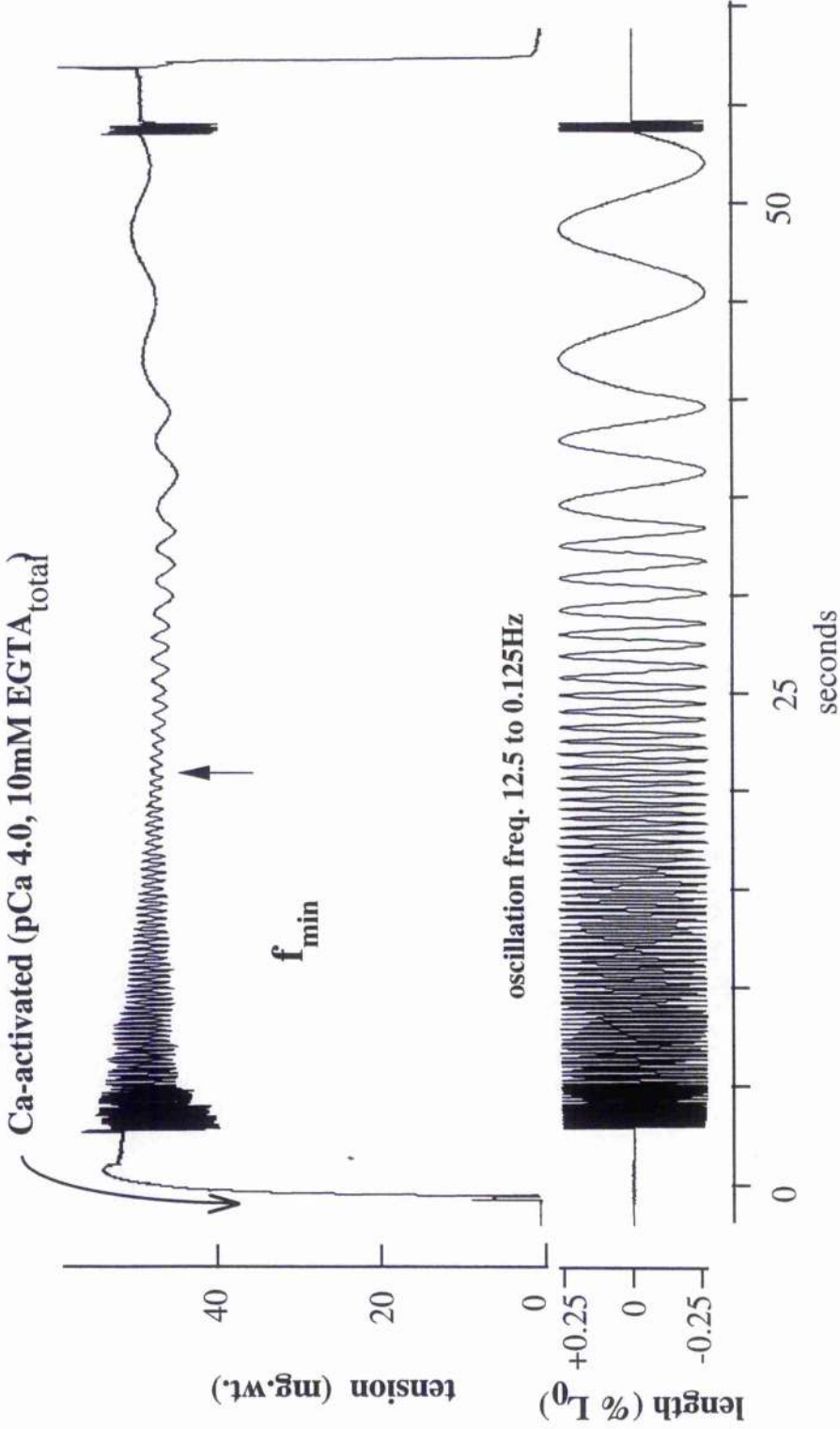


Figure 2.2 This shows a typical experimental trace where the muscle fibre is Ca-activated (Soln. C) and then oscillated at various frequencies (typically in 20 steps from 12.5 down to 0.125Hz then returning in 3 steps to 12.5Hz). The lower trace shows the sinusoidal length change imposed on the trabecula which is constant at the various frequencies. The upper trace shows the dependence of the force transients on the applied frequency of length change.

## THE OSCILLATION PROTOCOL

Sinusoidal analysis was used to determine the aspects of crossbridge muscle kinetics of the cardiac myofilaments. This method was first rigorously analysed and described by Kawai and Brandt in 1980. They used this protocol to analyse physiological processes in activated skeletal muscles of rabbit, frog and crayfish. However, it was previously described through Steiger and Rüegg (1969), who used sinusoidal analysis to study energetics of isolated contractile machinery of insect fibrillar muscle.

The small-amplitude oscillation ( $\pm 0.25\%$  of muscle length) was imposed on the trabecula at a range of frequencies from 0.125-20Hz. The working stroke of the crossbridges reported by various groups range from 4-20nm (Molloy *et al*, 1995, Ishijima *et al*, 1996, Mehta *et al*, 1997, Guilford *et al*, 1997). Therefore, the magnitude of the length change of  $\pm 0.25\%$  of muscle length, corresponding to  $\pm 2.5\text{nm}$  per half-sarcomere at a sarcomere length of  $2.2\mu\text{m}$  (Kawai *et al*, 1993), was chosen to avoid over-stretching the muscle to the point that causes the myosins to detach from the actin and then re-attach, as in stretch-release protocols (*e.g.* Jung *et al*, 1988, De Winkel *et al*, 1993) used to examine the kinetics of crossbridge reattachment.

Preliminary experiments under standard conditions showed that maximum muscle stiffness for rat myocardium was found at around 7.5Hz. The frequency for minimum stiffness ( $f_{\text{min}}$ ) was found usually between 2 and 3Hz. The range of frequencies used in the experiments of this thesis was from 0.125-12.5Hz in order to give a clear picture of the stiffness phenomenon above and below  $f_{\text{min}}$ . The sequence of the frequencies, applied typically in 15 steps, ranged from the highest to the lowest frequency, and then repeated the higher frequencies from 7.5Hz to 12.5Hz. This sequence was consistently employed to allow semi-automated analysis of the data after the experiment. Previous experiments using a variety of sequences showed that the order in which the frequencies were

imposed did not affect the mechanical behaviour of the preparations. The digital trace shown in Figure 2.2, obtained from a typical sinusoidal perturbation over the range of frequencies just described, show the tension and length outputs for a maximally Ca-activated trabecula.

The lever system was controlled by a 486 PC clone. In-house software allowed accurate control of the distance moved by the lever arm and the frequency at which the sinusoidal length changes were produced. A calibrated electron microscope graticule at 400X magnification had been used to calibrate the distance moved by the lever arm with a certain number of output pulses specified by the in-house software used. The length step-size imposed by a single pulse step was typically  $0.035\mu\text{m}$  (depending upon the exact length of the lever arm and mounting tubes). This means that for a typical trabecula of between 1 and 2mm in overall length, about 140 to 280 steps define the  $\pm 0.25\%$  length sinus wave.

The sinusoidal oscillations were applied at both resting and fully Ca-activated states, as well as the ATP withdrawal-induced rigor state for some experiments. Upon analysis of the length and corresponding tension traces at certain frequencies, the dynamic stiffness and phase data of the muscle preparation could be determined.

### **Basic Protocol**

Once the preparation was measured and  $\pm 0.25\%$  length of the specific preparation defined, the preparation was returned to the automated bath changing solution and set in 10R (Solution A). Resting tension of a healthy preparation was never above a few mg.wt. If resting tension was abnormally high, the sarcomere length was checked and adjusted or the preparation was not used. The preparation was then activated and relaxed until a steady contraction trace (as shown in Figure 2.2) was achieved. Once a steady contraction occurred and a tension plateau was achieved, the oscillation protocol was

implemented. A resting oscillation sequence was performed for every preparation at the beginning and end of the experiment. Further descriptions of protocol are specific to the type of experiment done and are given in the relevant chapters.

## **Data Handling and Analysis**

### *Muscle stiffness*

The ratio  $\Delta F/\Delta l$  defines dynamic muscle stiffness. The peak-to trough amplitude of the force transient was measured at each imposed frequency after the force sinusoid had stabilised. This typically occurs within less than one  $\Delta L$  cycle, even at the highest frequency. Dynamic stiffness can then be plotted as a function of oscillation frequency. This reveals a characteristic minimum in stiffness, in a Ca-activated muscle, at a discrete frequency termed  $f_{\min}$  (See Figure 3.8, in next chapter). This finding is similar to that obtained by other workers who have used sinusoidal analysis.  $f_{\min}$  is an index of mean crossbridge cycling rate (Kawai & Brandt, 1980; Rossmanith, 1986). The stiffness frequency plots for these preparations typically have two maxima, a lesser one slightly below  $f_{\min}$ , and a greater one around about 5-7.5 Hz. The number of frequencies used, as well as the specific frequencies explored were standardised for the bulk of experiments to facilitate comparisons. While the resolution around  $f_{\min}$  could be improved by testing more frequencies, this could prejudice ensuring the completeness of the range of frequencies analysed. In other experiments, which concentrated more frequencies narrowed around  $f_{\min}$ , we were able to conclude that the data reported here have sufficiently accurate resolution.

As generally found in the literature, dynamic stiffness should be virtually independent of frequency and phase shift virtually zero in resting and rigor muscle (Kawai & Brandt, 1980, Hajjar & Gwathmey, 1992). This was routinely confirmed in resting muscle before

proceeding with the  $\text{Ca}^{2+}$ -activated protocol, since a very large resting stiffness would indicate that a large percentage of the preparation was not functional myocardium, but rather connective tissue, thus unsuitable for mechanical analysis. The stiffness at rest provides information about the passive properties of the muscle and can be attributed to many factors, for example the giant protein titin (Linke *et al.*, 1994), collagen (Doering *et al.*, 1983, Kovanen *et al.*, 1984) and elastin (Granzier & Irving, 1995). Equally, rigor stiffness is frequency-independent, as indicated by the constant amplitude of the force waveform across the frequency range. In rigor conditions, crossbridges are permanently attached and therefore the observed stiffness should be high. It was found that stiffness in the rigor state was around three times the stiffness of  $\text{Ca}^{2+}$  activated muscle. Comparing the resting stiffnesses at two amplitudes of length change confirmed that a Hookean elastic characteristic holds over small amplitudes.

#### ***Number of crossbridges vs. tension and stiffness measurements***

McDonald *et al.* (1998) observed that shortening velocities were slower at virtually all relative loads when pCa was reduced to yield half-maximum force. This implies that there is a  $\text{Ca}^{2+}$  dependent mechanism that slows crossbridge cycling kinetics in myocardium. This slower cycling may arise from reductions in the level of thin filament activation associated with lower  $\text{Ca}^{2+}$  concentration and fewer crossbridges bound to the thin filament. However, it is established that isometric tension is a linear combination of probabilities of crossbridges at each state (Kawai & Zhao, 1993). Therefore, it is not possible to conclude the number of crossbridges involved at any time during activation from tension pCa relationships alone. This is because the availability of the calcium-binding sites depends on several factors. Thus it is crucial to also look at stiffness data as well.

It is known that stiffness represents the ratio between amplitudes of force and strength (Kawai & Brandt, 1980), and that it provides a measure of the number of crossbridge attachments to actin (Metzger & Moss, 1990). Metzger & Moss (1990) reported that at maximal  $\text{Ca}^{2+}$  activation stiffness and tension decreased proportionately at low pH. This linear relationship, between relative tension and relative stiffness, indicates that force per crossbridge is unchanged at various pH levels. This then indicates that pH decreases the number of attached crossbridges but does not alter the force produced in a single power stroke. In the same manner, Hofmann *et al* (1990) looked at the effect of lower pCas on this relationship between tension and length. This group looked at tension and stiffness at pCa values between 6.6 and 4.5, and found that the change in stiffness was proportional to that of tension at lower  $[\text{Ca}^{2+}]_s$ . This indicates that a lower pCa does not lower force per crossbridge. This agrees with the argument that muscle filaments do not reach maximum activation at lower pCas, thus resulting in a lower number of attached crossbridges. Therefore, it is clear, from these previous reports, that force per crossbridge is not reduced at lower pCas for those crossbridge that are attached and cycling.

### ***Phase Shift***

The phase relationship (with phase angle  $\Phi$ , expressed in degrees) between the force and length signals was examined. In these experiments, the development of the phase shift immediately after the frequency change, or at the start of the oscillation sequence altogether, could be observed. This confirms that phase shift was never greater than about  $90^\circ$ , i.e. the force wave never lagged or led by more than a fraction of one wavelength. As a starting point we consider  $\Phi$  as arbitrarily measured at the mid-point of the rising phase of the length waveform (the 'stretch' phase). This yielded a positive  $\Phi$ , indicating a phase lag of force behind length, a negative  $\Phi$ , indicating a phase lead of force before length, or zero  $\Phi$  where the force and length sinusoids were in phase. When

plotted as a function of frequency, the phase data produced a plot broadly similar in shape to that of the dynamic stiffness data.

Over the course of the experiments in this thesis, the number of frequencies imposed upon a trabecula was minimised to reduce the period of oscillation and to allow more interventions to be investigated within a single protocol. By examining several different protocols, we confirmed that the resultant 'profile' obtained with the shortened oscillation period did not distort the stiffness-frequency or phase-frequency plots.

### *Oscillatory work and power*

Net oscillatory work at a given frequency,  $W(f)$ , and the associated power,  $P(f)$ , output of the muscle can be derived from the information contained in the dynamic stiffness and the phase plots (Rossmannith *et al*, 1986), and are given by

$$W(f) = 2 M(f) \sin \Phi \quad (\text{Equation 2.4})$$

$$P(f) = W(f) * f \quad (\text{Equation 2.5})$$

where  $f$  donates frequency,  $\Phi$  phase shift and  $M(f)$  the value obtained when stiffness is normalised to the maximum force generated by the muscle. Positive values for  $W(f)$  indicate that, for that frequency, the muscle is generating net external work on the apparatus. Negative values indicate that, for that frequency, the apparatus is doing work against the muscle, or alternatively, the muscle is absorbing net oscillatory work. The frequency at which  $f_{\min}$  occurs, or which maximum work done ( $f_w$ ) or maximum power ( $f_p$ ) is displayed, have all been used as indicators of significant crossbridge kinetics (Steiger & Rüegg, 1969, Kawai & Brandt, 1980).

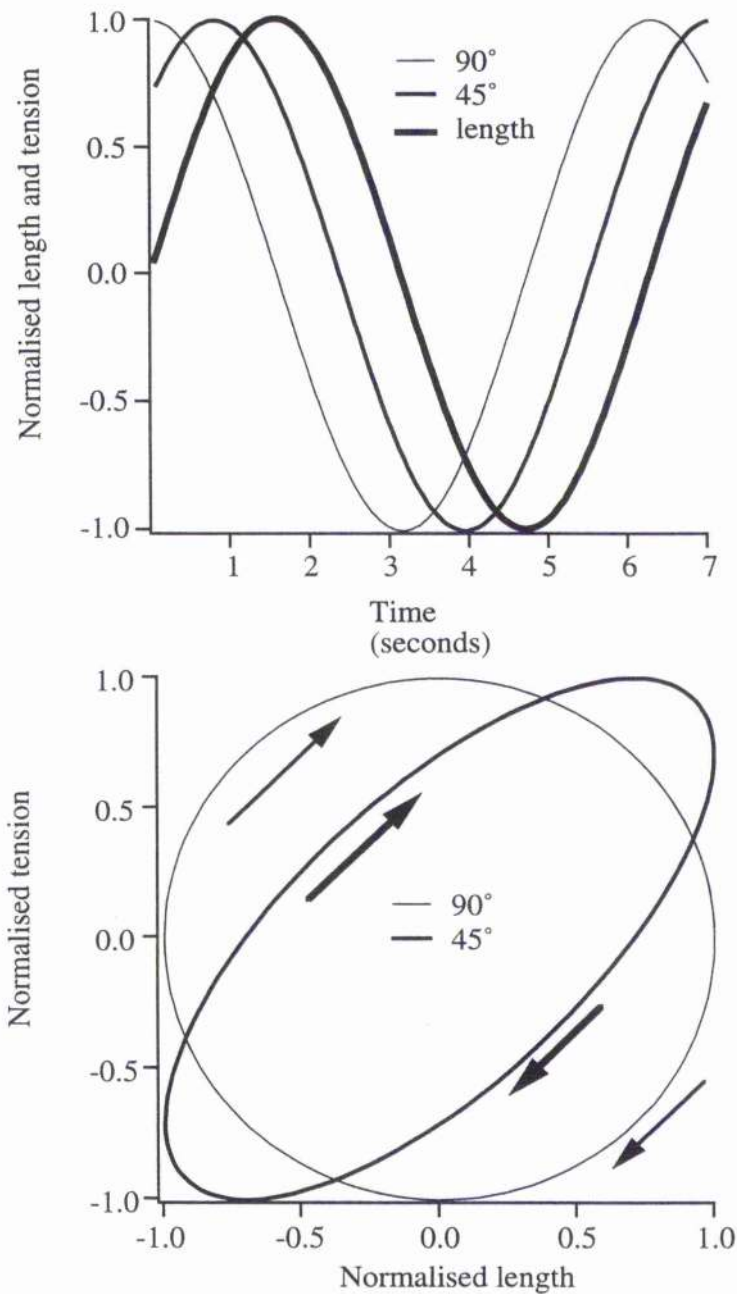


**Figure. 2.3.** Idealised phase shift for pure sinusoidal waves. **a.** diagrammatic representation of length and idealised tension waveforms corresponding to 45° and 90° phase shifts (note that tension *leads* length). **b.** the corresponding tension vs. length plots for the waveforms shown in **a.** The arrow shows the time relationship of the length vs tension data - the loops rotate clockwise in this case - phase lead. One rotation equates to about 6 seconds in this example.

As described in the text, a 90° phase shift describes a circle, whereas a 45° phase shift yields an ellipse.

(Modified after Fig. 2.7 PhD Thesis, G Wilson (Glasgow University, 1998))

### *Procedure for quantifying phase shift, oscillatory work and power values*

Equation 2.4 and 2.5, as given by Rossmanith (1986), used for calculating work and power, does not necessarily provide accurate assessment of the capacity of the muscle to generate or absorb oscillatory work. As reported here in more detail, the phase shift was not constant throughout a given cycle, although the pattern remained constant from one cycle to the next. Thus, the observed force waveform was not always a perfect sinusoid, as implied by Equation 2.4, unlike the imposed length waveform.

The ideal form is that produced by a constant phase shift throughout a cycle, which yields an elliptical length vs. force plot, also called a work loop. If the phase shift is  $90^\circ$ , the plot describes a circle, and an ellipse for  $45^\circ$  (see Figure 2.3). These work loops are created by plotting the change in length vs. the change in tension and shows the direction of the data. Counter-clockwise rotation of the work loop indicates a phase lag, where tension lags after length, *i.e.* positive work where work is done by the muscle. Clockwise rotation indicates a phase lead, where tension leads length, *i.e.* negative work where work is absorbed by the muscle. These loops are not derived from the phase data. Instead, the work loops are simply another way of looking at the phase data. Comparing the phase shift at  $90^\circ$  and  $45^\circ$  (Figure 2.3) to those in the next chapters show how the observed descending and rising phase of the Lissajous waveform differed from this ideal. If they differ at all, it was observed that the phase shift on the falling phase was generally of the same sign, but smaller or larger than the phase shift on the rising phase. Very occasionally, phase shift could reverse sign between the rising and falling phase (examples included in relevant chapters). The latter case produces an F vs. l loop that crosses over. The asymmetrical forms of loops are reported here by the difference, if any, in phase angle during the stretch ('phaseUp') and release ('phaseDown') parts of the waves.

In view of the departure of the observed results from a simple phase shift at a give frequency, it was necessary to quantify the extent of this departure from the ideal. Analysis routines (Igor macros written by Dr. D.J. Miller) quantified the phase shift initially as the time difference between each data point pair (length, tension) as described here.

**Smoothing:** Waves were first smoothed to reduce high frequency noise; this was done under direct observation to ensure that no artifactual distortion of the sinusoidal form was produced. (Smoothing used the box (=‘boxcar’) sliding average algorithm. This prevents any gross distortion to wave amplitude and overall form; typically only 2 (box ‘5’), 3 (‘box 7’) or 4 (‘box 9’) points either side of the test point are included in the averaging).

**Phase angle:** Once the waveforms for all test frequencies were satisfactory, the phase angle macro could be applied. Values were taken between about 6% and 94% of the tension sinusoid. (At the extremes of the sinus, measuring time-shifts this way becomes every unreliable due to ‘noise’ in the traces. A direct inspection of the plots of phase angles generated by the routines revealed any further obvious artifactual values that could then be deleted or recalculated). Phase angles were calculated from the time separation between the imposed length sinus and the tension waveform. The macro also confirmed whether the phase relationship between the tension and length waves was ‘lag’ or ‘lead’. The phase-shift times and direction (lag or lead) were converted to phase angle, knowing the wave frequencies. This process was completed, for each data point on the length wave, for 2, 3 or 4 complete waves, depending upon the number of waves sampled. At the highest oscillation frequencies, the first quarter to half wave after a frequency transition was ignored to ensure that the new tension waveform had stabilised. For a given frequency, the mean  $\pm$  SD of the observed phase shifts is reported for phaseUp and phaseDown. Thus, the larger the SD, the greater is the variation of phase shift as the length sinus proceeds. If the SD has gone up under the influence of the intervention, then

this shows that the intervention (*i.e.* change of pH, raised Pi, caffeine) has modified those elements of crossbridge kinetics that define the phase relationships.

### *Statistical data analysis*

One or two-tailed paired or unpaired Student's t-test was used (at P equal to 0.05) to determine if there was a statistically significant difference between the altered and control groups. Results from each test condition were compared with control values for maximum tension,  $f_{\min}$ , maximum stiffness, stiffness at  $f_{\min}$ , and phase data. One-tailed tests were used where a unidirectional change (*e.g.* slowing) was predicted. Two-tailed tests were performed elsewhere. Paired tests were appropriate where the preparation acted as its own control, unpaired for group comparisons.

All values (except in phase figures) are expressed as mean  $\pm$  standard error of the mean (SEM). Phase data shown in the phase figures include the standard deviation (SD), not the SEM of the phase angles, at each frequency. If the SD has changed under the influence of the intervention, this indicates that the change has modified those elements of crossbridge kinetics that define the extent of asymmetry in the phase relationships.

## CHAPTER 3 EFFECTS OF pH ON CROSSBRIDGE KINETICS

## INTRODUCTION

It has been recognised for over 100 years that acidosis in cardiac extracellular fluid reduces the contractility of the heart (Gaskell, 1880). To comprehend cardiac physiology and pathophysiology it is essential to understand the effects of pH on cardiac function. A decrease of intracellular pH is one of the most marked consequences of myocardial ischaemia. Usually a decrease of about 0.5 pH units is observed, but values as low as pH 6.2 have been reported (Garlick *et al*, 1979).

Although it is well established that extracellular acidosis causes a fall of developed force in cardiac muscle, the magnitude and rate of the force response depends on how the acidosis is produced. Previous work suggests that the major actions of pH are via changes in the intracellular pH (Orchard & Kentish, 1990). Therefore, it should be noted that the following experiments are concerned only with the mechanisms by which changes in intracellular pH affect cardiac muscle myofibrillar kinetics.

It is established that acidosis leads to a rapid decline of developed force followed by a slower partial recovery. Previous work has shown that acidosis alters the time course of both the twitch and the intracellular Ca transient that accompanies it; the onset of twitch relaxation is earlier, twitch relaxation is faster, and the intracellular Ca transient declines more slowly during acidosis.

The direct actions of pH changes on the contractile apparatus have been established using isolated preparations where the concentrations of  $\text{Ca}^{2+}$  and other ions were kept constant. For the experiments in this thesis, the intracellular space of the cardiac cells was brought under direct control by chemically skinning the preparation to destroy the membranes. Contractile activity, which in the past has been measured as ATPase activity or force development, follows a sigmoidal relationship to  $[\text{Ca}^{2+}]$  over the range of 0.5-50 $\mu\text{M}$ , but

the precise range depends on the experimental conditions. This activation is brought about by  $\text{Ca}^{2+}$  binding to one of the  $\text{Ca}^{2+}$ -specific' or 'low-affinity' sites on TnC (Holroyde *et al*, 1980), as described in the Introduction.

The relationship between  $[\text{Ca}^{2+}]$  and contractile activity of cardiac myofibrils is affected in two ways when solution pH is reduced. The apparent sensitivity of the myofibrils to  $\text{Ca}^{2+}$  diminishes so that a higher  $[\text{Ca}^{2+}]$  is needed to activate the myofibrils and the maximum ATPase activity or force production is reduced. There is evidence that these two effects are mediated by different processes (Orchard & Kentish, 1990).

Many studies have shown that a decrease in pH over the range 7.5-6.0 shifts the relationship between  $[\text{Ca}^{2+}]$  and myofibrillar ATPase activity (Kentish & Nayler, 1979) or force development (Fabiato & Fabiato, 1978) to higher  $[\text{Ca}^{2+}]$ , indicating that the sensitivity of the myofibrils to  $\text{Ca}^{2+}$  has been reduced. In adult cardiac preparations, the pCa required for 50% activation falls by about 0.1 pCa units for each 0.1 unit dropped in pH (Orchard & Kentish, 1990). The curves are shifted in parallel along the  $[\text{Ca}^{2+}]$  axis, with little or no change in the slope. Thus the threshold  $[\text{Ca}^{2+}]$  activation of the myofilaments is also increased as pH falls. Marban and Kusuoka (1987) used isolated perfused hearts to show a decrease in the  $\text{Ca}^{2+}$  sensitivity of cardiac myofibrils during respiratory acidosis. Previous work has also shown that the force is reduced even though the  $\text{Ca}^{2+}$  transient is potentiated (Allen & Orchard, 1983).

Although the inhibitory effect of acidosis on  $\text{Ca}^{2+}$  activation is now well established, the mechanism is still controversial. Several mechanisms have been proposed. Katz and Hecht (1969) proposed the idea that the decrease in  $\text{Ca}^{2+}$  sensitivity was due to competition between  $\text{H}^+$  and  $\text{Ca}^{2+}$  for the low-affinity  $\text{Ca}^{2+}$  binding site on the cardiac TnC. However, later studies provided contradictory results. In 1974, Fuchs reported no change in  $\text{Ca}^{2+}$  affinity over the pH range 8 to 5, and later studies with cardiac proteins indicated a similar lack of pH sensitivity of  $\text{Ca}^{2+}$  binding under physiological conditions

(Kohama, 1980, Stull *et al.*, 1978). However, Blanchard and Solaro (1984) measured the binding to TnC in situ in cardiac myofibrils and found that acidity caused a large reduction in  $\text{Ca}^{2+}$  binding to the  $\text{Ca}^{2+}$ -specific site; furthermore this reduced binding completely accounted for the decrease in  $\text{Ca}^{2+}$  sensitivity of the myofibrillar ATPase in acid solutions. Later in 1988 and 1989, Solaro *et al.* used fluorescently-labelled TnC to measure  $\text{Ca}^{2+}$  binding to the  $\text{Ca}^{2+}$ -specific sites alone. This sensitive technique showed that the  $\text{Ca}^{2+}$  affinity of these sites is indeed reduced in acid solutions.

Nevertheless, the effect of pH on the  $\text{Ca}^{2+}$  affinity of isolated TnC is only about one-half of the effect on the  $\text{Ca}^{2+}$  sensitivity of myofibrils and skinned fibres (Orchard & Kentish, 1990). This discrepancy may be because pH sensitivity does not depend completely on TnC. It has been shown that pH sensitivity is greater in adult preparations than in neonates (Solaro *et al.*, 1986, 1988), and is greater in cardiac muscle than in slow-twitch skeletal fibres, even though the TnC appears to be almost identical in all the preparations (Solaro *et al.*, 1986). However, TnI is known to exhibit different isoforms between adult and neonates and between cardiac and skeletal muscle. It was therefore suggested by Solaro *et al.* (1986, 1988) that the various pH sensitivities of the different muscle types are conferred by the type of TnI present. Solaro *et al.* (1986, 1988) have shown that the addition of TnI to TnC increases the pH sensitivity of  $\text{Ca}^{2+}$  binding to skeletal muscle, where  $\text{Ca}^{2+}$  sensitivity is lower compared to cardiac muscle. However, the mechanism by which TnI increases  $\text{Ca}^{2+}$  sensitivity is not yet clear.

### **Maximum Force Production**

Experiments with skinned muscles have demonstrated another effect of acidosis, a decrease of maximum force at saturating  $[\text{Ca}^{2+}]$  (Solaro, 1988). This effect occurs at all  $\text{Ca}^{2+}$  concentrations, but it can only be distinguished from the effect on  $\text{Ca}^{2+}$  sensitivity by using a saturating  $[\text{Ca}^{2+}]$  so that the latter action is eliminated. The reported effect on maximum force is variable, ranging from a 10% reduction (Fabiato & Fabiato, 1978) to a

30% reduction (Solaro *et al*, 1988) for a pH decrease from 7.0 to 6.5. This action is unlikely to be caused by the same mechanism as the decrease of  $\text{Ca}^{2+}$  sensitivity, because 1) it cannot be overcome by increasing the  $[\text{Ca}^{2+}]$  further, and 2) during development from neonate to adult, the effect of pH on  $\text{Ca}^{2+}$  sensitivity doubles but the effect on maximum force remains the same (Solaro *et al*, 1988). However the mechanism of the action of pH on maximum force remains unclear.

It had been generally accepted that the maximum force development of skinned fibres is affected much more by pH than is the maximum ATPase activity of isolated cardiac myofibrils (Blanchard *et al*, 1984, Kentish & Nayler, 1978). This suggests that there is a decrease in the cycling of the crossbridges (derived from ATPase activity), as well as a reduction in force produced in each cycle of the crossbridge. This is further interpreted as a fall in the efficiency of coupling ATP hydrolysis to force production at low pH. Earlier measurements of force and ATPase activity in the same preparation showed that force and ATPase activity were reduced in parallel by acidity (Schadler, 1967). Further studies indicate that force is depressed more than ATPase activity in skinned skeletal (Cooke *et al*, 1988) as well as skinned cardiac muscle (Godt & Kentish, 1989). Fabiato and Fabiato (1976) demonstrated that a decrease in pH reduced the force developed in a rigor contraction when myosin crossbridges are bound to actin in a stable state. This shows that pH alters the force of attached crossbridges. Kentish and Palmer (1989) used instantaneous stiffness of skinned cardiac and skeletal muscles during maximal  $\text{Ca}^{2+}$  activation as a measure of the number of attached crossbridges. This method was used to suggest that, as pH fell, the number of attached crossbridges was reduced, but by a smaller proportion than force, thus indicating that acidity also depressed force in each attached crossbridge.

The basis of the metabolic effect on myofibrillar energy usage is in the kinetic scheme for the actomyosin ATPase activity. There is a cyclic interaction between actin and myosin

during muscle contraction involving the forming and breaking of crossbridges, driven by the energy available from the hydrolysis of ATP into ADP and Pi, as previously discussed in Chapter 1. The net number of H<sup>+</sup> ions released during ATP hydrolysis is pH dependent (Ebus, 1994). Evidence using skeletal muscle (Cooke *et al*, 1988, Metzger & Moss, 1990) and cardiac muscle (Kentish, 1991) indicates that pH may influence the crossbridge cycle at more than one transition. Ebus (1994) gave evidence, using the pH dependence of ATPase activity, suggesting that ADP release and/or the number of crossbridges in the AM-ADP state are reduced at a low pH, and that association of protons is not rate limiting for crossbridge detachment.

Godt and Kentish (1989) assessed ATPase activity by measuring changes in fluorescence of NADH, which are dependent on the myosin contraction inside the measuring area. It is not clear whether the authors factored in the change in the myofilament lattice spacing due to low pH, which although causes a higher myosin concentration, causes a reduction in ATPase activity due to myofilament disarray (discussed further in the discussion section of this chapter) (Matsuda & Podolsky, 1986). Other evidence showed that the maximum Ca<sup>2+</sup>-activated ATPase activity in dog cardiac myofibrils did not vary significantly as a function of pH (Blanchard & Solaro, 1984). However, Kentish & Naylor (1979) had reported a 20% decrease in maximal Ca<sup>2+</sup>-activated ATPase activity in myofibrils from rabbit and guinea pig when pH was reduced from 7.2 to 6.4. However, the myofibrils did not contract isometrically, making a direct comparison with the isometric studies reported in this thesis impossible.

In terms of stiffness, Metzger and Moss (1990) reported no changes in stiffness as a function of pH in rabbit *soleus* slow muscle fibres, but a reduction of stiffness to about 75% at pH 6.2 in rat superficial (fast) *vastus lateralis* fibres at maximum activation. Ebus *et al* (1994) showed, using cardiac muscle at pH 6.2, a decrease in the amplitude of the force response during 1% lengthening (used as a measure of stiffness) to about 75%

of the control value at pH 6.2, thus showing that cardiac muscle is similar to fast skeletal muscle. Our experiments also examine the effects on force and stiffness in a range of pHs when rapid length changes are imposed on the rat cardiac muscle trabeculae using our sinusoidal oscillation method (explained in Chapter 2).

## METHODS

We investigated crossbridge properties using the sinusoidal oscillation method described previously in this thesis. Fine preparations of rat ventricle muscle were chemically skinned (as described in Chapter 2) to allow direct control of the ionic environment of the myofilaments. The preparation was activated in pCa 4.0 solutions of various pHs. The pHs used were 6.5, 6.75, 7.0, 7.25, and 7.5. The activating solution was made as described in Chapter 2 and then adjusted to the desired pH (KOH/HCl). Although the  $\text{Ca}^{2+}$  concentration is affected by the pH, the added Ca (as CaEGTA) was kept constant. The REACT program was used to calculate the free  $[\text{Ca}^{2+}]$  in the activating solutions at the specific pH. The trabecula was initially activated at pH 7.0 and oscillated. After every run in the various test pHs, the muscle was again activated and oscillated at pH 7.0. This was to evaluate the endurance of the preparation throughout the protocol. Once the force production in pCa 4.0 at pH 7.0 fell below 50% of the original contraction, the preparation was no longer used. This usually occurred after a total of 5 runs. Therefore, 3 different pHs were studied in each individual experiment.

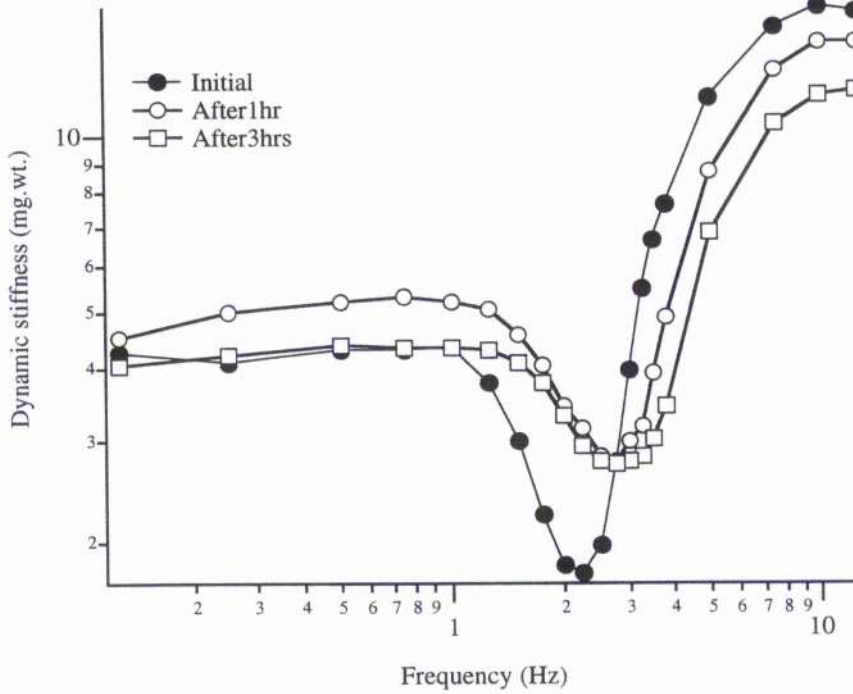
## RESULTS

Figure 2.2 shows an example of a typical experimental trace containing a maximal activation during which a series of small, sinusoidal length perturbations have been applied. Unlike the length signal, the tension signal clearly varies in amplitude with the different frequencies. It steadily decreases to a certain frequency and then begins to rise again. This frequency at which the amplitude reaches a minimum, is referred to as  $f_{\min}$ , and is generally accepted to reflect key kinetics aspects of the crossbridge cycle. The detailed reasons for this interpretation is explained in Chapter 2.

Each protocol began with an initial contraction and relaxation. This was repeated until a smooth contraction and a steady state of maximum tension was achieved. In many experiments the maximum tension and dynamic stiffness of the initial contraction was noticeably greater than the latter contractions. Reasons for this initial fluctuation in tension and stiffness development are not known. However, the maximum tension and dynamic stiffness was always similar in all the latter contractions in control solutions. The muscle was allowed to relax, after each contraction, until it reached a steady base line before activating the trabecula again.

If Ca-activated tension was allowed to persist until maximum tension fell appreciably, then it was observed that tension in the subsequent activation would be considerably reduced. To minimise this tension fall-off, the muscle was oscillated immediately after full activation was reached, and relaxed immediately after the oscillation sequence was completed.

Figure 3.1 shows results from an experiment where time was the only variable among the three activations and oscillations. Here it is shown that time has a slight effect on the deterioration of the maximum force produced by the muscle. The maximum force produced by the trabecula is 89% of the original contraction after 1hr, and 60% after 3



**Figure 3.1.** This figure shows the effect of time on rat myocardial stiffness. After the first activation and oscillation, the crossbridge cycle speeds up slightly. After further experimentation it is evident that this acceleration is not a result of time but rather the initial manipulation of the muscle. This acceleration can be seen always after the first and second activation, despite the time interval between the two activations. However, after the initial acceleration, the shape of the stiffness graph and the location of  $f_{\min}$  remain relatively the same despite the passage of time, as shown above.

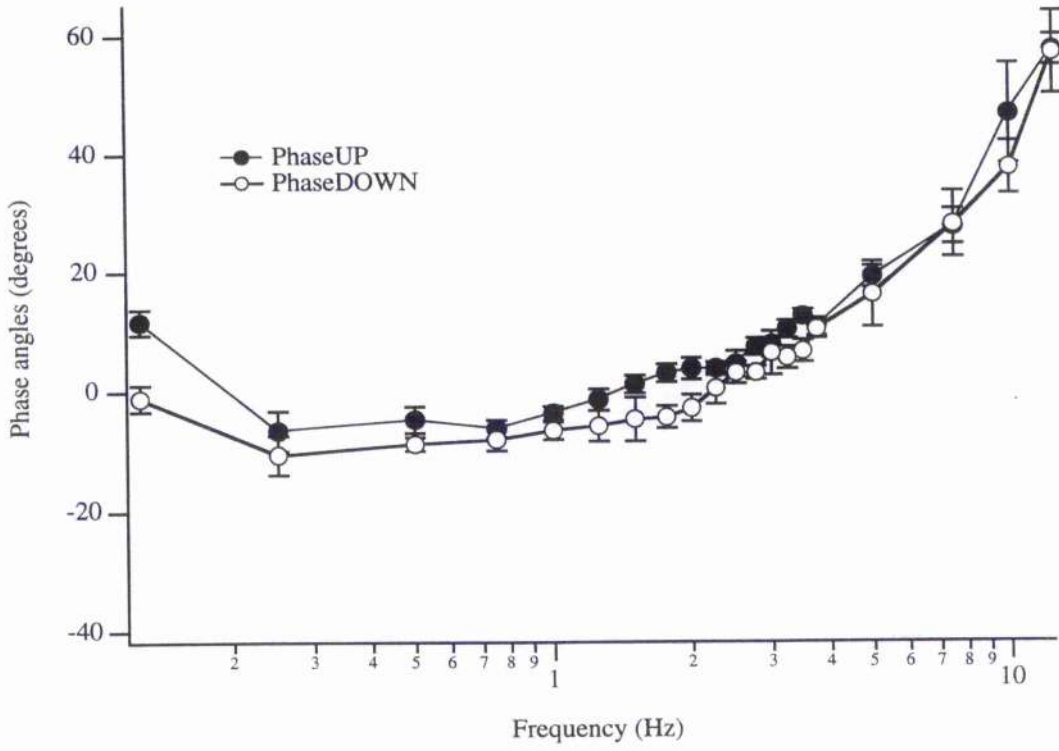


**Figure 3.2.** This is a typical phase plot for muscle at rest. At this state, the phase plot resembles its stiffness plot where there is no evidence of an  $f_{min}$ . There is no significant positive or negative work done by the muscle at rest.

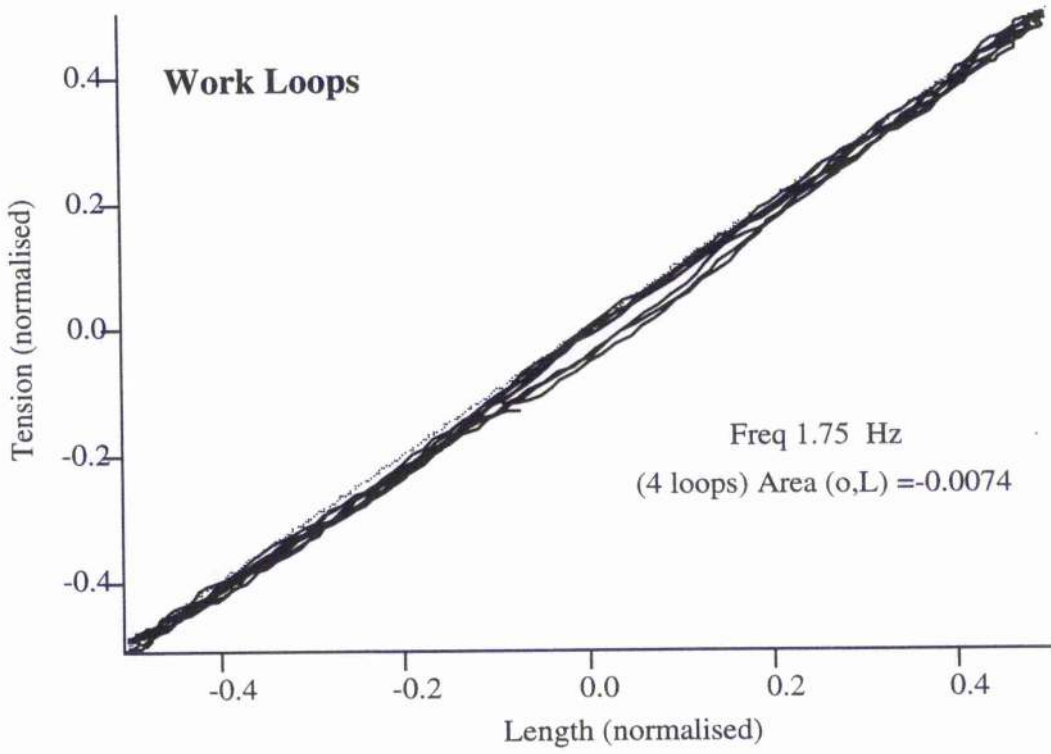


**Figure 3.3.** This is a typical set of work loops for muscle at rest. (o = tension, L = length) At this state, we anticipate that there is no significant work done or absorbed by the muscle at rest. This is confirmed by the (virtually) zero area enclosed by the length-tension loops.

**Figure 3.4**  
**A**

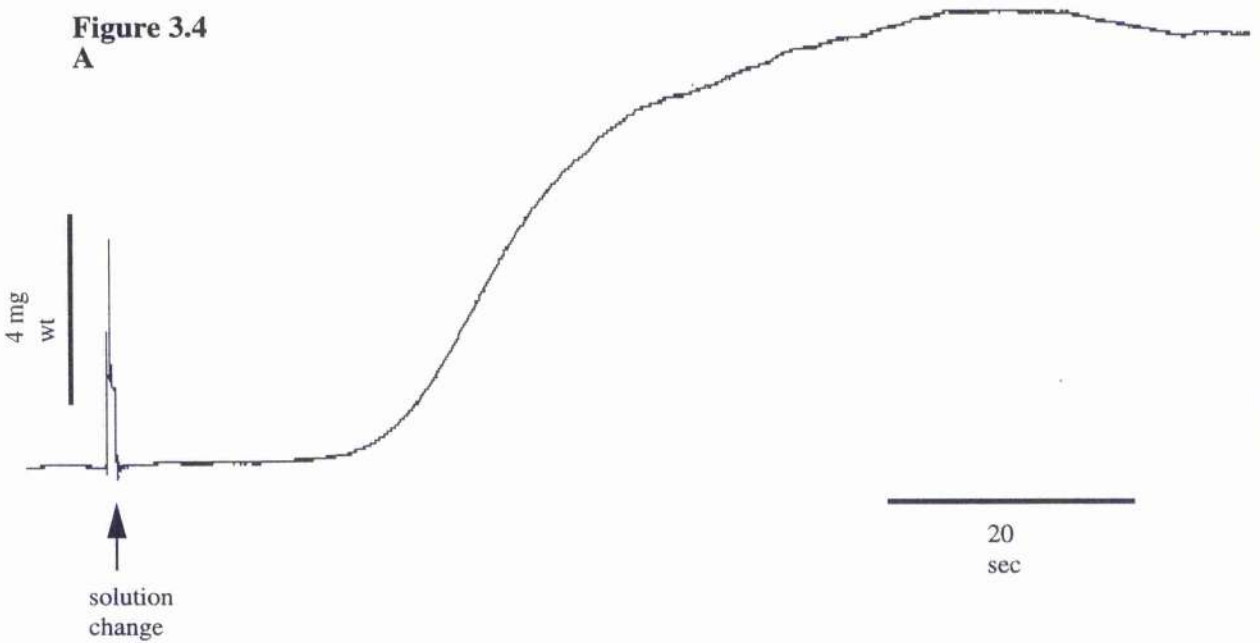


**Figure 3.4**  
**B**

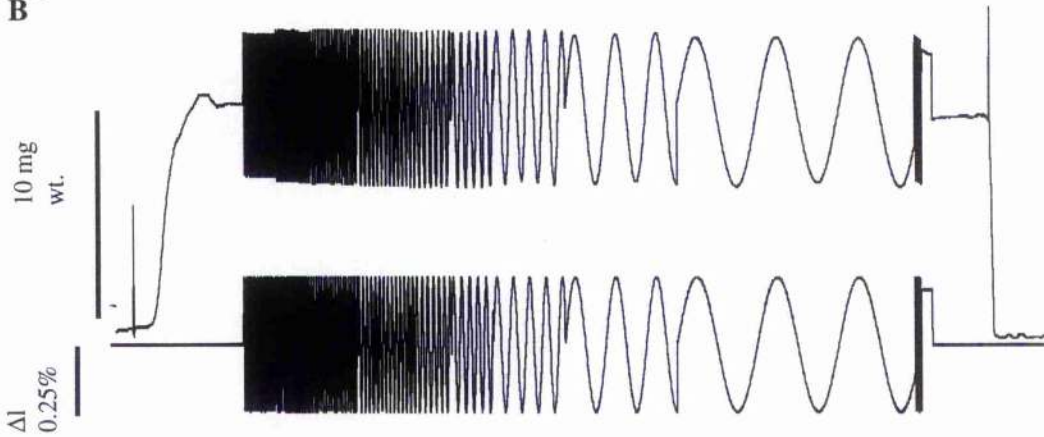


**Figure 3.4.** (A) The top panel shows a typical tension trace of rigor contraction. An arrow indicates where the fiber was transferred to rigor solution. Note that tension does not develop as fast that of calcium activated contraction. Rigor tension develops comparatively slower as the [ATP] within the fiber is depleted and cooperativity between attached bridges and teh regulatory proteins leads to the rigor state.

(B) The lower panel shows a typical experimental trace from rat myocardium in rigor. Note how, unlike Ca- activated records, there is no stiffness minimum during oscillation in rigor. The amplitude of the tension remains constant (apart from a small aliasing error at the highest frequencies) just as the length signal.

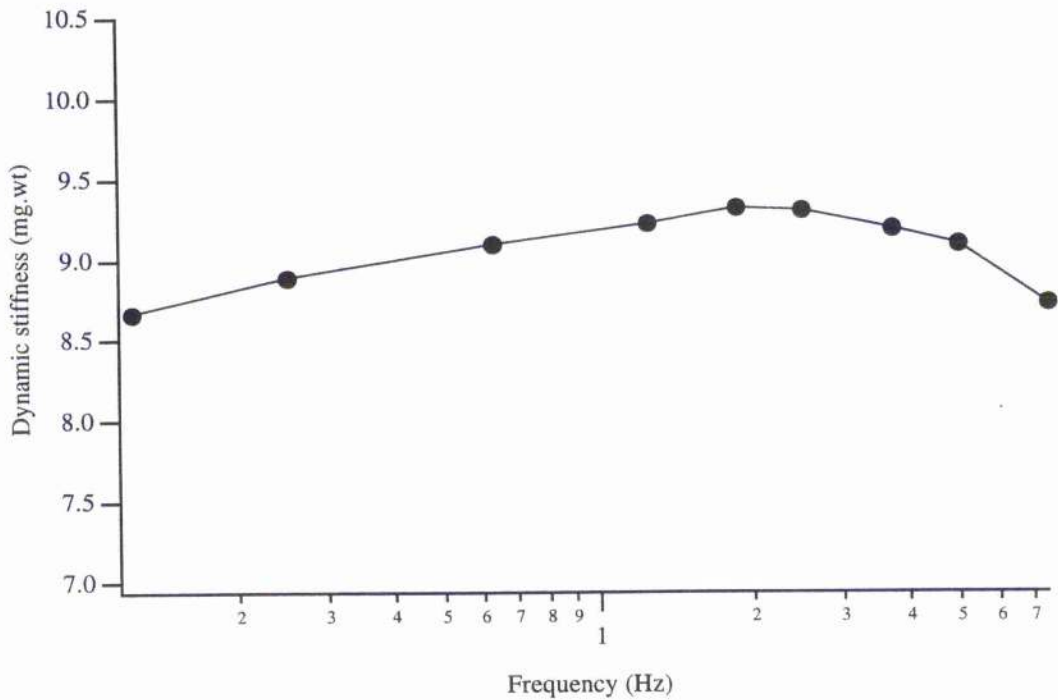


**Figure 3.5.** This figure shows the typical stiffness plot when the muscle is oscillated during rigor activation. Unlike  $\text{Ca}^{2+}$ -activated stiffness, rigor crossbridges are not cycling and obviously do not have an optimum cycling rate. Rather, the stiffness of rigor muscle is similar to a rubber band, where the elasticity is dependent on the change in muscle length during oscillation. This is however, a slight bend that can be seen in this figure and can be attributed to the recoil properties of the head and neck regions of the attached myosin molecule.

hrs. There is a discrepancy between the first and second contraction. This was seen throughout the experiments reported here, regardless of the time between the first and second contraction. This discrepancy can be seen in the results of maximum dynamic stiffness, reflecting the number of crossbridges. The shape of the dynamic stiffness graph is basically conserved throughout the protocol. However,  $f_{\min}$  does slightly increase after the first contraction. This is illustrated in Figure 3.1, where dynamic stiffness has been plotted against oscillation frequency to show where the minimum lies. Although the shape of the curve is slightly distorted with each subsequent activation,  $f_{\min}$  remains within a very small range of frequencies.

The protocol used for the various experiments simulating the effects of pH included a full activation and oscillation series in an activating solution at control at the beginning, in between every run at test pHs and again at the end. This was used as a time control within the experiment to evaluate the effect of time and the protocol itself on the trabecula. Previous experiments in this lab have shown that tension tends to deteriorate with time. The level of tension produced (or anticipated) can be corrected for a specific time, provided the fall-off rate of tension is known.

The resting stiffness of the muscle, mostly due to non-muscular tissue within the trabecula, was measured in each experiment using the same oscillation sequence used in the Ca-activated muscle. The oscillation sequence was repeated on the trabecula at rest after the first contraction and at the end of the experiment. The resting stiffness did not have a clear-cut minimum and is virtually frequency-independent. The plot of the resting stiffness shows a relationship similar to that of any passive elastic material. This shows that no, or very few, crossbridges are involved in the resting stiffness, but is rather a result of the non-muscular tissue present in the trabecula. The value of the average stiffness of resting trabecula was taken and subtracted off all the values of the Ca-

activated stiffness. This gave the stiffness value purely attributable to the crossbridges or of the crossbridges against the length change made to the muscle.

A muscle at rest is not capable of generating external work. This was verified by plotting the phase shift data extracted from the imposed sinusoidal length perturbations to a trabecula at rest. Figure 3.2 show that a very small phase shift is observed between the waveforms in a resting muscle. There is no phase shift observed between the two waveforms on the rising limb, however, there is a small phase lead on the descending limb. Figure 3.3 shows the corresponding tension *vs.* length loop that is produced when the waveforms in Figure 3.2 are plotted. As expected, the loop is quite flat, but rotates in a clockwise direction (with respect to time), therefore a small net amount of work is being absorbed by the trabecula when oscillated at rest.

Figure 3.4 shows an experimental trace, with both length and tension waveforms illustrated. It shows the stiffness-frequency relationship for a trabecula in rigor (*i.e.* zero ATP). Rigor stiffness is frequency-independent, as indicated by the constant amplitude of the tension waveform (Figure 3.5). The stiffness of the activated or rigor muscle is high, consistent with the number of attached crossbridges being maximal. In rigor conditions, all available crossbridges are permanently attached, unlike the dynamically and randomly cycling crossbridges in Ca-activated muscle where only a small proportion is attached at any one time. Therefore, the observed stiffness in rigor muscle is higher than in maximally Ca-activated muscle.

When rigor is fully developed, all the crossbridges are able to attach, but are unable to cycle due to the absence of ATP. Therefore, the preparation becomes very stiff as detected by the increase in the oscillation tension amplitude (discussed previously). During rigor, just a small positive phase shift is observed between the length and tension waveform. Correspondingly, the length-tension loop produced during rigor is virtually flat.

## Effect of pH on Max. Tension

Various factors contributed to the amount of force produced by the trabecula. These factors will be listed and discussed in the next section. One of the aims of the present experiments was to compare the tension production by rat myocardium at various pHs, both alkaline and acidic. However, due to the uncontrollable differences that may exist between various trabeculae, such as the extent of fibrous tissue or degree of muscle damage, *etc.*, tensions could not be compared directly. Instead, all data are converted to percentages with the maximum force produced by the control run at pH 7 defined as 100%.

The mean maximum Ca-activated force produced were (% relative tension)  $117.6 \pm 13.5$  at pH 7.2 (n=5),  $134.5 \pm 7.4$  at pH 7.5 (n=6), and  $137.0 \pm 3.3$  at pH 7.8 (n=2). Acidic pH has the opposite effect from alkaline pHs, since acidic pHs decrease force production. The mean tensions (% relative tension) were  $90.4 \pm 8.5$  at pH 6.75 (n=5),  $66.4 \pm 3.7$  at pH 6.5 (n=8), and  $30.9 \pm 0.4$  at pH 6.2 (n=2). (see Table 3.1) Data returns to control values (data not shown) when muscle is returned to the control solutions.

<b>Table 3.1</b>	<b>Change in Maximum Ca-activated force vs. pH</b>		
<b>pH</b>	<b>Relative Tension (%)</b>	<b>n=</b>	<b>P=</b>
<b>7.8</b>	137.0 ± 3.3	2	n too small
<b>7.5</b>	134.5 ± 7.4	6	p < .01
<b>7.2</b>	117.6 ± 13.5	5	p < .05
<b>7</b>	Determined 100%	N/A	N/A
<b>6.75</b>	90.4 ± 8.5	5	P = .05
<b>6.5</b>	66.4 ± 3.7	8	P < .01
<b>6.2</b>	30.9 ± 0.4	2	n too small

### **Dynamic Stiffness**

As length was oscillated sinusoidally, the tension transients produced by the trabeculae were also approximately sinusoidal in all the various pH activating solutions used. At lower frequencies there were slight variations near the crests of the sinusoidal force transient. These variations were found mainly between 1.75 and 0.5 Hz.

### **Control conditions**

In Figure 3.6, the amplitude of the tension trace (*i.e.* stiffness) is plotted against frequency for a trabecula activated at pCa 4, pH 7. The plot is generally characterised by a downward deflection in the middle of the frequency range, showing a minimum

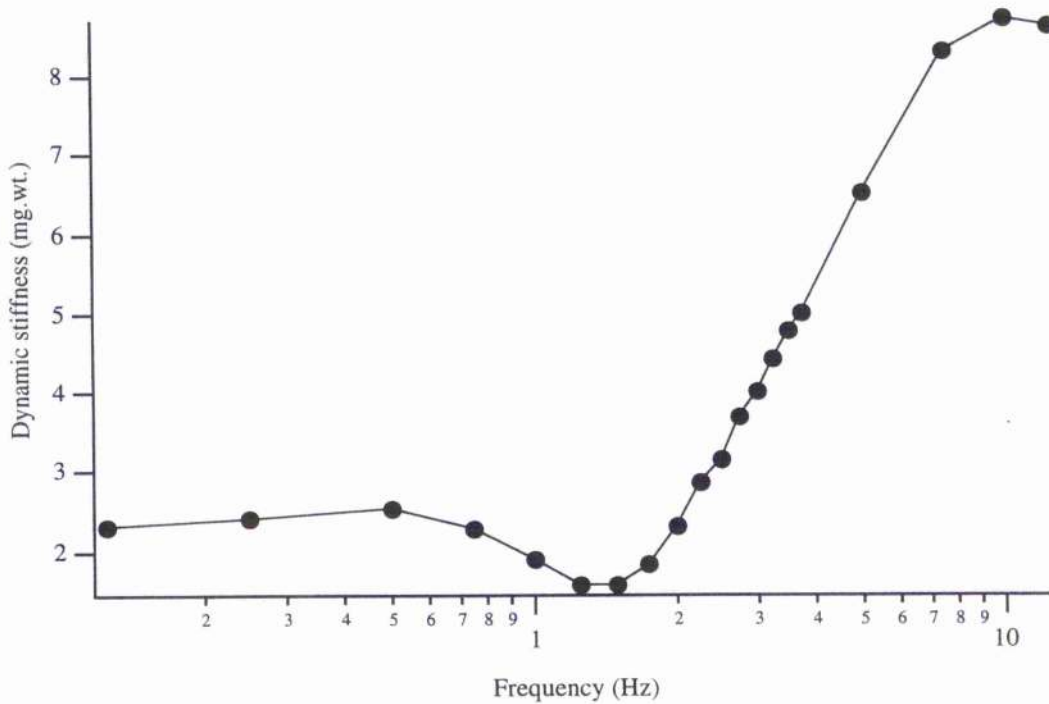


**Figure 3.6.** This figure shows typical graph of muscle stiffness at pH7. The tension transient is plotted against the frequency at which the muscle was oscillated to show the stiffness of the fiber at the various frequencies. Muscle stiffness, and thus the amount of tension production, is clearly dependent on the oscillation frequency. A distinct minimum can be seen between 1 and 2 Hz. This is where the  $f_{\min}$  of most rat myofibrils were found. The  $f_{\min}$  varied with species and experimental manipulation.

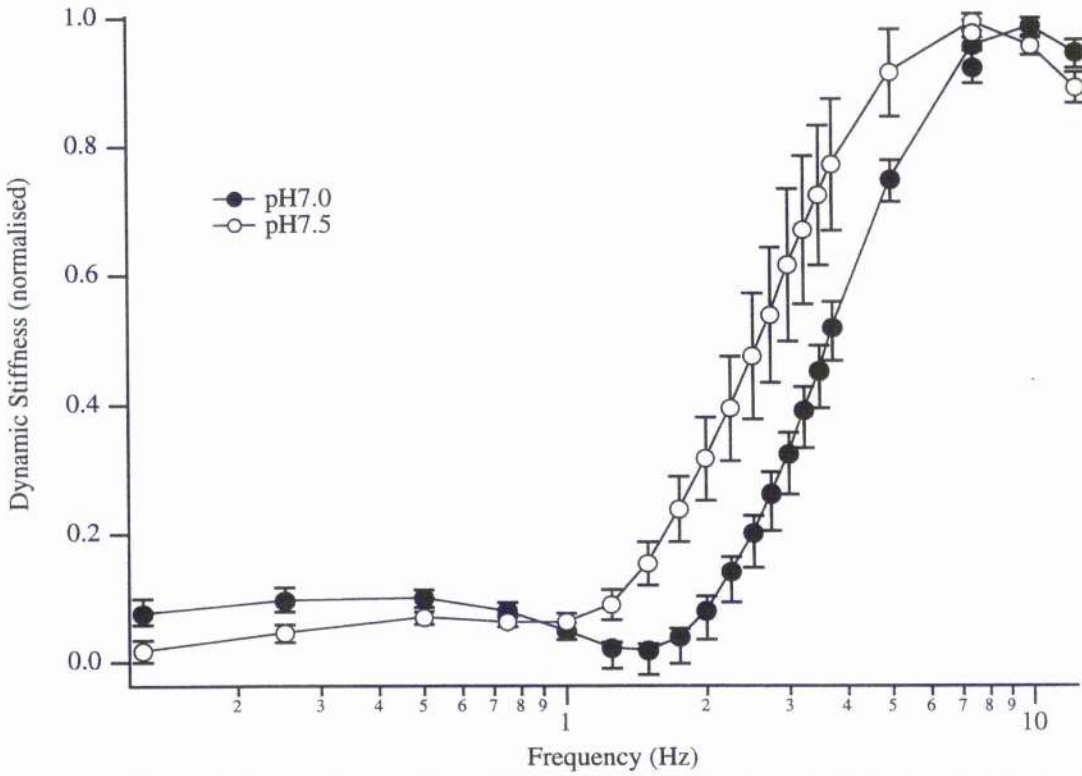


**Figure 3.7.** This figure shows the combined data (mean  $\pm$  sem) of 8 experiment for pH 7 and 6 experiments for pH 7.5. The whole relationship is shifted leftward, to lower frequencies, and thus  $f_{min}$  is lower at pH 7.5 that 7.0. The shape of the stiffness-frequency relationship is well defined at both pHs at frequencies near  $f_{min}$ .

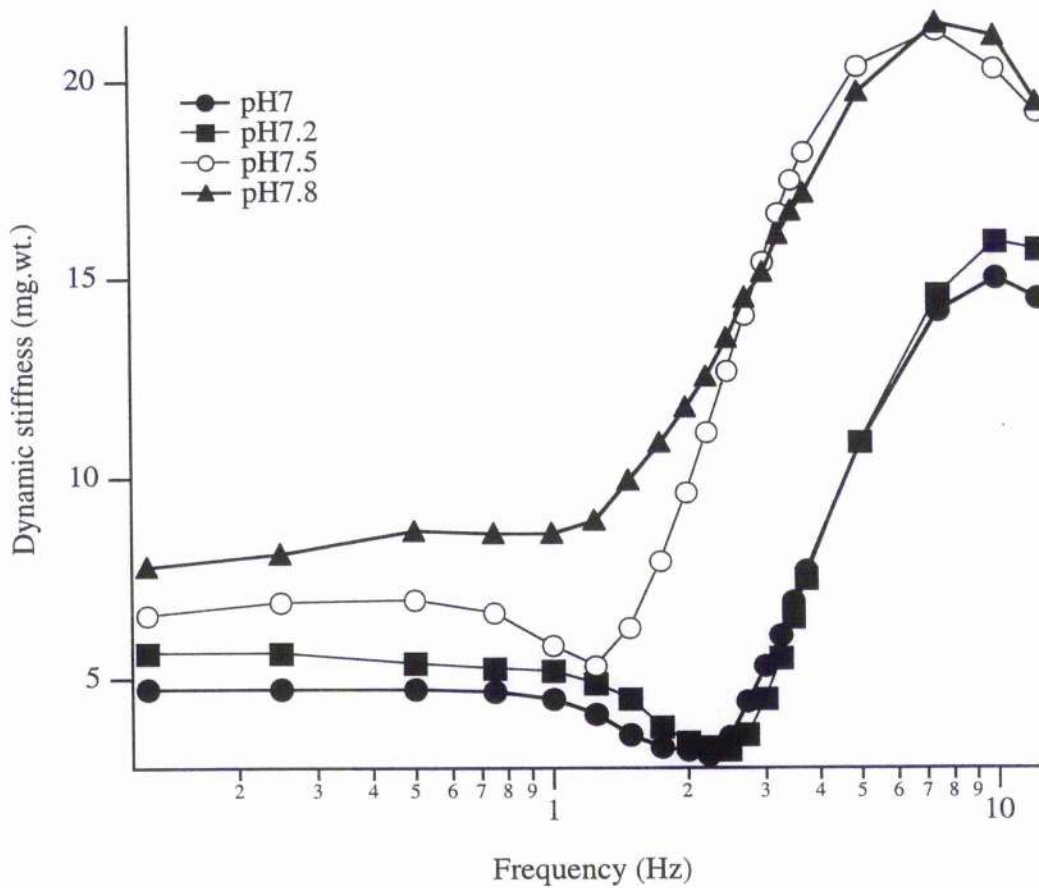


**Figure 3.8.** This figure shows individual stiffness-frequency plots for pH 7 to pH 7.8 taken from a single experiment.  $f_{\min}$  is slightly higher at 7.2 than 7.0 and lower at more alkaline pHs. This indicates that the pH for fastest crossbridge cycling may be around pH 7.2, which is similar to normal intracellular pH. Stiffness at all frequencies is greater at more alkaline pH, reflecting the overall increase in tension.

dynamic stiffness, with an increase in stiffness especially at higher frequencies,  $f_{\min}$ , corresponds to the point of reversal in the descending part of the stiffness-frequency curve.  $f_{\min}$  was clearly defined in most preparations. Occasionally the absolute minimum stiffness occurred at the lowest frequency. However, a clear downward deflection could be seen further along the curve at the mid-range of frequencies where  $f_{\min}$  was normally found. At pH 7,  $f_{\min}$ , for rat myocardium, was  $1.60 \pm 0.15$  Hz at pCa 4.  $f_{\min}$  can be altered by a change of pH, depending on the direction and extent of the pH change.

### *Alkaline pHs*

Increasing the pH from 7 to 7.2 shifts the entire stiffness-frequency curve to the right, bringing  $f_{\min}$  to a higher frequency. However, at pH 7.2 to pH 7.8, the entire stiffness-frequency curve was shifted progressively to the left, thus bringing the  $f_{\min}$  to lower frequencies. Dynamic stiffness varied greatly between the trabeculae as it does for maximum force. Therefore, all data are converted to percentages, with the stiffness in the control run at pH 7 defining as 100%. Dynamic stiffness at  $f_{\min}$  was higher at pH 7.2 with a mean of  $150.6 \pm 27.1\%$ , of that at pH7. Dynamic stiffness at  $f_{\min}$  also rises beyond pH 7.2 to  $186.0 \pm 24.8\%$  at pH 7.5. In alkaline pHs beyond 7.2, the range of dynamic stiffness in the stiffness-frequency plot decreased, although the plot was moved to higher values. The maximum dynamic stiffness found at the higher frequencies beyond 3 Hz was found to increase at higher pH. Compared with pH 7, the maximum dynamic stiffness was (in %)  $115.62 \pm 6.05$  at pH 7.2 (n=5),  $125.14 \pm 4.35$  at pH 7.5 (n=6), and  $139.92 \pm 12.75$  at pH 7.8 (n=2). (see Table 3.3) These features can be seen in Figure 3.7 for pH 7.5 vs. pH7. Figure 3.8 shows the gradual change in stiffness from pH 7 to pH 7.8. Although the frequency at which the maximum stiffness occurs is perhaps not physiologically relevant, it gives a picture of the functional capacity of the crossbridges.

This increase in dynamic stiffness was accompanied by a spreading out of the inflection in the relationship that defines  $f_{\min}$ . However, a clear  $f_{\min}$  can still be seen at pH 7.8. This increase in  $f_{\min}$  between pH 7 and pH 7.2, and subsequent decrease in  $f_{\min}$  at higher pHs indicates that the optimum pH for fastest crossbridge cycling lies close to pH 7.2 (at 20° C, at least).

All dynamic stiffness data were normalised to the maximum of each run. The stiffness minimum was then subtracted and the data re-normalised to facilitate comparison of the shapes of the various stiffness-frequency curves.  $f_{\min}$  occurs at slightly different frequencies in each case so that averaging traces from different experiments tends to smooth the relationship and obscure the appearance of  $f_{\min}$ . However, an individual trace, such as Figure 3.8, shows the features mentioned more clearly.

### *Acidic pHs*

At pH 6.5, the entire dynamic stiffness plot was clearly shifted to the right, i.e. to higher frequencies. However,  $f_{\min}$  was no longer clearly defined. There is a distortion in the shape of the plot that can be described as a flattening out of the curve. This effect, seen in every experiment, was reproducible as indicated by the plots of the compiled data in Figure 3.9 (same as above). However, it was possible to determine the general area in which  $f_{\min}$  was located by drawing a line down the straight upward part of the plot near the higher frequencies and another line tangent to the bottom of the 'dip' in the stiffness-frequency. The frequency that lay at the crossing of the two lines was taken to be  $f_{\min}$ . (see Figure 3.2) The mean  $f_{\min}$  at pH 6.5, 7 and 7.5 determined by this method is stated in Table 3.1. It should be noted that the phase curve shifts, reported in the next section, indicate the same shift and also provide ready quantification.

Table 3.2	Average $f_{min}$ vs. pHs (Hz)		
	pH 6.5	pH 7	pH 7.5
n=6	$3.17 \pm 0.27$	$1.83 \pm 0.29$	$1.25 \pm 0.24$
p Value	> 0.05	N/A	> 0.001

The dynamic stiffness at  $f_{min}$  is progressively greater at pHs below pH 7. At pH 6.75, the mean dynamic stiffness at  $f_{min}$  was  $150.4 \pm 10\%$  (n=5) that of pH 7. Below pH 6.75,  $f_{min}$  was no longer clearly defined to measure the minimum dynamic stiffness. Maximum dynamic stiffness found at the higher frequencies beyond 3 Hz was reduced at lower pH. Compared with pH 7 (taken as 100%), the maximum dynamic stiffness (in %) was  $93.15 \pm 0.97$  at pH 6.75 (n=5),  $71.96 \pm 3.29$  at pH 6.5 (n=8), and  $44.56 \pm 6.65$  at pH 6.2 (n=2). These features can be seen in Figure 3.9 for pH 6.5. (see Table 3.3) Figure 3.10 shows the gradual change in stiffness from pH 7 to pH 6.5. Due to decrease in maximum stiffness and the increase in minimum stiffness in acidic pHs below 7, the range of stiffness change in the stiffness-frequency plot became more narrow. Data returns to control values for both alkaline and acidic pHs (data not shown) when muscle is returned to the control solutions.

<b>Table 3.3</b>	<b>Change in Maximum Dynamic Stiffness vs. pH</b>		
<b>pH</b>	<b>Stiffness (%)</b>	<b>n=</b>	<b>p=</b>
<b>7.8</b>	139.92 ± 12.75	2	n# too small
<b>7.5</b>	125.14 ± 4.35	6	p < 0.001
<b>7.2</b>	115.62 ± 6.05	5	p = 0.17
<b>7</b>	Determined 100%	N/A	N/A
<b>6.75</b>	93.15 ± 0.97	5	p = 0.14
<b>6.5</b>	71.96 ± 3.29	8	p < 0.001
<b>6.2</b>	44.56 ± 6.65	2	n# too small

The 'flattening-out' effect on the stiffness-frequency curve observed at acidic pH was further examined by oscillating the muscle at various acidic pHs. As shown in Figure 3.10, this flattening effect is greater progressively with lower pHs.

The comparison of the maximum stiffnesses with the maximum tensions was done at each pH to see whether they scale proportionately. Figure 3.22 show that they do indeed scale proportionately.

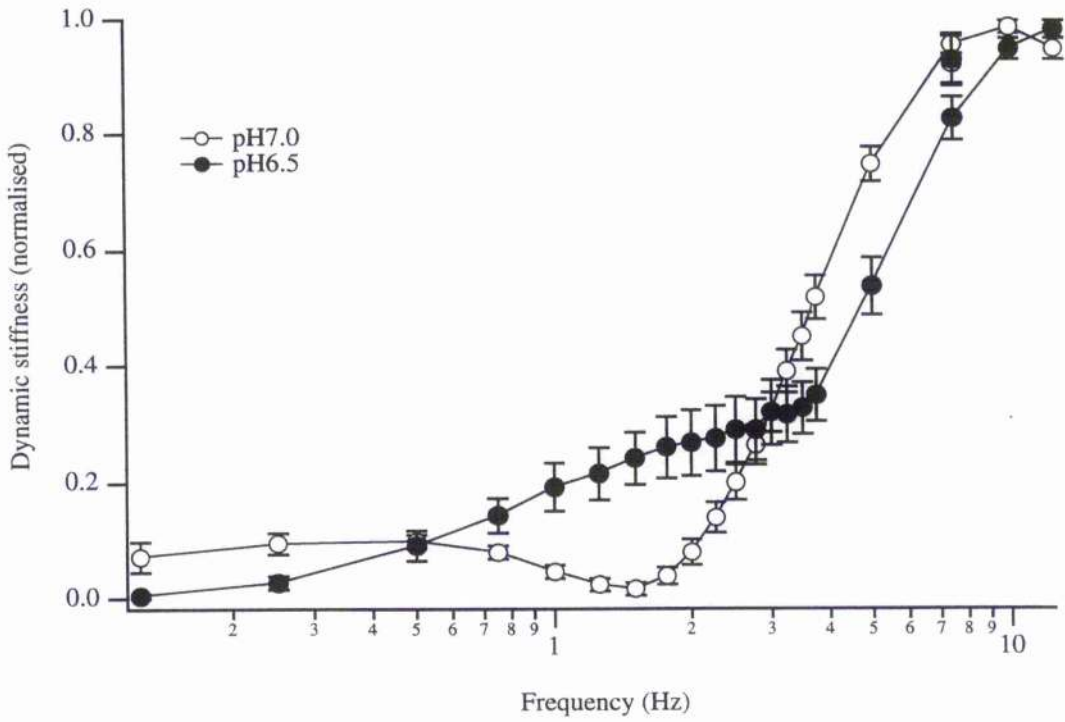


**Figure 3.9.** This figure shows the combined data of 8 experiments for pH 7 and pH 6.5. Any increase in  $f_{\min}$  at pH 6.5 is not apparent because the shape of the stiffness-frequency relationship is altered at pH 6.5 around  $f_{\min}$  so the  $f_{\min}$  inflection becomes unclear.

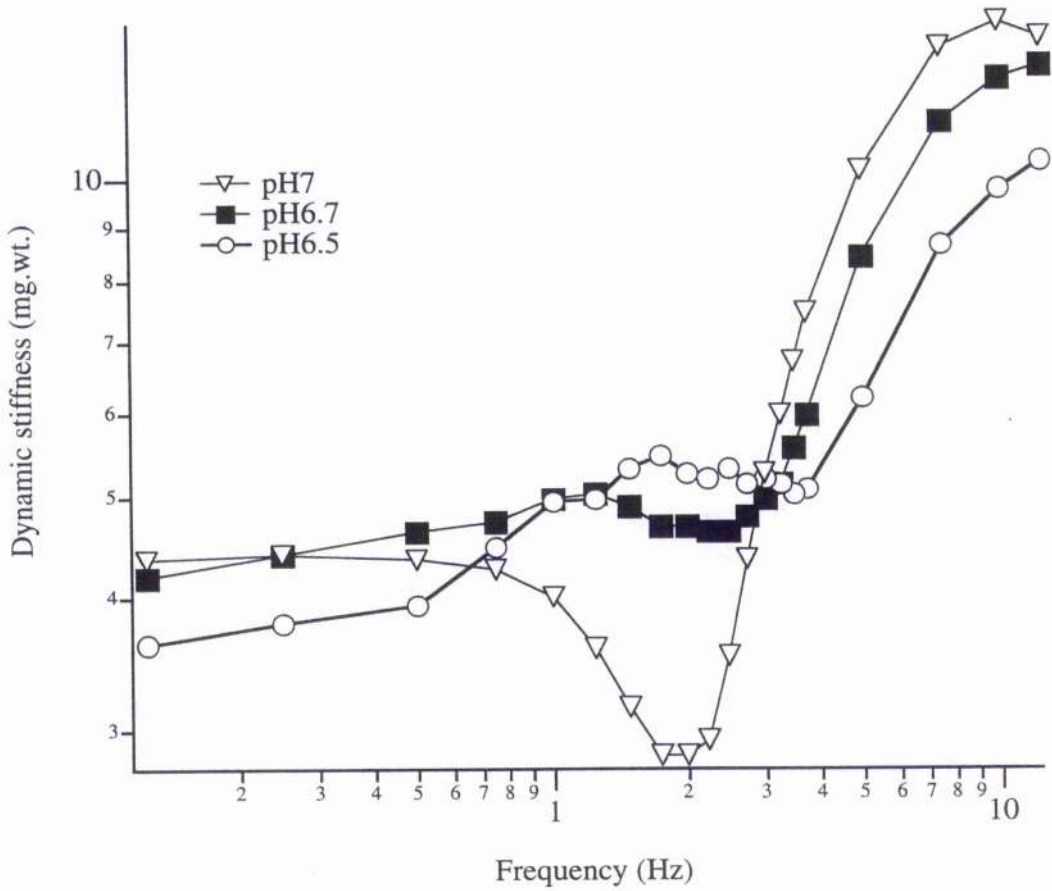


**Figure 3.10.** This figure shows examples of individual stiffness-frequency plots for pH 6.5 to pH 7. All traces originated from the same experiment. The lower the pH the higher is  $f_{min}$ . The spread of the inflection defining  $f_{min}$  can also be seen to be wider at the lower pHs.

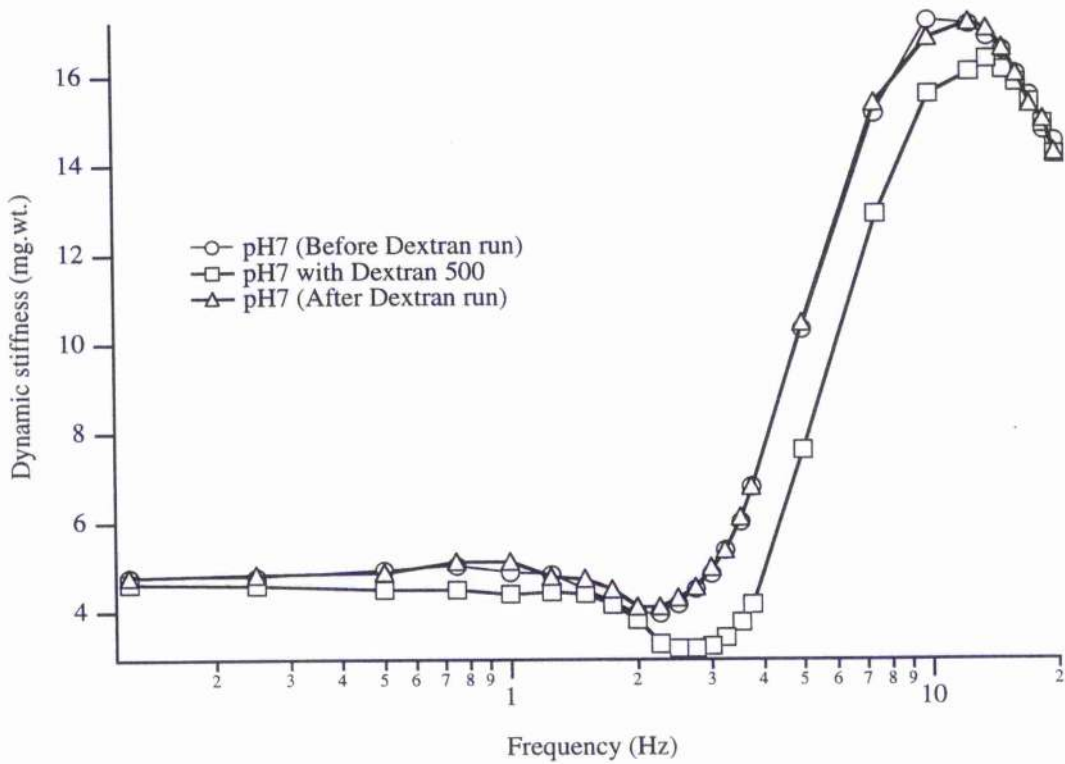


**Figure 3.11.** This figure shows the effect that Dextran 500 has on rat myocardial stiffness during sinusoidal oscillation. The increase in  $f_{min}$  seen in acidic pH can also be seen here. Note that there is no 'spreading out' effect in the Dextran 500 experiments.

### *Lattice Shrinkage Effects*

It has been reported that acidic conditions will cause shrinkage of the myofilament lattice (Matsuda & Podolsky, 1986). A change in lattice dimensions would obviously affect crossbridge kinetics, independent of the effect of acid pH itself. Dextran T-500 is a neutral, large molecule (a sugar polymer) that causes an osmotic effect on the myofilament lattice because it is large enough to be excluded from the intra-lattice fluid space. Therefore, Dextran T-500 was used to mimic the shrinkage effect of acidic muscle. The amount of Dextran added to the solution allowed a comparable shrinkage of the myofilament lattice to that of pH 6.5. Unpublished data from the lab of DJ Miller showed that 2.5 % Dextran T-500 or pH 6.5 caused about a 5 % shrinkage of the muscle fibre (Shields & Miller, 1991, University of Glasgow, Scotland). Rat myocardium was oscillated in a pCa 4 solution with 2.5% Dextran T-500 at pH 7. There is small but significant change in maximum tension where tension is  $94.9 \pm 1.3$  % that of control ( $P < 0.05$ ,  $n = 3$ ). Stiffness at  $f_{min}$  is slightly but significantly higher, at  $110.47 \pm 1.9$  % that of control ( $P < 0.05$ ,  $n = 3$ ). There is no significant change in  $f_{min}$ , or maximum stiffness ( $P > 0.05$ ,  $n = 3$  for both). Figure 3.11 shows that shrinkage did not have any significant effect on  $f_{min}$ . (Note that Figure 3.11 is an individual experiment. Thus the increase in  $f_{min}$  seen in Figure 3.11 does represent the average.) However, there was no distortion of the stiffness-frequency plot of the kind seen in acid conditions. Instead, there was a clear  $f_{min}$  inflection and the shape of the curve resembled the control with no Dextran (see Figure 3.11).

## Phase shifts

### *Control conditions*

The phase shift between the length and tension traces was analysed in two parts. The phase angle was plotted for the sinusoid moving in the upward direction (*i.e.* during the stretching part of the length change) and separately for the downward direction. This is because the (mean) phase angle between phaseUp (when the preparation is being stretched) and phaseDown (when the preparation is being released) often differ significantly. However, the phase angle often did not change substantially within either of these two parts of the sinus. Figure 3.12 shows a typical phase plot of a maximally Ca-activated trabecula at pH 7. The plot closely resembles that of the stiffness-frequency plot. Like the stiffness frequency plot, the phase plot is highly frequency dependent. There is virtually no phase shift at the lower frequencies. This is followed by a small inflection towards positive phase angles (positive angles meaning an increase in phase lag) for phaseUp and indicates a small amount of positive work, or work done, by the muscle. Despite this inflection, rarely was positive work actually done by the muscle. This is demonstrated in the work shown in Figure 3.18. The mean maximum phase angle in the physiologically relevant areas for the control was  $-9.85 \pm 1.19\text{deg}$  for phaseUp and  $-22.73 \pm 2.86\text{deg}$  for phaseDown ( $n=5$ ). The SD in these experiments is an index of how much the phase angle varies along a single loop (or set of loops). Therefore it shows how far the loop deviated from the 'ideal' sinusoid with a constant phase shift where SD would be zero. (Refer back to the end of the 'Phase Shift: phase angle' section in Chapter 2 for further explanation). If the SD has gone up under the influence of the intervention, then this shows that the change of has modified those elements of crossbridge kinetics that define the phase relationships.

Next, there is a sharp increase in phase lead at the frequencies immediately before  $f_{min}$  in the stiffness-frequency curve. In Figure 3.12, this is indicated by the sharp deflection into negative phase angles. This deflection continues until a maximum negative value is reached. This was true for both phaseUp and phaseDown data where the mean minimum phase angle for the control was  $-30.61 \pm 7.66$  deg for phaseUp and  $-28.47 \pm 7.84$  deg for phaseDown (n=5). There is no significant difference ( $P>0.1$ ) between the maximum negative phase angles reached by the phaseDown plot compared to phaseUp. The downward deflection corresponds to negative work, or work done on the muscle by the puller. It is clear that a large amount of work is done on the trabecula at the frequencies surrounding  $f_{min}$ .

### *Alkaline pHs*

At higher pH,  $f_{min}$  is moved to lower frequencies. It has also been shown that the shape of the phase plot directly correlated to the position of  $f_{min}$  in the stiffness-frequency plot. Therefore, it was expected that the phase plot for alkaline conditions would shift to the left, to lower frequencies, in order to correspond to the results shown for the alkaline stiffness-frequency plots. This relationship was evident in these experiments and can be observed in Figure 3.13-15. At higher pH, the phase plot is shifted to the left just as for  $f_{min}$ . The mean shift between the control and pH 7.5 for the maximum phase angles was  $-0.50 \pm 0.15$  Hz for phaseUp and  $-0.90 \pm 0.42$ Hz for phaseDown and minimum phase angles was  $-0.75 \pm 0.23$ Hz for phaseUp and  $-0.60 \pm 0.25$ Hz for phaseDown. (See Table 3.4)

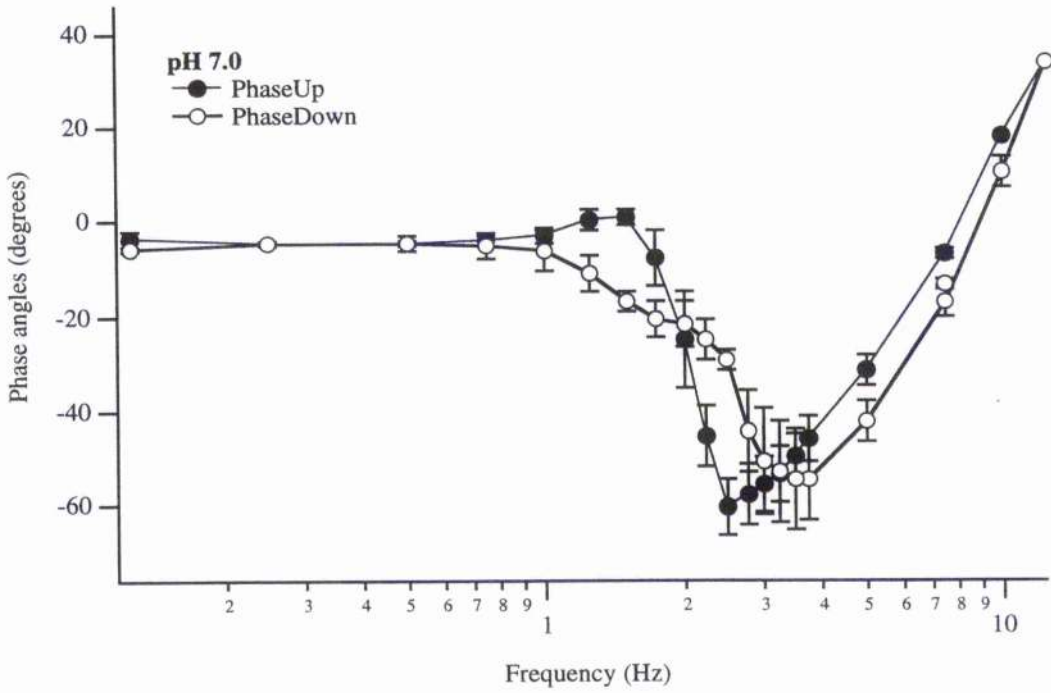


**Figure 3.12.** This figure shows a typical phase plot for pH 7. The frequency at which  $f_{\min}$  occurs in the dynamic stiffness plots is typically midway along the down slope of the phaseUp vs frequency relationship. Positive oscillatory work by the myocardium, possibly physiologically relevant, is done where the phase shift is positive. This thus occurs at frequencies just below  $f_{\min}$ .

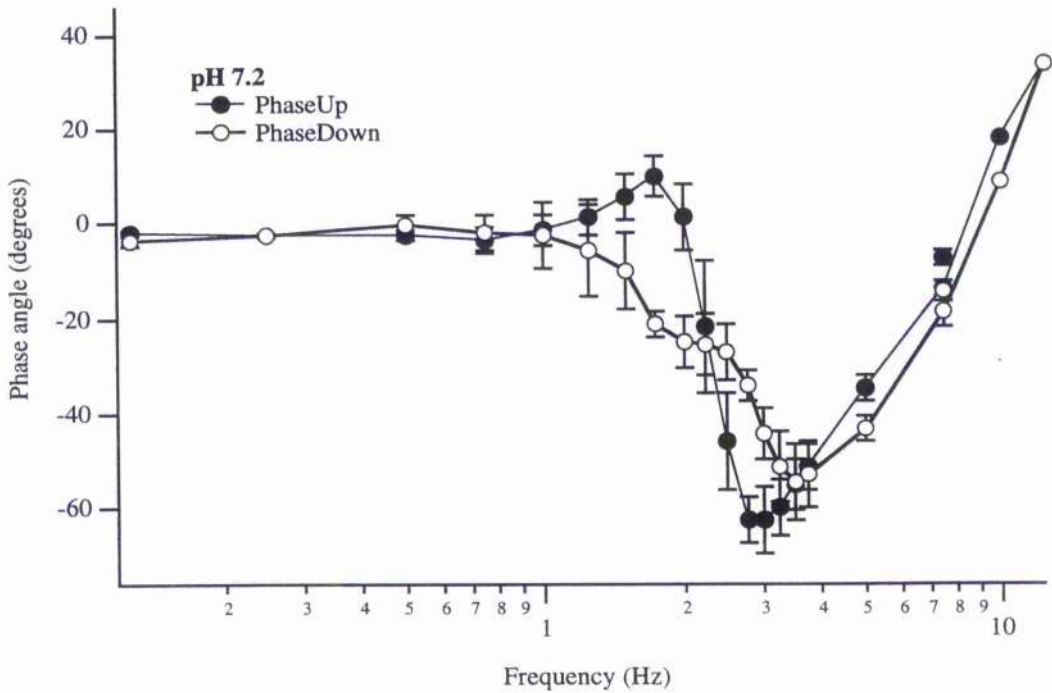


**Figure 3.13.** This figure shows a typical phase plot for pH 7.2. As with pH 7, the frequency at which  $f_{min}$  occurs in the dynamic stiffness plots is typically midway along the down slope of the phaseUp vs frequency relationship. Positive oscillatory work by the myocardium, possibly physiologically relevant, is done where the phase shift is positive. This thus occurs at frequencies just below  $f_{min}$ . As mentioned in this chapter, the optimum pH for rat myocardium is around pH 7.2. In the experiments of this chapter, the most positive work is seen at this pH.

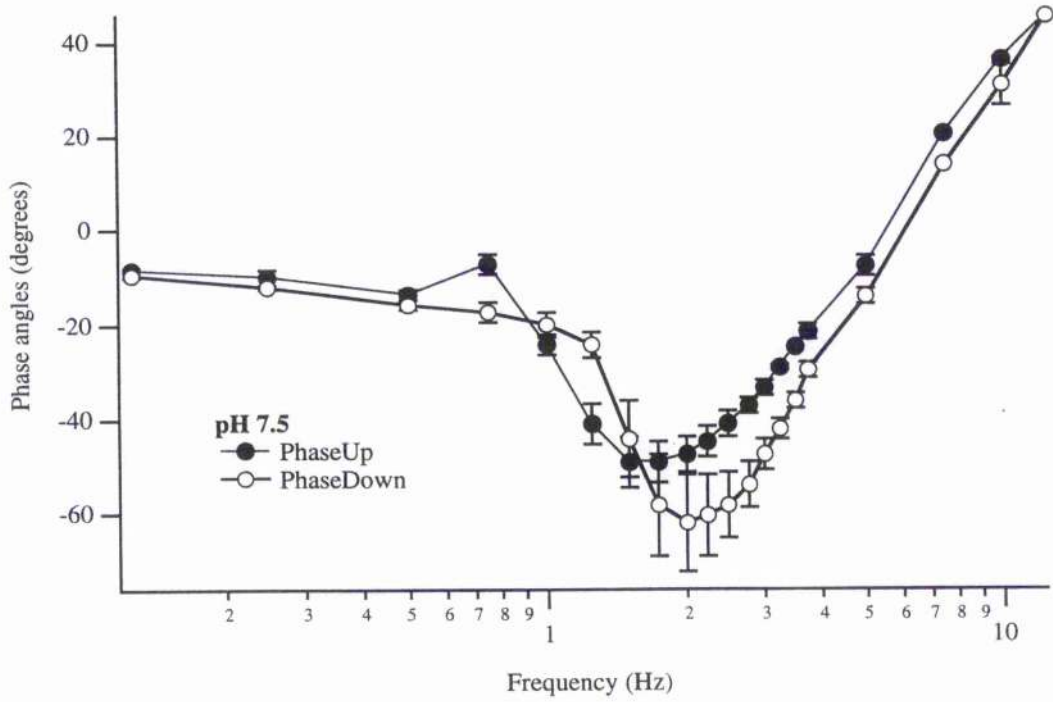


**Figure 3.14.** This figure shows a typical phase plot for pH 7.5. At this pH there is no positive phase angles but rather a large amount of negative phase angles within the physiologically relevant areas. This indicates that no positive oscillatory work is generated at the frequencies near  $f_{\min}$ .

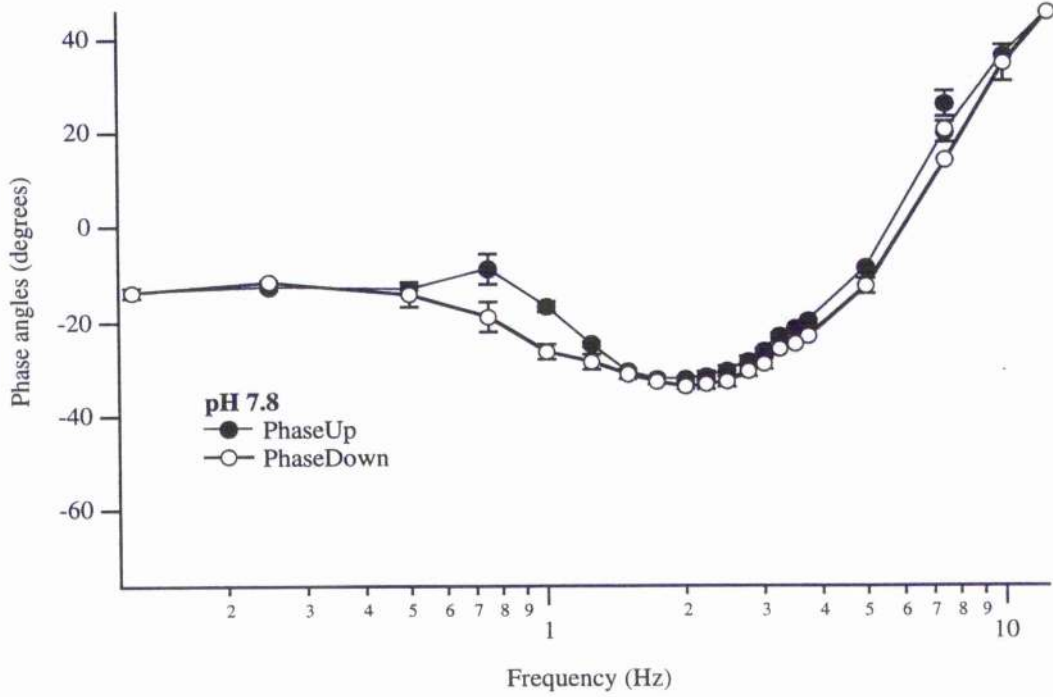


**Figure 3.15.** This is a typical phase plot for pH 7.8. At this pH, the phase plot has begun to resemble that of acidic pHs where the negative work or work absorbed by the muscle has been greatly reduced. There is also no positive work done by the muscle at this pH.

Table 3.4	Shift of Phase Plot from pH 7 to pH 7.5 (Hz)			
	Shift at Max Phase Angle	P=	Shift at Min Phase Angle	P=
PhaseUp	-0.50 ± 0.15	P< 0.5	-0.75 ± 0.23	P< 0.5
PhaseDown	-0.90 ± 0.42	P= 0.7	-0.60 ± 0.25	P= 0.6

\*n=5 for all experiments.

For alkaline conditions, the shape of the phase shift plot at alkaline pH also has a few differences from that at pH 7. Figure 3.13 shows that at pH 7.2 the initial inflection to positive phase angles for phaseUp is greater, indicating work being done by the muscle at these physiologically relevant frequencies. At more alkaline pH, however, this initial inflection is reduced slightly. This indicates that the optimum pH for work production for rat myocardium lies close to pH 7.2. The n numbers for the phase data were too small to do statistical analysis at pH 7.2 and 7.8.

The other change in the shape of the phase plot is with the deflection to negative phase angles around the value of  $f_{min}$  from the stiffness-frequency graph. This deflection reaches maximum negative values at pH 7.2. At more alkaline pH, however, this deflection becomes smaller. This indicates that the rat myocardium also absorbs the most work at pH 7.2.

### *Acid pHs*

It has been shown, with alkaline pHs, that the position of the phase plot directly correlated to the position of  $f_{min}$  in the stiffness-frequency plot. This is also true for acid

pHs although a clear  $f_{min}$  cannot often be seen at pHs lower than 6.75. However a comparison between Figure 3.12 and 3.16 of pH 7 and pH 6.75 shows that  $f_{min}$  is increased at lower pH. (n numbers were too small to do statistical analysis) Therefore, it was expected that the phase plot for acidic conditions would shift to the right, to higher frequencies, in order to correspond to the results shown for the acidic stiffness-frequency plots. This relationship was evident in these experiments and can be observed in Figure 3.16-17. At lower pH, the phase plot is shifted to the right, just as expected. The mean shift in frequencies between the control and pH 6.5 for the maximum phase angles was  $+0.95 \pm 0.48\text{Hz}$  for phaseUp and  $+0.90 \pm 0.53 \text{ Hz}$  for phaseDown and minimum phase angles was  $+1.95 \pm 0.65\text{Hz}$  for phaseUp and  $+0.90 \pm 0.38\text{Hz}$  for phaseDown. (See Table 3.5)

Table 3.5	Shift of Phase Plot from pH 6.5 to pH 7 (Hz)			
	Shift At Max Phase Angle	P=	Shift At Min Phase Angle	P=
PhaseUp	$+0.95 \pm 0.48$	P< 0.01	$+1.95 \pm 0.65$	P< 0.05
PhaseDown	$+0.90 \pm 0.53$	P= 0.13	$+0.90 \pm 0.38$	P= 0.7

\*n=5 for all experiments.

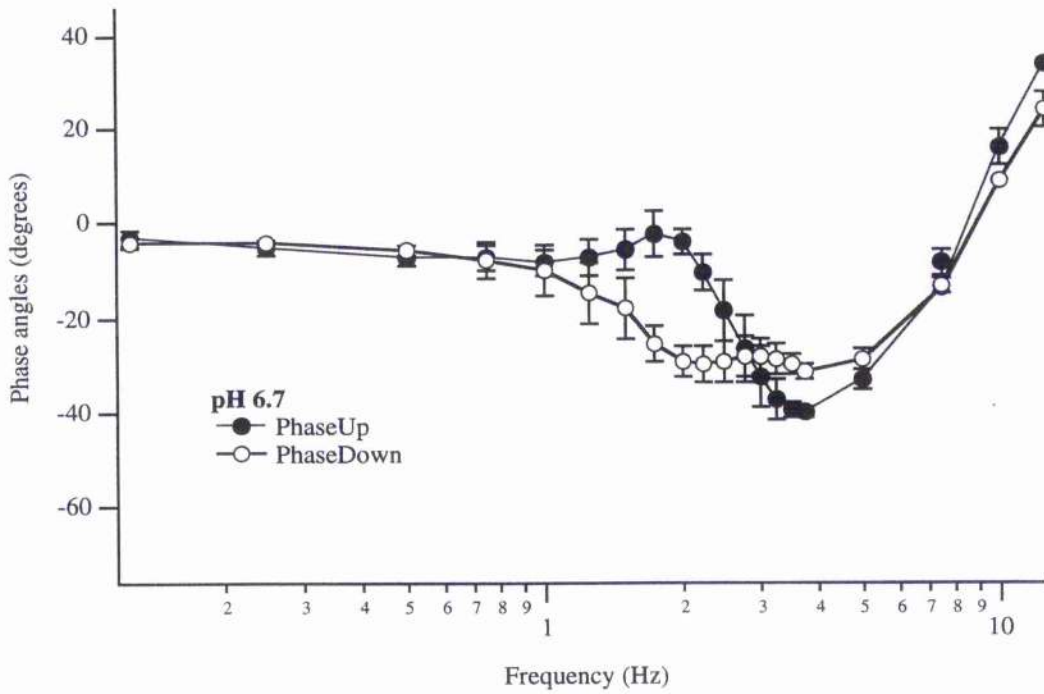
The shape of the phase shift plot also has a few changes at acid pHs. Figure 3.16 shows that, at pH 6.75, the initial inflection to positive phase angles for phaseUp has decreased. This indicates that the amount of work being done by the muscle has decreased. (n numbers were too small to do statistical analysis) At more acidic pHs, this initial inflection is decreased progressively.

The other significant change in the shape of the phase plot is with the deflection to negative phase angles around the value of  $f_{\min}$  from the stiffness-frequency graph. This deflection becomes less negative at progressively lower pH. The mean shift in phase angles between the control and pH 6.5 for the maximum phase angles was  $10.89 \pm 5.26\text{deg}$  for phaseUp ( $P < 0.1$ ) and  $12.01 \pm 5.89\text{deg}$  for phaseDown ( $P = 0.12$ ) and minimum phase angles were  $36.63 \pm 9.06\text{deg}$  for phaseUp ( $P = 0.01$ ) and  $33.15 \pm 8.70\text{deg}$  for phaseDown ( $P = 0.01$ ).

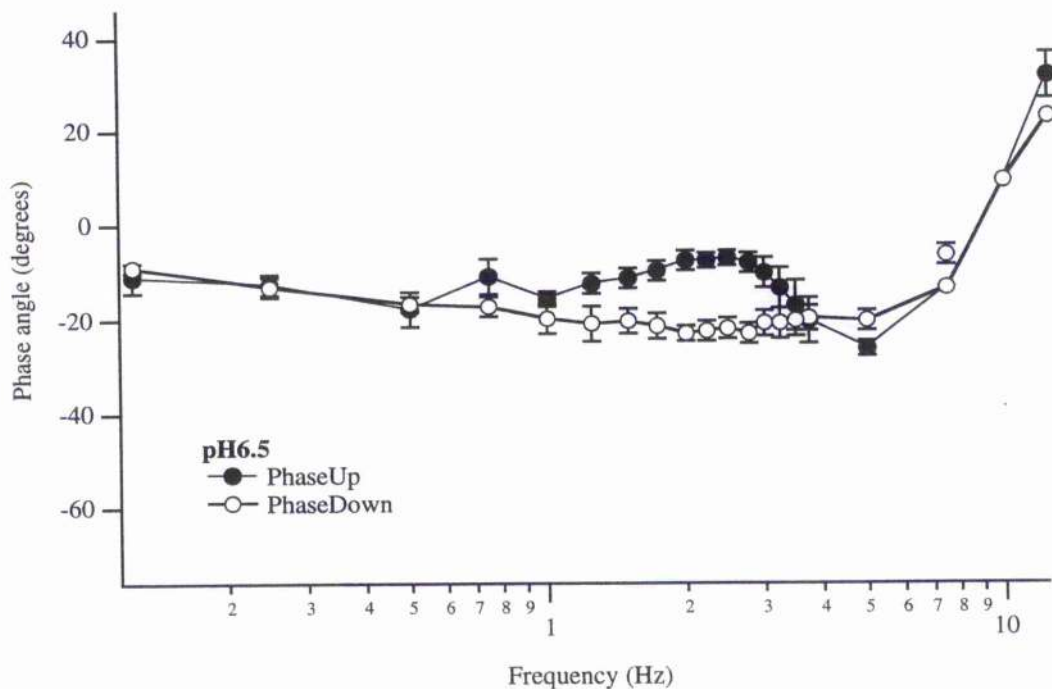
Perhaps that most striking observation was that, unlike the stiffness-frequency plot, there is no major distortion in the shape of the phase plot. There are only shifts in the position of the curves as corresponding to  $f_{\min}$  frequency, as well as change in the range of phase angles existing between the two sinusoidal traces. However, the general shape of the phase-frequency plot remains fairly constant. Data returns to control values (data not shown) for the phase plots and work loops when muscle is returned to the control solutions.

### **Work and Power Values**

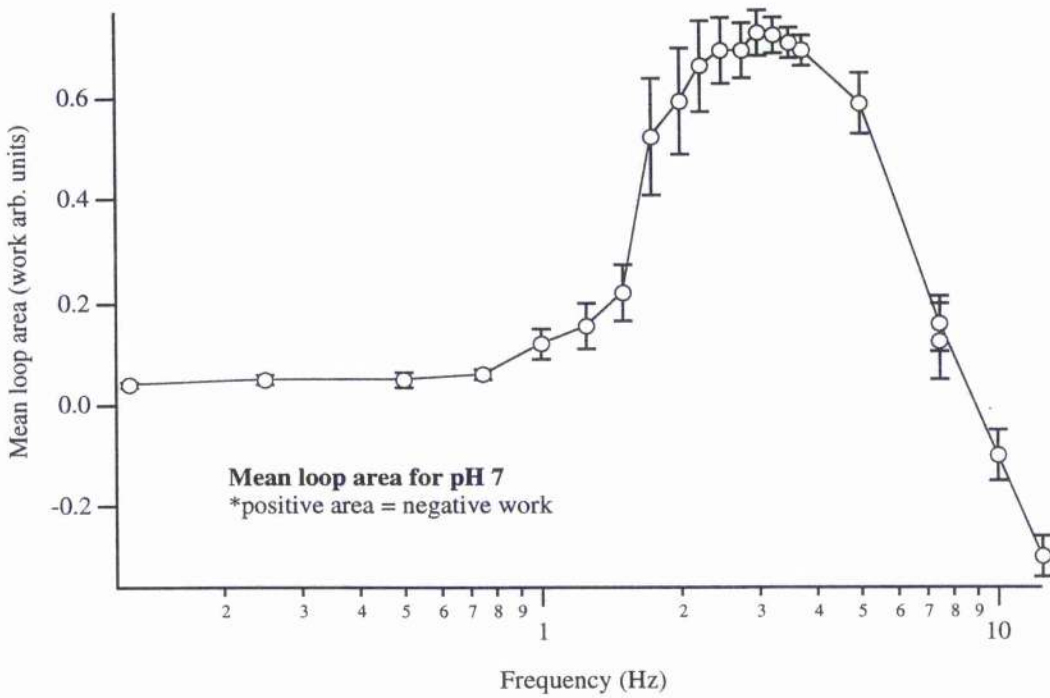
Calculations for the change in work and power output between pH 6.5, 7.0 and 7.5 were attempted using equation 2.4 and 2.5. However, due to the lack of positive phase values, physiologically relevant work and power values were not able to be obtained.



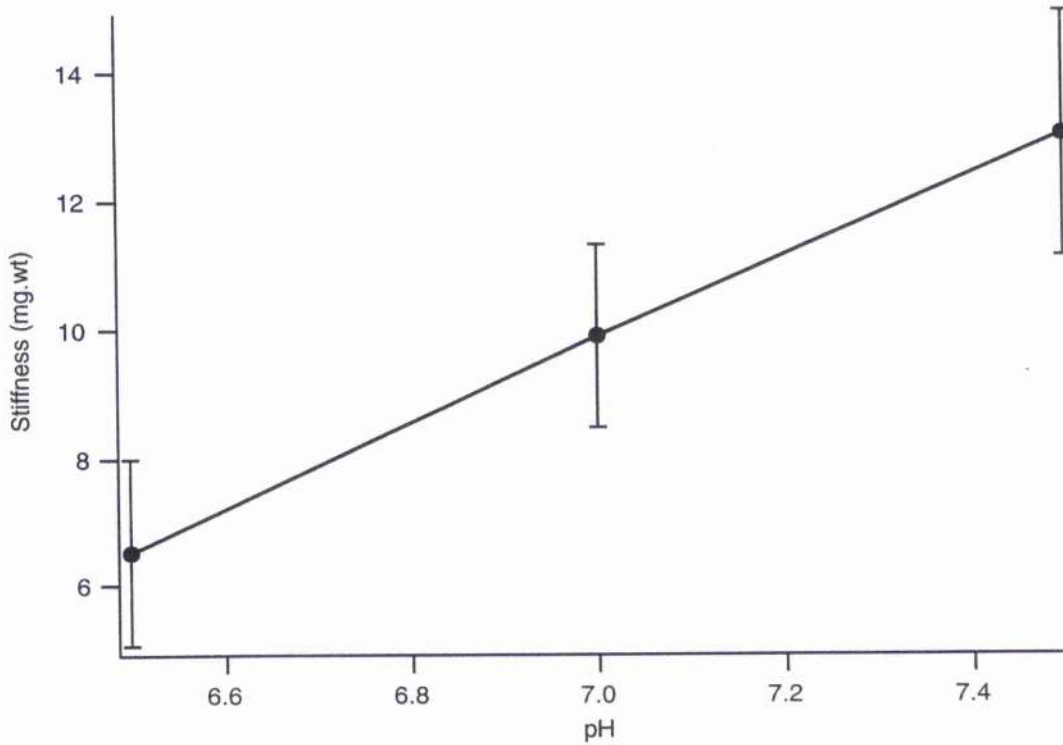
**Figure 3.16.** This figure is a typical phase plot for pH 6.7. Occasionally there may be a minute amount of positive work done at this pH. However, the phase plot has already begun to become shallower, showing that the muscle fibre is no longer able to absorb as much work as it did at pH 7 or pH 7.2.



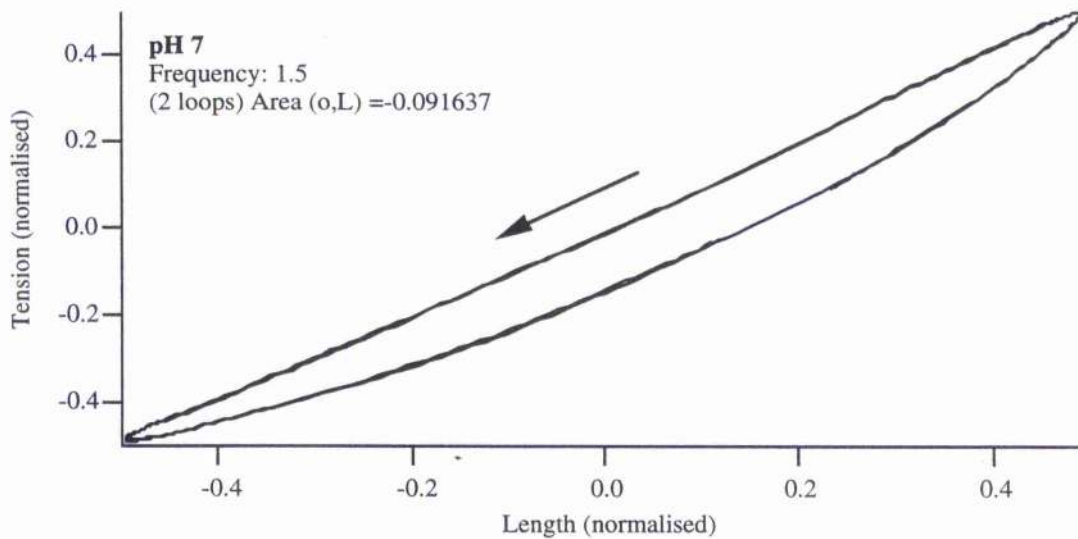
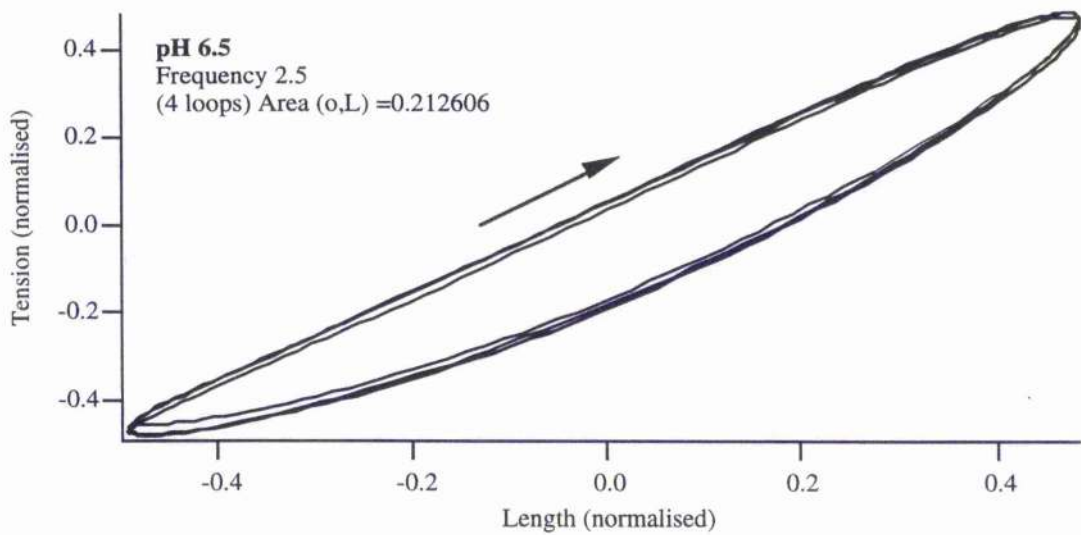
**Figure 3.17.** This figure shows a typical phase plot for pH 6.5. At this pH there is no positive and very little negative work within the suggested physiologically relevant range of frequencies. The reasons for this phenomenon are discussed in the chapter.



**Figure 3.18.** This figure shows the work loop area plotted against frequencies at pH 7 (n=7). Note that positive areas represent negative work done. The error bars represent the sem. This graph reveals that no physiologically-relevant positive work is done by the cardiac muscle fibre. Positive work is associated with anti-clockwise loops which define a negative area within the present descriptions.



**Figure 3.19.** This figure shows the change in stiffness during sinusoidal oscillation of fully  $\text{Ca}^{2+}$ -activated muscle fibres at different pHs. ( $n=4$ ) Note that each experiment used for this graph contained activations at each pH shown.



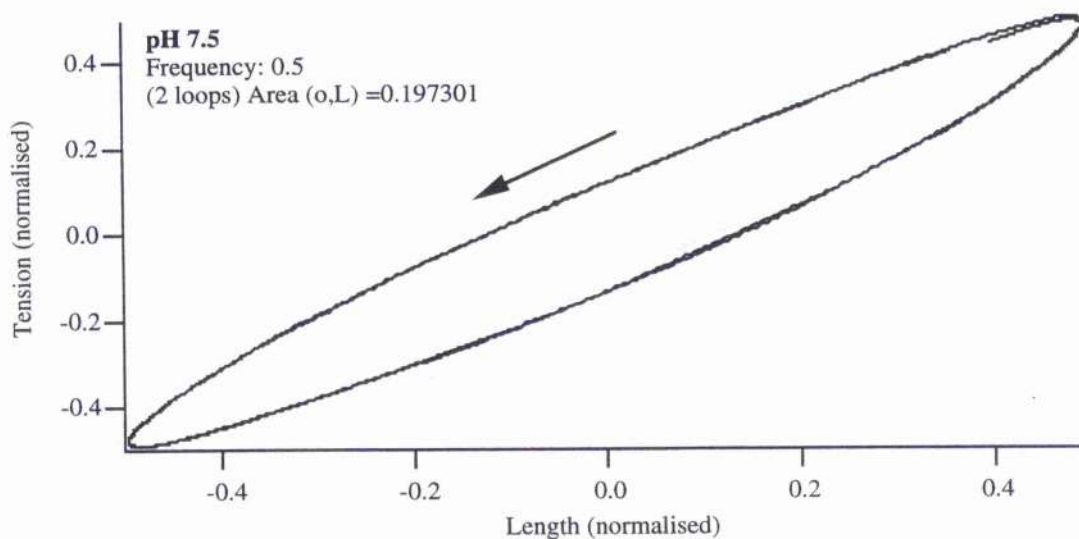


**Figure 3.20.** This figure shows an example of work loops obtained at pH 6.5, pH 7 (control), and pH 7.5. (o = tension, L = length) All three loops are from the same experiment and are typical of all pH experiments done in this thesis. The work loop graphs shown are at the frequencies where the maximum phase angle (i.e. most positive work) existed within the physiologically relevant area. The arrows indicate the direction of the loop.

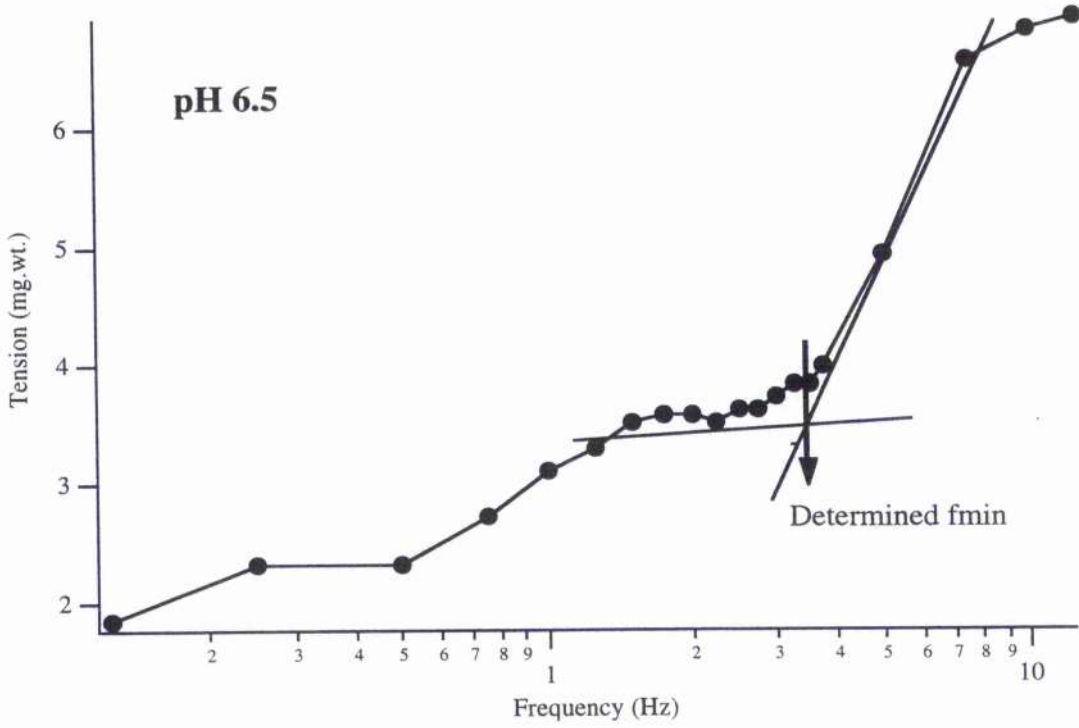


**Figure 3.21.** This figure shows an example of the method of how the location of  $f_{\min}$  was determined, on an individual trace, when there was no clear  $f_{\min}$ . This situation was frequently present for acidic pHs.

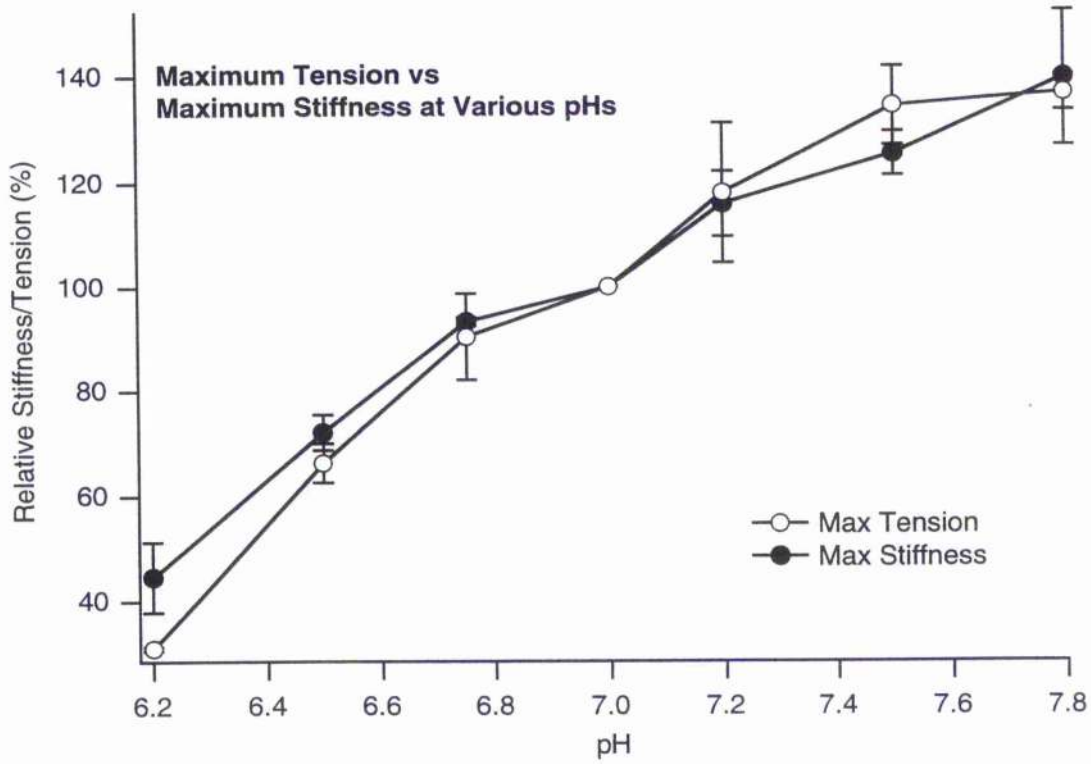


**Figure 3.22.** This figure shows the mean data for maximum tension vs maximum stiffness at various pHs. The error bars represent the sem for each value. There is no sem at pH7 because pH7 acted as the control and was therefore regarded as 100%.

## DISCUSSION

It has been well documented that acidosis occurs during hypoxic or ischaemic conditions in cardiac muscle. The aim of this study was to determine the effect of pH on different aspects of cardiac muscle function such as maximum force, stiffness, work and power, using the sinusoid oscillation technique.

Acidosis is established to be responsible, at least in part, for the rapid and pronounced fall of Ca-activated force observed in ischaemia/hypoxia. We looked at the effect of pH on maximum Ca-activated force. This effect probably occurs at all  $\text{Ca}^{2+}$  concentrations, but it can only be distinguished from the effect of Ca-sensitivity by using a saturating  $[\text{Ca}^{2+}]$  so that the latter effect can be eliminated (Orchard & Kentish 1990).

There have been several studies examining the effect of pH on force. In 1991, Kentish showed that a decrease in pH from 7.0 to 6.2 results in a reduction of  $\text{Ca}^{2+}$ -activated isometric force by 55%. The relationship between force and pH went in the opposite direction for alkaline pH, where maximum isometric force continued to rise at pH 7.4. Later in 1994, Ebus *et al.* also showed that maximum isometric force increased gradually from pH 6.2 to pH 7.5. Our results were comparable to those reported for maximum isometric force from cardiac skinned fibres for a pH range from 7.5 to as low as pH 6.5, where it was reduced by around 30% (*e.g.* Ebus *et al* 1994). However, the proportional relationship between tension and stiffness as seen in Figure 3.22 can be taken to mean that force per crossbridge may be assumed to be unaltered by changes of pH.

The mechanism through which pH affects Ca-activated force has not been clearly established, though many widely accepted theories do exist. One possible explanation is that the simple mass action effect suppresses the release of protons during the transition between detached cross-bridge states. This would promote an increase in the fraction of weakly bound cross-bridges (Ebus *et al* 1994). These weakly bound crossbridges are

considered to contribute less to force production and would explain these results. It has been established that maximum force development is much more effected by pH than is ATPase activity. Therefore, it has been suggested that there is also a reduction in the force produced in each cycle of the crossbridge (Orchard & Kentish 1990). This may be due to a fall in the efficiency of coupling ATP hydrolysis to force production at low pH. Fabiato and Fabiato obtained evidence for this hypothesis in 1978. They demonstrated that a decrease in pH reduced the force of a rigor contraction, where the myosin crossbridges are bound to actin in a stable state.

A primary finding of this study was that at maximal  $\text{Ca}^{2+}$  activation, stiffness (at all frequencies) reduced progressively as pH was lowered (illustrated in Figure 3.19). It is assumed that stiffness provides a measure of the number of attached crossbridges. Therefore, we conclude that a decrease in pH somehow inhibits crossbridge attachment. However, how this inhibition is caused is still unclear. If acidosis does reduce the binding constant of  $\text{Ca}^{2+}$ , it does so by increasing the off-rate rather than by decreasing the on-rate. This is because the on-rate is thought to be diffusion limited (Orchard & Kentish 1990). ( $K = k_{on} / k_{off}$ ) This increase in the off-rate of  $\text{Ca}^{2+}$  may help to explain the increase in relaxation rate that occurs in intact muscle during acidosis as reported in Chapter 5.

In addition to this effect, the increase in  $[\text{H}^+]$  may be inhibiting the individual crossbridges from moving forward in the crossbridge cycle. During normal cycling, once myosin catalyses the breakdown of one molecule of ATP to ADP, Pi and  $\text{H}^+$ ; myosin then attaches to actin in a weakly bound state. It is considered that at this point the crossbridge has greatly flexibility and therefore produces less stiffness when the muscle is manipulated. According to current crossbridge cycling models, the crossbridge must release the  $\text{H}^+$  before it can enter the strongly bound state. The increase in  $[\text{H}^+]$  will

inhibit the crossbridge from releasing the  $H^+$  and thus may increase the proportion of bridges remaining in the weakly bound or unattached states.

Our results showed that crossbridge cycling rate is progressively decreased at higher pH and increases at lower pH (See Table 3.2). Using the sinusoidal oscillation method, with  $f_{min}$  as an indicator of crossbridge cycling rate, we found that  $f_{min}$  is found at significantly lower frequencies at alkaline pH ( $P < 0.001$ ). The effect is reversed when looking at acidic pH. The position of  $f_{min}$  at higher frequencies reported in our results was concluded from consistent results of  $f_{min}$  being found at significantly higher frequencies at pH 6.7 ( $P < 0.05$ ). Thus, from the consistent progression of  $f_{min}$  to higher frequencies as pH is changed from 7.8 to 6.7, it was concluded that  $f_{min}$  would be found at even higher frequencies for pHs below 6.7. This hypothesis was supported by a few experiments where a characteristic ' $f_{min}$  dip' could be found at higher frequencies for pH 6.5 (n numbers were too small for statistical analysis), although the plot showed the beginnings of the flattening out effect.

However, these results are different from those frequently reported using the ATPase measurements which, before now, have been used to identify the rate at which the crossbridges are cycling (Orchard & Kentish 1990, Ebus *et al* 1994). ATPase measurements can only report the *average* crossbridge cycling rate from the amount of ADP released using an indirect fluorescence method. Sinusoidal analysis on the other hand, measures the activity at many frequencies to reveal the frequency,  $f_{min}$ , at which the greatest proportion of the crossbridges are cycling. Therefore, this allows for the observation of specific crossbridge activity that would otherwise be masked under the average. This advantage of the sinusoidal oscillation method was crucial to see that, as pH drops, there is not only a change in the crossbridge cycling rate, but also a spreading of the rates to a wider range of frequencies. It is noticeable that the distinctness of the  $f_{min}$  feature was lost below pH 6.75. Between pH 6.75 and 6.5, or lower, we conclude that

crossbridge cycling is no longer concerted over a narrow range of frequencies. We suggest that some aspect of crossbridge interaction that normally brings individual rates into a narrow range is thereby disturbed in acidic conditions. Measurements of ATPase rate by conventional methods can only reveal the average rate of ATP consumption. The present findings reveal that this average might obscure what is happening to a potentially more important property reflecting the narrowness of the frequency range that normally typifies crossbridge rate.

One possibility is that the rate constants for intermediate steps in the crossbridge cycle are changed or disrupted at lower pH. There are many chemical constants involved in muscle contraction. It seems that some are affected just below pH 6.7, while other only alter markedly at far lower pH. However, it seems, from our results, that most constants are altered beyond 6.5.

Another possibility involves changes in the myofilament lattice at increased  $[H^+]$ . It was thought that a higher concentration of  $H^+$  outside the myofilaments would cause an osmotic effect and result in myofilament shrinkage. This shrinkage would result in altered space among the crossbridge causing a decrease in efficiency. However, the present results using T-500 Dextran, which mimicked the effect of filament shrinkage at pH 6.5, showed that shrinkage alone does not account for the discrepancy in muscle function at low pH. Matsuda and Podolsky (1986) have shown, using X-ray diffraction studies, that the myofilament lattice not only shrinks but is also disrupted at low pH, notably the regularity of the actin hexagonal array. One explanation is that the increase in  $[H^+]$  allows binding to negative charged residues causing a significant disturbance to the pattern of protein charges found within the myofilament. The resulting disruption the myofilaments reduced their ability to interact normally with each other. The result is a decrease in cooperativity, which thus leads to the crossbridge rates to spread out since the crossbridges are now cycling at more 'independent' rates than usual without being

influenced by neighbour crossbridges. This feature, rather than lattice shrinkage, could contribute to the observed spreading of crossbridge rates.

The scenario described here could explain why myocardial pump function is grossly reduced in acidosis. The known reduction in isometric force underestimates the extent to which the ability to deliver work is actually reduced.

Many preparations examined were able to produce net positive work, at control conditions, at least at one frequency. However, most preparations only just failed to exceed zero net work. By contrast, Iwamoto (1995) reported a large proportion of frog fast twitch skeletal fibres examined were not able to generate any positive sinusoidal work (named 'idler' fibres), attributing this to 'greater non-linearity' (broadly equivalent to the loop asymmetries discussed here) in kinetic properties. There seems little doubt that the muscles in Iwamoto's report, as well as the present study, would generate external work under physiological conditions (i.e. undergoing significant shortening whilst under load). The lack of oscillatory work thus merely indicates that aspects of the experimental protocol are critical to its magnitude. Although with this protocol the phase curve may not cross to positive angles (just below  $f_{min}$ ), that region of the curve still relates to the ability to generate work (or at least absorb the least work) at those frequencies.

Our results using phase shift analysis show that the positive phase angles (near  $f_{min}$ ) decrease at lower pH ( $P < 0.1$ ). This means that the muscle is doing less oscillatory work. This decrease is reinforced by the decrease in work-loop areas as seen in the previous section (See Figure 3.20). The change in the loop direction must also be taken into account when viewing Figure 3.20. The work loop for pH 6.5 is going clockwise (i.e. negative work) while the loops for pH 7 and 7.5 are going counter-clockwise (i.e. positive work.)

There are a few possible explanations for this phenomenon. First, it has been established from the force data that there is a reduction in the number of attached crossbridges at lower pH. Therefore, the overall ability of the muscle to produce positive work is reduced.

There are also the many factors affecting the crossbridges that are attached. It can be assumed from the  $f_{min}$  data that the crossbridge cycling rate is increased at lower pH. However, this effect is not clear using the stiffness-frequency plots. Then again, we do know that the phase plots shift in the same direction as the frequency-stiffness plots. Therefore, we can conclude that crossbridge cycling rate does increase at lower pH. Analysis approximating  $f_{min}$  location using the method shown in Figure 3.21 shows a significant increase in  $f_{min}$  at lower pH ( $P < 0.05$ ). It is probable that this is the result of the increase in the off-rate of the crossbridge due to the reduction in the binding constant. This increase in the off-rate is consistent with a reduction of the time the myosin head is in the power stroke. This decrease in the power stroke time can thus lead to the decrease in force, but also work and power.

Another factor, as previously discussed, is the degree of disarray in the myofilament lattice during acidosis. As with force, the present results show that it is the disorganisation within the lattice rather than the shrinkage that affects work. It is reasonable to expect that this disorder among the crossbridges will reduce the efficiency of the attached crossbridges to do work. This coincides with the decrease in cooperativity that is interpreted from the spreading of the crossbridge rate.

The data from the stiffness frequency plot and the phase plots can be used to determine how cardiac muscle power output is affected with changes in pH. It has been stated that power is determined by the equation:  $P(f) = W(f) * f$ . We have already seen that crossbridge rate does increase during acidosis. However, the amount of work generated is more drastically lower (significant decrease in positive phase angle at pH 6.5  $P < 0.01$ ).

Although the phase curves are shifted to higher frequencies, the reduction in maximum phase angles and absolute force multiply together to give a much lower oscillatory power output. This decrease in power will cause a reduction in the functional ability of the heart to pump adequate blood to the body. If not reversed, this dysfunction will lead to further deterioration of the heart muscle leading to more complications, including larger increases in acidosis, and eventually lead to tissue death.

## CHAPTER 4 EFFECT OF PHOSPHATE ON CROSSBRIDGE KINETICS

## INTRODUCTION

During ischaemia/hypoxia the heart muscle undergoes a decrease or loss of contractile activity. The mechanism of this early contractile failure is not well established, but many early theories have now been discarded due to various findings. It was thought that the early decrease in the twitch amplitude was due to the reduced availability of Ca ions. However, it was shown that the electrical activity and the Ca current are not changed during the decrease in contractile force (Kohlhardt & Kubler, 1975, Ventura-Clapier & Vassort, 1980). Also, the absence of changes in the Ca transient (Allen and Orchard 1983) confirms that the duration and magnitude of the changes in internal Ca following excitation are not altered at the time of force decrease.

Acidification (previous chapter), which occurs during prolonged hypoxia or ischaemia, is able to depress force development of skinned fibres (Fabiato & Fabiato 1978). However, a change in pH is not an early phenomenon in ischaemia (Allen *et al* 1985). In addition, studies by Hoerter *et al* (1986) showed that, upon mitochondrial inhibition, the fall in force occurs without acidification.

It has been suggested that the decrease in the cytoplasmic phosphorylation potential may decrease the free energy of ATP hydrolysis (Gibbs 1985); force could be affected either by a direct effect on the contractile machinery or by an effect on Ca<sup>2+</sup> release from the sarcoplasmic reticulum. However, Kentish and Allen (1986) have brought some evidence that the fall of phosphorylation potential is not the direct cause of the reduced force production. Early contractile failure is accompanied by a rapid hydrolysis of creatine phosphate (CrP) that induces an increase in inorganic phosphate (Pi). Herzig and Rüegg (1977) were the first to propose that the increase in Pi may be involved in the fall of tension observed after hypoxia or ischaemia. Many studies have shown that Pi decreases maximal force and stiffness in skinned fibres; this effect is greater in cardiac

and slow muscles than in fast muscle (Herzig & Rüegg 1977, Godt *et al* 1985, Kentish 1986).

Many labs have begun to study the effects of Pi on the kinetics of contraction since the mid- 1980s. It has been shown that Pi does not seem to alter maximal speed of shortening, (Altringham & Johnston 1985, Cooke & Pate 1985). However Pi does affect the frequency of oscillatory work (Kawai *et al* 1987) as well as the recovery of tension following quick stretch and length activation, which are accelerated by Pi (Herzig & Rüegg 1981, Altringham & Johnston 1985). Studies looking at the influence of Pi on actomyosin ATPase rates have shown either no change (Altringham & Johnston 1985) or a slight decrease (Ebus *et al* 1994) in the energy cost of tension. It has also been shown that Pi accelerates the relaxation of rigor tension upon photolysis of caged ATP. This result suggests that the dominant force-generating cross-bridge state is reversibly coupled to the release of Pi (Hibberd *et al* 1985).

During muscle contraction, there is a cyclic interaction between myosin (M) and actin (A) with hydrolysis of ATP to ADP and Pi. The net reaction provides energy for force production and shortening (Huxley 1957). The reaction pathway for the crossbridge ATPase cycle is shown in chapter 1.

According to this mechanism, ATP (as  $MgATP^{2-}$ ) rapidly binds to the actomyosin (AM) rigor cross-bridge (Step 1) and is hydrolysed directly in step 3', or in step 3 after crossbridge detachment (step 2). The AM-ATP and AM-ADP-Pi, occur as steps 2 and 4. Product release is accelerated upon binding of M-ADP-Pi to actin, forming AM-ADP-Pi.

The specific reaction step coupled to the force generating transition may be the release of Pi from the low force AM-ADP-Pi state to form a high-force AM'-ADP state (step 5). There are several observations that strengthen this theory. First, the free energy change for this step is large ( $\sim 40\text{kJ mol}^{-1}$ ), (White & Taylor, 1976). Second, isometric force is

reduced as [Pi] is increased within an activated skinned muscle fibre (Brandt *et al* 1982, Cooke & Pate 1985). It is presumed this reduction in force is due to the shifting of the equilibrium of step 5 (in the above scheme) to the left. Third, the apparent rate constant for force generation from rigor following photolysis of caged ATP increases at high [Pi] (Hibberd *et al* 1985). This is consistent with the force-generating transition being associated with step 5 since the observed rate would then be given by  $k_{+5} + k_{-5} [Pi]$ , where  $k_{+5}$  is the first order rate constant from left to right and  $k_{-5}$  is the second order rate constant from right to left in step 5, and so would increase as [Pi] is raised (Dantzig *et al* 1992).

Under ischaemic-hypoxic conditions, the intracellular [Pi] rises from a value of 1-3 mM to 20 mM or more (Herzig & Rüegg, 1977, Kentish, 1986). If the AM'-ADP state is significantly populated during an isometric contraction, sudden introduction of Pi within the fibre should decrease force, with kinetics related to  $k_{+5}$  and  $k_{-5}$ . If AM-ADP-Pi is in rapid equilibrium with M-ADP-Pi, sudden introduction of Pi should also cause a rapid decrease of muscle stiffness.

Previous studies have shown that both  $Ca^{2+}$ -activated maximum tension and dynamic stiffness decrease with the introduction of a high [Pi] (Kawai *et al* 1987, Kentish 1991, Ebus *et al* 1994). The experiments done in this chapter attempt to repeat and extend these results. Although alterations in myofilament  $Ca^{2+}$  sensitivity and isometric force are well reported, effects on myocardial work and power are less so. Therefore, further analysis was also performed using the sinusoidal oscillation protocol, to analyse other effects Pi has on the kinetic properties of cardiac muscle, specifically work and power.

## METHODS

Crossbridge properties were investigated using the sinusoidal oscillation method described previously in this thesis. Fine preparations of rat ventricle muscle were chemically skinned (as described in Chapter 2) to allow direct control of the ionic environment of the myofilaments. The preparation was activated in pCa 4.0 solutions of various [Pi]. The [Pi]s used were nominally zero Pi (as the control), 2 mM, 5 mM and 10mM. The activating solution was made as described in Chapter 2 with desired [Pi] added at the same time. The trabecula was initially activated under control conditions (nominally zero Pi, pH 7) and oscillated. After every run in the various [Pi]s, the muscle was again activated and oscillated under control conditions. This was to evaluate the endurance of the preparation throughout the protocol. If the force production in pCa 4.0 at zero Pi fell to 50% of the original contraction, the preparation was no longer used. The order of the protocol was switched around in every experiment. This was to ensure than the amount of damage inflicted at one [Pi] would not affect the muscle kinetics at the next [Pi].

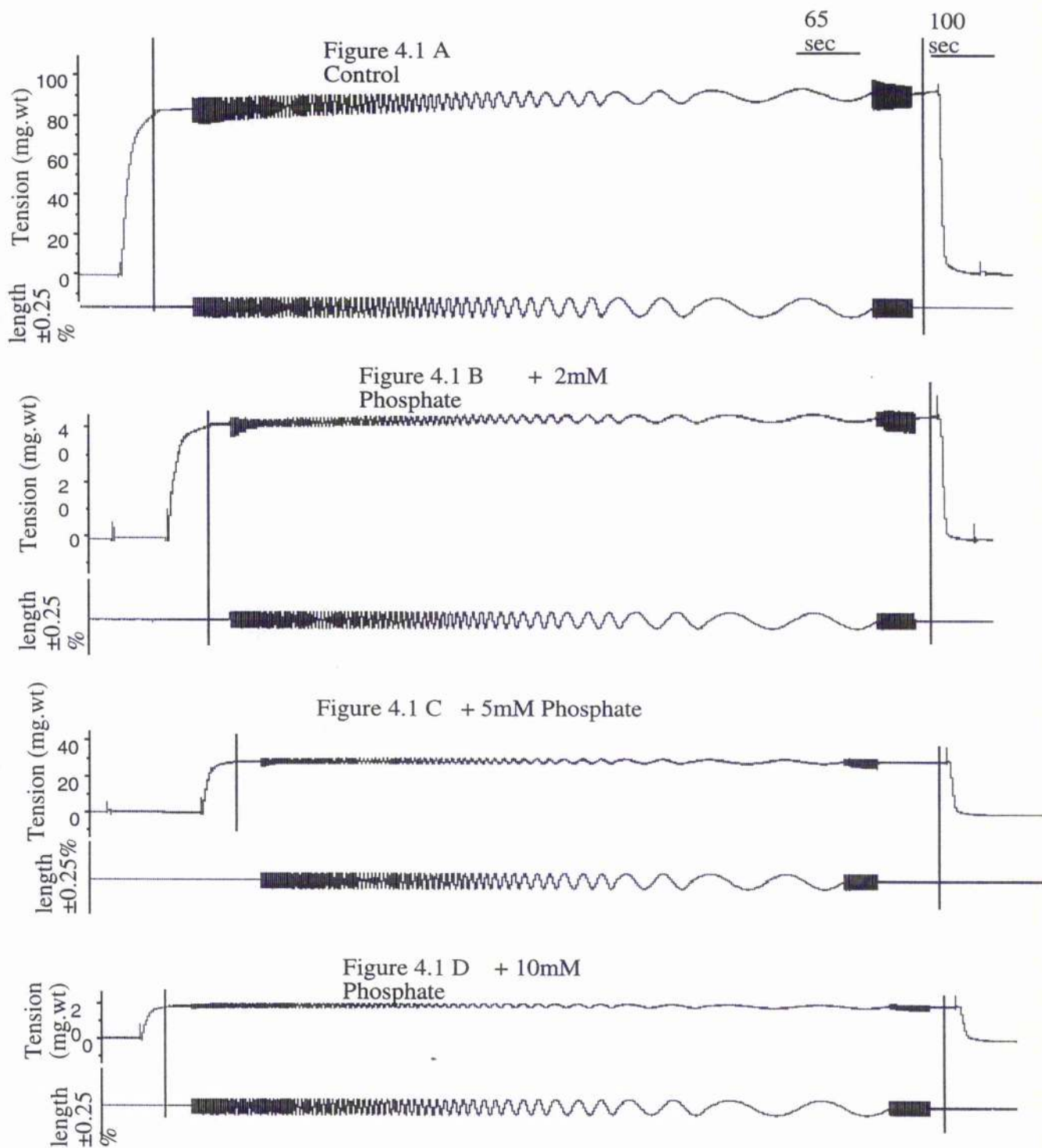
## RESULTS

Figure 4.1 shows an example of a typical experimental trace for a phosphate experiment beginning with a maximal activation and including a control activation and oscillation between every phosphate affected activation. A series of small, sinusoidal length perturbations have been applied during each activation. Details of the precautionary and control measures included in each experiment are identical to those used in the pH experiments. Thus, these measures can be reviewed in the Results section of the previous chapter.

### Effect of Phosphate on Max. Tension

Various factors contributed to the force produced by the preparation. These factors will be listed and discussed in the next section. One of the aims of these experiments was to compare tensions produced by rat myocardium at various [Pi]. However, due to the differences that may exist between the various trabeculae, such as diameter, degree of muscle damage, *etc.*, force production could not be compared directly between them. Instead, all data were normalised with the maximum force produced by the control run (nominally phosphate free) defining 100%.

The relationship between [Pi] and force production is not linear, as is shown in Figure 4.2. It shows that at higher [Pi], force is significantly decreased. The mean force produced was (in %)  $59.63 \pm 3.40$  (n=6) at 2 mM Pi,  $42.94 \pm 5.69$  (n=6) at 5 mM Pi, and  $39.84 \pm 5.96$  (n=13) at 10 mM Pi. (All p values < 0.01) (See Table 4.1)



**Figure 4.1.** A-D This set of figures shows the effect of phosphate on muscle force production and the dynamic stiffness. Note that at higher phosphate concentrations, steady-state force and stiffness are both significantly smaller. The reasons for this phenomenon are discussed in this chapter. The number of points recorded per second had been increased during sinusoidal oscillation in order to increase the resolution of the trace. Thus the time recorded between the vertical markers were recorded in milliseconds opposed to seconds during the rest of the experiment. In the time shown above milliseconds has been converted to seconds.

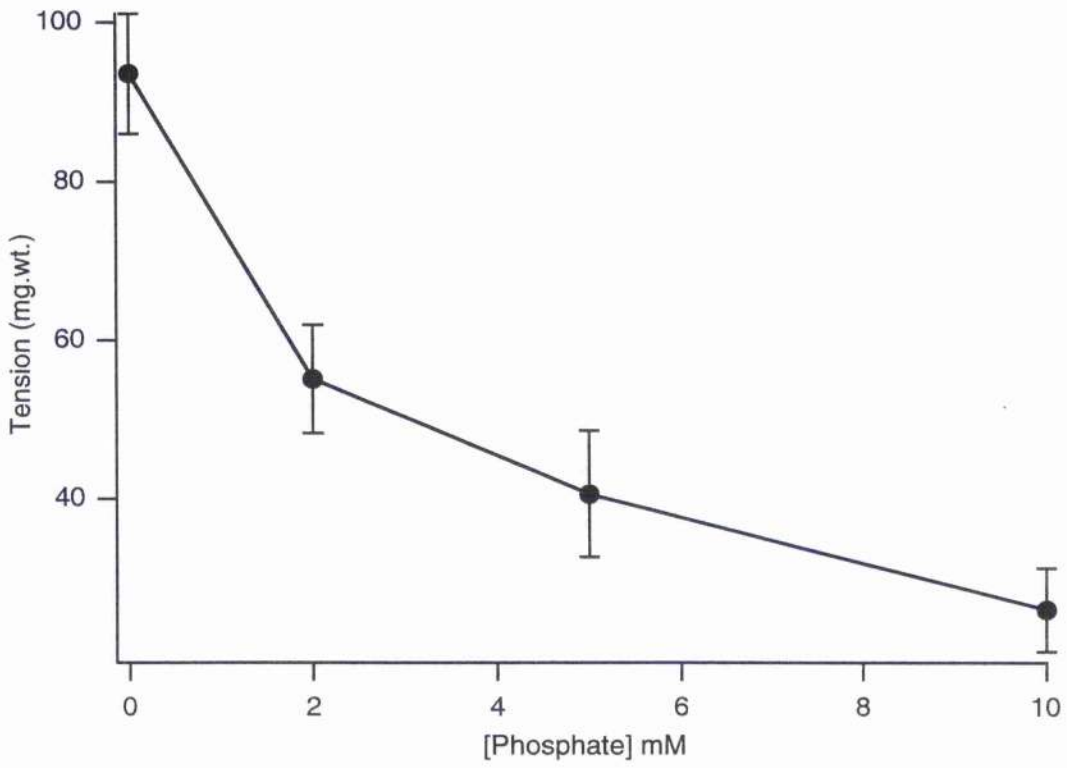


**Figure 4.2.** This figure shows the relationship between phosphate concentration and maximal force production. The points are the mean  $\pm$  sem for  $n=6$  preparations.

<b>Table 4.1</b>	<b>Change in Maximum Ca-activated force vs. [Pi]</b>		
<b>[Pi] (mM)</b>	<b>Relative Tension (%)</b>	<b>P=</b>	<b>n=</b>
<b>0</b>	Determined 100%	N/A	N/A
<b>2</b>	59.63 ± 3.40	< 0.01	6
<b>5</b>	42.94 ± 5.69	< 0.01	6
<b>10</b>	39.84 ± 5.96	< 0.01	13

## **Dynamic Stiffness**

### ***Control conditions***

The control activations and oscillations are identical to those of the control in the experiments where pH was the experimental variable and can be reviewed in the Chapter 3. For a brief summary, reading from low to high frequencies, the plot is generally characterised by a downward deflection, until reaching  $f_{\min}$ , followed by an increase in stiffness. This increase continues until a maximum is reached at about 7-10Hz, and then begins to decline. The control runs in this set of experiments did not have a clear  $f_{\min}$  for the majority of the trabeculae. This may have several explanations and have been considered in the discussion section of Chapter 3.

It has been established by many labs that, under the conditions used in this experiment, the zero phosphate solutions will usually have a small level of phosphate contamination of around 0.9 mM, mostly from Pi generated by the active tissue (Xiang & Kentish, 1995).

### ***Raised Phosphate***

The increase in [Pi] has three main effects on the stiffness-frequency plot. The first is to shift the whole curve to higher frequencies. The second is that the inflection defining  $f_{\min}$  becomes noticeably more pronounced at higher [Pi]. The third is the depression of the stiffness-frequency plot.

Between 0.9 mM and 2 mM Pi, the entire stiffness-frequency curve is shifted to the right, thus bringing  $f_{\min}$  to higher frequencies. This phenomenon holds at phosphate concentration up to 10 mM. The entire stiffness-frequency curve is shifted to the right, consistent with a speeding of crossbridge kinetics. The mean  $f_{\min}$  value was  $3.08 \pm 0.25$  Hz (n=6) at 2 mM Pi,  $3.71 \pm 0.36$  Hz (n=6) at 5 mM Pi, and  $5.67 \pm 0.70$  Hz (n=12) at 10 mM Pi. (All p values < 0.01)

It was obvious that at raised [Pi] the inflection point of  $f_{\min}$  becomes more clear, as shown in Figure 4.3. This effect is even more pronounced in these experiments where the control stiffness frequency plot lacked a clear  $f_{\min}$  inflection.

The third effect of Pi was the severe depression of the stiffness-frequency plot at higher [Pi]. Compared with values plotted at 0.9 mM [Pi] (which was taken as the [Pi] in nominally zero Pi conditions and tension defined as 100%), dynamic stiffness at  $f_{\min}$  was far lower than control with added Pi, with mean values (in %) of  $73.79 \pm 16.86$  (n=6) at 2 mM [Pi] (P= 0.05),  $74.54 \pm 15.89$  (n=6) at 5 mM [Pi] (P< 0.01), and  $59.56 \pm 6.95$  (n=12) at 10 mM [Pi] (P< 0.01). The maximum dynamic stiffness found at the higher frequencies beyond 3 Hz was also found to be decreased greatly at higher [Pi]. However,

due to the extreme shift to the right, the maximum stiffness was not reached for 5 and 10 mM phosphate. Further studies could include oscillation at still higher frequencies to obtain these values. Compared with (nominally) 0.9 mM [Pi], the maximum dynamic stiffness was  $60.12 \pm 4.42\%$  at 2 mM [Pi] ( $P = 0.05$ ). All these features can be seen in Figure 4.3. Although the frequencies at which the maximum stiffness occurs may not be physiologically relevant, they give a picture of the functional capacity of the crossbridges (see Methods chapter).

<b>Table 4.2</b>		<b>Change in Dynamic Stiffness at <math>f_{\min}</math> vs. [Pi]</b>	
<b>[Pi] (mM)</b>	<b>Stiffness (%)</b>	<b>P=</b>	<b>n=</b>
<b>0</b>	Determined 100%	N/A	N/A
<b>2</b>	$73.79 \pm 16.86$	< 0.05	6
<b>5</b>	$74.54 \pm 15.89$	< 0.05	5
<b>10</b>	$59.56 \pm 6.95$	< 0.01	12

In order to facilitate comparison of the shapes of the various stiffness-frequency curves, all stiffness data were normalised to the maximum for each experiment individually. The minimum was then subtracted and the data re-normalised  $f_{\min}$  occurs at slightly different frequencies in each case, so that averaging several traces from different experiments tends to smooth the relationship, as was noted in the chapter on pH. However, an individual trace, such as Figure 4.4, shows the features described more clearly.

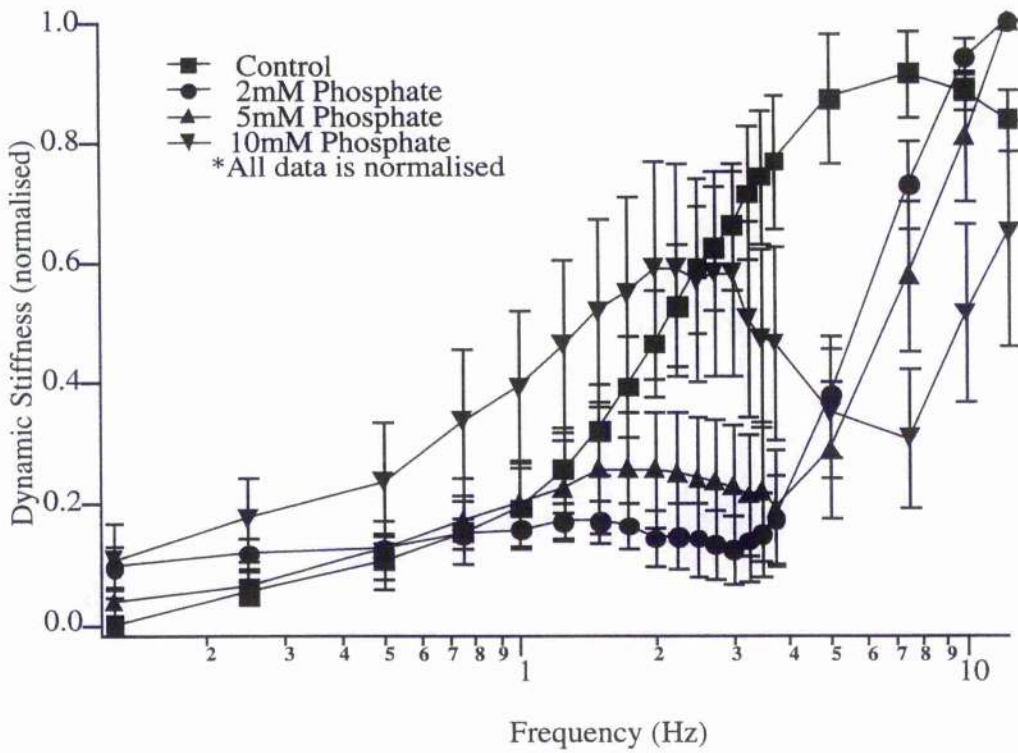


**Figure 4.3.** This figure shows the combined phosphate data for 6 experiments. Note that the  $f_{\min}$  was not well defined for the control for the fibers used in this study. (See example of individual experiment stiffness plot in Figure 4.4) However, the effect of phosphate can clearly be seen. This figure shows that the higher the phosphate concentration is, the faster and more defined  $f_{\min}$  becomes. The implications of these results are further discussed in this chapter.

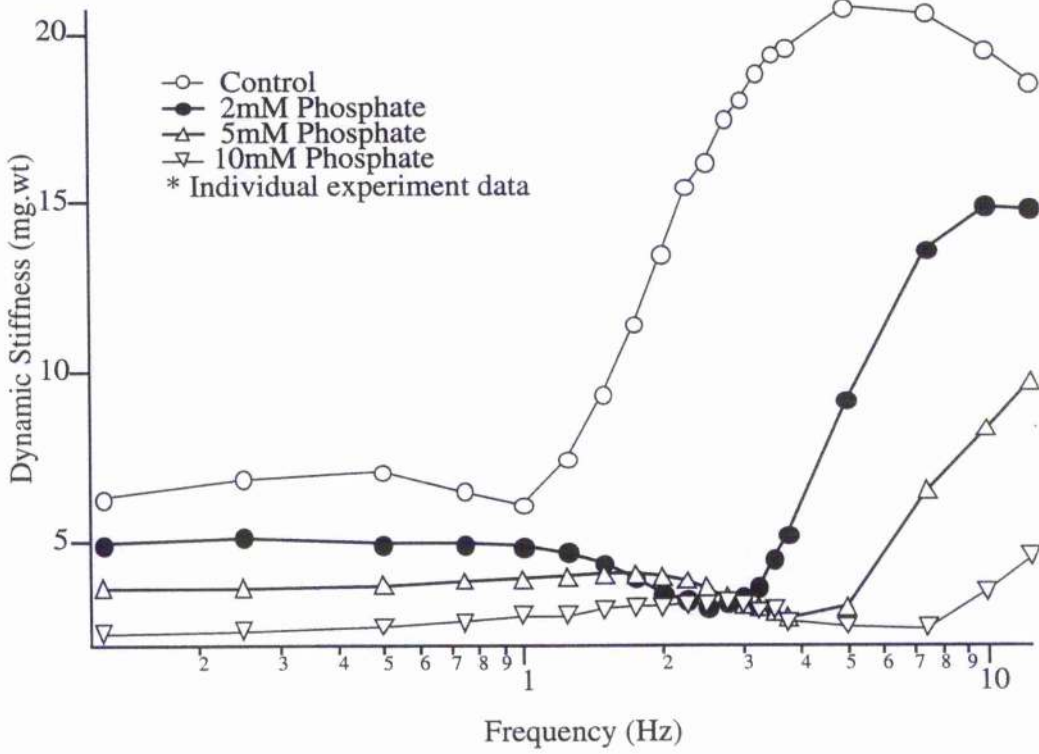


**Figure 4.4.** This figure shows a stiffness-frequency plot from a single experiment. Unlike the stiffness plot of the combined data (Fig 4.3), it is clear that the control curve does have a clear  $f_{\min}$ . Just as in the combined data graph, phosphate increases the frequency at which  $f_{\min}$  is found and creates a clearer  $f_{\min}$  inflection.

## Phase

### *Control conditions*

The phase shifts between the length and tension traces were analysed in two parts, as in the previous chapter. Figure 3.13, in Chapter 3, shows a typical phase plot of a maximally Ca-activated trabecula. This plot is explained in detail in the previous chapter. Refer back to the beginning of the 'Phase Shift: control conditions' for the explanation of the way phaseUp and Down curves differ, *i.e.* the stretching phase of the cycle (phaseUp angles) tends to be more affected than the lengthening phase (phaseDown angles). The SD in these experiments is an index of how much the phase angle varies along a single loop (or set of loops). Therefore it shows how far the loop deviated from the 'ideal' sinusoid with a constant phase shift where SD would be zero. (Refer back to the end of the 'Phase Shift: phase angle' section in Chapter 2 for further explanation). If the SD has gone up under the influence of the intervention, then this shows that the change in [Pi] and/or acidity has modified those elements of crossbridge kinetics that define the phase relationships.

### *Raised Phosphate*

It has been shown in the previous chapter that the position of characteristic features in the phase plot directly correlated with the position of  $f_{\min}$  in the stiffness-frequency plot. This is also true for the experiments involving phosphate. The comparison in Figure 4.3 of 2 mM added Pi, 5 mM added Pi, and 10 mM added Pi shows that  $f_{\min}$  does indeed increase as [Pi] rises. Therefore, it was expected that the phase plot would shift to the right to

higher frequencies at higher [Pi] in order to correspond to the results shown in the stiffness-frequency plots. This relationship was evident in these experiments and can be observed in Figures 4.5-4.7. The phase plot steadily shifts to the right with increased [Pi] just as  $f_{\min}$  does. The mean shift in frequencies between the control and 2mM added phosphate for the maximum phase angles was  $+1.50 \pm 0.18\text{Hz}$  for phaseUp and  $+1.3 \pm 0.62\text{ Hz}$  for phaseDown and minimum phase angles was  $+2.75 \pm 0.53\text{Hz}$  for phaseUp and  $+3.08 \pm 0.97\text{Hz}$  for phaseDown (n=3 for all values). The mean shift in phase angles between the control and 2mM added phosphate for the maximum phase angles was  $+13.82 \pm 2.02\text{ deg}$  ( $P < 0.05$ ) for phaseUp and  $+6.46 \pm 3.43\text{ deg}$  ( $P < 0.15$ ) for phaseDown and minimum phase angles was  $+8.30 \pm 2.73\text{ deg}$  ( $P > 0.50$ ) for phaseUp and  $+17.38 \pm 8.50\text{ deg}$  ( $P > 0.20$ ) for phaseDown (n=3 for all values). The mean shift in phase angles between the control and 2mM added phosphate for the maximum phase angles was  $+28.60 \pm 2.78\text{ deg}$  ( $P < 0.01$ ) for phaseUp and  $+17.72 \pm 13.16\text{ deg}$  ( $P < 0.15$ ) for phaseDown. The mean shift in frequencies between 2mM and 10mM added phosphate for the maximum phase angles was  $+4.42 \pm 0.87\text{Hz}$  for phaseUp (n=3) and  $+7.42 \pm 3.18\text{Hz}$  for phaseDown (n=3) and the minimum phase angles was  $+6.5 \pm 0.00\text{Hz}$  for phaseUp (n=1) and  $+1.25 \pm 0.00\text{Hz}$  for phaseDown (n=1). (See Table 4.3-4 for p values) The shift between 2mM and 10mM added phosphate for the minimum phase angles and frequencies for both phaseUp and phaseDown could not be quantified in most experiments because the minimum values lay beyond the frequencies used in these experiments.

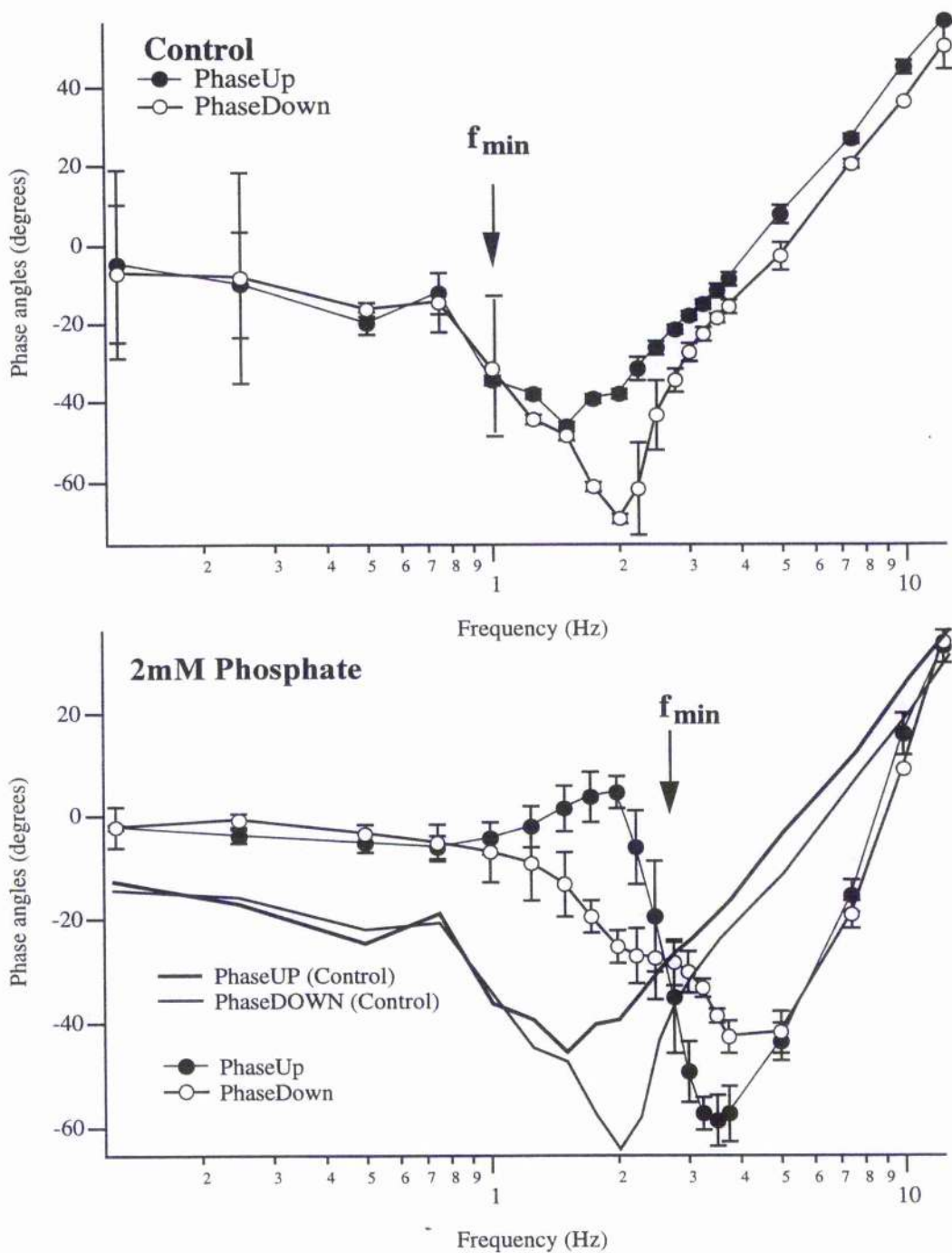


**Figure 4.5.** This figure shows the phase shift plot for a typical individual phosphate experiment. The thicker lines representing the control data (from panel A) are superimposed on those in the presence of 2mM phosphate (Panel B) to facilitate comparison. The error bars represent the standard deviation of shifts in phase at each frequency. At this [Pi], the phase plot still resembles that of the control. However, the point of most work absorbed (near 3.5Hz in both curves) is found at a slightly higher frequency.

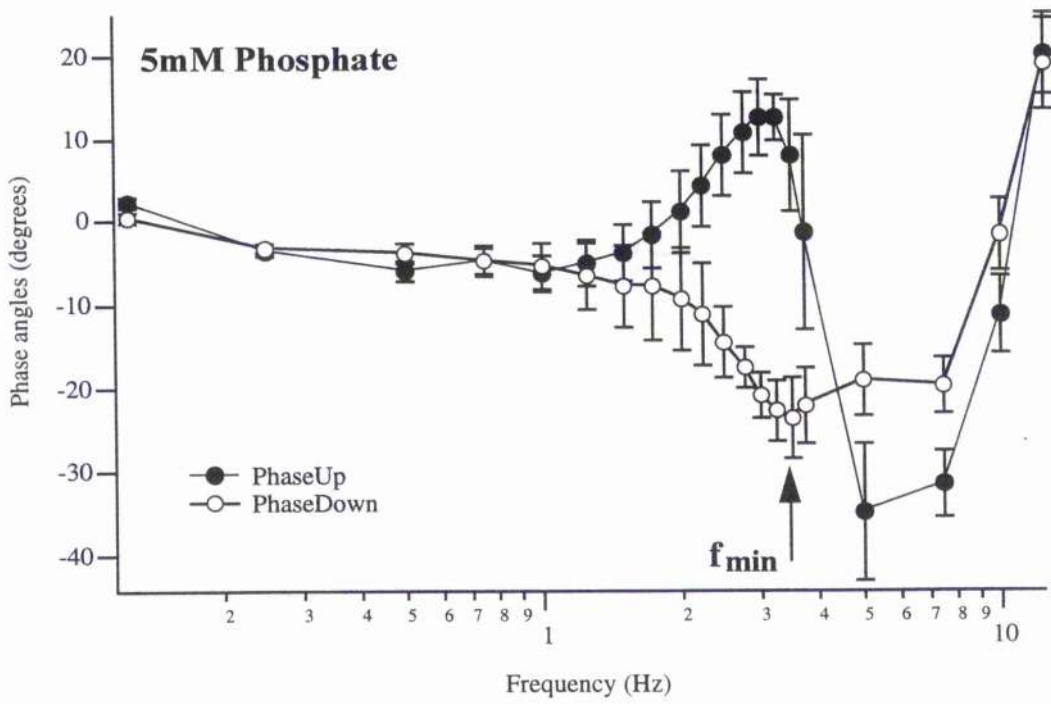


**Figure 4.6.** This is a typical phase plot with 5mM phosphate added to the activating solution. Because of the higher  $f_{min}$  with 5mM phosphate, the phase plot has also shifted comparatively to the right. At this [Pi], the phase plot no longer resembles that of the control. Instead there is a large amount of positive work done just below the where  $f_{min}$  is seen in the stiffness plot. Also, the amount of work absorbed has decreased significantly.

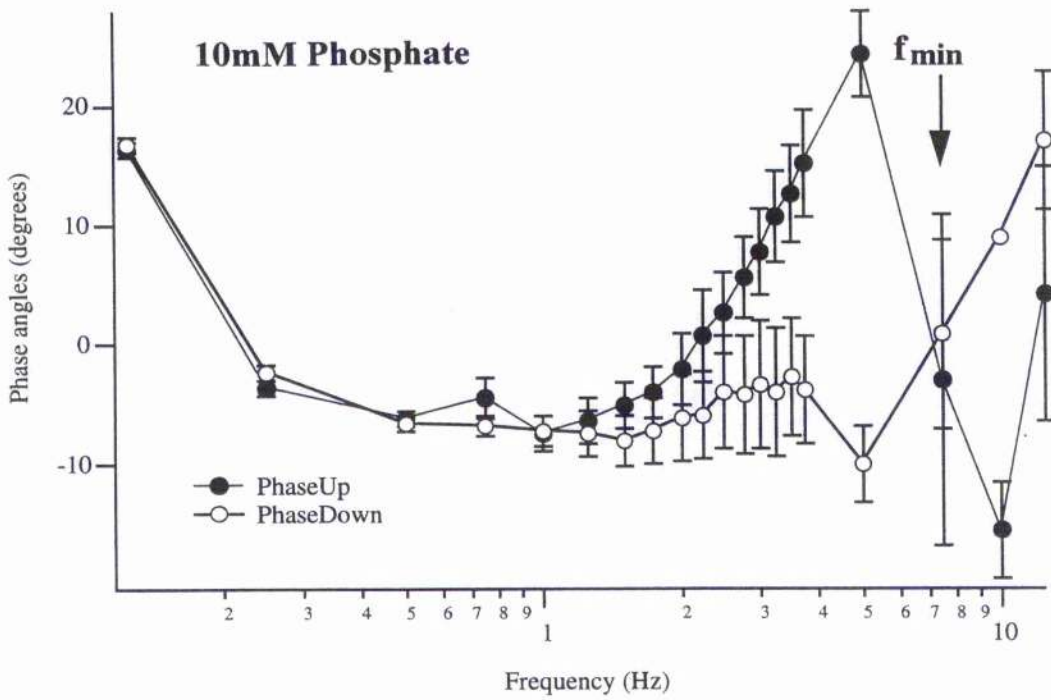


**Figure 4.7.** This is a typical phase plot obtained with 10mM phosphate. In keeping with the higher  $f_{\min}$  with 10mM phosphate, the phase plot has also shifted to the right. At this [Pi], the phase plot no longer resembles that of the control. Instead there is a large amount of positive work done just below the frequency (see Figure 4.6) where  $f_{\min}$  is seen in the stiffness plot. This amount of positive work has increase considerably compared with 5mM phosphate. Also, the amount of work absorbed has decreased significantly.

Table 4.3	Shift of Phase Plot from Control to 2mM added Phosphate (Hz)			
	Shift at Max Phase Angle	P=	Shift at Min Phase Angle	P=
PhaseUp	+1.50 ± 0.18	< 0.05	+2.75 ± 0.53	< 0.05
PhaseDown	+1.3 ± 0.62	= 0.12	+3.08 ± 0.97	= 0.06

\*n=3 for all experiments.

Table 4.4	Shift of Phase Plot from 2 to 10mM added Phosphate (Hz)			
	Shift at Max Phase Angle	P=	Shift at Min Phase Angle	P=
PhaseUp	+4.42 ± 0.87	< 0.05	+6.5 ± 0.0	*(n=1)
PhaseDown	+7.42 ± 3.18	= 0.10	+1.25 ± 0.00	*(n=1)

\* n=3 for all experiments except where noted.

The shape of the phase shift plot also shows a few changes at higher [Pi]. Figures 4.5-4.7 show that the initial inflection to positive phase angles for phaseUp shows a striking increase at higher Pi. Also, with an increase in [Pi], an inflection to positive phase angles develops for phaseDown where there was none at 0.9 mM [Pi]. This increase in positive

phase angles obtained near  $f_{min}$  reveals that the oscillatory work being done by the muscle has greatly increased.

The other change in the shape of the phase plot is with the deflection to negative phase angles typically just above the value of  $f_{min}$  from the stiffness-frequency graph. This deflection becomes less negative at higher [Pi]. This indicates that a rise in [Pi] reduces the negative work (work absorbed) at frequencies just above  $f_{min}$ . It is also apparent in Figure 4.7 that at higher [Pi], a shift between the overall phaseUp and phaseDown relationships becomes significant where the phaseUp curve is located significantly to the right of phaseDown.

Unlike the stiffness-frequency plot, there is no depression in the shape of the phase plot by Pi; actually the opposite is apparent. Positive work is increased while negative work is decreased. There is a shift in the position of the curve as corresponding to frequency, as well as change in the relative position between the phaseUp and phaseDown plots.

### **Work and Power Values**

Calculations for the change in work and power output between the control, 2mM and 10mM [Pi] were attempted using equation 2.4 and 2.5. However, due to the lack of positive phase values, physiologically relevant work and power values were not able to be obtained.

### **Phosphate and Acidic pH Combined**

#### ***Maximum Tension***

Maximum force varied greatly between the trabeculae. Therefore, all data are converted to percentages, with the maximum tension produced for the control run at pH 7 defined as 100%. Maximum tension in pH 6.5 and 10mM Pi combined was  $37.6 \pm 0.3$  % that of the

control ( $n = 2$ ). Since  $n = 2$  experiments of the pH 6.5 and 10mM Pi combination, there is no statistical analysis available.

### *Stiffness*

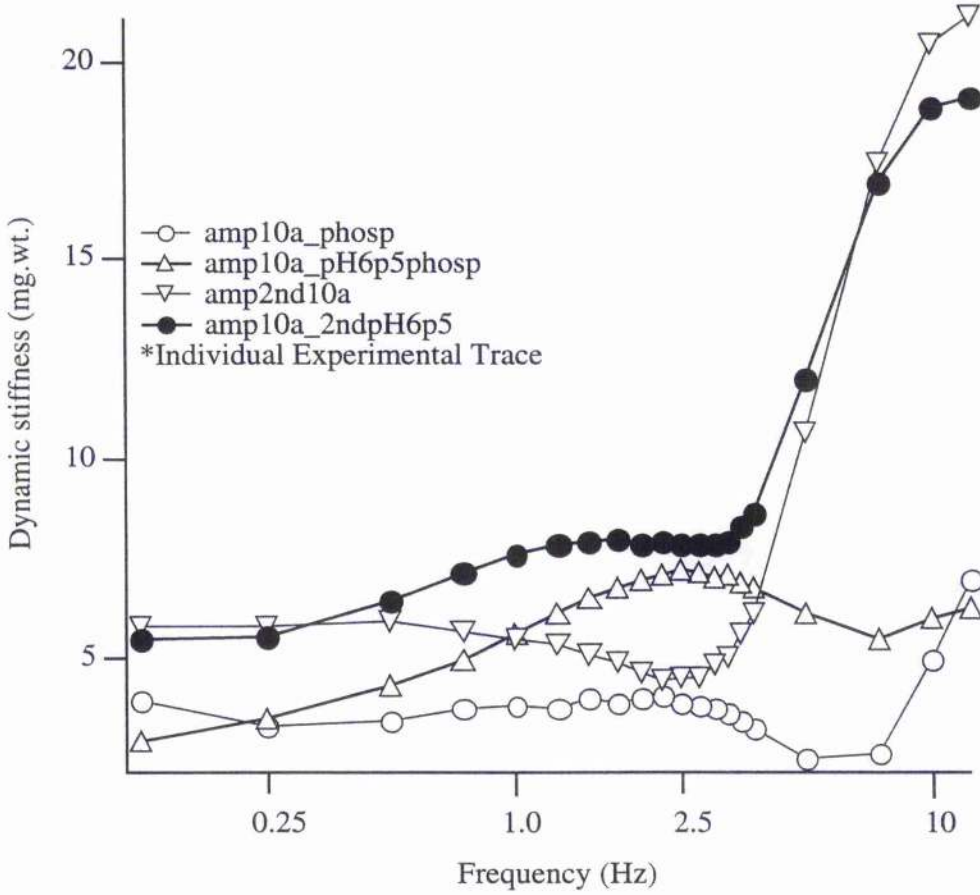
At pH 6.5 combined with 10mM phosphate, the entire stiffness-frequency curve shifts to the right, bringing  $f_{min}$  to a higher frequency, higher than with pH or Pi alone. Dynamic stiffness varied greatly between the trabeculae as it does for maximum force. Therefore, all data are converted to percentages, with the stiffness in the control run at pH 7 defined as 100%. The mean shift in  $f_{min}$  was  $466.7 \pm 188.6 \%$  that of control ( $n = 2$ ). Dynamic stiffness and the stiffness at  $f_{min}$  were higher than that at Pi alone but lower than at pH 6.5 alone. Dynamic stiffness was  $29.4 \pm 3.1\%$  of control ( $n = 2$ ). Dynamic stiffness at  $f_{min}$  was  $172.1 \pm 74.2\%$  of control ( $n = 2$ ). These features can be seen in Figure 4.8. Table 4.5 shows, for comparison, the values in % for one experiment where control and all three variables were examined on the same muscle fibre ( $n = 1$  for table, thus no SEM values available). Although the frequency at which the maximum stiffness occurs is perhaps not physiologically relevant, it gives a picture of the functional capacity of the crossbridges.

### *Phase*

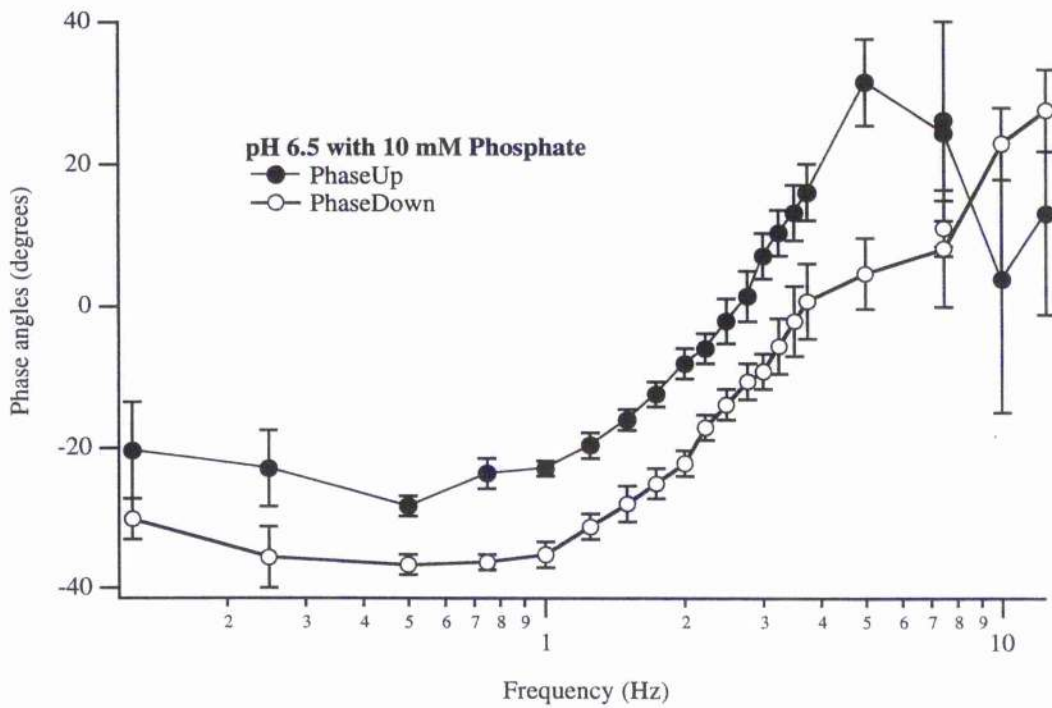
The shape of the phase shift plot also has a few differences compared to pH and Pi alone. Figure 4.9 shows that, at pH 6.5 with 10mM phosphate, the initial inflection to positive phase angles for phaseUp and phaseDown has shifted to higher frequencies just as the stiffness–frequency plot. The increase of phase angles just before  $f_{min}$  resembles the shape seen for 10mM phosphate alone. The quantitative analysis of the shifts between pH 6.5 combined with 10mM phosphate vs. control could not be done for either phaseUp or phaseDown because the data around  $f_{min}$  for the former has shifted beyond the values

of the graph (see Figure 4.9). Higher frequencies must be examined to reveal the entire shape of the curve relationship around where  $f_{\min}$  is found before complete analysis can be done.

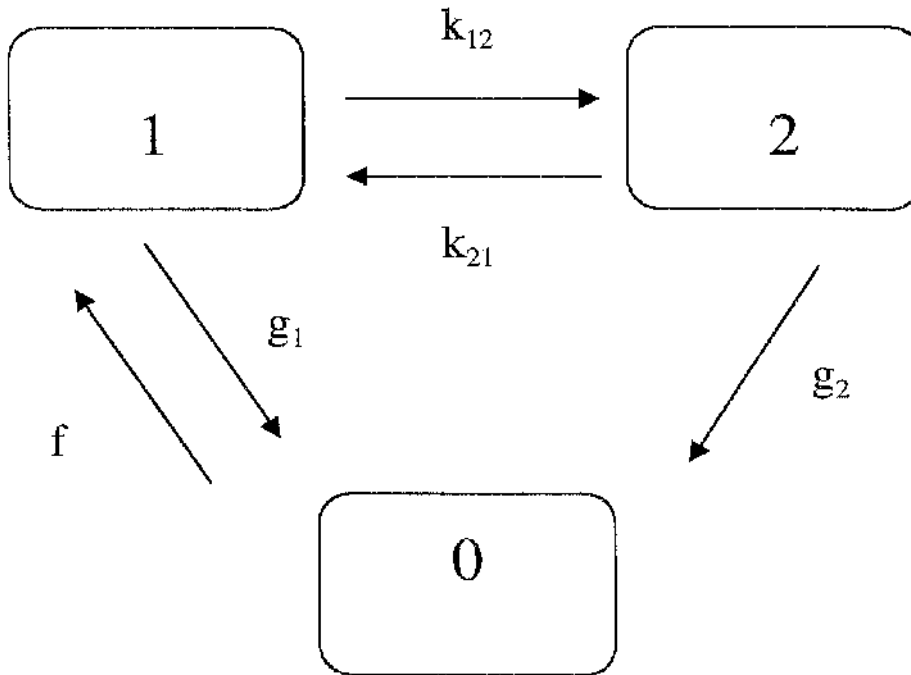
<b>Table 4.5</b>	pH 6.5 (% of control)	10mM Pi (% of control)	pH + 10mM Pi (% of control)
Maximum Tension	53.3	81.6	37.8
$f_{\min}$	222.2	144.4	333.3
Maximum Stiffness	34.9	85.7	31.6
Stiffness at $f_{\min}$	60.9	132.0	119.6



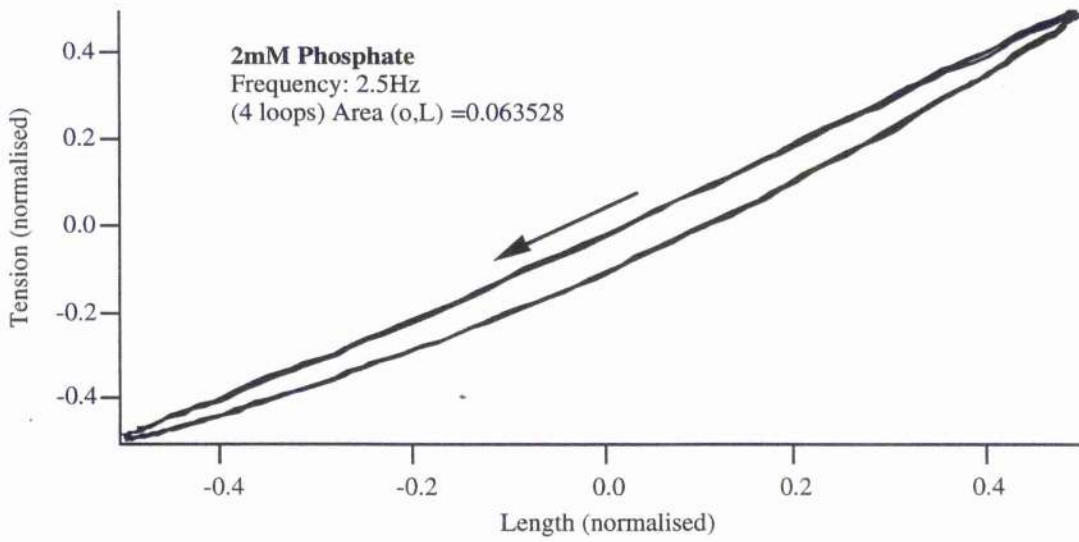
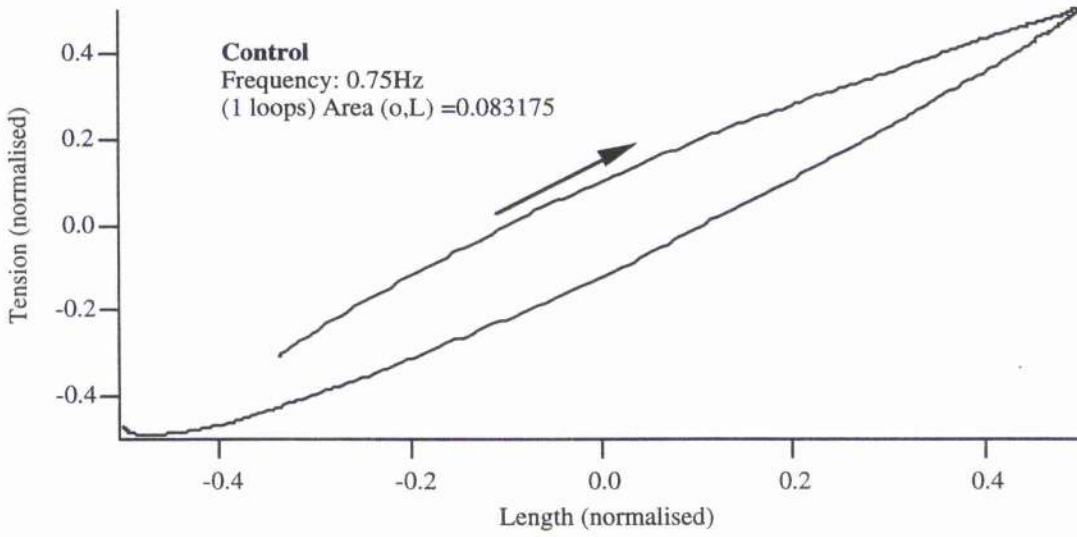
**Figure 4.8.** This figure shows a typical stiffness-frequency plot from a single experiment for pH 6.5 combined with 10mM phosphate.



**Figure 4.9.** This figure shows a typical phase plot for pH 6.5 combined with 10mM phosphate. The error bars represent the standard deviation of shift in phase at each frequency.



**Figure 4.10.** A schematic of the three-state model of Julian *et al* (1974), with modification to allow detachment from the low-tension state. (Rossmanith *et al* 1998) Crossbridges can occupy a detached state (state 0) and the two attached states (state 1 and state 2). State 2 is attained by crossbridges that have undergone a powerstroke, converting structural energy into mechanical energy. These three states are governed by the rate constant for attachment,  $f(x)$ , the two rate constants for detachment,  $g_1(x)$  and  $g_2(x)$ , along with the power stroke rate constant,  $k_{12}(x)$ , and the reverse rate constant,  $k_{21}(x)$ .



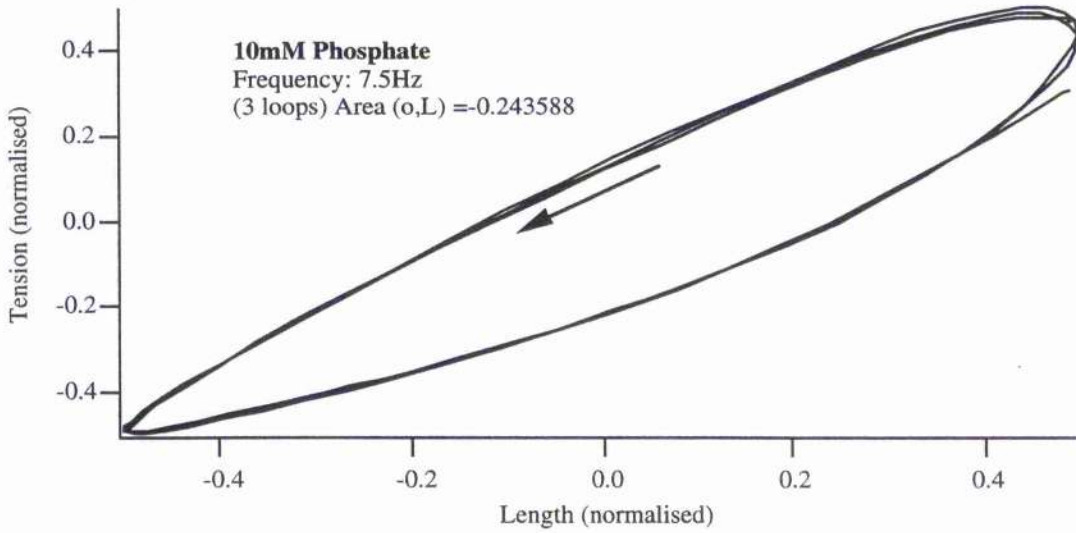


**Figure 4.11.** This figure shows an example of work loops obtained at control, 2mM and 10mM phosphate. (o = tension, L = length) All three loops are from the same experiment and are typical of all phosphate experiments done in this thesis. The work loop graphs shown are at the frequencies where the maximum phase angle (i.e. most positive work) existed within the physiologically relevant area. The arrows indicate the direction of the loop.

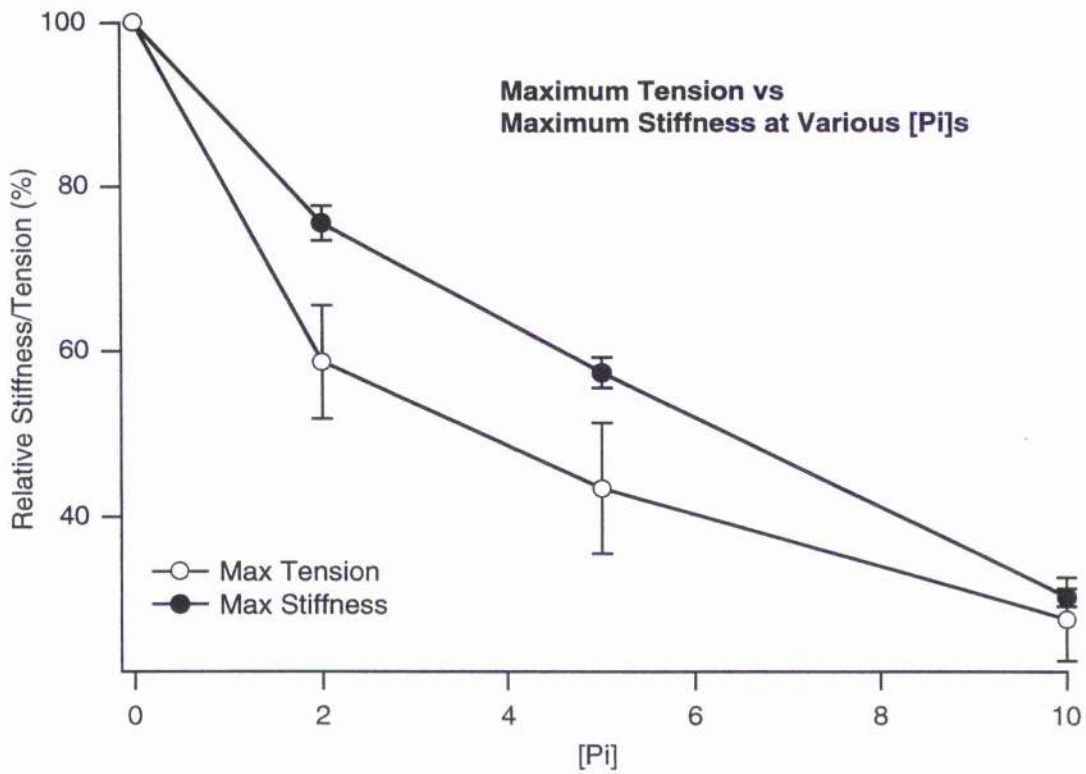


**Figure 4.12.** This figure shows the mean data for maximum tension vs maximum stiffness at various [Pi]s. The error bars represent the sem for each value. There is no sem at 0 mM Pi because 0 mM Pi acted as the control and was therefore regarded as 100%.

## DISCUSSION

### *Phosphate Alone*

On the conventional crossbridge cycle model, we can anticipate that Pi will favour bridges remaining longer in the pre-power stroke (Pi release) state i.e. weakly attached as {AM.ADP.Pi} bridges. This readily accounts for the widely observed force and stiffness reductions. Our results using the sinusoidal oscillation technique are similar to those reported earlier. The decrease in both maximum tension ( $P < 0.01$ ) and stiffness ( $P < 0.01$ ) (Figure 4.2-3) and the overall decrease in stiffness at all frequencies in the stiffness-frequency plots support the theory that increased [Pi] inhibits the crossbridge from entering the power-stroke state. The reliability of sinusoidal oscillation to obtain these results has been defended by recent analysis by Rossmannith and Tjokorda (1998). They have shown that crossbridge kinetic properties from conventional measurements, like maximum shortening velocity, or the rate of tension redevelopment after stretch and release, can be compared with those from sinusoidal oscillation. Their analysis showed that  $f_{min}$  is sensitive to the forward rate of the power stroke, and the detachment rate for the crossbridge under strain. To investigate the relationship between the various states in the crossbridge cycle, we can look at the three-state model of Julian *et al* (1974) with modifications proposed by Rossmannith and Tjokorda (1998) to allow detachment from the low tension state (state 1) as seen in Figure. 4.10. Under steady-state isometric conditions, crossbridges that occupy the first attached state contribute only to stiffness, because they are assumed to attach with no strain. The crossbridges that have undergone the power stroke and occupy the second attached state generate both stiffness and tension.

Actions of phosphate are significantly different between cardiac and fast skeletal muscle; Pi reportedly slows relaxation upon Ca reduction in the latter but speeds it in the former.

However, Pi binding at the ATP site is reportedly identical across cardiac, slow and fast skeletal (Cremona *et al*, 1990). This suggests that Pi may regulate force at a further site. Smith and Barsotti (1992) reported a reduction in maximum velocity of shortening ( $V_{max}$ ) for cardiac muscle whereas no change is reported for skeletal muscle (Altringham & Johnston 1985, Pate & Cooke, 1989b). This is supported by the analysis by Rossmannith and Tjokorda (1998) which reports  $V_{max}$  to be sensitive to the forward rate  $g_1$ . This seems consistent with a reduced isometric ATPase rate (skeletal, Kawai *et al* 1987, cardiac: Schmidt-Ott *et al*, 1990). These effects on force were thought to be explained by reversal of the Pi-release step in the crossbridge cycle by mass action of Pi. However, if force were proportional to the number of attached crossbridges, mass action would imply that the overall crossbridge cycling rate and the isometric force would decrease in proportion. Yet, it has been shown that tension falls more steeply than ATPase (Ebus *et al* 1994). Our results show that maximum tension does fall more steeply than maximum stiffness in cardiac muscle (Figure 4.12). (Data approaching significance with  $p = 0.20$ ,  $n$  only = 6) This implies fewer bridges entering the power stroke step(s) and decreased mean force per XB. Our results show a decrease in force proportional to previous reports, but also show that crossbridge kinetics relating to the crossbridge cycling rate actually speed up with increased [Pi]. This disproportion between force and stiffness (also reported by others for cardiac m.; Mekhfi & Ventura-Clapier, 1988, Smith & Barsotti, 1993, and for skeletal m., Kawai *et al*, 1987, Hibberd *et al* 1985, Martyn & Gordon, 1992) seems to require actions additional to the simple 'mass action' of Pi as a reaction product.

Release of caged Pi in skeletal muscle in isometric contraction results in a decline of force. This is interpreted to mean that a transient {AM.ADP.Pi} force-generating state exists. Raised [Pi] favours the crossbridge to persist in this step and thus explains slowed relaxation seen in skeletal muscle. Since the opposite is reported to occur in cardiac muscle (Simnett *et al*, 1998) it may be that this step is too short lived to contribute here.

Several experimental circumstances demonstrate increased crossbridge cycling under Pi. Our results, using sinusoidal oscillation, show a significant speeding of crossbridge kinetics, even with the addition of as low as 2 mM Pi ( $P < 0.05$ ). Releasing caged Pi in rigor muscle speeds relaxation (low Ca) and force redevelopment (high Ca) in both skeletal and cardiac muscle (Hibberd *et al* 1985, Barsotti & Ferenczi, 1988). This can be explained if Pi binding to {AM.ADP} bridges reverses the power stroke and thus favours other 'back' reactions, provided significant relaxation occurs by that route (but see *e.g.* Hoskins *et al*, 1999). It is also energetically favourable, because the energy otherwise dissipated in the power stroke is regained, apart from energy expended in Pi rebinding itself.

The interpretation of the phase analysis despite the lack of positive phase angle has been discussed in the Discussion section of Chapter 3 and is also relevant to this chapter. In summary it states that although the phase curves may not cross to positive angles (just below  $f_{min}$ ), that region of the curve still relates to the ability to generate work (or at least absorb the least work) at those frequencies. Our frequency-phase plots indicated a significant increase in positive phase shift just below  $f_{min}$  in the presence of 2mM Pi ( $P < 0.05$ ) and 10 mM Pi ( $P < 0.01$ ). This increase indicates that the attached crossbridges are doing a larger amount of oscillatory work at raised [Pi]. This conclusion is supported by the length-tension loops, which show an increase in area at higher [Pi] (Figure 4.11). The change in the loop direction must also be taken into account when viewing Figure 4.11. The work loop for the control is going clockwise (*i.e.* negative work) while the loops for 2 and 10mM phosphate are going counter-clockwise (*i.e.* positive work.) This increase in work-loop areas probably requires that other steps, such as the forward power stroke,  $k_{12}$ , are also increased. The oscillation protocol forces crossbridges to redistribute their attachment states from the steady-state isometric distribution. This reveals that, for the reduced population of attached bridges at high Pi, the ability to generate work (Figure 4.7) is actually greater.

Since the optimum frequency at which this achieved is also higher, greater power per bridge is possible. For overall contractile function, these features will tend to mitigate the other effects of raised Pi, possibly in an energetically favourable way. This is a previously unsuspected and unreported result of cardiac myofilament function under conditions of high [Pi].

### ***Phosphate and Acidic pH Combined***

It has been established that acidosis has a detrimental effect on crossbridge kinetics. An increase of  $[H^+]$  could potentially depress crossbridge kinetics by changing the rates of reactions in the crossbridge cycle, either by mass action at steps where  $H^+$  participates in the reaction, or by  $H^+$  influencing enzyme activity, or by other actions such as changing myofilament spacing. The effects of Pi have also been studied here and show a negative effect on force but a positive effect on oscillatory work and occasionally power. The combined effects of these chemical factors associated with ischaemia and hypoxia on cardiac muscle kinetics have only been explored in terms of force but not regarding work and power.

It has been shown recently that the effects of Pi and of pH on isometric force are independent in cardiac muscle (McLaughlin & Godt, 1990, Kentish, 1991, Ebus *et al.*, 1994) and that  $H^+$  and Pi release are unlikely to occur at the same step in the crossbridge cycle. It has been suggested that, in skeletal muscle, Pi and  $H^+$  release occur at nearby reactions (Bagshaw & Trentham, 1974). Kentish (1991) stated that this is true for cardiac muscle also, and suggested that  $H^+$  release may immediately precede that for Pi. If this is true, it is improbable that the main action of  $H^+$  is by reversal of the Pi release step. However, mass action by  $H^+$  could be involved in other steps. The reduction of force could result from the reversal of the transition of  $M^*.ATP$  to  $M^{**}.ADP.Pi$ , (Step 2 in Figure 1.6) thus inhibiting crossbridge attachment, or by encouraging the transition from

AM\*.ADP to AM (Step 6 in Figure 1.6) and thus promoting crossbridge detachment (Kentish 1991).

These conclusions are drawn from their results showing how the average force under ischaemic conditions is not significantly different from the product of the relative reductions in force of increased [Pi] or decreased pH separately (Kentish 1991, Ebus 1994). Our results differ with these previous reports, where we found that a decrease in acidity and Pi separately yield more than a 50 to 60% reduction in force. However, the combined effect of acidity and Pi yielded around a 30% decrease in force. This difference can be due to the variation in concentrations of Pi and H<sup>+</sup> in the experimental protocol. Both Kentish and Ebus used 30mM Pi with the pH at 6.2. It has been well established that during heart failure, pH falls as low as 6.2 and that the full effects of Pi are reached at concentrations of 20mM or more. Our study did not involve the full effect of Pi or pH. Therefore, it can be concluded that, at sub-maximal concentrations of Pi and H<sup>+</sup>, the synergistic effect of Pi and acidity are greater on average force than that of Pi or H<sup>+</sup> independently. It has been concluded by other workers that Pi and H<sup>+</sup> act as if they have completely different effects on maximum force production. However, taking our results into account, it seems that they definitely do affect each other although the mechanisms remain unclear.

Although our results concerning force reduction do not give evidence for independent actions of acidity and Pi, our results regarding stiffness,  $f_{min}$ , and work clearly testify that the release of Pi and H<sup>+</sup> must be at different steps in the crossbridge cycle and that their effects work through independent mechanisms. Unlike the effects on force, acidity and Pi, independently, had opposite effect on stiffness and work. However, when applied together, the results combined the effects of both factors. These effects may help to reduce the potentially fatal effects of acidosis plus raised [Pi] during ischaemia in cardiac muscle in terms of pump function.

**CHAPTER 5 RELAXATION KINETICS OF RAT CARDIAC TRABECULAE  
USING AN 'EGTA-JUMP' PROTOCOL**

## INTRODUCTION

CHF does not only develop in heart with systolic dysfunction. It is established that diastolic dysfunction can begin the CHF process at a much earlier stage, before contraction becomes inadequate (Braunwald & Ross, 1963, Hirota, 1980). Diastolic dysfunction is the major pathophysiological mechanism in approximately 40% of patients with symptoms of CHF (Soufer *et al*, 1985, Nwasokwa, 1993, Vassen *et al*, 1996). Most treatments for CHF involve treatment for systolic dysfunction. This is useless, or even detrimental, for a patient suffering from diastolic dysfunction (Lorell, 1991). Therefore it is vital to understand the diastolic properties of cardiac muscle, which include aspects of relaxation as well as the resting properties (such as passive elasticity) of myocardium in order to develop appropriate treatment.

In smaller mammals, such as rat, the slowing of the crossbridges associated with the development of CHF can be accounted for by a change in the predominant myosin isoform within the ventricles. The predominant myosin isoform, found in normal rat myocardium, is the  $V_1$  type ( $\alpha\alpha$ -homodimer). However, with chronic overload, a shift in the predominant isoform from the  $V_1$  to the  $V_3$  type ( $\beta\beta$ -homodimer) occurs. The former of these isoforms has a faster ATPase rate (Lompre *et al*, 1979), but lower force generating capacity than the latter (Van Buren *et al*, 1995). This isoform shift is considered to be an energy-efficient adaptation to myocardial stress (Alpert & Mulieri, 1982) such that normal tension can be developed at a lower ATP cost. In larger mammals such as the rabbit and human, a change in the distribution of myosin isoforms cannot account for the slowing of the intrinsic crossbridge cycling rate (Mercadier *et al*, 1983), since the predominant isoform present in the normal myocardium is already of the slowest,  $V_3$  type.

Assessing myocardial relaxation in the working whole heart is complicated due to the variations in the load imposed on the heart (Brutsaert *et al*, 1980) and the non-uniformity of adjacent myocardial segments (Blaustein & Gaasch, 1983, Brutsaert, 1987). Collectively, these can alter the variables used to define the lusitropic state. Therefore, the majority of studies examining the activation and relaxation kinetics of cardiac muscle have used isolated preparations, such as papillary muscles, trabeculae or single myocytes, rather than the whole heart. Using these isolated preparations in kinetic studies removes the complications just described.

In diastole, cytosolic free  $[Ca^{2+}]_i$  is about 0.2  $\mu M$ . Muscle relaxation begins after  $[Ca^{2+}]_i$  starts to return to resting concentrations. The initial removal of free  $Ca^{2+}$  occurs via uptake into the SR. As the  $[Ca^{2+}]_i$  falls in the cytosol, the dissociation of  $Ca^{2+}$  from TnC on the thin filament is favoured. The free  $[Ca^{2+}]_i$  is thus partially buffered by the release of  $Ca^{2+}$  from TnC. Once TnC is deactivated, the associated Tm is able to relocate in its inhibitory position along the thin filament, provided there is no steric hindrance by active bridges still in mid-cycle. The return of Tm to its resting position prevents any further crossbridge attachment. As the crossbridges detach, and are not replaced by new attachments, force declines and relaxation occurs. The rate at which force declines in intact preparations depends on the efficiency of these mechanisms.

In these experiments, the preparation is chemically skinned (as described in the Methods Chapter) before examining its relaxation kinetics. The SR and sarcolemma are completely disrupted throughout the preparation and are no longer functional. This means that the bathing solution surrounding the preparation essentially becomes an extension of the intracellular environment. This allowed the relaxation kinetics of the myofilaments alone to be studied without the intervention of the SR; the rate at which the SR sequesters  $Ca^{2+}$  no longer needs to be considered as a possible rate limiting factor in relaxation. Thus, the main factor now governing the rate decline of  $[Ca^{2+}]_i$  is the rate and

extent of  $\text{Ca}^{2+}$  binding to the Ca buffer used in these experiments. Provided the Ca-buffer capacity is sufficient, any observations on relaxation rate can be confidently attributed to the properties of the myofilament proteins themselves.

Relaxation is produced when the  $[\text{Ca}^{2+}]$  bathing a previously Ca-activated muscle is abruptly reduced. We have combined  $[\text{Ca}^{2+}]$  reduction with [Ca-buffer] increase to accelerate relaxation as far as possible. If a sufficiently high [EGTA] gradient can be used, where Ca (and its buffer) diffusion is no longer rate limiting, relaxation speed should reflect crossbridge detachment rate. In these experiments, preparations are maximally Ca-activated (*c.* pCa 4) but only weakly Ca-buffered (0.2mM total EGTA, ionic balance with 50 or 100mM HDTA). Relaxation was induced by immersion in a range of [EGTA] (0.5-100mM), nominally Ca-free solution (pCa 7.2 or greater)

The complexities of the diffusion problem involved, of Ca-buffering and of the highly non-linear relationship between  $[\text{Ca}^{2+}]$  and tension required that the assumptions about buffering speed produced by the [EGTA] step be tested. A mathematical model was constructed (by D.J. Miller, 1999, University of Glasgow), taking account of the diffusion-with-buffering process in the muscle as [EGTA] rises,  $[\text{Ca}^{2+}]$  falls and of the relationship of  $[\text{Ca}^{2+}]$  to tension. Here, the rate of  $[\text{Ca}^{2+}]$  (and therefore tension) decline is assumed to be diffusion-limited and thus it is predicted to increase with total [EGTA] step.

The mathematical model of the experimental situation of an instantaneous change in external [EGTA] leading to the diffusion-limited movement of EGTA into the preparation was set up in the following way:

In order to calculate the relative tension expected at a given time during relaxation produced by lowering  $[\text{Ca}^{2+}]$  with EGTA, the following assumptions and simplifications have been made:

i. each preparation is regarded as cylindrical in shape and initially fully equilibrated to the external solution.

ii. the preparation cross section is initially treated as fifty concentric annuli of equal thickness that fill its entire cross-section (see Figure. 5.1).

iii. to model the effects of an 'unstirred layer' or even a superficial layer of damaged myofibrils, the outermost annulus of the preparation (*i.e.* no. 50) was considered not to contribute to the force generation of the trabecula.

iv. the Hill equation adequately describes the instantaneous relationship between  $[Ca^{2+}]$  and tension.

v. the inward diffusion of free EGTA only was considered *i.e.* the simultaneous outward diffusion of CaEGTA, was neglected. In those cases of greatest relevance, the higher [EGTA] steps, the latter process will hardly have time to develop before the situation within the tissue is effectively dominated by incoming free EGTA.

The solution for the conditions described is given by Crank (1956, equation 5.22):

$$\frac{C - C_1}{C_0 - C_1} = 1 - \frac{2}{a} \sum_{x=1}^{20} \frac{e^{-D\alpha x^2} J_0(r\alpha)}{J_1(a\alpha)} \quad (\text{Equation 1})$$

where C is the concentration for a particular annulus and a particular time,  $C_0$  is the surface concentration,  $C_1$  is the initial concentration in the cylinder,  $J_0$  is the zero order Bessel function of the first kind,  $J_1$  is the first order Bessel function, D is the diffusion coefficient for EGTA,  $t$  is time in seconds,  $\alpha_n$  is the  $n$ th root of the Bessel function,  $r$  is the radius of interest and  $a$  is the outer radius of the cylinder. For computational stability, the first twenty roots of the Bessel functions were taken. D was taken as  $5 \cdot 10^{-7} \text{ cm}^2 \text{ sec}^{-1}$  (Kushmerick & Podolsky 1979).

By solving Eqn 1 for various times after an increase in extracellular [EGTA] (=C<sub>0</sub>), [EGTA] (=C) in each annulus can be calculated. (This calculation would also predict the fall of the [CaEGTA] as that species can be considered to diffuse outward.) Knowing both [EGTA<sub>free</sub>] and [CaEGTA] in each annulus for a given time, we can calculate [Ca<sup>2+</sup>] (by solving the following quadratic equation from an unpublished derivation: DJ Miller and DG Moisescu, 1976):

$$(Ca_{free})^2 * K + Ca_{free} * (1 + K(EGTA_{total} - Ca_{total})) - Ca_{total} = 0$$

(Eqn: 2)

The initial [Ca<sub>total</sub>] was taken as 0.22 mM, that of initial [CaEGTA] plus 20μM, the known contamination level. *K* adequately describes the interaction of EGTA and Ca under the prevailing conditions (5\*10<sup>6</sup>M).

Next, we consider how to derive tension from the momentary value of [Ca<sup>2+</sup>]. Knowing [Ca<sup>2+</sup>] for each annulus, relative tension is calculated (from the Hill equation below):

$$\frac{C_x}{C_{max}} = \frac{K_{Ca}^{-h} [Ca^{2+}]^h}{1 + K_{Ca}^{-h} [Ca^{2+}]^h} \quad (\text{Eqn: 3})$$

where *h* is the Hill coefficient, *C<sub>max</sub>* is the maximum force at saturating Ca<sup>2+</sup> levels, *C<sub>x</sub>* is the force at a given [Ca<sup>2+</sup>] and *K<sub>Ca</sub><sup>-h</sup>* is the reciprocal of the [Ca<sup>2+</sup>] producing half *C<sub>max</sub>* raised to the power *h*. This simplification that Equation 3 applies instantaneously has been used by other authors in similar circumstances (*e.g.* Westerblad & Allen, 1994).

Tension attributable to each annulus was assumed proportional to its fractional area (A<sub>n</sub>=r<sub>2</sub><sup>2</sup> - r<sub>1</sub><sup>2</sup> / r<sub>0</sub><sup>2</sup>), where *r<sub>1</sub>* and *r<sub>2</sub>* are the outer and inner radii of the annulus and *r<sub>0</sub>* the overall preparation radius). Summing tension for all the annuli at a given time yields total

relative tension. Typically, tensions for each of 20 times covering the total time of interest were calculated for a given condition.

The model was run in MS Excel. Graphical output showed both relative equilibration of the cross section and relative activation of the annuli. When the mathematical solution proved unstable (*e.g.* at very brief times), or where the relative tension changes very steeply, spatial resolution was increased by modelling 20 to 40 additional annuli across the region of steepest buffer or  $[Ca^{2+}]$  concentration change.

## **METHODS**

### **Protocol**

The trabeculae were mounted for isometric force measurements, as previously described in Chapter 2, and skinned in Triton-X100. The preparations were then activated in 0.2A (Solution B), allowing tension to develop until reaching its maximum. Once this had occurred, the digitising rate was increased to 400 Hz, to ensure that enough data points were recorded to examine the rate of relaxation as the preparation was relaxed in the appropriate relaxing solution. This protocol was repeated for each of the relaxing solutions E-I (Table 5.1 below), which differed in their [EGTA]. A 2-4 minute period was allowed between each cycle of contraction and relaxation where the preparation was immersed in solution B. The [EGTA] steps were applied in random order to examine whether the sequence of application of these solutions affected the results. (The results did not significantly differ with various orders of relaxing solutions).

### **Solution composition**

The composition of the solutions used for these experiments is shown in Table 5.1:

Table 5.1 [EGTA] of relaxing and activating solutions							
Solution components	0.5mM 'E'	2mM 'F'	5mM 'G'	15mM 'H'	50mM 'I'	100mM 'J'	0.2mM Activating
EGTA (mM)	0.5	10	5	15	50	100	-
HDTA (mM)	99.5	98	95	85	50	-	98.8
CaEGTA (mM)	-	-	-	-	-	-	0.2
MgCl <sub>2</sub> (mM)	6.5	6.5	7	7	8	8.5	6.5
HEPES (mM)	25	25	25	25	25	25	25
Na <sub>2</sub> ATP (mM)	5	5	5	5	5	5	5
Na <sub>2</sub> CrP (mM)	15	15	15	15	15	15	15
DTT (mM)	10	10	10	10	10	10	10

### Curve Fitting

The relaxation transients were well fitted in virtually all cases with a single exponential curve after the first 5-10% of tension fall (examples are shown in Figure 5.1). It is important to note that forcing a two exponential fit invariably resulted in two components of almost identical time constant, or one with a significantly slower time constant that only contributed a few percent to the total relaxation amplitude.

Fitting was done, with the program Igor Pro ver 3.3, to the following equation:

$$y=A+B*\exp(-kr*t)$$

where **A** is the residual (or baseline 'offset') tension, **B** is the initial tension value minus the residual (*i.e.* the extent of the exponential fall), **kr** is the rate constant for relaxation and **t** is time in seconds. The value of **kr** obtained from each relaxation transient, for a

single preparation, was then plotted against [EGTA]. A best-fit saturating equation of the form:

$$y=C*[1-\exp(-kE*D)]$$

was fitted to the resulting plot, where **C** is the offset, **kE** is the rate constant for the rate of change of tension at the various [EGTA] and **D** is the [EGTA]. Equation 5 therefore predicted the maximum rate of relaxation for each preparation obtained from the line of best fit, and this value was compared with the maximum rate obtained experimentally. Both the individual and mean data sets were fitted in this manner. It was found that the mean curve and maximum rate were representative of the data set.

## RESULTS

Values calculated from the diffusion-equation model (as tension vs. time) were well fitted with single exponentials (as illustrated); this proved adequate to describe most of the theoretical tension fall, as with real relaxations (shown later). The time constants derived from this process are plotted for various [EGTA] steps (Figure 5.2).

From the tension vs. time plot obtained with the diffusion modelling described earlier, the experimental model predicts that the relaxation rate will continue to increase if  $\text{Ca}^{2+}$  is the only rate limiting factor in these experiments (Figure 5.3). Some properties of the model have been explored to test its behaviour. For a given modelled diameter, an increase in diffusion coefficient ( $D$  in equation 5) produces a parallel, upward shift in the log rate vs. log [EGTA] plot. Further, the effect of a reduction in radius at a given value of  $D$  is to steepen the slope and displace upward on the Y axis. These properties conform to what one would expect for the model.

Figure 5.1 shows the relaxation transients obtained (for the step to 100mM EGTA) during a typical experiment. The transients were well fitted with a single exponential curve fit. The exponential curve fit so well at some [EGTA] concentrations that it is difficult to distinguish between the original data and the curve fit at various sections of the curve (Figure 5.1 and 5.4). The relaxation was repeated at each [EGTA] on each fibre and showed that there was no significant difference between both either runs ( $P > 0.25$  or more for all [EGTA]s).

Figure 5.2 shows the relaxation rate constants obtained from the exponential curve fitting process for all the EGTA step experiments. The range of rate constants derived over the range of [EGTA]-steps is well fitted with a rising '1-exponential' curve as shown in Figure 5.1 (from Eqn 5). In this particular example, the best fit curve reaches a defined

plateau, indicating that at this [EGTA]-step some other slower intervention, other than the rate of  $[Ca^{2+}]$  decline, is limiting the rate of trabecular relaxation.

The results obtained from these experiments gave the strong impression the rate saturates at the highest [EGTA] step (see Figure 5.3). However, the slope of the theoretical relationship is shallow, making it difficult to conclude with confidence, from linear plots, that there is a significant departure between the theoretical and practically-observed rates of relaxation. However, when the diffusion model and actual data are compared on the double log axes, the deviation is more apparent (Fig. 5.3). The extent of deviation between observed and modelled behaviour implies that the preparations do reach a region where the relaxation rate is no longer defined by the rate of fall of  $[Ca^{2+}]$ .

Figure 5.3 shows a log-log plot of the rates of relaxation at different [EGTA]-steps. This figure clearly shows a deviation between the actual and model-based rate of relaxation at, or beyond, the 50mM [EGTA]-step. Data for this figure is shown in Table 5.2. It shows that the diffusion-limited rate of tension decline is still predicted to increase, though the actual data indicates a rate plateau. At this point, some slower factor, such as crossbridge kinetics, becomes rate-limiting for relaxation. Since the rate of relaxation is beginning to saturate in the preparations, it indicates that we are approaching the maximal rate that is governed solely by myofilaments with this protocol.

**Table 5.2      Theoretical vs. Actual Relaxation Rates at Various [EGTA]s**

<b>[EGTA]</b>	<b>Theoretical Data (approx. figures) (sec<sup>-1</sup>)</b>	<b>Actual Data (mean figures) (sec<sup>-1</sup>)</b>	<b>P Values (Theoretical vs. actual)</b>
<b>100</b>	7.75	3.51 ± 0.59	< 0.01
<b>50</b>	5.95	3.33 ± 0.66	< 0.01
<b>15</b>	3.25	2.60 ± 0.55	> 0.10
<b>5</b>	1.90	1.91 ± 0.51	> 0.20
<b>2</b>	1.30	1.16 ± 0.27	> 0.20
<b>0.5</b>	0.67	0.68 ± 0.30	> 0.20

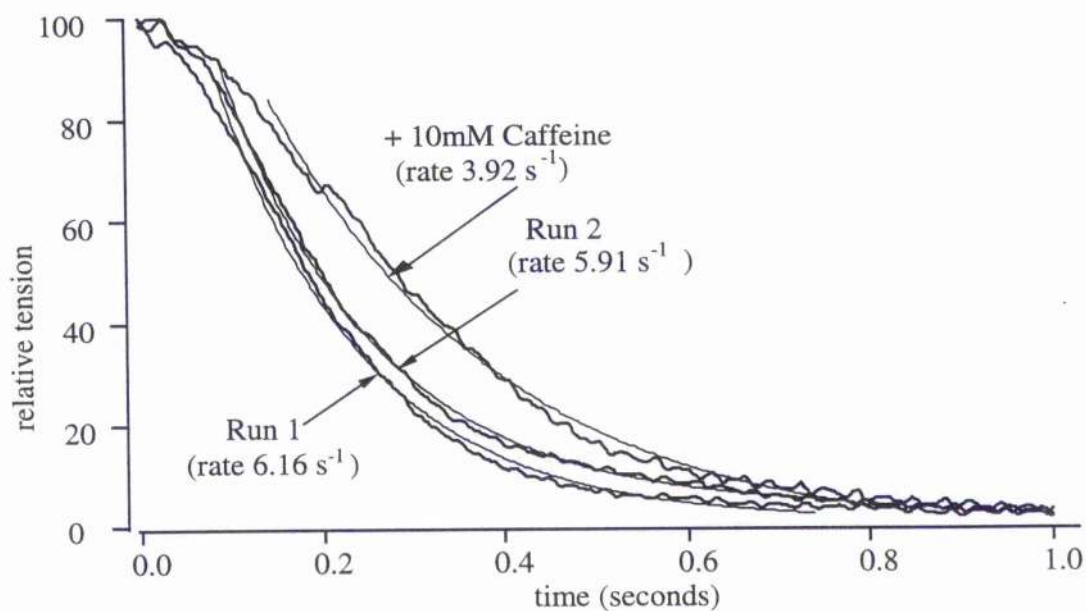


**Figure 5.1.** This figure shows three experimental traces at the 100mM EGTA step including one with 10mM Caffeine present. Single exponentials (thinner, smoother curves) have been fitted for each relaxation curve and, after the initial delay, provide a satisfactory fit to most of the relaxation time-course. (rate constants shown)

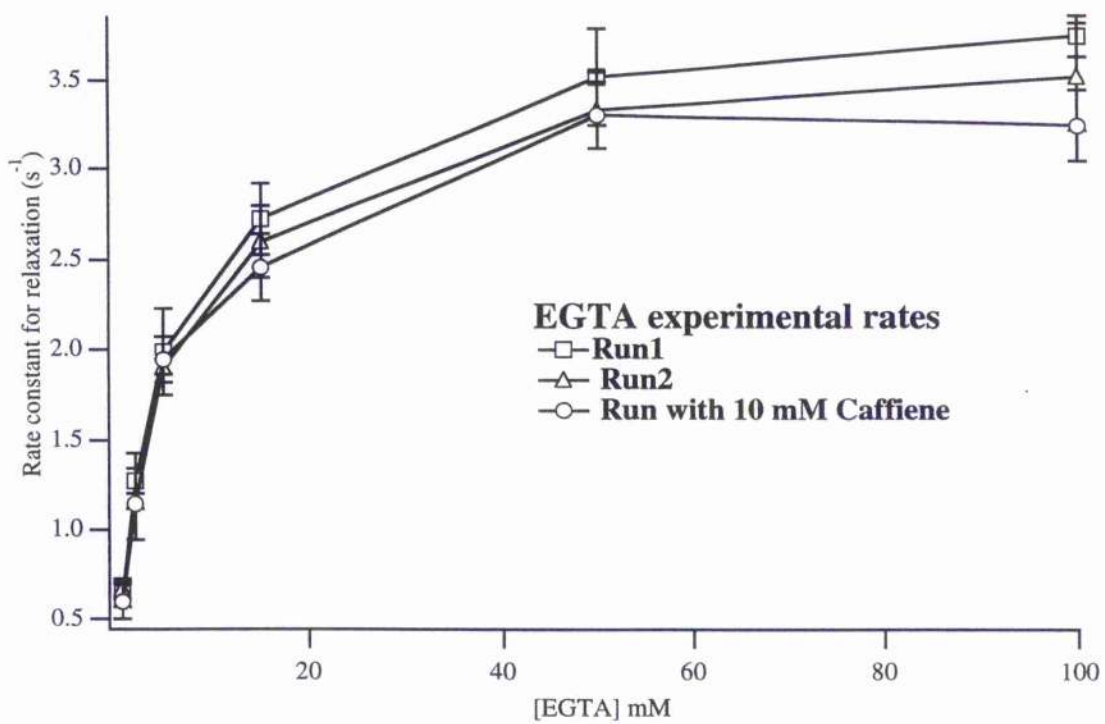


**Figure 5.2.** This figure shows the average from all the EGTA step experiments (n=5) of the rates constants obtained from best-fit curve fitting for each concentration and run.

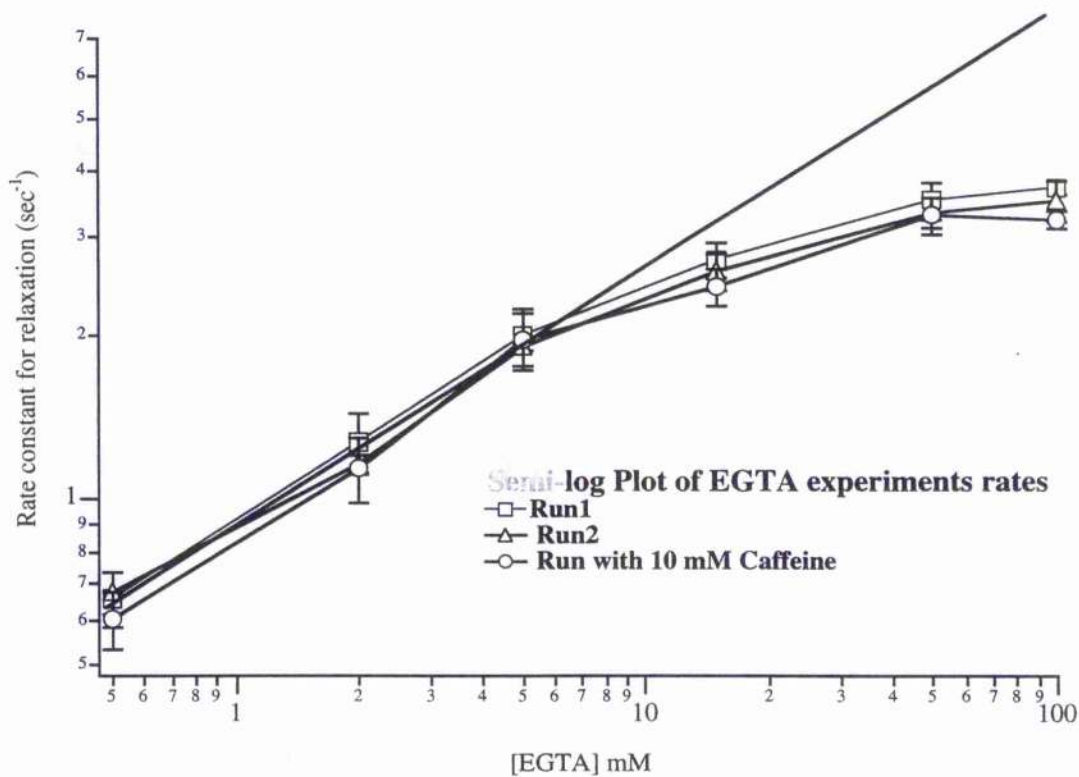


**Figure 5.3.** This figure shows a log-log plot of the rate constant averages from all the EGTA experiments. The straight black line represents the progression in relaxation speed predicted by the model. The actual data separate from the theoretical data around the 20mM EGTA step, indicating that another rate limiting factor exists at these speeds, which has been identified in this chapter as the crossbridge detachment rate.

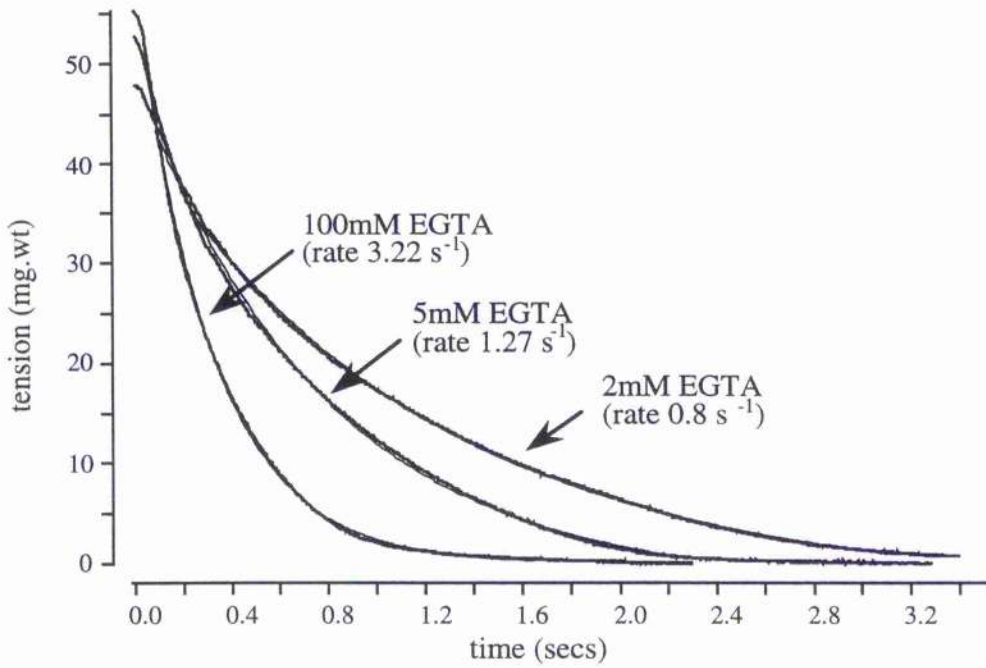


**Figure 5.4.** This figure shows three experimental traces at the 100mM, 5mM, and 2mM EGTA steps including the single exponentials (thinner, smoother curves) have been fitted for each relaxation curve. Note that the fitted exponentials provide a satisfactory fit to most of the relaxation time-course. (rate constants shown)

## DISCUSSION

The rate of relaxation of skinned trabeculae from rat myocardium was investigated by applying a range of different concentrations of the  $\text{Ca}^{2+}$  buffer EGTA within the bathing solution. The skinning procedure ensured that any influence of the SR would have had on relaxation, by re-sequestering  $\text{Ca}^{2+}$  or acting as a diffusion barrier, was eliminated. With no functional SR, the main factor controlling the uptake of free  $[\text{Ca}^{2+}]$  is the binding of the ion to available EGTA, with the rate of dissociation of  $\text{Ca}^{2+}$  from TnC influencing the level of free  $\text{Ca}^{2+}$ .

Previous literature shows other labs altering the concentration of the Ca-buffer (usually NITR-5) within the preparation by using the flash photolysis method to study relaxation rates. These labs have used a chemically caged chemical relative of BAPTA and EGTA, which is 'activated' (*i.e.* raising its Ca-binding affinity) by a flash of light of the appropriate wavelength and thus bringing forth rapid relaxation by initiating a rapid uptake of  $\text{Ca}^{2+}$  simultaneously across the diameter of the muscle. However, when one examines the method of flash photolysis where a laser is employed, we can see that the release of NITR-5 is not necessarily uniform within the muscle, but localised to the area affected by the laser beam. If the laser beam illuminates the transducer the tension signal is lost probably by extreme local heating as many photons are absorbed by the semiconductor elements. The laser light is thus restricted in those experiments to pass only through the middle portion of the muscle between the two attachment sites, it can only rapidly reduce  $[\text{Ca}^{2+}]$  in a limited area of the muscle. This causes variations in the state of activation along the preparation due to greater relaxation rates in the middle portion compared with the areas nearer the two ends not directly affected by the laser. What will then be observed is the fall of tension in the middle portion. This allows the still-contracted ends to shorten, stretching the middle, relaxing, portion of the muscle. This need only proceed to a small extent (a little over 1% of local length in the 'relaxing'

portion of the muscle) to force detachment of all the remaining crossbridges in the middle portion – rather in the manner of a ‘quick-release’ experiment. This will allow tension to fall not at the intrinsic detachment rate of the bridges, as the experiment is designed to measure, but rather because relative sliding is occurring.

The [EGTA]-step method used here, with various EGTA concentrations in separate baths, has advantages over the flash-photolysis method. First and foremost, the entire trabecula is immersed in the EGTA bath, allowing equal radial diffusion of EGTA at all points along the length of the tissue. This relaxation proceeds equally at all point along the muscle’s length, precluding localised shortening and stretch. We have used trabeculae of up to only a certain diameter to ensure that the relaxation data at maximum rates are not limited by the time needed for the chemical diffusion. Another benefit of the EGTA bath method is the minimal damage to the muscle and the ability to repeat the experiment with the same preparation under various experimental conditions. The high concentration of EGTA is easily washed out of the trabecula by placing it in the ‘standard’ 10mM EGTA relaxing solution (Solution A). (In fact, the muscle is never equilibrated to the higher concentration of EGTA since the solution was routinely changed as soon as relaxation was complete. This occurs once the *average* concentration of EGTA within the tissue is about 0.2mM, long before it has reached *e.g.* 100mM except in the outermost parts of the trabecula - see below). Upon reactivation and relaxation in high [EGTA], the data are reproducible - the activation force and relaxation rates compare favourably with the original activation and relaxation. Statistical analysis show no significant difference between data of repeated control run ( $P > 0.30$ ). By contrast, flash photolysis, has the drawback of the ability of chemicals in the solution around the muscle to absorb light of the wavelengths needed for photolysis within the muscle preventing an accurate measurement of relaxation potential (Palmer & Kentish 1997).

We developed a model to investigate the kinetics of relaxation of skinned trabeculae using an EGTA-jump protocol, as described earlier in this chapter. The model, basing the time course of relaxation solely on the speed of appearance of inwardly-diffusing EGTA, obviously predicts that the rate of relaxation of ventricular trabeculae would continue to increase significantly as the [EGTA]-step is increased, by accelerating the decrease of intracellular free  $[Ca^{2+}]$ . (See Table 5.2) Thus, provided that the change in  $[Ca^{2+}]$  is the rate-limiting factor (see Figure 5.4), as would be the case if the preparation were too large, for example, we would not predict any saturation of maximum relaxation rates.

At the lower range [EGTA] steps, where diffusion delays are expected to be dominant, the model predicts a relaxation time course that corresponds quite well to that observed in a representative preparation. This can be seen by comparing data in Figure 5.4 for [EGTA]-steps of up to 20mM EGTA. There is no significant difference between theoretical and experiment relaxation rates for [EGTA]-steps of up to 20mM EGTA ( $P > 0.2$  and higher). This encourages us to believe that our modelling assumptions are reasonable. It is worth noting that, in order to substantiate this model, the solutions were ionically balanced with appropriate [HDTA] at the various [EGTA], constant free  $Mg^{2+}$ , *etc* (see Table 5.1). Thus, the transition from activation to relaxation was not affected by changes of ionic conditions, other than the fall of  $[Ca^{2+}]$ . It should be noted, however, that the concentration of EGTA within the trabeculae never reached very high levels in the present experiments. Once the average free [EGTA] has exceeded about 0.2mM, as it diffuses inward from a much higher surface concentration, the free Ca will be too low to sustain force. (A mixture of 0.2mM EGTA and 0.2mM CaEGTA, that can be considered to exist locally, results in a free Ca of about  $2 \cdot 10^{-7}M$ , given that apparent  $K_{Ca}$  for EGTA is  $5 \times 10^6M$ ). Later, as [EGTA] continues to rise, tension will already be undetectably low in that region, so the ionic conditions that prevail then are of no consequence for the present analysis.

The results shown in this chapter demonstrate that the rate of relaxation continue to increase with higher [EGTA]-steps, over the range of [EGTA]s used, until around 20 or 50mM EGTA (for preparations of the dimensions employed here). Beyond this concentration range, the trabeculae appear to have reached their maximal rate of relaxation (Figure 5.4). There is a further difference between the theoretical and experimental relaxation curves ( $P < 0.01$  for [EGTA]s of 50 and 100mM). At the higher [EGTA] steps, the experimental relaxations are very well described by a single exponential curve, those of the diffusion model are not; they can be fitted with two exponentials, although given the underlying complexities, this 'fit' is not of any theoretical significance. Kentish and Palmer (1997) reported a 2-exponential fall of tension. However, the results from this chapter shows no compelling evidence that the fall needs more than a single exponential to describe it adequately, even when the fibre is not EGTA-diffusion limited. Also, it is unclear what a two-exponential fall relates to if a single population of crossbridges is 'sampled' during the relation. The single process is clearer as that associated with the 'detachment' rate for the crossbridges after Ca has fallen too low to permit re-attachment. Since the actual results show a saturation of relaxation rate, it would suggest that the rate-limiting factor governing the rate of relaxation at higher [EGTA] steps might no longer be the fall of  $[Ca^{2+}]$ , but most probably the crossbridge detachment rate. Therefore, we conclude that at the highest [EGTA] employed, we are seeing relaxation rate being limited by the myofilaments themselves rather than diffusion. This approach thus provides a technique to study whether some of the factors studied here can alter crossbridge detachment kinetics. This could help to explain any changes in  $f_{min}$ , or other kinetically determined parameters such as phase shift, that these agents have been found to produce.

**CHAPTER 6 EFFECTS OF CAFFEINE ON RELAXATION RATES AND  
MUSCLE WORK AND POWER**

## INTRODUCTION

During heart failure, the decrease in myocardial force production may be overcome by either increasing the  $\text{Ca}^{2+}$  available to the myofibrils or by increasing the responsiveness of the myofibrils to the available  $\text{Ca}^{2+}$ . The latter can be augmented by 'Ca<sup>2+</sup>-sensitising' drugs, and prevents the complication of causing arrhythmias. However, a disadvantage of the Ca<sup>2+</sup>-sensitising agents is their tendency to slow the rate of relaxation of the cardiac twitch (Palmer *et al.* 1996, Wolska *et al.* 1996).

It has been established that caffeine influences myofilament responsiveness to  $\text{Ca}^{2+}$  and ATPase activity (Wendt & Stephenson 1984, Steele & Miller 1990, Powers & Solaro 1995, Palmer & Kentish 1996). Caffeine has shown to raise  $\text{Ca}^{2+}$  sensitivity in adult ventricle, adult atrium, and neonate ventricle of the rat, yet decreases submaximal force. However, Pi and acidosis has been shown to reduce  $\text{Ca}^{2+}$  sensitivity, though they also decrease force. This contrast suggests that caffeine acts by a completely different mechanism to Pi and acidosis and could act as a useful check on its ability to alter  $f_{\text{min}}$  and phase relationship.

Although the  $\text{Ca}^{2+}$  sensitivity of myofilament activity was increased by caffeine, there was no effect on the  $\text{Ca}^{2+}$  binding to TnC (Powers & Solaro 1995). Therefore, it has been suggested that caffeine affects myofilament function via a mechanism that is independent of TnC- $\text{Ca}^{2+}$  binding but may instead involve direct effects on actin-crossbridge interactions.

This interaction of caffeine with the myofilaments was studied using the oscillation protocol described in earlier chapters. Previous studies have focused on the effect of caffeine on isometric force production and  $\text{Ca}^{2+}$  sensitivity. However, there is a lack of information on the effect caffeine has on muscle work and power. In our experimental protocol, we oscillated the fully activated muscle in the presence of 10mM caffeine. In

addition we have looked at the effects of 10mM caffeine on the relaxation rates of the rat myocardial muscle. Although there is evidence showing a decrease in relaxation rates, we re-examine this effect using the [EGTA]-step protocol described in Chapter 5.

## METHODS

Crossbridge properties were investigated using the sinusoidal oscillation method described previously in this thesis. Fine preparations of rat ventricle muscle were chemically skinned (as described in Chapter 2) to allow direct control of the ionic environment of the myofilaments. The preparation was activated in pCa 4.0 solutions with or without caffeine. The activating solution was made as described in Chapter 2 with desired [caffeine] added at the same time. The trabecula was initially activated under control conditions and oscillated. After every run in the activating solution with 10mM caffeine, the muscle was activated again and oscillated caffeine-free. This was to evaluate the endurance of the preparation throughout the protocol. Once the control force production in pCa 4.0 at had fallen to 50% of the original contraction, the preparation was no longer used.

The caffeine relaxation experiments were done at the end of each [EGTA]-step relaxation experiment reported in Chapter 5. Thus, the methods for this section are the same as those in chapter 5 except where 10mM caffeine was present in each EGTA relaxing solution and the 0.2mM CaEGTA activating solution.

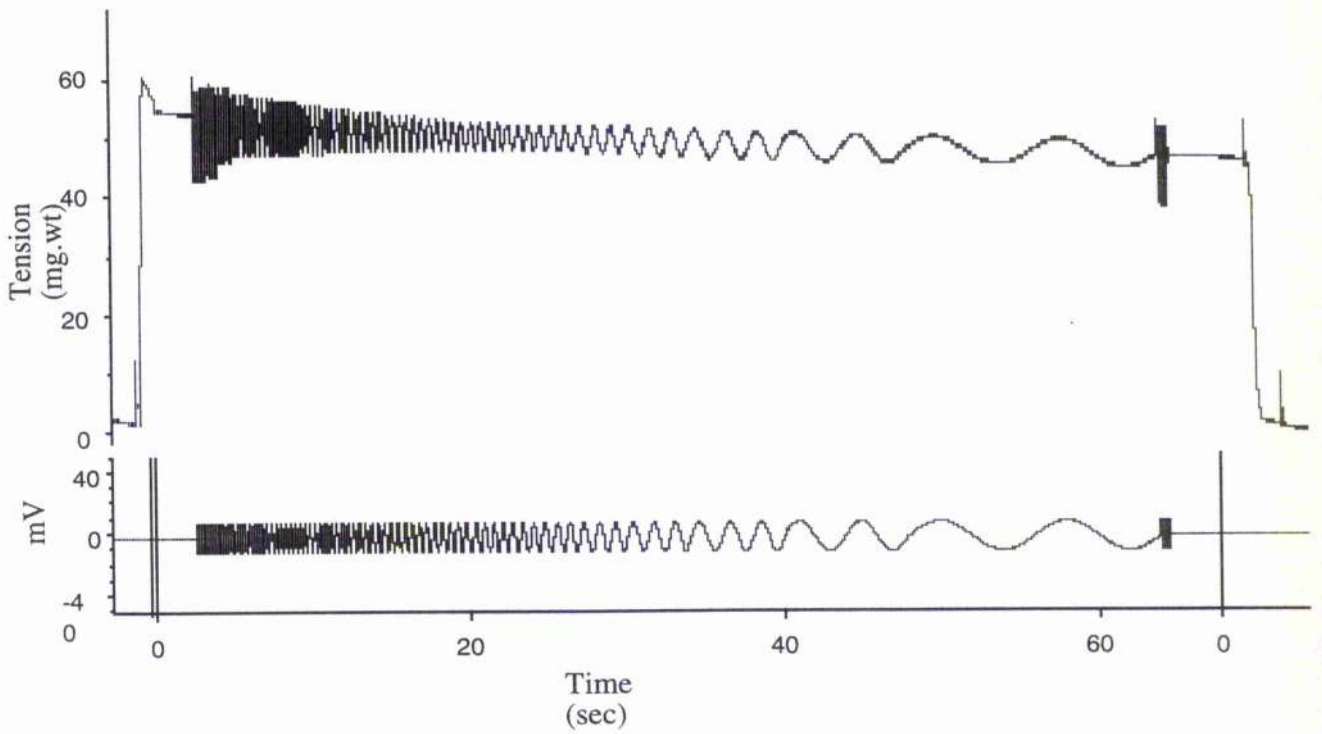
## RESULTS

Figure 2.2. shows an example of a typical experimental trace for an experiment beginning with a maximal activation and oscillation including those done for this chapter. A series of small, sinusoidal length perturbations was applied during each activation. Details of the precautionary and control measures included in each experiment are similar to those explained in Chapter 2.

### Effect of Caffeine on Maximum Tension

Various factors contributed to the force produced by the trabecula. These factors will be listed and explained in the Discussion section of this chapter. One of the aims of these experiments was to compare how caffeine affects the tension produced by rat myocardium. However, due to the differences between the various trabeculae, such as diameter, degree of muscle damage, *etc.*, it was considered that force production could not be compared directly between preparations. Instead, all data were normalised with the control response defined as 100%. The mean force produced was (in %)  $88.13 \pm 2.50$  ( $n=3$ ) at 10mM caffeine ( $P<0.01$ ).

<b>Table 6.1</b>	<b>Change in Maximum Ca-activated force vs. [Caffeine]</b>	
<b>[Caffeine] (mM)</b>	<b>Relative Tension (%)</b>	<b>n=</b>
<b>10</b>	$88.13 \pm 2.50$	3



**Figure 6.1.** This figure shows a typical experimental trace of rat myocardium when activated and oscillated in standard activating solution (Solution C) + 10mM Caffeine. The top trace is of the tension transient, which shows a dependency on oscillation frequency. The bottom trace shows the change in length applied during activation and oscillation.

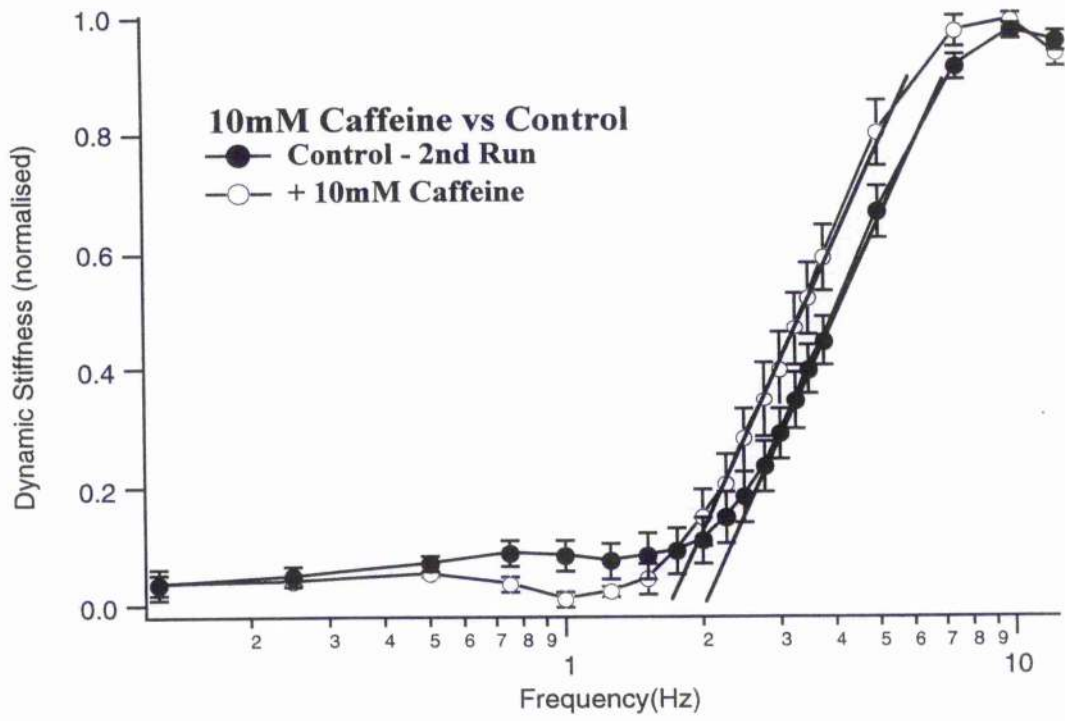


**Figure 6.2.** This figure shows the combined data for three caffeine experiments. The data for the individual experiments were normalised to the maximum and minimum dynamic stiffness before they were pooled. The error bars represent the sem at each frequency. The parallel lines fitted to the major part of the relationship between 2 and 6 Hz allow one to estimate the relative shift of the whole relationship. The leftward shift produced by caffeine represents a slowing by approximately 20%.

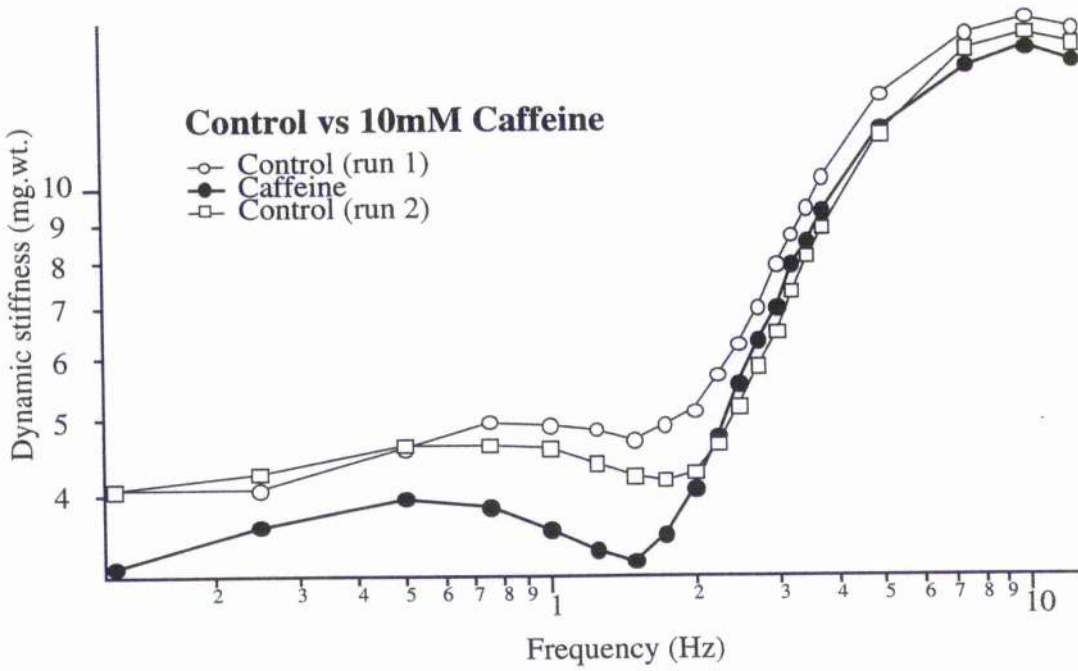


**Figure 6.3.** This figure shows the stiffness-frequency plot for an individual caffeine experiment. The run with 10mM Caffeine came after control run 1 and 2.

## Dynamic Stiffness

### *Control (Caffeine absent)*

The control activation and oscillations were done with zero caffeine. These data are identical to the controls reported in Chapter 3. For a brief summary, at progressively higher oscillation frequencies, the plot of dynamic stiffness against frequency is generally characterised by a downward deflection, until reaching  $f_{\min}$ , followed by an increase in stiffness. This increase continues until a maximum is reached, and then begins to decline again.

### *Effect of 10mM Caffeine*

Caffeine has three major, obvious effects on the stiffness-frequency plot (Figure 6.2). The first is to shift the curve to lower frequencies. The second is that the inflection defining  $f_{\min}$  becomes noticeably more pronounced with caffeine. The third is the large depression in stiffness before and around  $f_{\min}$  with caffeine as well as a slight fall to lower stiffness ranges for the entire plot.

In five experiments with 10mM caffeine present, the stiffness-frequency curve does shift to the left, bringing the  $f_{\min}$  to lower frequencies. Mean  $f_{\min}$  value was  $1.42 \pm 0.20$  Hz for the control, and  $1.17 \pm 0.20$  Hz with 10mM caffeine. In each experiment ( $n=3$ ) there was a decrease of 0.25 Hz. Although this is only a small shift compared to those seen in previous chapters, it is significant ( $P= 0.05$ ). It was obvious that when caffeine was added the inflection point of  $f_{\min}$  became more well defined, as shown in Figures 6.2 and 6.3. The downward inflection that characterises  $f_{\min}$  became deeper than without caffeine.

The third effect of caffeine addition was the severe depression of the stiffness vs. frequency plot, especially for the points at frequencies below or around  $f_{min}$ . Dynamic stiffness at  $f_{min}$  was significantly lower with added caffeine, with a mean value of  $87.67 \pm 4.94$  % of the control ( $P < 0.05$ ). Maximum dynamic stiffness at frequencies greater than 3 Hz was also found to decrease in the presence of caffeine. Compared with the control, the maximum dynamic stiffness with 10mM caffeine was also found to decrease, with a mean value of  $94.40 \pm 2.54$  %. However, the difference in Maximum stiffness was not significant ( $P > 0.1$ ). These features can be seen in Figure 6.2. Although the frequencies at which the maximum stiffness occurs is perhaps not physiologically relevant, they give a picture of the functional capacity of the crossbridges.

To facilitate qualitative comparisons, all data were normalised to the maximum of each experiment. The minimum was then subtracted and the data re-normalised to allow comparison of the shapes of the various stiffness-frequency curves.  $f_{min}$  occurs at slightly different frequencies in each case, so that averaging several traces from different experiments tends to smooth and flatten the relationship (see Figure 6.2). However, an individual trace, such as Figure 6.3, shows the features mentioned more clearly.

Table 6.2	Change in Dynamic Stiffness at $f_{min}$ vs. [Caffeine]	
[Caffeine] (mM)	Stiffness (%)	n=
10	- $87.67 \pm 4.94$	3

## Phase

### *Control (Caffeine absent)*

Phase shift between the length and tension traces was analysed in two parts. Phase angle was plotted for the length sinusoid in the upward (which equals stretch, 'phaseUp') direction and separately for the downward (which equals release, 'phaseDown') direction. Figure 3.13, in Chapter 3, shows a typical phase plot of a maximally Ca-activated trabecula. This plot is explained in detail in Chapter 3. The SD in these experiments is an index of how much the phase angle varies along a single loop (or set of loops). Therefore it shows how far the loop deviated from the 'ideal' sinusoid with a constant phase shift where SD would be zero. (Refer back to the end of the 'Phase Shift: phase angle' section in Chapter 2 for further explanation). If the SD has gone up under the influence of the intervention, then this shows that caffeine has modified those elements of crossbridge kinetics that define the phase relationships.

### *Effect of 10mM Caffeine*

It has been shown in Chapter 3 that the position of the phase-frequency plot correlated with the position of  $f_{\min}$  in the stiffness-frequency plot. This is also true for the experiments described in this chapter with caffeine present. A comparison of the curves in Figures 6.2 and 6.3 shows that  $f_{\min}$  does indeed decrease when 10mM caffeine is present. However, the shift in the stiffness-frequency plot when caffeine is present is not as large as the shifts reported in the previous chapters with other agents. Therefore, it was expected that the phase plot for increased [caffeine] would shift to the lower frequencies in order to correspond to the results shown in the stiffness-frequency plots. This relationship was evident in these experiments and can be observed in Figure 6.4. With caffeine present, the phase plot shifts to the left just as  $f_{\min}$  does.

The phase shift plot is also different in the presence of 10mM caffeine. (No numerical data shown ( $n=3$ ) but all the experiments yielded similar shift patterns. Figure 6.4 used as representative graph.) Figure 6.4 shows that, in caffeine, the frequency difference between the minimum phase angles between phaseUp and phaseDown becomes greater. PhaseUp shifts more to the left than does phaseDown. Also, with caffeine, the standard deviation of the phase angles at any given frequency becomes greater. The phenomenon is greatest around the most negative points of the phase plot. There is no significant change in the range of phase angles between protocols (All  $p$  values  $> 0.2$ ).

Unlike the stiffness-frequency plot, there is no major depression in the shape of the phase plot with caffeine. The positive and negative work is relatively the same. There is a small shift in the position of the curve as corresponding to frequency, as well as a change in frequency separation between the phaseUp and phaseDown plots.

### **Work and Power Values**

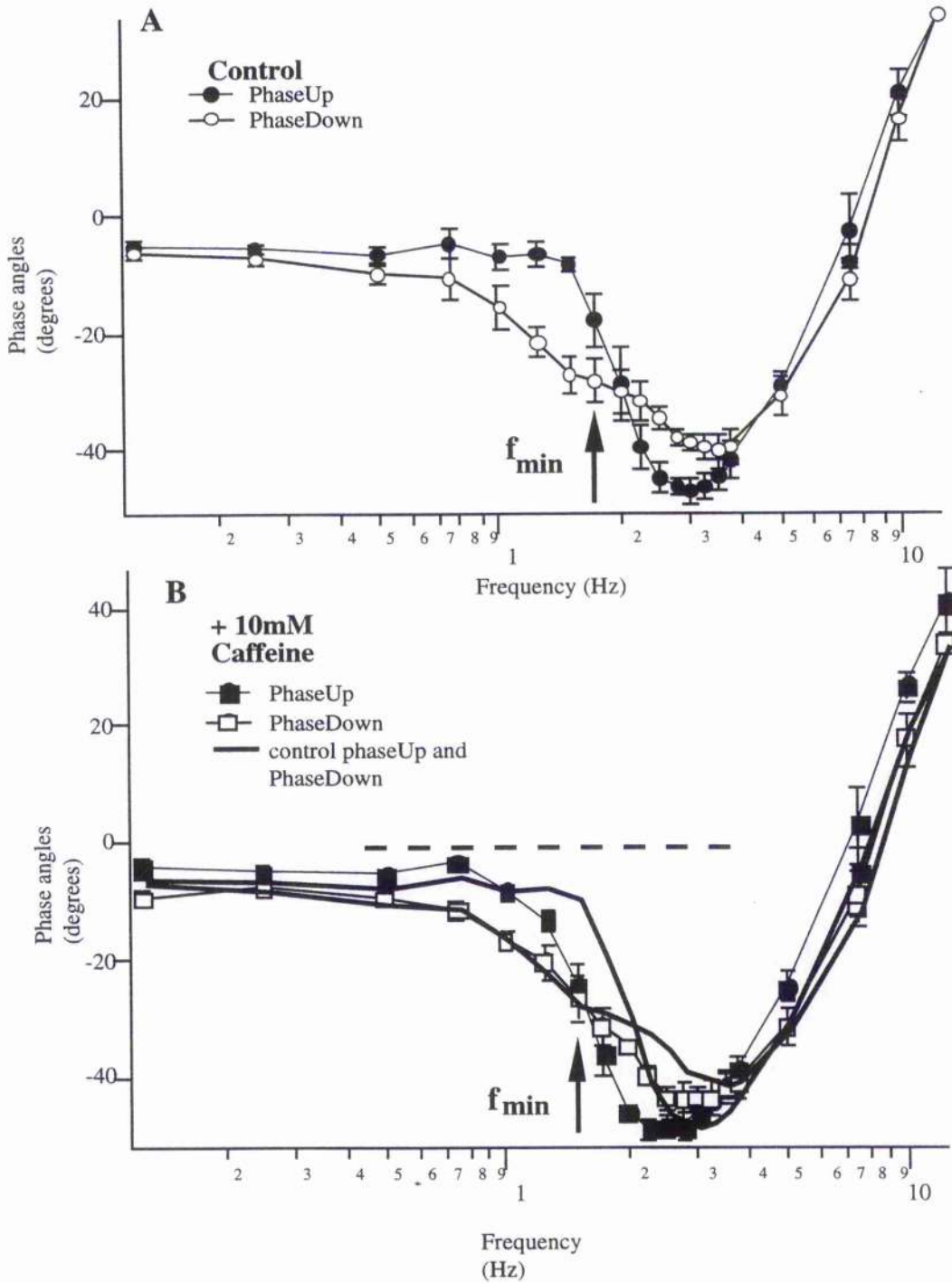
Calculations for the change in work and power output between control and 10mM caffeine were attempted using equation 2.4 and 2.5. However, due to the lack of positive phase values, physiologically relevant work and power values were not able to be obtained.

### **EGTA-Step Relaxation**

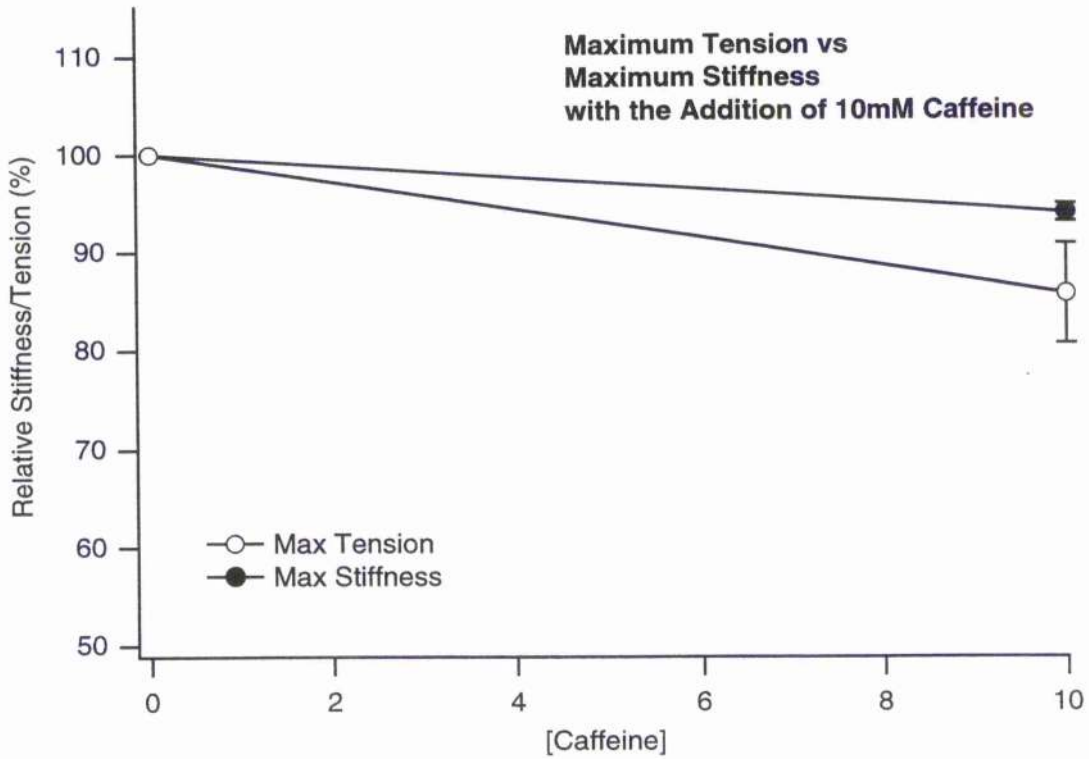
The data from the [EGTA]-step experiments with 10mM caffeine shows that muscle relaxation was delayed as a result of the addition of caffeine to the bath solution. These experiments were done in conjunction with the experiments from chapter 5. Therefore the representing figures are combined with those from the previous chapter.

Figure 5.1 shows the relaxation transients obtained during a typical experiment. As with the initial [EGTA]-step runs, the transients of the [EGTA]-caffeine runs were also well fitted with a single exponential curve fit. The exponential curve fit so well that it is difficult to distinguish between the original data and the curve fit. This figure clearly reveals that relaxation kinetics were not altered with the addition of caffeine despite the initial delay.

Figure 5.2 shows the relaxation rate constants obtained from the exponential curve fitting process for all the EGTA step experiments. The range of rate constants derived over the range of [EGTA]-steps is well fitted with a rising exponential curve as shown in Figure 5.1 (from Eqn 5 in Chapter 5). Although it is clear from Figure 5.1 that the addition of 10mM caffeine has significantly delayed the onset of the exponential phase of relaxation of the skinned rat cardiac muscle trabeculae at the [EGTA]-steps of 20mM EGTA and above, the relaxation rates are not affected. Statistical analysis showed that there was no significant difference between control and added caffeine at any [EGTA] (All p values > 0.5). These results can also be seen in the semi-log plots of the relaxations rates shown in Figure 5.3.



**Figure 6.4.** This figure shows the phase shift plot for a typical individual caffeine experiment. The thicker lines representing the control data (from panel A) are superimposed on those in the presence of caffeine (Panel B) to facilitate comparison. Note that the muscle does no positive oscillatory work at the frequencies near  $f_{min}$ . (no points fall above the broken line). The error bars represent the standard deviation of shifts in phase at each frequency.



**Figure 6.5.** This figure shows the mean data for maximum tension vs maximum stiffness with the addition of 10mM Caffeine. The error bars represent the sem for each value. There is no sem at 0 mM Caffeine because 0 mM Caffeine acted as the control and was therefore regarded as 100%.

## DISCUSSION

Several labs have shown that, at concentrations around 10mM or greater, caffeine reduces maximal force production in cardiac muscle (Palmer & Kentish 1996). This effect is similar to the effect of acidity and Pi on cardiac muscle force development (Palmer & Kentish 1996). In addition, Figure 6.5 shows that the fall of tension is greater than the fall of stiffness with added caffeine. This is similar to the phosphate results obtain for this thesis, and implies a decreased mean force per XB as explained in Chapter 4. However, the similarities do not carry over in all muscle kinetic values. In terms of  $Ca^{2+}$  sensitivity, the effects of caffeine are opposite to those of acidity and Pi; caffeine increases myofilament responsiveness to  $Ca^{2+}$  whereas Pi and acidity reduce it significantly as seen in our results and from the labs of Palmer and Kentish (1996). This suggests that caffeine may work through different mechanisms than acidity and Pi to reduce force. It is probable that by comprehending the manner through which caffeine works, we can also better understand the possible mechanisms through which reduced pH and increased [Pi] work to reduce myocardial contractility during ischaemia or hypoxia.

It has been established that caffeine does not increase  $Ca^{2+}$  sensitivity by affecting the affinity of TnC for  $Ca^{2+}$  (Solaro 1995). Solaro and colleagues showed that caffeine had no effect on the interaction between TnC and  $Ca^{2+}$ . This suggests that caffeine may be working through direct interaction on the crossbridge. This idea is supported by ATPase activity data provided by Solaro *et al* showing that caffeine decreases crossbridge cycling (1995). This decrease in crossbridge cycling rate indicated through decreases in  $f_{min}$  and stiffness values could be seen in individual caffeine experiments done in our lab. This indicates a decrease in crossbridge kinetics that is beyond the interactions between TnC and  $Ca^{2+}$ , since all measurements were taken at full  $Ca^{2+}$  activation. The compiled  $f_{min}$  and stiffness (at  $f_{min}$ ) data in this thesis show a small but significant difference attributable to caffeine and thus does support this idea ( $P=0.05$  for  $f_{min}$ ,  $p < 0.05$ , stiffness at  $f_{min}$ ).

Caffeine also differs from Pi and acidity in terms of work. Our results, using phase analysis show that there is no significant change in the positive or negative work output ( $P > 0.20$  or more). Caffeine seems to leave most of the kinetics of muscle work relatively untouched. The results shown in Figure 6.4 show that the muscle kinetics shift to lower frequencies during phaseUp and phase Down, which correspond to the decrease in  $f_{min}$ . Refer back to the beginning of the 'Phase Shift: control conditions' for the explanation of the way phaseUp and Down curves differ, *i.e.* the stretching phase of the cycle (phaseUp angles) tends to be more affected than the lengthening phase (phaseDown angles).

Taking equation 2.5 for power, we know that this result tells us that the muscle is generating less power. Since power is a product of work and time, these results coincides with our [EGTA]-step experiments showing a delay in relaxation with the addition of caffeine. The interpretation of the phase analysis despite the lack of positive phase angle has been discussed in the Discussion section of Chapter 3 and is also relevant to this chapter. In summary it states that although the phase curves may not cross to positive angles (just below  $f_{min}$ ), that region of the curve still relates to the ability to generate work (or at least absorb the least work) at those frequencies.

Chapters 3 and 4 have shown that pH and Pi cause significant changes in both work and power. Figure. 4.10 shows the schematic of the three-state model of Julian *et al* (1974), and shows a simplified version of the crossbridge cycle. Pi was mentioned to affect both  $k_{12}$  and  $g_2$ , while acidosis, decreases force and work, is thought to effect  $k_{12}$  but not  $g_2$ . The decrease in relaxation rates mentioned above show that caffeine probably affects the  $g_2$  value mentioned by Rossmannith *et al* (1998) by slowing the  $g_2$  kinetics.

More interesting is the relationship between the decrease in force with the accompanying decrease in  $f_{min}$  ( $P = 0.06$ ), with no significant change in work. The combination of these results suggests that caffeine does not affect the myofilament at either the pre-power

stroke steps where pH or Pi are released. If it affected the power stroke step as Pi or H<sup>+</sup> does, we would see a change in the work value along with the change in power. Steele and Smith (1992) showed that caffeine failed to increase rigor tension when applied after contracture had fully developed. This confirms that caffeine does not affect the strongly bound state of the crossbridge or the  $k_{12}$  value. The inhibitory effect of caffeine on  $g_2$  may explain the relaxation delay but not the decrease in tension development and  $f_{min}$ . (Note that the model did take Ca<sup>2+</sup>-sensitivity into account. Due to the high calcium buffering action of EGTA at [EGTA] above 20mM, Ca<sup>2+</sup>-sensitivity is no longer a variable at this point. However, the delay was seen at all [EGTA].) Therefore, we must consider the third variable in this three-state model, which is the rate constant for attachment,  $f$ , or the reverse rate constant,  $g_1$ , for the crossbridges in the weakly bound state. A reduction in  $f$  can explain why we observe the decrease in tension development,  $f_{min}$ , and ATPase activity without any change in work.

**CHAPTER 7 EFFECTS OF TnC ISOFORM CHANGES ON CROSSBRIDGE  
KINETICS**

## INTRODUCTION

Ca regulated contraction begins after Ca binds to sites on the TnC. This in turn starts a cascade of conformational changes throughout the thin filament, ultimately allowing the formation of a crossbridge between actin and myosin. The rate at which actin and myosin attach and detach, as the muscle contracts or relaxes, is the 'crossbridge cycling rate'. This cycling of the crossbridges causes the muscle to shorten and/ or create force.

Contractile dysfunction is one of the many symptoms observed during heart failure (de Tombe, 1998). The decreased contractility is characterised by depressed systolic and diastolic function. This involves slowed contraction and relaxation as well as an overall prolongation of contraction duration. This contractile dysfunction can occur as a result of altered intercellular  $Ca^{2+}$  handling (E-C coupling), upon which much work has been focused. Additionally, altered energy utilisation, or the result of changes in the properties and functioning of the contractile proteins could be implicated. One possible factor contributing to the contractile dysfunction, at the sub-cellular level, could be alterations in crossbridge function. It is associated with changes in the distribution and content of myocardial proteins both in human CHF and in animal ventricular hypertrophy (VH) (Schwartz *et al* 1992, Nadal-Ginard *et al* 1989) and in animal CHF (Li *et al*, 1997). It appears that these changes are of functional significance, since decreased myocardial myofibrillar ATPase activity has been demonstrated in the failing human heart (Pagani *et al*, 1988) and in the hearts of animal models of VH (Alpert, 1983).

In small animal models of VH and CHF, the decrease of ATPase activity has been shown to be associated with a marked shift in the myosin isoform expression from V1 to the V3 (Schwartz *et al* 1992, Nadal-Ginard *et al* 1989). It is known that the V3 form of myosin has a lower ATPase activity (Pope *et al*, 1980) and that expression of this isoform is correlated with a reduction in the maximum velocity of sarcomere shortening (de Tombe

*et al*, 1991). However, an isoform shift of V1 myosin to V3 myosin is not seen in diseased myocardium of larger species, such as human, since cardiac myosin in these species are already of the V3 form under control conditions (Schwartz *et al* 1992, Nadal-Ginard *et al* 1989). This is consistent with the observation that the ATPase activity of purified cardiac myosin is not altered in human heart failure (Mercadier *et al*, 1983). Therefore, it is likely that alterations in other contractile proteins play a role in determining the contractile properties of failing myocardium (Solaro & Van Eyk, 1996).

We used the sinusoidal length oscillation technique on rat myocardial tissue on rat myocardial tissue to show the changes of the stiffness-frequency relationship with the removal and restoration of TnC. It has been shown that TnC can be extracted from skinned muscle fibres without disrupting the myofilament structure. With the removal of TnC, Ca regulated tension decreases significantly, depending on the fraction of TnC extracted. Replacing the TnC into the myofilament, restores Ca regulated tension, typically up to 70% (Babu *et al*, 1987). Using such extraction and replacement protocols, we have produced similar data. This chapter reports experiments on the consequences of the extraction of rat cardiac TnC and its replacement with human or rabbit skeletal TnCs. We have then analysed the stiffness data to quantify key parameters such as the crossbridge cycling rate, length-tension phase shift, integrated work loop, and total oscillatory power.

## METHODS

The effect of different TnC isoforms on crossbridge properties was investigated using the sinusoidal oscillation method described in-depth in chapter 2. The oscillations consisted of a length change of  $\pm 0.25\%$  length change. The range of frequencies used was from 0.125-12 Hz. The sequence, shown in the tension trace in Figure 2.2, begins at the high frequencies and goes down to 0.125 Hz and then have a brief burst of high frequencies at the end. In pilot experiments, the order of the frequencies was shown not to have an effect on the position of  $f_{min}$ . The return to high frequencies at the end was used to check reversibility by observing whether the stiffness has fallen.

Fine preparations of rat ventricle muscle were chemically skinned (as described in Chapter 2) to allow direct control of the ionic environment of the myofilaments. The preparation was activated in pCa 4.0 solution and oscillated, as described in earlier chapters. This first activation served as a control for the rest of the experiment.

The next step was to extract the current TnC from the trabecula. Various methods have been used by many labs. Our first extraction trials included a EGTA solution of a low total ionic strength (Babu *et al* 1987). The method finally chosen for these experiments, derived from the solutions used by Morimoto and Ohtsuki (1987), involved a *trans*-1,2-cyclohexanediamine-*N,N,N',N'*-tetraacetic acid (CDTA) solution of a low total ionic strength. The CDTA extraction solution contains 100mM CDTA, 100mM Imidazole-HCl, and 0.1mM TFP. The pH of the solution was around 7.8 and was not adjusted by acid or base.

To achieve TnC extraction from the rat cardiac preparations, the trabeculae were first transferred from a version of relaxing solution B with no CrP, to a rigor solution at pH 7, 20°C. The composition of the rigor solution is shown in Table 2.3, Chapter 2. Once a state of rigor was achieved, the preparation was placed into the extraction solution

between 30-35°C for 30 minutes. The preparation was then returned to the relaxing solution at 20°C and checked for tension response in pCa4 solution. The extraction process was repeated for another 15 minutes to increase the extent of TnC extraction if needed. However, the length of extraction was found to be optimal at 30 minutes. This was determined by extracting TnC for about 5 minutes at a time and measuring tension immediately afterwards. On average 50% of tension was lost after 15 minutes and about 90% was lost after 30 minutes. Longer extraction periods showed little effect in terms of maximum Ca<sup>2+</sup> activated tension. Extraction was stopped when the Ca-activated tension was down to 10-20% of the initial level, or if there was a change in the fall of tension between the consecutive extractions. The preparation was returned to the relaxing solution at 20°C and checked for tension response in pCa4 solution after every extraction. Once maximal extraction was achieved, the trabecula was activated at pCa4 and oscillated.

Restitution with the experimental TnC isoform was done by 60 minute incubations with 2 to 6 mg/ml TnC in relaxing solution B (composition in chapter 2). The optimum temperature for restitution was found to be between 5 and 10°C. Higher temperatures had proved less effective with a significantly lower return of original tension. The preparation was then returned to relaxing solution B at 20°C, and then transferred to relaxing solution A before checking the tension response at pCa4.

TnC mutants were constructed in the labs of Ian P Trayer at the University of Birmingham using methods that rely on the over-expression of recombinant TnC in *Escherichia coli*. These methods are described in detail by Al-Hillawi *et al* (1995).

## RESULTS

A typical experimental trace for a TnC extraction and restitution experiment began and ended with a maximal activation and oscillation to act as a control within the experiment. During every activation, a series of small sinusoidal length perturbations was applied. Details of the precautionary and control measures included in each experiment are identical to those used in Chapter 3. Thus these measures can be reviewed in the results section of this previous chapter.

### **Effect of extraction, restitution and TnC isoform on Maximum Tension**

Various factors contributed to the force produced by the trabecula. These factors were listed and explained in the Discussion section of Chapter 3. One of the aims of these experiments was to compare the tension produced by rat myocardium between various TnC isoforms. However, due to the differences that may exist between the various trabeculae, such as diameter, degree of muscle damage, *etc.*, the absolute force production could not usefully be compared directly between them. Instead, all data were converted to percentages with the maximum force produced by the control run defining as 100% for individual preparations.

The extent of TnC extraction was judged by the tension development in pCa4 following the extraction. The maximum degree of extraction observed produced less than 10% tension compared to that of the original pre-extraction tension.

The extent of TnC restitution into the muscle was also measured by the tension development in pCa4 following TnC restitution. The maximum TnC restitution observed produced up to 70% tension compared to that of the original pre-extraction tension.

( $P < 0.05$ ). This occurred with the restitution of human TnC and rabbit skeletal TnC into the rat myocardial preparation. However, there was no significant difference in maximum force produced after replacement of human TnC or rabbit skeletal TnC ( $P > 0.30$ ).

## **Dynamic Stiffness**

### ***Before TnC Extraction***

The control activation and oscillations were done before TnC extraction. These data are identical to those reported in Chapter 3. For a brief summary, the plot is generally characterised by a downward deflection, until reaching  $f_{\min}$ , followed by an increase in stiffness. This increase continues until a maximum is reached, and then begins to decline again. This frequency of minimum stiffness, termed  $f_{\min}$ , corresponds to the point of reversal in the descending part of the stiffness-frequency curve. This characteristic  $f_{\min}$  was clear in most preparations.

### ***After extraction***

The extraction of TnC removed the muscles ability to initiate crossbridge attachment and hence reduced the muscle contraction to very low fractions. The dynamic stiffness properties, perhaps not surprisingly, reflected closely those of the muscle at rest. There was no distinct minimum or maximum stiffness ( $P < 0.01$ ). The stiffness frequency plot in Figure 7.1 shows that with the extraction of TnC, the frequency of oscillation has little discernible effect on the stiffness of the preparation.

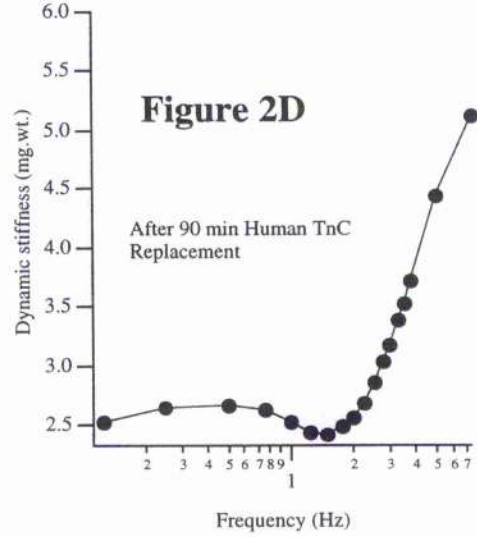
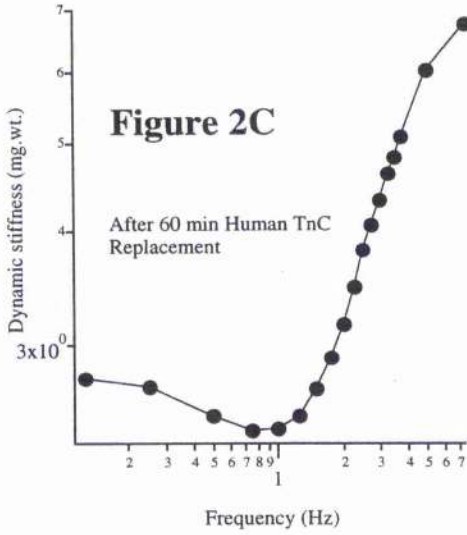
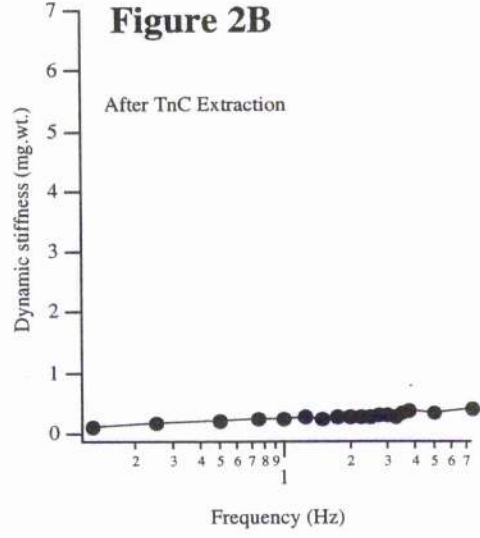
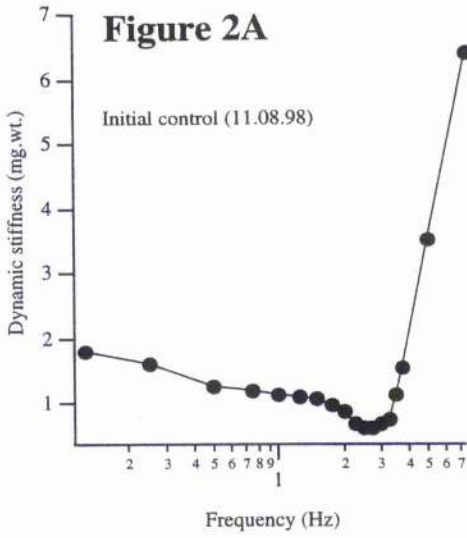


**Figure 7.1.** This figure shows, in respective order, the typical stiffness-frequency plots during a Human TnC replacement experiment. Figure A shows the initial stiffness plot and is followed by Figure B with shows the stiffness after extraction. Note that there is no inflection defining  $f_{\min}$  in Figure B. In Figure C,  $f_{\min}$  then returns after 60 minutes of TnC reconstitution in a bath with a [Human TnC] of  $220\mu\text{M}$ . After an additional 30 minutes in the TnC bath, Figure D shows how  $f_{\min}$  has come closer to its original frequency.

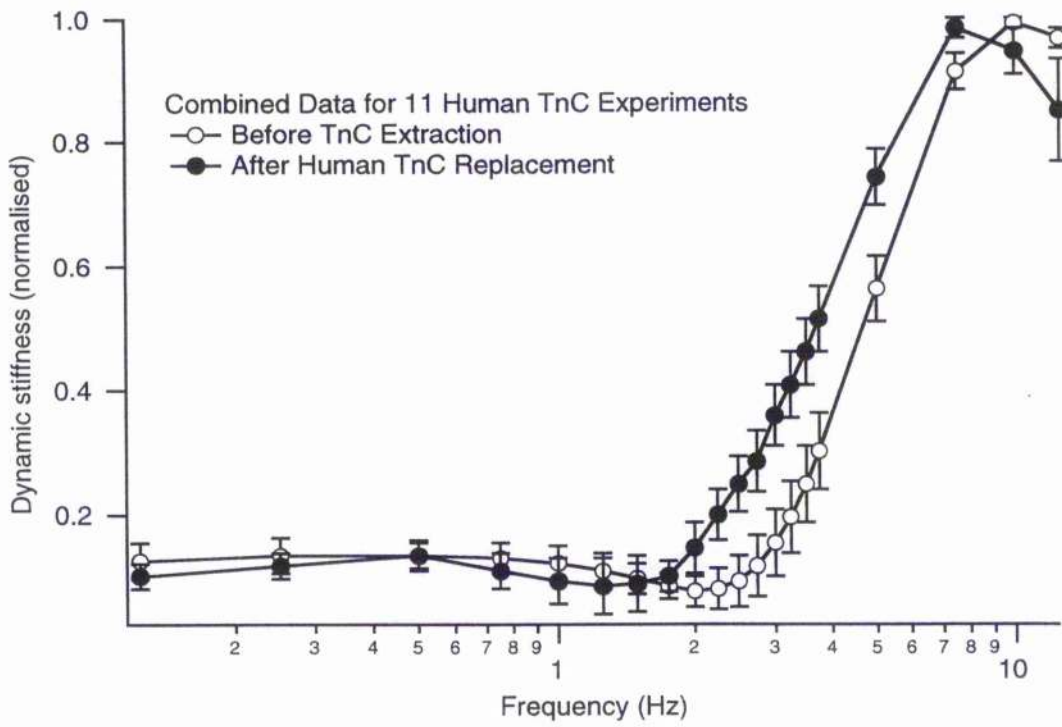


**Figure 7.2.** This figure shows the combined dynamic stiffness data for 11 Human TnC replacement experiments (as mean  $\pm$  sem).

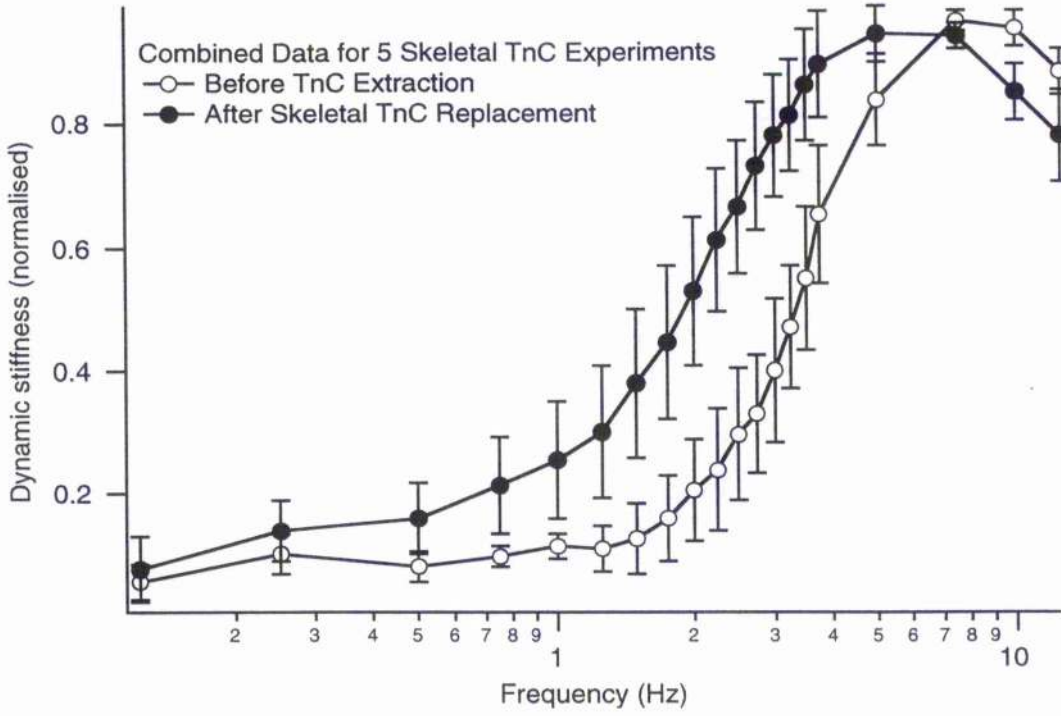


**Figure 7.3.** This figure shows the combined dynamic stiffness data for 5 Skeletal TnC replacement experiments (as mean  $\pm$  sem). The data was normalised to the maximum and minimum points observed, regardless of frequency.

### *After restitution*

The restitution process had three main effects on the stiffness-frequency plot. First is the shifting of the curve to lower frequencies. Second is that the inflection defining  $f_{\min}$  becomes less pronounced. Third, there is a depression through the entire plot to a lower range of stiffness ( $P < 0.05$ ). With restitution using human cardiac TnC, the entire stiffness-frequency curve shifts to the left, thus bringing the  $f_{\min}$  to lower frequencies. This phenomenon occurred with the restitution using rabbit skeletal TnC. The entire stiffness-frequency curve shifts to the left, showing a decrease in crossbridge cycling rate.

The inflection point of  $f_{\min}$  began to show a spreading-out effect with the reconstituted TnC as shown in Figure 7.2 and 7.3. This effect was less pronounced in the experiments where the inflection for  $f_{\min}$  was not as steep for the control stiffness-frequency plot.

The third effect was the depression of the stiffness frequency plot compared with the stiffness before extraction ( $P < 0.05$ ). This effect was most clearly seen with the decrease in the maximum dynamic stiffness found at the higher frequencies beyond 3 Hz. These features can be seen in Figure 7.2 and 7.3. Although the frequencies at which the maximum stiffness occurs is not physiologically relevant, they give a picture of the functional capacity of the crossbridges.

However, there was no significant difference in any of the features describes above between human TnC or rabbit skeletal TnC (All p values  $> 0.30$ ).

### ***Double Extraction and Restitution***

Double extraction and restitution of with Human TnC reveals similar data to the initial extraction and restitution. Just as with the first extraction, the characteristic stiffness-frequency plot could no longer be seen after the second extraction. There was no distinct minimum or maximum stiffness, and the frequency of oscillation has little discernible effect on the stiffness of the preparation (Figure 7.6).

The effects of the second restitution process on the stiffness-frequency plot of the first restitution were similar to the three main changes seen from the first restitution on the original stiffness-frequency plot. The shifting of the curve to lower frequencies and the general depression through the entire plot to a lower range of stiffness was maintained after the double restitution. The data from the first and second restitution had a similar relationship to the data of the first restitution to the original stiffness-frequency plot where maximum stiffness was around 70% of the stiffness before the corresponding extraction.

### **Phase**

Note that no statistical analysis was done on the phase data in this chapter because of insufficient n numbers. Due to inappropriate conditions (such as high electrical noise), there was a lack of experiment where phase analysis could be done.

### ***Before Extraction***

The phase shift between the length and tension traces were analysed in two parts. The phase angle was plotted for the sinusoid in the upward direction and separately for the downward direction. Figure 3.14, in Chapter 3, shows a typical phase plot of a maximally Ca-activated trabecula under control conditions before TnC extraction. This

plot is explained in detail in Chapter 3. Refer back to the beginning of the 'Phase Shift: control conditions' for the explanation of the way phaseUp and Down curves differ, *i.e.* the stretching phase of the cycle (phaseUp angles) tends to be more affected than the lengthening phase (phaseDown angles). The SD in these experiments is an index of how much the phase angle varies along a single loop (or set of loops). Therefore it shows how far the loop deviated from the 'ideal' sinusoid with a constant phase shift where SD would be zero. (Refer back to the end of the 'Phase Shift: phase angle' section in Chapter 2 for further explanation). If the SD has gone up under the influence of the intervention, then this shows in this chapter that the extraction/replacement protocol or the change in TnC isoform has modified those elements of crossbridge kinetics that define the phase relationships.

### ***After Restitution***

It has been shown in previous chapters that the position of the phase plot directly correlated with the position of  $f_{min}$  in the stiffness-frequency plot. This is also true for the experiments reported in this chapter. A comparison between Figure 7.4 of skeletal muscle and 7.5 of cardiac muscle of the phase before TnC extraction and after TnC restitution shows that  $f_{min}$  does indeed decrease after TnC restitution. Therefore, it was expected that the phase plot after TnC restitution would shift to the left to lower frequencies in order to correspond to the results shown in the stiffness-frequency plots. This relationship was evident in these experiments and can be observed in Figure 7.4 and 7.5.

The shape of the phase shift plot also has a few significant changes after TnC restitution. Figure 7.4 and 7.5 show that after replacing the rat cTnC with either human cardiac or rabbit skeletal TnC, there is a change in the deflection to negative phase angles after the

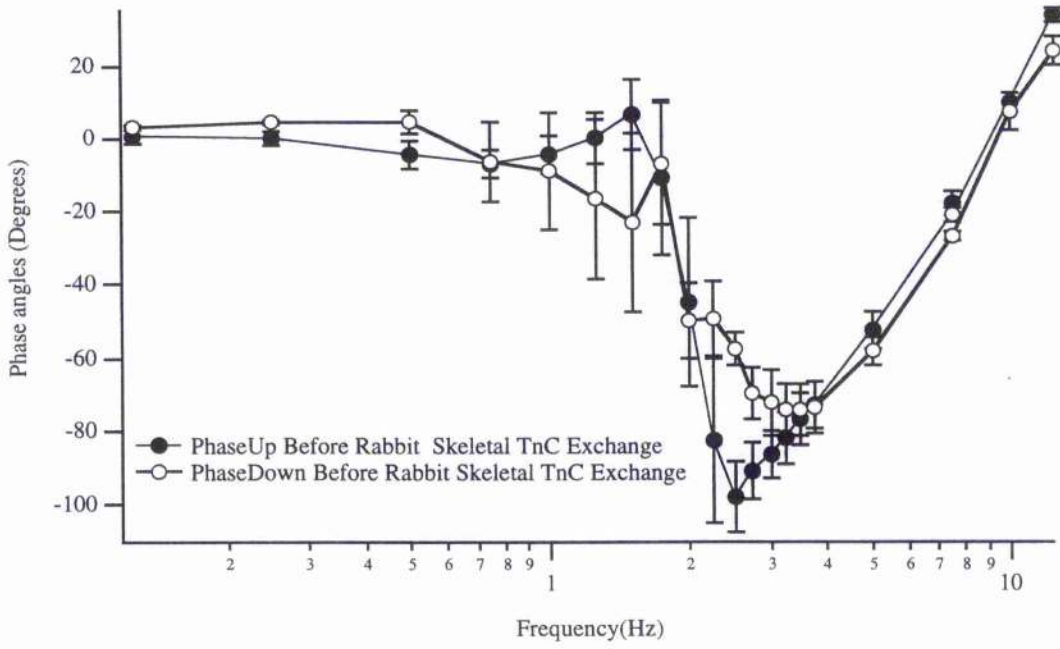
value of  $f_{\min}$  derived from the stiffness-frequency graph. These values become less negative in both phaseUp and phaseDown.

The other change in the shape of the phase plot is with the peak positive phase angles around 1.5 Hz or the 'initial inflection' toward positive phase angles for phaseDown. As seen in Figure 7.4 and 7.5, these angles become less positive, and in some experiments, more negative after TnC replacement of either isoform. However, our data show inconclusive evidence to support any significant directional change of shape of the initial inflection toward positive phase angles for phaseUp. Although significant changes can be seen in Figure 7.4 and 7.5, it must be noted that these figures are a representation of single experiments rather than combined data. The shape of the phase plot of the combined data is similar to the single experiment shown except for the initial inflection toward positive phase angles for phaseUp. The data for the initial inflection toward positive phase angles for phaseUp differed among each experiment and could not be used to draw any conclusions. The other change in the shape of the phase plot is with the initial inflection toward positive phase angles for phaseDown. As seen in Figure 7.4 and 7.5, these angles become less positive, and in some experiments, more negative after TnC replacement of either isoform.

### **Work and Power Values**

Calculations for the change in work and power output before after TnC replacement were attempted using equation 2.4 and 2.5. However, due to the lack of positive phase values, physiologically relevant work and power values were not able to be obtained.

A



B

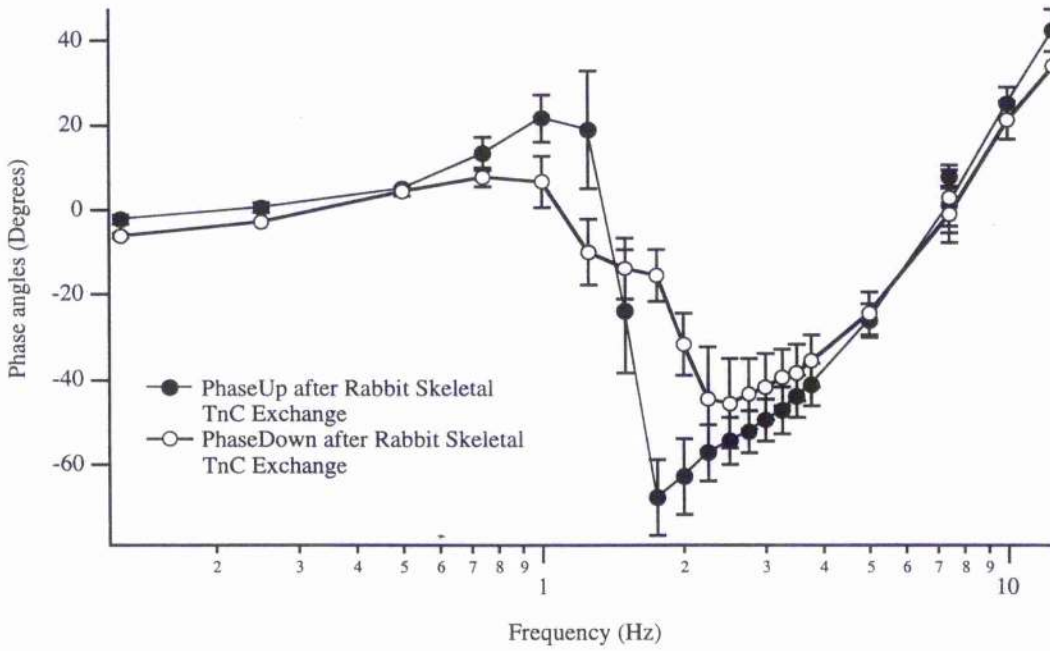
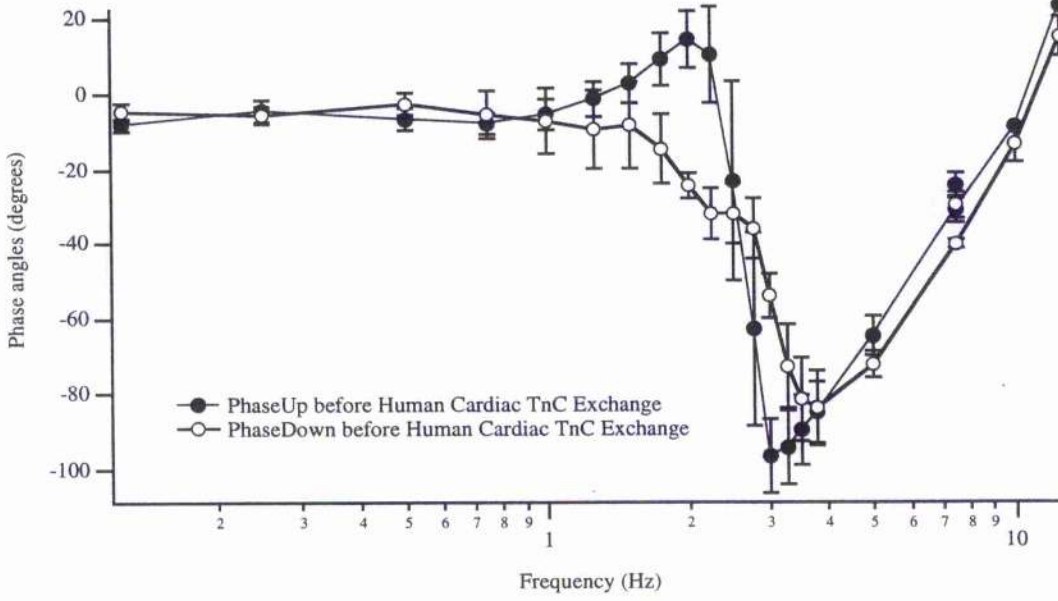


**Figure 7.4.** This figure shows a typical example of the phase plots before and after the fibre is reconstituted with rabbit skeletal TnC.

A



B

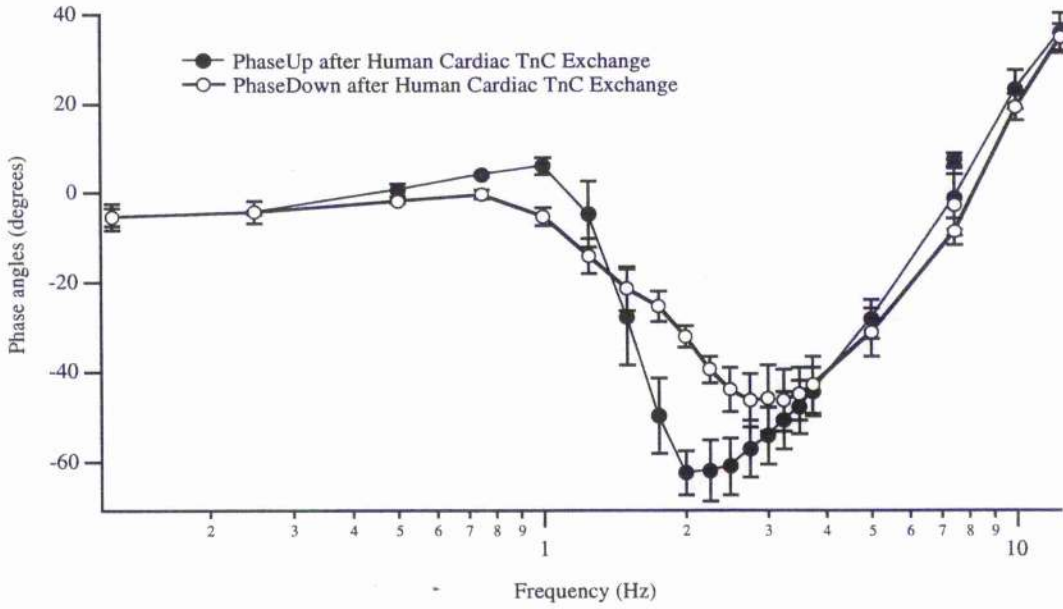


**Figure 7.5.** This figure shows the typical trace of the phase plots before and after the fiber is reconstituted with human cardiac TnC.

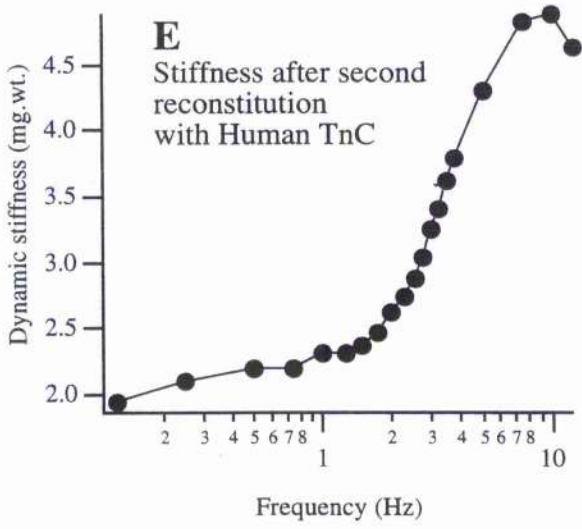
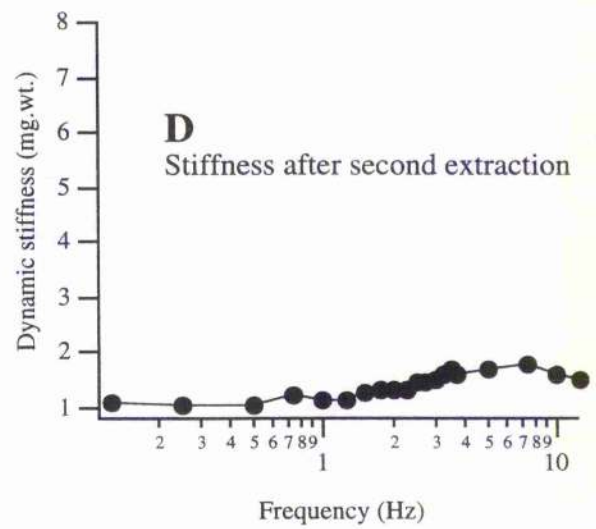
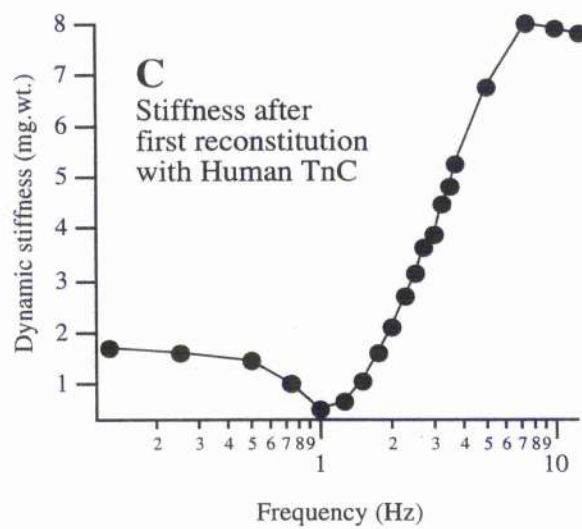
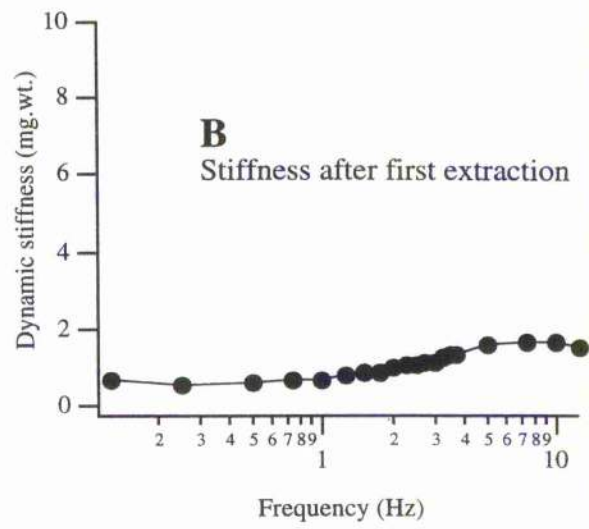
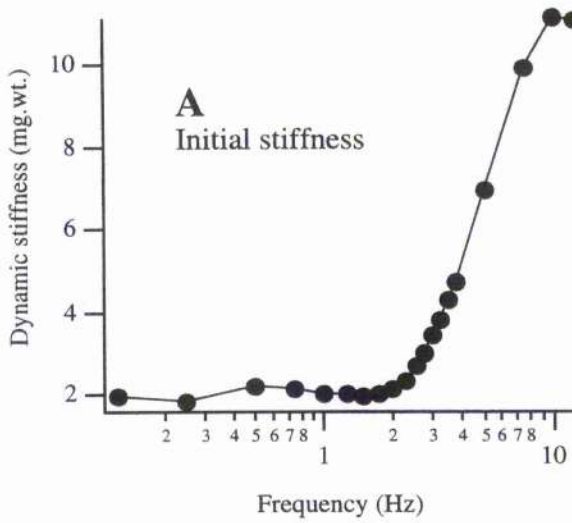


**Figure 7.6.** This figure shows, in sequence, the typical stiffness-frequency plots obtained during a Human TnC double replacement experiment. Panel A shows the initial stiffness plot. Panel B shows the stiffness profile immediately after extraction. Note that there is no discernible  $f_{\min}$  in Panel B. In Panel C, obtained after the first TnC reconstitution in a bath with a [Human TnC] of 220 $\mu$ M, a clearly defined  $f_{\min}$  then returns with about 70% of original maximum stiffness. Panel D with shows the stiffness after the second extraction where again there is no  $f_{\min}$ . Panel E then shows how, after the second reconstitution, a discernible  $f_{\min}$  returns (at least a sharp inflection at about 1.5Hz), again with about 70% of the maximum stiffness of the first TnC reconstitution remaining.

## DISCUSSION

The results in this study looked at the effects of interchanging human cardiac TnC versus rabbit skeletal TnC into skinned rat cardiac myofibrils using a CDTA extraction and replacement protocol. It has been established previously in other labs that rabbit skeletal TnC is considered the faster compared to the slow human cardiac TnC (Babu *et al*, 1987, Dohet *et al*, 1995, Morimoto & Ohtsuki, 1996). Therefore, it was hypothesised that the replacement of human cardiac TnC into the rat myofibril would not change the muscle kinetics within the fibres, but the replacement of rabbit skeletal TnC would change the muscle kinetics, specifically in terms of work and power.

However, before the effect of the TnC isoform could be tested, the efficiency of the extraction and replacement protocol needed to be determined. It is stated by Babu *et al* (1986) that 75% of tension is lost after about 30% of the TnC is extracted. With the present results of over 85% loss of maximum tension ( $P > 0.01$ ), it can be speculated that over 30% of the native TnC was removed by the extraction protocol used in this chapter.

Another point to consider is any irreversible damage caused to the trabecula during the extraction protocol. It can be seen from the experiments in this chapter that only a maximum of about 60-70% of original tension and 70% of the original stiffness returned after TnC replacement. There are two possible explanations for this discrepancy. The first is that the percentage of tension lost is due to damage imposed on the trabecula during extraction. It is possible that the low ionic extraction solution causes molecular damage to the myofilaments. This damage may prevent the new TnC isoforms from attaching. It may also render newly attached TnC inactive due to incomplete or improper attachment. Further evidence for this damage can be seen in our double extraction experiments. About 60-70% of the maximum tension and stiffness produced after the first replacement experiment returned after the protocol was repeated on the same

trabecula. The similarity between of the results between the first and second protocol may point to some damage being incurred by the muscle during the experimental protocol.

The entire discrepancy probably cannot be attributed to 'chemical' damage to the trabecula. The other possibility for the disparity can be due to the duration of the replacement protocol. As explained in the Methods section, the fibres were immersed in the new TnC isoform solution for one hour. Experiments were conducted to see if longer immersion would lead to a higher uptake of TnC. Looking at the stiffness results in Figure 7.1, it can be seen that stiffness does increase slightly after an additional 30 minutes in the TnC solution. However, there was no large increase in the maximum tension produced. (n numbers too small for statistical analysis of double extraction experiments and experiments with additional TnC replacement time) Therefore, some of the decreased muscle kinetics can be attributed to non-uptake of TnC due to time rather than lack of native TnC removal during the extraction phase.

The next step was to determine the efficiency of the replacement protocol. According to our results, we found that 60 minutes in the TnC replacement bath was the optimum time for this phase of the protocol. As seen in previous time control experiments discussed in chapter 3, the passage of time alone does have a detrimental effect of the state of the muscle filaments (n numbers too small for statistical analysis time control experiments). In the present case, specific damage by oxygen-derived free radical for example, plus any non-specific, time-dependent degeneration of the structure of the fibre will contribute to a fall in force. This can be seen in the muscle kinetics of a fibre *in vitro*. Thus, the additional 30 minutes in the TnC replacement bath was eliminated due to the minimal restoration of maximal tension.

This 60-minute TnC replacement time was sufficient for the return of 60-70% of the original tension, around 70% of the original stiffness, and a full return of the general

shape of the stiffness-frequency plot ( $P < 0.01$ ). These results give evidence that the kinetics of physiologically relevant functioning muscle returned after the replacement of TnC to the thin filament. This return of function after TnC replacement allows for a clearer understanding of certain kinetic aspects of cardiac muscle function.

The absence of  $\text{Ca}^{2+}$  activated tension after TnC extraction and the return of  $\text{Ca}^{2+}$  activated tension after TnC replacement demonstrates the integral part that TnC plays in muscle contraction ( $P < 0.01$ ). It is known that tension development within the muscle is due to myosin heads changing formation against a resistance while in the power stroke portion of the crossbridge cycle. In the case of the experiments in this chapter, the resistance comes from the ends of the trabecula that are firmly attached to the transducer and lever arm by a loop of nylon monofilament. *In vivo*, this resistance would come from the ends attached to bone by tendons in skeletal muscle or the blood volume in the chambers of the heart and its own internal fibrous connective tissue for cardiac muscle. Our results indicate that the absence of TnC from the thin filament prevents the initiation of the crossbridge cycle. Previous studies have shown that TnI, the inhibitory component of troponin, prevents filament activation and that TnC, once bound with  $\text{Ca}^{2+}$ , removes the inhibitory effect of TnI. Therefore, our results give further evidence that the removal of TnC enters the muscle into a quasi-permanent inhibited state. It was mentioned that previously published work as well as our own shows that the protocol does not result in the removal of all the TnC during extraction. In fact, less than 50% of the native TnC are thought to be removed by the extraction protocol. One may reasonably question why the remaining TnC does not allow for the development of significant tension within the muscle. This brings back the concept of cooperativity of the muscle. Babu *et al* (1986) stated that tension is reduced by 70% with the removal of 30% of TnC. With the removal of each TnC, the communication pathway along the muscle filament is potentially disrupted. Cooperativity involves the Tm filaments interacting end-to-end with one another (Brandt & Schachat, 1997). It seems that only partial saturation of TnC is

required for full activation (Fitzsimons *et al*, 2001). When some regulatory units (comprising a TnC plus its associated Tm) lose their TnC, the 'activation' of that Tm becomes dependent on the long-range allosteric effect (cooperativity) of its neighbours. Force does not fall 'stoichiometrically' with TnC extraction, reflecting the ability of this cooperativity to enable crossbridge activation despite the lack of direct TnC-Ca based regulation of each Tm domain.

Altogether, these widely accepted views of cooperativity in Ca-dependent activation along the thin filament would predict that force should be well sustained until only a very small fraction of the normal TnC complement remains. However, it has also been discussed previously (Chapter 3) in regards to low pH that non-cooperativity among the crossbridges under those conditions may allow the myosin head to cycle at more widely variable speeds instead of over a narrower range. Thus the distances between the sections of 'normally' Ca<sup>2+</sup> activated crossbridges may prevent the muscle from working effectively and developing a significant amount of tension. This suggests that questions still remain about the exact nature of the interrelationship between active crossbridges, Ca-dependent TnC-TnI-TnT-Tm controlled disinhibition of actin-myosin binding and cooperativity between regulatory units in striated muscle.

The second and third muscle kinetic features that are instrumental in judging the efficiency of the extraction and replacement protocol were the shape of stiffness-frequency plot and the maximum stiffness of the trabecula. It has been established that stiffness relates to the number (proportion) of crossbridges in the strongly bound state (Kentish *et al*, 2001). The present data from stiffness measurements during rest and rigor attest to this argument. At rest, where there is effectively no Ca<sup>2+</sup> activation and no cycling crossbridges but sufficient ATP, there is minimal stiffness. This is interpreted to mean that there is no resistance against the mechanical oscillation applied to the muscle attributable to strongly attached crossbridges. However, it is clearly shown that during

rigor, where the maximum number of crossbridge are attached in the strongly bonded state due to the lack of ATP, stiffness is at a maximum because of the increased resistance to the mechanical oscillation by the large number of less compliant myosin heads. This deduction has been used in this chapter to determine the effectiveness of the extraction and replacement protocol. During extraction, a decrease in stiffness is seen, similar to that of resting muscle ( $P < 0.01$ ). This inability for the crossbridges to activate and cycle in the presence of ample  $\text{Ca}^{2+}$  gives evidence that TnC was successfully removed. After the replacement protocol, greater muscle stiffness signifies restoration of TnC to the thin filament. However, the present results show that there is not a full recovery to the original stiffness ( $P < 0.05$ ). This decrease in stiffness may be due to the same reasons as the normal decrease in tension that is seen, as discussed earlier. This post-extraction, replacement protocol decrease in stiffness may be due to either damage incurred by the thin filament during extraction or insufficient amounts of TnC replacement.

The shape of the stiffness-frequency plot can also be used to determine kinetic properties of the muscle preparation after TnC extraction and replacement. The return of the shape of the stiffness-frequency plot after TnC replacement indicates that the kinetic properties of crossbridge action were well preserved during the extraction protocol. The kinetic properties was not expected to be fully restored because that would suggest that the extraction process would not affect proteins other than TnC or that the replacement process would reverse those effects caused to the other thick or thin filament proteins. It can only be stated, from our data, that crossbridge cycling was inhibited due to the absence of TnC. Our results do not give any evidence for the presence or absence of effects on any other molecules other than TnC. However, it has been stated that the extraction protocol may, for example, also extract a small percentage of myosin (Moss 1992). We did not reconstitute other proteins along with the TnC so that it was possible to isolate the effects of TnC alone. This possible extraction of other proteins could also

explain some of the discrepancies seen between the original values and those after TnC replacement. It may account for the trabecula's inability to sustain full tension, stiffness, and the shape of the stiffness-frequency plot after TnC restitution. These discrepancies may also be due to the decrease in the number of TnC binding sites available to the  $\text{Ca}^{2+}$ . As mentioned before, this could be due to damage during extraction or insufficient length of time in the TnC replacement bath.

Last, the possibility must be considered that the stiffness-frequency plot did not return completely to its former shape, including the position of the  $f_{\min}$ , because of the change in the TnC isoform. However, this argument is unlikely to account for any significant change for the two main reasons. First, there are not sufficient data to determine how much of the changes are due to the TnC isoform versus the effects of the extraction and replacement protocol. The accurate control experiment to rule out or measure the exact effects of the experimental protocol would be to reconstitute the preparation with its own native TnC. However, purified rat TnC was not available to carry out these experiments. Nevertheless, our results from restitution of skeletal TnC indicate that the discrepancies may have been largely due the extraction and replacement protocol. This is because no significant change in  $f_{\min}$  was seen between human cardiac TnC and skeletal TnC ( $P > 0.70$ ).

Once the effects of the experimental protocol were determined, the differences between human cardiac and rabbit skeletal TnC could then be deduced from our results. This includes effects on maximum tension, stiffness, shape of the stiffness-frequency plot, and phase. In terms of tension the results showed that there was no difference in maximum tension produced ( $P > 0.60$ ). This is in agreement with what would be expected theoretically. Different isoforms of TnC may alter the rate of tension development, but would not necessarily alter the steady-state tension produced. The difference between the two isoforms lies in the trigger speed due to the additional  $\text{Ca}^{2+}$  binding site on fast TnC

isoforms, but the additional binding site does not increase the number of crossbridges attached at one time. This additional binding site will increase cooperativity (Morimoto & Ohtsuki, 1996) and thus increase the rate of tension development. Any such change is not expected to increase  $f_{min}$  that, although affected by the 'on' rate for attachment (Rossmannith & Tjokorda, 1998) as a steady-state parameter, is not sensitive to Ca-activation speed.

Our results showed that maximum stiffness was decreased after the replacement with either human cardiac and rabbit skeletal TnC. There was no significant difference in the stiffness or  $f_{min}$  between the TnC isoforms ( $P > 0.50$ ). Again, this is in agreement with what would be expected theoretically. As explained before, stiffness within the muscle is determined by the number of crossbridges attached in a strongly bound state. Thus the isoform of TnC should not affect stiffness within the muscle. Also, once  $Ca^{2+}$  is bound to TnC, it remains bound to TnC till  $Ca^{2+}$  is taken up by the SR and the contraction process ends. Thus the TnC isoform may affect the initial rate of force development and the rate of relaxation, but should not affect the crossbridge cycling speed (*i.e.*  $f_{min}$ ), maximum stiffness, or maximum tension. However, a decrease in  $f_{min}$  and maximum stiffness may be seen universally, regardless of TnC isoform, due to the possible damage on the crossbridge as well as myosin or other proteins lost during TnC extraction.

The arguments for the lack in difference in tension and stiffness between human cardiac and rabbit skeletal TnC also apply to our results in the phase analysis. The interpretation of the phase analysis despite the lack of positive phase angle has been discussed in the Discussion section of Chapter 3 and is also relevant to this chapter. In summary it states that although the phase curves may not cross to positive angles (just below  $f_{min}$ ), that region of the curve still relates to the ability to generate work (or at least absorb the least work) at those frequencies. Although TnC is integral in turning on the muscle, it seems from the results that the work and power output of the muscle is a function of the

crossbridges. Our results support this because there was no difference in the phaseUp or phaseDown between the two isoforms used in this chapter (n numbers for phase data are too small for statistical analysis). One significant finding that should be mentioned, however, is the universal decrease in the negative spike of both phaseUp and phaseDown. This means that there is a decrease in the work absorbed by the muscle. This cannot be related to the TnC isoform because the change is seen equally in both sets of results. This result may be due to the loss of myosin molecules during TnC extraction. Since work and power has been said to be a function of the crossbridges, a decrease in the number of attached or functioning crossbridges could explain the decrease in the work absorbed. However, it must be noted that this is speculative since histological studies were not performed to confirm the loss of myosin.

**CHAPTER 8 EFFECTS OF TNT MUTATION ARG<sup>93</sup>GLN ON CA<sup>2+</sup>  
SENSITIVITY AND CROSSBRIDGE KINETICS**

## INTRODUCTION

Contraction of cardiac muscle involves the complex and extensive interlinking of protein-protein interactions that begin with Ca binding to the thin filament. Any differences to the make up or position of these proteins may result in functional changes of the contraction process. An understanding of the roles and interactions of these muscle proteins during normal muscle contraction will help to unveil the causes for functional discrepancies that are due to protein alterations.

In the absence of Ca, the muscle exists in a state of relaxation where tropomyosin sterically blocks the myosin binding site on actin, preventing the formation of the actomyosin link (see Chapter 1). Steric blocking mechanisms also involve TnI, and possibly TnT, as well as Tm. The movement of these proteins after Ca-activation are involved in removing inhibition of the actin-myosin crossbridge mechanism.

During relaxation, the TnC C-terminus, with the two high affinity  $\text{Ca}^{2+}/\text{Mg}^{2+}$  binding sites, is tightly bound to actin via the N-terminus of TnI. The N-terminus of TnC is free of Ca and only interacts weakly with TnI. In cardiac muscle, the N-terminus of TnC has only one Ca binding site, which binds to  $\text{Mg}^{2+}$  weakly and exchanges  $\text{Ca}^{2+}$  quick enough to regulate the transition from relaxed to activated state. After the influx of Ca into the cell and release from the SR, Ca binds to the N-terminus of the TnC.

The experiments reported in this chapter looks at the functional effect of the Arg<sup>92</sup>Gln mutation on the so-called CB2 region of TnT (Palmiter & Solaro 1997). (Arg = Arginine, Gln = Glutamine) Previous studies have shown that the function of TnT is to anchor the Tn complex onto the thin filament (Pearlstone & Smillie, 1977, Willadsen *et al*, 1992). Four of the eight mutants found in TnT of familial hypertrophic cardiomyopathy (FHC) cases are point mutations that affect the amino acids located in or near the CB2 region. The Arg<sup>92</sup>Gln mutation replaces a basic amino acid with a neutral

one and thus involves a charge change. The mutant has protein structural changes that locally destabilise the highly helical CB2 region. This structural alteration may result in changes to the Ca<sup>2+</sup>-insensitive TnT<sub>1</sub>-Tm interactions. This study looks at the effect that the Arg<sup>92</sup>Gln mutant has on Ca sensitivity in cardiac muscle.

Ischaemia of the cardiac muscle itself is seen in a high percentage of heart failure cases. It is known that during acute ischaemic episodes, the pH within the cardiac muscle can drop as low as 6.2. Heart failure is seen in the most severe FHC cases, as evidenced by sudden death due to electrophysiological as well as mechanical complications (Palmiter & Solaro, 1997). Therefore, we decided to look at the effect of pH changes on the Ca sensitivity of heart tissue expressing the Arg<sup>92</sup>Gln mutation.

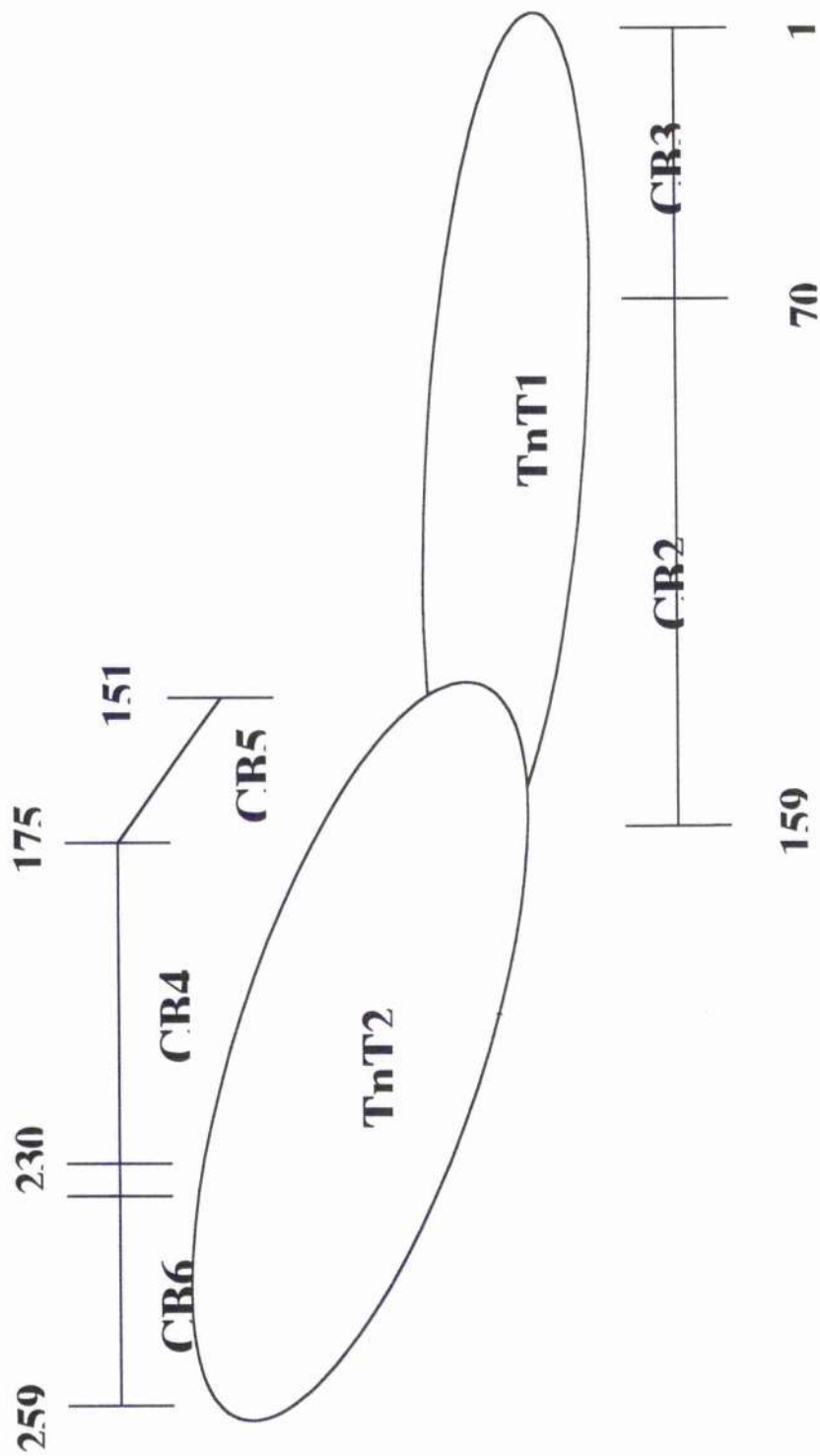


**Figure 8.1.** This figure shows a schematic representation of fast skeletal TnT. The mutant used in this experiment, Arg<sup>92</sup>Gln, is located in the CR2 region of TnT1.

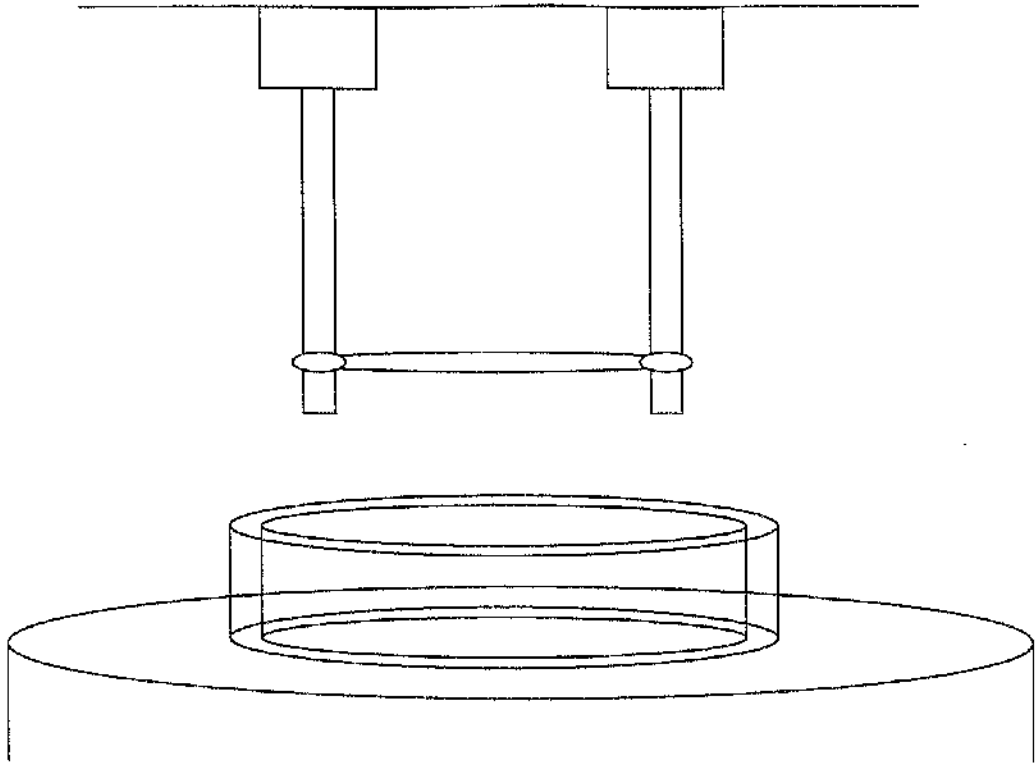


**Figure 8.2.** This figure shows a schematic drawing of the skinned fibre suspended between a fixed arm and a force transducer using cellulose-acetate glue at both ends. A small vial with the appropriate solution was placed below the fibre on a platform and the fibre was then lowered into the vial.

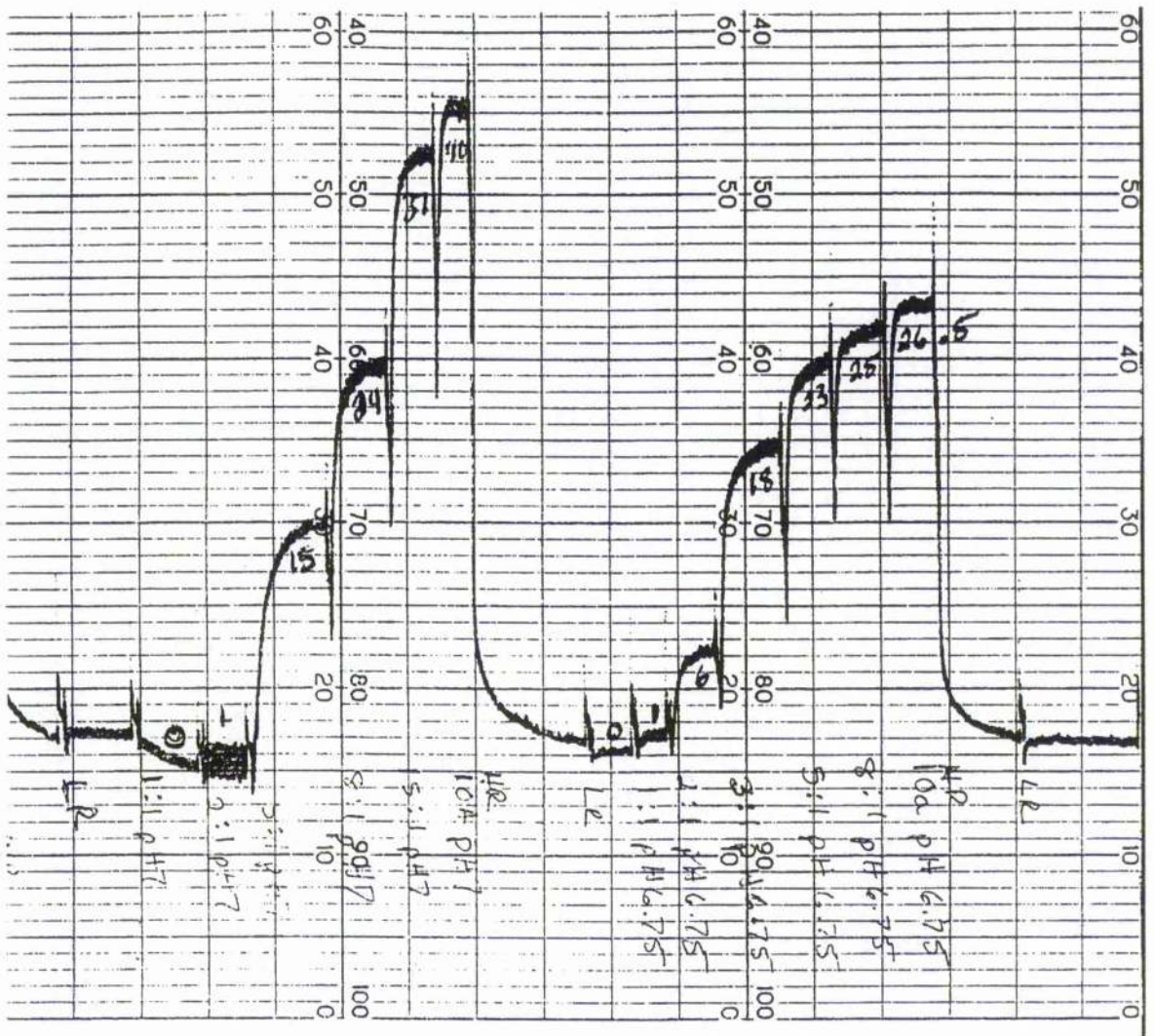


**Figure 8.3.** This figure shows a typical experimental trace from a  $\text{Ca}^{2+}$  sensitivity experiment.

## METHODS

### Mouse Model Transgenics

The experiments done in this chapter were done using transgenic mice from A.J. Marian's Lab at Baylor University, Texas USA. The transgenic mice were engineered by the following techniques. A single 1.1-Kb human cardiac TnT (cTnT) complementary DNA (cDNA) fragment was isolated from a normal human heart cDNA library using a library screening method (Sambrooks *et al*, 1989). The Arg<sup>92</sup>Gln mutation, associated with a high incidence of Sudden Cardiac Death in patients with HCM, was then introduced into the fragment using oligonucleotide-mediated, site-directed mutagenesis (Nelson *et al*, 1989). The human cTnT cDNAs, either normal or mutant type, were placed downstream from the promoter region of the cytomegalovirus (CMV) insert. The CMV/cTnT-Arg<sup>92</sup>Gln inserts were then cloned into a shuttle vector and then rescued by homologous recombination. Recombinant replication-deficient viruses carrying the cTnT cassettes were created using a transfection method and purified. The transgenic mice that expressed the Arg<sup>92</sup>Gln mutation were generated by the methods described by Marian *et al* (1997).

### Fibre Preparation

Some small differences in technique were used for the experiments reported in this chapter which were done in Professor Solaro's labs in Chicago. These relate to minor details of the solutions used and method of mounting the preparation, setting sarcomere length and so on, as detailed below.

The relationship between force and pCa was determined at different pHs on mice cardiac fibres prepared as follows: Adults CD1 mice expressing the human cTnT cDNA (normal

and Arg<sup>92</sup>Gln mutants) were humanely killed by exposure to a lethal concentration of ether vapour. The hearts were promptly removed and placed into 'high relaxing' solution (see Table 8.1) on ice. The left ventricle was then opened via a single cut from the aorta to the apex. Muscle bundles from ~150 to 200  $\mu\text{m}$  in diameter and from ~ 2 to 3mm in length were prepared from the papillary muscles of the left ventricle. These preparations were then chemically skinned by placing them in 'high relaxing' solution containing 1% Triton-X 100 for a minimum of 1 hour to a maximum of 24 hrs.

## Solutions

The three main solutions used throughout the experiments were termed 'high relax', 'low relax', and 'activating' solutions. The composition of these solutions is shown in Table 8.1. 'High relax' was used for dissecting, storing, skinning, and relaxing the fibre. 'Low relax', had 1/50th of the concentration of EGTA (Ca chelator) of high relax. 'Low relax' was used before each activation or pCa series to speed up the contraction by decreasing the time for Ca to rise in the tissue and thus to produce a steady state of tension. The pCa of 'Activating solution' was enough to activate the fibre maximally at all test pHs. The ionic strength of these solutions ranged between 0.175M and 0.185M. All solutions also included dithiothreitol (DTT) 5mM, phosphocreatine (10000 International Units/litre), and protease inhibitors pepstatin a (2.5  $\mu\text{g}/\text{ml}$ ), and leupeptin (1  $\mu\text{g}/\text{ml}$ ).

The pCa solutions were made by mixing 'high relax' and 'activating' solutions to produce the various ratios shown in Table 8.2. The React computer program was used to determine the free  $[\text{Ca}^{2+}]$  in each solution and thus the pCa.

The pHs tested were 6.25, 6.5, 7.0, 7.25, and 7.5. The 'high relax' and 'activating' solutions were mixed to the various ratios at the control solution C and then readjusted to the desired pH using KOH and HCl. All pH adjustments were done at 22°C. Due to the marked temperature dependence of the pH buffer (imidazole), care was taken for the

solutions to reach 22°C before use, and the pH was periodically checked during experiments (as in other experiments reported in this thesis).

<b>Table 8.1</b>	<b>EGTA (mM)</b>	<b>KCl (mM)</b>	<b>CaCl<sub>2</sub> (mM)</b>	<b>MgCl<sub>2</sub> (mM)</b>	<b>Imidazole (mM)</b>	<b>ATP (mM)</b>	<b>CP (mM)</b>
High relax pH 6.5	10.00	52.66	0.00	8.35	25.00	5.27	15.00
Low relax pH 6.5	0.20	82.16	0.00	8.16	25.00	5.28	15.00
Activating solution pH 6.5	10.00	34.82	8.97	8.18	25.00	5.30	15.00
High relax pH 7	10.00	58.42	0.00	8.81	25.00	5.19	15.00
Low relax pH 7	0.20	88.34	0.00	8.16	25.00	5.19	15.00
Activating solution pH 7	10.00	39.06	9.93	8.15	25.00	5.21	15.00
High relax pH 7.5	10.00	63.22	0.00	10.34	25.00	5.16	15.00
Low relax pH 7.5	0.20	93.86	0.00	8.16	25.00	5.17	15.00
Activating solution pH 7.5	10.00	45.82	10.04	8.16	25.00	5.19	15.00

Table 8.2 Activating solution ratios	Activation in 5ml (ml)	High Relax in 5ml (ml)	pH 6.5 free [Ca <sup>2+</sup> ] μM	pH 6.5 pCa	pH 7 free [Ca <sup>2+</sup> ] μM	pH 7 pCa	pH 7.5 free [Ca <sup>2+</sup> ] μM	pH 7.5 pCa
Of 1:1	2.50	2.50	4.58*10 <sup>-05</sup>	5.34	4.85*10 <sup>-07</sup>	6.31	5.85*10 <sup>-08</sup>	7.23
Of 2:1	3.33	1.67	9.12*10 <sup>-06</sup>	5.04	9.71*10 <sup>-07</sup>	6.01	1.20*10 <sup>-07</sup>	6.92
Of 3:1	3.75	1.25	1.36*10 <sup>-05</sup>	4.87	1.46*10 <sup>-06</sup>	5.84	1.82*10 <sup>-07</sup>	6.74
Of 5:1	4.17	0.83	2.24*10 <sup>-05</sup>	4.65	2.43*10 <sup>-06</sup>	5.61	3.08*10 <sup>-07</sup>	6.51
Of 8:1	4.45	0.55	3.47*10 <sup>-05</sup>	4.46	3.87*10 <sup>-06</sup>	5.41	4.98*10 <sup>-07</sup>	6.30
Of 10:1	4.55	0.46	4.23*10 <sup>-05</sup>	4.37	4.82*10 <sup>-06</sup>	5.32	6.25*10 <sup>-07</sup>	6.20
Of 15:1	4.69	0.31	5.90*10 <sup>-05</sup>	4.23	7.16*10 <sup>-06</sup>	5.15	9.42*10 <sup>-07</sup>	6.02
Full Activation	5.00	0	1.66*10 <sup>-04</sup>	3.78	5.24*10 <sup>-05</sup>	4.28	1.87*10 <sup>-05</sup>	4.73

## Calcium-Sensitive Force Measurements

In the experiments described in this chapter, the skinned preparation was suspended between a fixed arm and a force transducer using cellulose-acetate glue at both ends. Once the glue was applied, the preparation was immediately immersed in 'high relax' until the glue hardened and the fibre was secure. The preparation was then changed to low relax in preparation for activation. Low relax was also used before activating the preparations in any of the pCa solution sets. The preparation was first activated in maximum activating solution at pH 7 until a steady state of force was achieved and the contraction pattern was consistent. The sarcomere pattern was then adjusted to 2.2 $\mu$ m (using laser diffraction). The fibre was again activated at low pCa at pH 7 to obtain a consistent contraction pattern, before using the sets of pCa solutions prepared at the various pH values.

The series of pCa solutions were used from lowest to highest  $[Ca^{2+}]$  and then relaxed in 'high relaxing' solution. The number of repeat applications of the full pCa sets investigated per preparation ranged from 2 to 4, depending on the fall-off rate of tension produced by the fibre. The fall-off rate was determined by comparing the original tension produced with the pH 7 maximum pCa solution and the tension of subsequent activations with the same solution, including a final activation at the end of the experiment. A maximum fall off rate of 30% across the entire sequence was the criterion for the use of a fibre for the third or fourth pCa run. Isometric tension was recorded on a paper chart. The experiments were conducted at ~22°C.

## **Analysis of Ca<sup>2+</sup> Sensitivity Experiments**

All data from the chart recorder was measured by hand and recorded on Microsoft Excel. The Prism and Igor graph programs were used for all further analysis and graph plotting. Best-fits to the Hill equation were derived and plotted using the mean  $\pm$  SEM of data from various pCa points at each different pH. The best-fit pCa<sub>50</sub> and Hill coefficients were plotted against pH. The maximum tension at the various pHs was also plotted and compared between the wild-type and Arg<sup>92</sup>Gln mutant.

## **Sinusoidal Analysis**

We investigated crossbridge properties using the sinusoidal oscillation method described previously in this thesis. Freshly excised hearts were glycerinated and sent to the lab in Glasgow on dry ice (initially at -20°C). The glycerination process involved submerging the fresh heart into 50% glycerine, instead of a water based solution. This prevented crystallisation of cell components at low temperatures and prevented further damage to the dying muscle. The hearts were then stored at -20°C until time of use. Before experimentation the hearts were allowed to warm up to room temperature for about 1 hr and used immediately.

Fine preparations of mouse papillary muscle from the left ventricle were chemically skinned (as described in Chapter 2) to allow direct control of the ionic environment of the myofilaments. Both transgenic and non-transgenic preparations were activated in pCa 4.0 solutions at pH 7.0 and oscillated. This protocol was repeated twice to ensure that the data were reproducible. However, due to the fragile nature of these preparations, no more than three protocol runs were done in one experiment. The data were analysed using the same methods as described earlier.

## RESULTS

### Ca<sup>2+</sup> Sensitivity Data

Figure 8.4 demonstrates the results from the pCa solution sets done at the different pHs for both wild-type and mutant cardiac myofibrils. Compared with the wild-type preparations, those with Arg<sup>92</sup>Gln showed an increase in Ca sensitivity at each pH. Also, the extent of the Ca sensitivity increase was greater at the lower pHs.

pCa<sub>50</sub> was determined off of Figure 8.4 using cursors to determine exact locations of pCa<sub>50</sub> values. The number after the pCa value does not denote the SEM but rather the difference between the wild-type and mutant preparations. The n numbers indicate the number of experiment involved in the Figure 8.4. Since pCa<sub>50</sub> values were not determined from graphs of individual experiments (due to time constraints), statistical analysis could not be done. pCa<sub>50</sub> was 6.09 ± 0.15 (n=5) at pH 7.5, 5.53 ± 0.18 (n=10) at pH 7, and 4.80 ± 0.34 (n=2) at pH6.5 for the wild-type preparations. However, pCa<sub>50</sub> was 6.24 ± 0.15 (n=7) at pH 7.5, 5.71 ± 0.18 (n=10) at pH 7, and 5.14 ± 0.34 (n=10) at pH6.5 for the mutant preparations. These results are shown in Figure 8.5. pCa<sub>30</sub> for also determined (off of Figure 8.4) at each pH for both wild-type and mutant preparations and are also illustrated in Figure 8.5.

The Hill coefficient was also determined off of Figure 8.4 using cursors to determine exact locations of the coefficient values. The number after the Hill coefficient value does not denote the SEM but rather the difference between the wild-type and mutant preparations. The n numbers indicate the number of experiment involved in the Figure 8.4. Since Hill coefficient values were not determined from graphs of individual experiments (due to time constraints), statistical analysis could not be done. The Hill coefficient was 6.19 ± 0.48 (n=5) at pH 7.5, 3.16 ± 0.34 (n=10) at pH 7, and 3.71 ± 0.24 (n=2) at pH6.5 for the wild-type preparations. However, the Hill coefficient was 4.86 ±

0.81 (n=7) at pH 7.5,  $2.99 \pm 0.16$  (n=10) at pH 7, and  $2.31 \pm 0.24$  (n=10) at pH6.5 for the mutant preparations. This change in Hill coefficient between the two fibre types is illustrated in Figure 8.6.

The maximum force generated increased with an increase in alkalinity (Figure 8.7). The maximum force generated was higher at pH 7.5, and lower at pH6.5 in comparison to the maximum force generated at pH 7 for both mutant and wild-type preparations (all p values  $\leq 0.05$ ). As shown in Figure 8.7, there was no significant difference between wild-type and Arg<sup>92</sup>Gln mutant fibres when comparing the maximum force generated at individual pH values ( $P > 0.15$ ).

### **Sinusoidal Analysis**

No data is shown in this thesis from the sinusoidal oscillation analysis. All data and analysis for these experiment (n=6 for wild-type, and n=6 for mutant) were discarded due to the poor muscle performance during activation and oscillation. Suggestions for future attempts are discussed briefly in the next section.

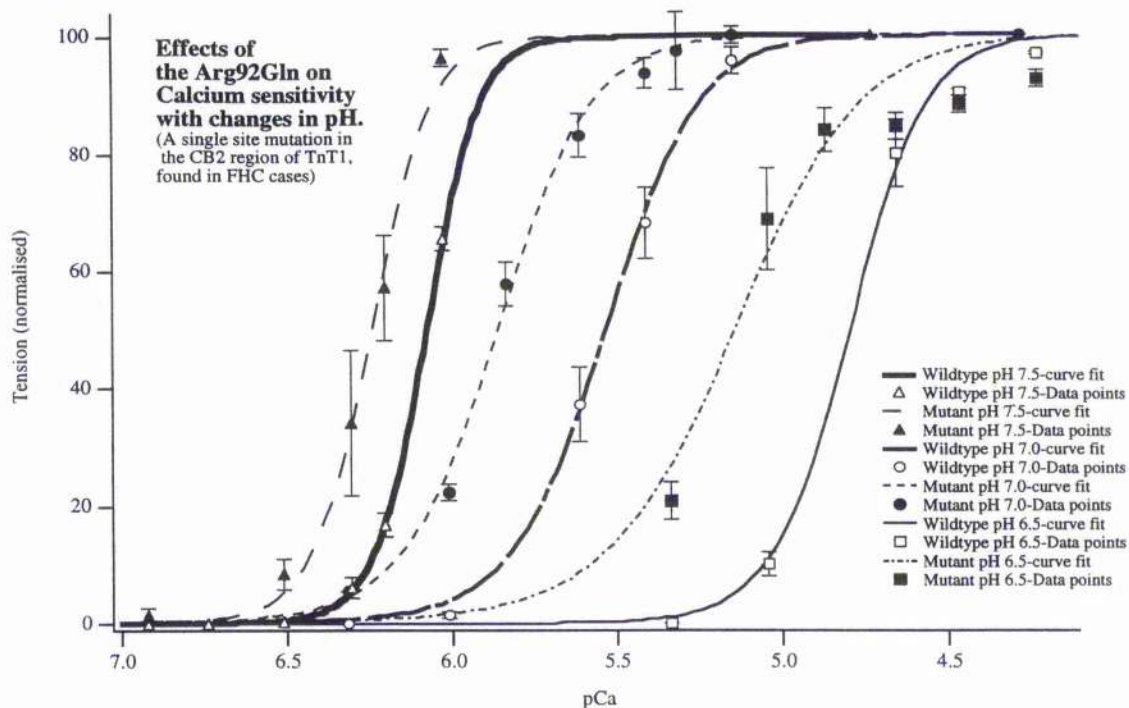


**Figure 8.4.** This figure shows the Hill-fit curves of the data points from the calcium-sensitivity experiments. This graph displays the effects of the Arg92Gln on calcium sensitivity with changes in pH. The tension development has been normalised.

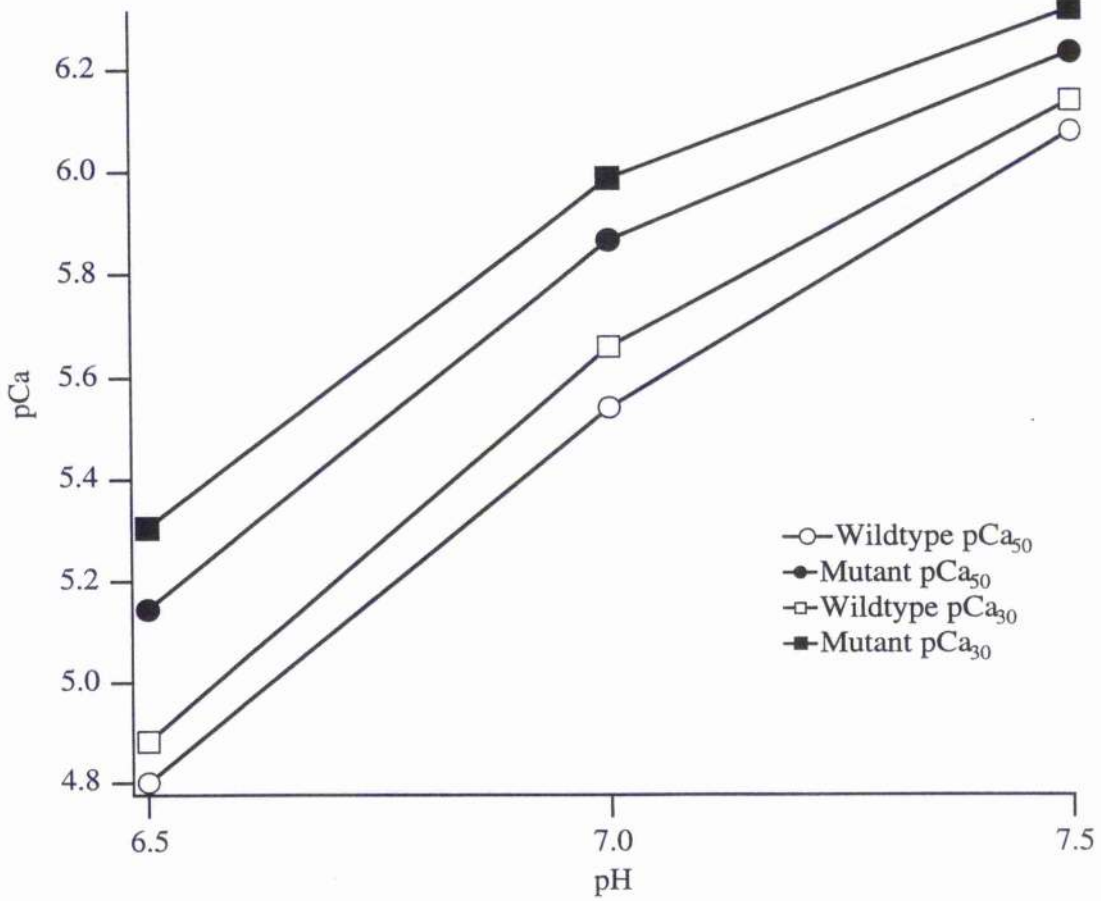


**Figure 8.5.** This figure shows the pCa<sub>50</sub> and pCa<sub>30</sub> data for wild-type vs. mutant myofibrils at three pHs using the mean data. For the wild-type preparations n=5 at pH7.5, n=10 at pH7, and n=2 at pH6.5. For the mutant n=7 at pH7.5, n=10, at pH7, n=10 at pH6.5.

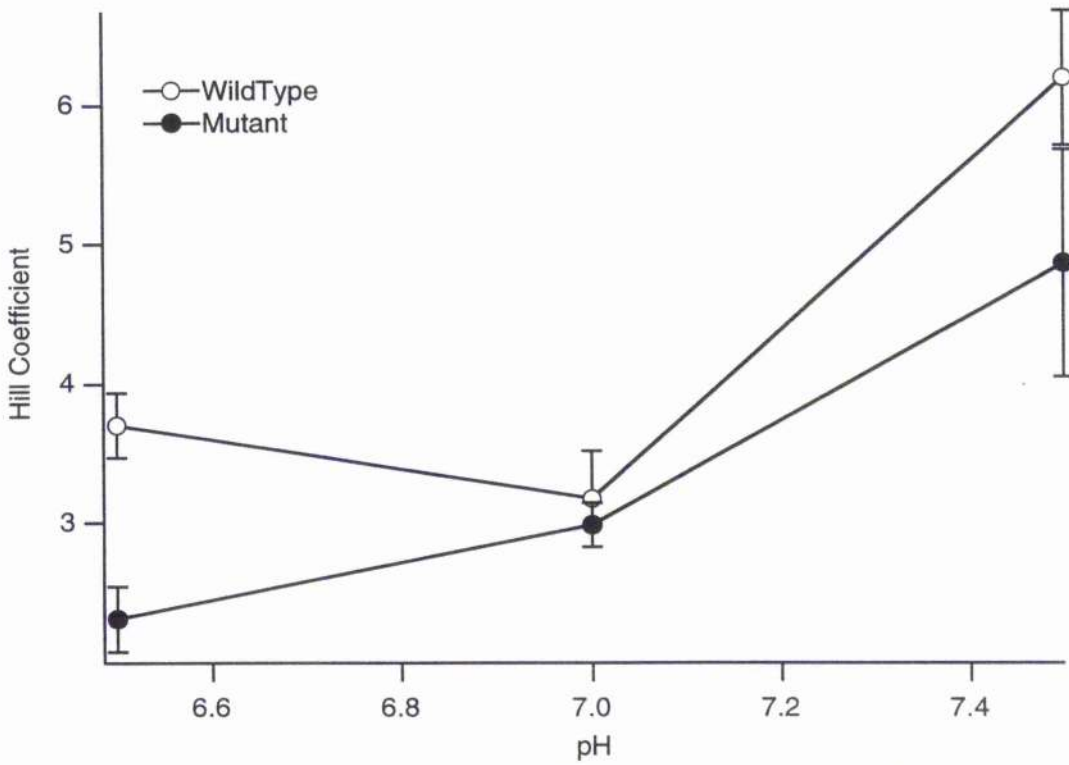


**Figure 8.6.** This figure shows the mean Hill coefficients for the wild-type and mutant myofibrils at three different pHs. The error bars represent the standard deviation of the results. For the wild-type preparations n=5 at pH7.5, n=10 at pH7, and n=2 at pH6.5. For the mutant n=7 at pH7.5, n=10, at pH7, n=10 at pH6.5.

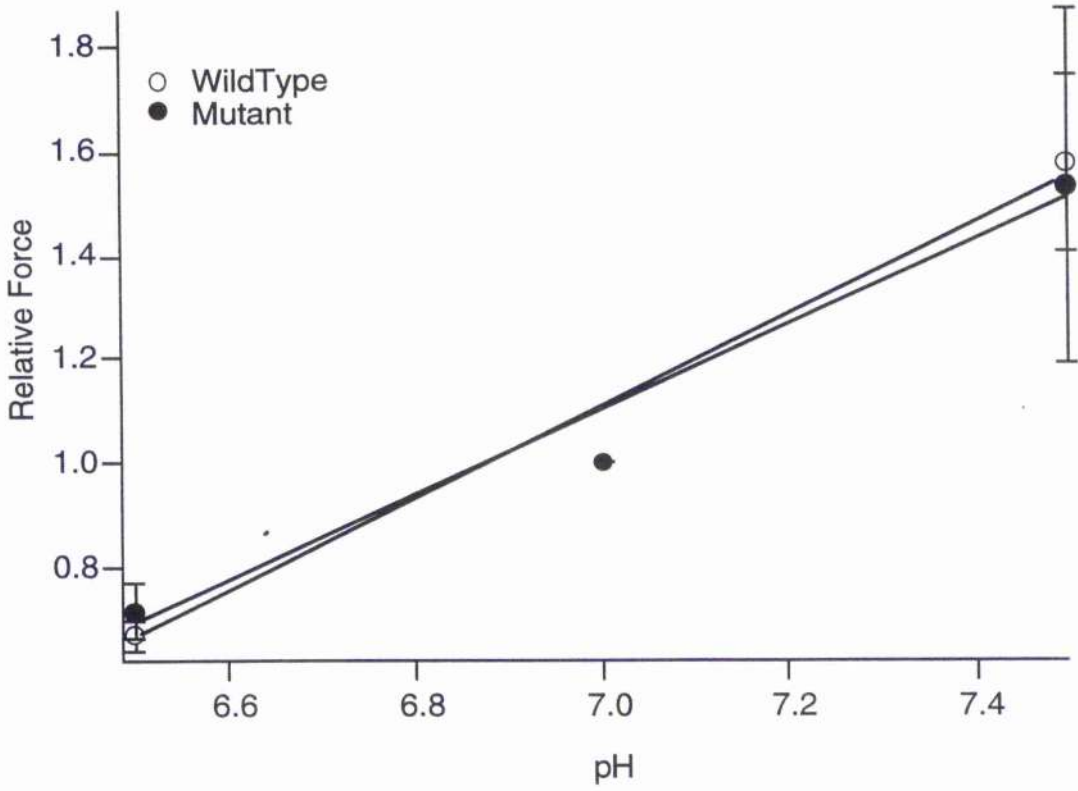


**Figure 8.7.** This figure shows the average maximum force produced by the wildtype vs. mutant mice myofibrils. All data was normalised to pH 7 values. The error bars represent the standard deviation. For the wild-type preparations n=5 at pH7.5, n=10 at pH7, and n=2 at pH6.5. For the mutant n=7 at pH7.5, n=10, at pH7, n=10 at pH6.5.

## DISCUSSION

### *Effect of the Arg<sup>92</sup>Gln mutation on Ca<sup>2+</sup>-sensitivity*

Hypertrophic cardiomyopathy, a paradigm of cardiac hypertrophy and failure, is caused by mutations in genes coding for sarcomeric proteins. It has postulated that a primary defect caused by mutations in the sarcomeric proteins is impaired contractility. These mutations have been found mainly in the genetic code for  $\beta$ -myosin heavy chain,  $\alpha$ -tropomyosin, and troponin T proteins. There have already been eight mutations discovered in TnT that can cause FHC. This study has focused on the point mutation Arg<sup>92</sup>Gln in the CB2 domain of TnT1 region on cTnT.

It has been established that TnT plays a key role in structurally bridging the regulatory protein to the thin filament. It has been shown that the CB2 region of TnT binds to Tm, supporting the idea that the function of TnT was to anchor the Tn complex onto the thin filament (Pearlstone & Smillie 1977). The importance of the CB2 region in linking the TnT2 domain and the extreme N-terminal region of TnT lies in its effect on the Tm end-to-end interactions. A mutation in this region may result in structural modifications that locally destabilise the highly  $\alpha$ -helical CB2 domain. It has been suggested that destabilisation will result in disruption of the transmission of the activating signal, which could change the Ca<sup>2+</sup>-insensitive TnT<sub>1</sub>-Tm interactions. This can be explained by the idea that the TnT<sub>1</sub> domain acts as the link tethering the troponin complex to Tm in the presence of Ca<sup>2+</sup> (White *et al* 1987). This would result in a reduction in activation speed with a decrease in the pCa value. However, our results show an increase in Ca<sup>2+</sup>-sensitivity and an increase in the pCa value of maximum muscle contraction with the Arg<sup>92</sup>Gln mutation.

TnT is also known to participate directly in the  $\text{Ca}^{2+}$ -dependent regulation of striated muscle contraction (Potter *et al* 1995). This is strongly supported by the present results, which show an increase in  $\text{Ca}^{2+}$ -sensitivity once a mutation is introduced to the TnT. This specific result may be due to the location of the mutation on TnT. Yanaga *et al* (1999) reported that certain TnT mutations induced this same increase in  $\text{Ca}^{2+}$ -sensitivity, while others had no effect on  $\text{Ca}^{2+}$ -sensitivity but did increase the maximum ATPase activity. From the present result, the Arg<sup>92</sup>Gln mutation has no effect on force-production by the muscle. Morimoto *et al* (1998) also saw the same effect where TnT with the Arg<sup>92</sup>Gln mutation was exchanged into rabbit cardiac muscle fibres. They reported increased  $\text{Ca}^{2+}$ -sensitivity but no significant differences in tension generation under maximal activating conditions, or in cooperativity (as reflected in the Hill coefficient). The results of this chapter indicate that muscle fibres with the Arg<sup>92</sup>Gln mutation associated with FHC activate at lower pCas but then requires the pCa to fall to that same low pCa to relax. This leads to longer  $\text{Ca}^{2+}$ -activation of the muscle fibres. The heart muscles of FHC patients are reported to hypercontract and be less compliant and thus present clinically with reduced left ventricular (LV) volume capacity, small stroke volumes, little or no volume reserve, and, in some patients, thickened LV septa obstructing flow through the mitral valve (Palmiter & Solaro 1997). This altered architecture may play a large role in the episodes of sudden death seen in patients with FHC.

The mechanism by which TnT causes the increase in  $\text{Ca}^{2+}$ -sensitivity has been the subject of some debate. There are two possible mechanisms by which TnT can influence the activity of the thin filament. The first is by changing the affinity of TnC to  $\text{Ca}^{2+}$ . The second is by altering the ability of TnI to inhibit contraction. However, it seems unlikely that it is the interaction between TnI and TnC that causes the increase in  $\text{Ca}^{2+}$ -sensitivity. It has been shown that there is no change in the TnC-  $\text{Ca}^{2+}$  affinity with mutation in the CB2 region of TnT (Lin *et al* 1996). On the contrary, a study by Yanaga *et al* (1999),

looking at the interaction between TnI and TnT, shows an increase in  $\text{Ca}^{2+}$ -sensitivity due to impairment in the inhibitory action of TnI.

### *Influence of pH in the presence of the Arg<sup>92</sup>Gln mutation*

The hearts of patients with FHC are known to hyper contract and are less compliant. This leads to reduced ventricular volume and rapid emptying of a small stroke volume (Palmiter & Solaro 1997). This results in an inadequate cardiac output and thus creates an ischaemic condition. FHC is a disease that prove fatal during strenuous exercise or other types of activity that suddenly raise the body's oxygen demands during strenuous exercise (McKenna & Camm 1989). Therefore, during exercise, since the metabolic needs of the heart muscle are higher than normal, hearts with FHC are put into a more severe state of ischaemia with the likelihood of increased myocyte acidosis. It is informative to examine the effect of acidosis on muscle function of cardiac myocytes affected by FHC mutations.

It is well established that during ischaemia or hypoxia the intracellular pH of cardiac muscle drops to as low as 6.2. This chapter looks at the effects of the Arg<sup>92</sup>Gln mutation at pH 6.5 and pH 7.5. It is known that acidity and alkalinity lower and raises  $\text{Ca}^{2+}$ -sensitivity respectively in cardiac muscle (*e.g.* Potter *et al* 1997).  $\text{H}^+$  does this by changing the affinity of TnC to  $\text{Ca}^{2+}$ . The present results agree with those from previous studies. We see that at pH 6.5, the  $\text{Ca}^{2+}$ -sensitivity was drastically lower for both the wild-type and mutant muscle fibres. We also see that, at pH 7.5, the  $\text{Ca}^{2+}$ -sensitivity is greatly increased for both muscle fibre types. However, we see that the tissues with the Arg<sup>92</sup>Gln mutation are more  $\text{Ca}^{2+}$ -sensitive at each pH. Therefore, we can conclude that alterations in pH do not override the effect of the TnT mutation and that these factors influence muscle kinetics through different mechanisms. This is further supported by the data on maximum force production. The results show that, although acidity and

alkalinity lower and raise force production respectively, there was no significant difference between the force produced by the wild type and mutant preparations ( $P > 0.15$ ).

We also see that the difference between the  $\text{Ca}^{2+}$ -sensitivities of the mutant and wild-type tissues increases, the lower the pH. This, in contrast to the previous comments, suggests that acidity somehow enhances the effect of the Arg<sup>92</sup>Gln mutation to raise  $\text{Ca}^{2+}$ -sensitivity. This may be due to the effect of acidic pH on the inhibitory action of TnI. Although, pH works through a different mechanism to decrease  $\text{Ca}^{2+}$ -sensitivity, at the same time, it may affect TnI to decrease inhibition to contraction just as the Arg<sup>92</sup>Gln mutation does. However, the mechanisms through which each factor affects TnI inhibition may differ. Further studies are required to determine the precise mechanism through which alterations in pH and TnT mutations affect the  $\text{Ca}^{2+}$ -sensitivity. This information is essential in understanding the nature of FHC and its resultant complications.

### *Sinusoidal Analysis*

Due to strict national quarantine laws regulating the shipment of live animals coming from outside the country, we were not able to work with fresh tissue for the sinusoidal oscillation section of this chapter. Instead, experiments were done on glycerinated preparations shipped back to the lab in Glasgow. As mentioned in the Result section, the quality of all data obtained for every experiment was very poor. Thus, we were unfortunately unable to quantify work and power output differences between the wild-type and transgenic muscle.

We have already established in the previous chapters that certain muscle kinetic parameters, such as  $f_{\text{min}}$ , can be seen in intact muscle filaments. Also, though we have

seen  $f_{min}$  at various frequencies, a similar stiffness-frequency and phase relationship was evident in all experiment with identical variables. However, this was not the case for the wild-type or transgenic experiments in this chapter. None of the data within the wild-type or the transgenic experiments showed any statistically relevant relationship. This could be due to the how the tissue was stored, warmed up, or removed from the glycerine solution. Further development in methods of transporting these transgenic hearts is necessary to provide accurate sinusoidal oscillation data. Other options are to either bring the sinusoidal oscillation equipment to the country where the mice are raised or create these transgenic and wild-type mice here in the UK.

## CHAPTER 9 CONCLUSION

Contraction, relaxation and the coupling between these stages in mammalian muscle are regulated by multiple parameters, including intracellular conditions, and protein isoforms. Both these factors can independently alter contraction and relaxation through different pathways. Moreover, these factors exert their regulatory impact on contraction and relaxation through interdependent mechanisms as well. Thus, their regulatory effects may not be mutually exclusive. Understanding myocardial contraction therefore requires understanding of mechanisms that underlie interactions between effects these mentioned factors on myocardial force development and work produced. These factors may regulate contraction via crossbridge recruitment, crossbridge cycling kinetics or a combination thereof. Accordingly, in the studies described in this thesis, we aimed to unravel some of the mechanisms via changes to either intercellular conditions or protein isoforms (as well as a combination of the two in Chapter 8) to examine the impact they make on regulation of myocardial contraction and relaxation.

Before the results in this thesis can be compared, the methods for experimentation must be discussed. Most of our experimentation involved the sinusoidal-oscillation technique. Here cardiac muscle kinetics were measured and compared using such indicators as maximum tension,  $f_{min}$ , dynamic and maximum stiffness, and phase degrees. Of these parameter,  $f_{min}$  and phase analysis has been used and their validity and accuracy reviewed in multiple recent papers as mention in both Chapter 1 and 2.

### $f_{min}$

$f_{min}$ , as defined in Chapter 1, is the frequency on the stiffness-frequency plot where stiffness comes to a minimum. Here, at  $f_{min}$ , the crossbridges exert the least resistance force perhaps because the oscillation frequency of the imposed length changes corresponds with the frequency at which the mean number of crossbridges are cycling. Sinusoidal analysis was first described by Kawai and Brandt in 1980 and has been used by various labs ever since (Rossmannith & Tjokorda, 1998, Kentish, 2001). Various other

kinetics parameters, such as  $V_{max}$  and  $k_{tr}$ , have also been used in the past to study crossbridge cycling. In 1998, Rossmanith and Tjokorda interpreted their  $f_{min}$ ,  $V_{max}$ , and  $k_{tr}$  results using a simple-strain-dependent three-state model formulated by Julian *et al* (1974). This model showed two attached states (weakly and strongly bound) the detached state, as well as the forward and reverse reaction rates involved at each step. A review of the comparison of these parameters is in Chapter 1.

Kawai and Brandt (1980) initially looked at  $f_{min}$  in rabbit psoas and crayfish muscle and stated that the frequency at which the dynamic modulus is minimal is found at a frequency slightly higher than the optimal frequency for oscillatory work. They found  $f_{min}$  around 25 Hz for the former and around 30 Hz for the latter (both experiments were done at 20°C). Rossmanith *et al*, 1998, also found  $f_{min}$  at around 22 Hz for rabbit psoas muscle, though these experiments were done at 25°C. Although these  $f_{min}$  values are much higher than the values found in this thesis, the difference in muscle type used must be taken into consideration. This thesis reports  $f_{min}$  results using rat cardiac muscle. The change in muscle kinetics with different muscle types plays a crucial role. This is seen in a previous report by Rossmanith *et al*, 1986, where  $V_3$  muscle kinetics were only half that of the  $V_3$  isoform (at 25°C). Kentish *et al*, (2001) also found  $f_{min}$  around 1.9 Hz in mouse myocardium at 24°C. These  $f_{min}$  values are favourably comparable to  $V_{max}$  results by Pope *et al* (1980). Our results were similar for rat cardiac muscle to that of Kentish *et al* (2001) and Rossmanith *et al* (1986). Any differences in  $f_{min}$  values between other labs and ours may also be due differences in the protocol used, including the experimental temperature. Rossmanith *et al*, 1986, looked at the effect of temperature on  $f_{min}$  and found that  $f_{min}$  is located at higher frequencies for higher experimental temperatures. This could one of the reasons for the difference between results from Rossmanith *et al* (1986) and Kentish *et al* (2001), obtained at 25°C, and results reports in this thesis, obtained at 20°C.

We must look at how  $f_{\min}$  compares to published ATPase measurements under identical chemical situations. Previous ATPase measurement at pH 6.5 published by Ebus *et al* (1994) reports a decrease in ATPase activity compared to that of control. Our results at pH 6.5 are different to these reports, where we see an increase in  $f_{\min}$  at pH 6.5 compared to control. Previous ATPase measurement at pH 7.5 published by Ebus *et al* (1994) also reports a decrease in ATPase activity compared to that of control. Our results at pH 7.5 are comparable, where we too see a decrease in  $f_{\min}$ . Previous ATPase measurement at 10mM phosphate published by Ebus *et al* (1994) reports a decrease in ATPase activity compared to that of control. Our results at 10mM phosphate are very different, where we see a large increase in  $f_{\min}$ . Previous ATPase measurement at 10mM caffeine published by Solaro *et al* (1995) reports a decrease in ATPase activity compared to that of control. Our results at 10mM caffeine are comparable, where we see a small decrease in  $f_{\min}$ .

There may be several reasons for the differences seen between our  $f_{\min}$  values and results using ATPase measurements. It has already been shown that others do have similar  $f_{\min}$  values. Therefore it cannot be a discrepancy in the  $f_{\min}$  protocol. One must take into consideration that  $f_{\min}$  analysis involves measuring the mechanical dynamics of the muscle fibre that ultimately produce work and power. ATPase measurements, however, only look at the product of a chemical reaction that takes place during muscle activity. Furthermore, recent studies showing multiple crossbridge cycles per one ATP molecule (Yanigida, 1999) demonstrate that ATP measurements alone can be misleading in terms of crossbridge kinetics.

However, this does not explain why  $f_{\min}$  values are so low in this thesis and previously mentioned studies. Converted to beating rate of the heart *in vivo*, these results are too slow to be 'real'. There are two factors to take into consideration when looking at  $f_{\min}$  values. First, the experimental temperature of around 20°C is far below *in vivo* temperatures of around 37°C. It is well established that higher temperatures increase the

rate of chemical reactions (Rossmannith, 1986). The second factor is the idea that increased strain on the muscle will decrease the crossbridge cycling rate. This idea is based on the well-established 'Fenn Effect' which Kawai & Brandt (1980) used to describe muscle mechanochemistry as load sensitive. Thus the greater the load, the greater the strain on the individual crossbridges, causing a decrease in crossbridge cycling speed. In terms of experiments described in this thesis, the load is the greatest in isometric contractions and will thus result in the slowest mean crossbridge cycling frequency. These two factors help explain some of the discrepancy for the low mean cycling rate. However, other factors such as the species, experimental protocol, and solutions used, may always play some role in changes in  $f_{min}$  values.

### **Oscillatory Work**

The second part of our phase analysis involved deriving, from phase data, oscillatory work produced or absorbed by the muscle. The methodology of this analysis is described in Chapter 2. Just as  $f_{min}$ , oscillatory work, work done by cycling crossbridge, has also been examined by various groups, including Kawai & Brandt, 1980, and, more recently, Rossmannith & Tjokorda, 1998.

Kawai & Brandt, 1980, reported that the fibre absorbed work from the oscillating length driver in high and low frequency ranges, while it generated oscillatory work at medium frequencies. Now the range of frequencies used in this thesis is supported by the arguments presented above for  $f_{min}$ . This argument states that data at frequencies higher than those used in this thesis, may provide information on certain muscle kinetic properties but do not correspond to the rate at which the crossbridges are cycling in our experimental set-up. Therefore, our finding, of where maximum work was found, compare favourably to what was observed by Kawai & Brandt in 1980. Results from Chapters 3, 4, and 6 show that maximum positive work was found at the middle range of frequencies that were used in this thesis. Another observation throughout this thesis is

that the frequency at which maximum positive work was done was always found just below  $f_{\min}$ . This is similar to the results reported by Rossmannith & Tjokorda, 1998, who also found the frequency of maximum positive work, with they term  $f_w$ , just below  $f_{\min}$ . Rossmannith & Tjokorda, 1998, compared  $f_w$  to  $V_{\max}$  and  $k_{tr}$ , just as they compared  $f_{\min}$ . Their comparison is identical to that of  $f_{\min}$ , which is found in Chapter 1 of this thesis. They also show that  $f_{\min}$  and  $f_w$  are influenced by the same step in the three-state model by Julian *et al* (1974). This would explain why maximum positive work was found at the frequencies reported in this thesis. This would also make the arguments stated above for the frequencies of  $f_{\min}$  correspond to the frequencies at with maximum positive work was done as well.

### **Intracellular Conditions and Protein Isoforms**

Previous studies have shown that the effects of pH, Pi and caffeine are similar for certain muscle kinetic parameters but differ in others (McLaughlin & Godt, 1990, Kentish, 1991, Ebus *et al*, 1994). Although our results from Chapter 3, 4, and 6 do not always match previously reported results, they do show this same trend between pH, Pi and caffeine. This suggests that pH, Pi, and caffeine work through different mechanisms and influence different steps of the crossbridge cycle. It is well established, as mentioned in both Chapter 3 and 4, that both  $H^+$  and Pi is released during a crossbridge cycle. Kentish (1991) suggested that  $H^+$  release may immediately precede that of Pi. Our results support that idea that  $H^+$  is indeed released at a different step than Pi. This is again reinforced by the results in this thesis of pH and Pi combined. These results show that the combination of pH and Pi does not have an additive effect on muscle kinetics but rather an averaging effect as described in Chapter 4 see Figure 4.8–9). This is supported furthermore by our caffeine results that are similar to that of acidic pH for certain kinetic parameters and similar to Pi for other parameters. However, there is a clear relationship

between the three intracellular conditions because there are consistent results for certain parameter for all three factors.

Muscle kinetics is not only influenced by the intracellular biochemical conditions but also by the different protein isoforms expressed within the myofilament. It is well established that in various disease states, different isoforms, more often the slower isoforms, are expressed for various protein structures of the myofilament. As explained in the Introduction section of both Chapter 7 and 8, this leads to decrease myocardial function.

These ideas are supported by the results of Chapter 8, where a point mutation in the CB2 region of TnT cause a shift in the pCa curve as well as hill coefficients. Here, although the myofilament contracts at lower pCas, the rate of contraction is slower. Another important issue is the effect of different isoforms combined with chemical factors such as intracellular acidic conditions. The results in Chapter 8 show that acidic pH increases the Ca<sup>2+</sup> sensitivity above that of the mutation alone. Therefore, along with the result of of pH and Pi combined, we can be conclude that intracellular conditions, and protein isoforms not only influence muscle kinetics directly but also influence each other.

## CHAPTER 10 REFERENCES

- AL-HILLAWI, E., BHANDARI, D.G., TRAYER, H.R., TRAYER, I.P. (1994) Over-expression of human cardiac troponin-I and troponin-C in *Escherichia coli* and their purification and characterisation. Two point mutations allow high-level expression of troponin-I. *European Journal Biochemistry*, **225**, 1195-1201.
- AL-HILLAWI, E., BHANDARI, D.G., TRAYER, H.R., TRAYER, I.P. (1995) The effects of phosphorylation of cardiac troponin I on its interactions with actin and cardiac troponin C. *European Journal Biochemistry*, **228**, 962-970.
- ALLEN, D.G., ELLIOTT, A.C., ORCHARD, C.H. (1987) The metabolic effects of acidosis in isolated ferret hearts (Abstract). *Journal of Physiology*, **394**, 40P.
- ALLEN, D.G., MORRIS, P.G., ORCHARD, C.H., PIROLO, J.S. (1985) A nuclear magnetic resonance study of metabolism in the ferret heart during hypoxia and inhibition of glycolysis. *Journal of Physiology*, **361**, 185-204.
- ALLEN, D.G., EINSENER, D.A., PIROLO, J.S., SMITH, G.L. (1985) The relationship between intracellular calcium and contraction in calcium-overloaded ferret papillary muscles. *Journal of Physiology*, **364**, 169-182.
- ALLEN, D.G., ORCHARD, C.H. (1983) Intracellular calcium concentration during hypoxia and metabolic inhibition in mammalian ventricular muscle. *Journal of Physiology*, **339**, 107-122.
- ALPERT, N.R. (1983) Myocardial hypertrophy and failure. New York, Ravens press.
- ALPERT, N.R., GORDON, M.S. (1962) Myofibrillar adenosine triphosphatase activity in congestive heart failure. *American Journal of Physiology*, **202**, 940-946.
- ALPERT, N.R., MULIERI, L.A. (1982) Increased myothermal economy of isometric force generation in compensated cardiac hypertrophy induced by pulmonary artery constriction in the rabbit. *Circulation Research*, **50**, 491-500.
- ALTRINGHAM, J.D., JOINSTON, I.A. (1985) Effects of phosphate on the contractile properties of fast and slow muscle fibres from an Antarctic fish. *Journal of Physiology*, **368**, 491-500.
- AMPHLETT, G.T., VANAMAN, T.C., PERRY, S.V. (1976) Effect of the troponin C-like protein from bovine brain (brain modulator protein) on the  $Mg^{2+}$  stimulated actomyosin ATPase of skeletal muscle actomyosin. *FEBS Letters*, **72**, 163-168.
- ANDERSON, P.A.W., GREIG, A., MARK, T.M., MALOUF, N.N., OAKELEY, A.E., UNGERLEIDER, R.M., ALLEN, P.D., KAY, A.B. (1995) Molecular basis of human cardiac troponin T isoforms expressed in the developing, adult and failing heart. *Circulation Research*, **76**, 681-686.
- ANDERSON, P.A.W., MALOUF, N.N., OAKELEY, A.E., PAGANI, E.D., ALLEN, P.D. (1992) Troponin T isoforms expression in the normal and failing human left ventricle: a correlation with myofibrillar ATPase activity. *Basic Research in Cardiology*, **87**, 117-127.

- ASHLEY, C.C., LEA, T.J., MULLIGAN, I.P., PALMER, R.E., SIMNETT, S.J. (1993) Activation and relaxation mechanisms in single muscle fibres. *Advances in Experimental Medicine & Biology*, **332**, 97-115.
- ASHLEY, C. C., MOISESCU, D. G. (1977) Effect of changing the composition of the bathing solutions upon the isometric tension-pCa relation in bundles of crustacean myofibrils. *Journal of Physiology*, **270**, 627-652
- BABU, A., SCORDILIS, S.P., SONNENBLICK, E.H., GULATI, J. (1987) The control of myocardial contraction with skeletal fast muscle Troponin C. *Journal of Biological Chemistry*, **262**, 5815-5822.
- BABU, A., SONNENBLICK, E.H., GULATI, J. (1988) Molecular basis for the influence of muscle length on myocardial performance. *Science*, **240**, 74-76.
- BACKX, P.H., GAO, W-D., AZAN-BACKX, M.D., MARBAN, E. (1994) Mechanism of force inhibition by 2,3-butanedione monoxime in rat cardiac muscle: Roles of  $[Ca^{2+}]_i$  and cross-bridge kinetics. *Journal of Physiology*, **476**, 487-500.
- BAGSHAW, C.R., TRENTHAM, D.R. (1974) The characterisation of myosin-product complexes and of product-release steps during the magnesium ion-dependent adenosine triphosphatase reaction. *Biochemical Journal*, **141**, 331-349.
- BARSOITI, R.J., FERENCZI, M.A. (1988) Kinetics of ATP hydrolysis and tension production in skinned cardiac muscle of guinea pig. *Journal of Biological Chemistry*, **79**, 997-1016.
- BIANCHI, C.P. (1968) Pharmacological actions on excitation-contraction coupling in striated muscle. *Federation Proceedings*, **27**, 126-131.
- BLANCHARD, E.M., SOLARO, R.J. (1984) Inhibition of the activation and troponin calcium binding of dog cardiac myofibrils by acidic pH. *Circulation Research*, **55**, 382-391.
- BLAUSTEIN, A.S., GAASCH, W.H. (1983) Myocardial relaxation. Effects of beta-adrenergic tone and synchrony on LV relaxation rate. *American Journal of Physiology*, **244**, H417-H422.
- BODOR, G.S., OAKELEY, A.E., ALLEN, P.D., CRIMMINS, D.L., LADENSON, J.H., ANDERSON, P.A.W. (1997) Troponin I Phosphorylation in the Normal and Failing Adult Human Heart. *Circulation*, **96**, 1495-1500.
- BODOR, G.S., PORTERFIELD, D., VOSS, E.M., SMITH, S., APPLE, F.S. (1995) Cardiac troponin-I is not expressed in fetal and healthy or diseased adult human skeletal muscle tissue. *Clinical Chemistry*, **41(12 Pt 1)**, 1710-1715.
- BRANDT, P.W., SCHACHT, F.H. (1997) Troponin C modulates the activation of thin filaments by rigor cross-bridges. *Biophysical Journal*, **72**, 2262-2267.

- BRANDT, P.W., DIAMOND, M.S., RUTCHIK, J.S., SCHACHT, F.H. (1987) Co-operative interactions between troponin-tropomyosin units extend the length of the thin filament in skeletal muscle. *Journal of Molecular Biology*, **195**, 885-896.
- BRANDT, P.W., COX, R.N., KAWAI, M., ROBINSON, T. (1982) Regulation of tension in skinned muscle fibres. Effect of crossbridge kinetics on apparent  $Ca^{2+}$ -sensitivity. *Journal of General Physiology*, **79**, 997-1016.
- BRAUNWALD, E., ROSS, J. Jr. (1963) The ventricular end-diastolic pressure: appraisal of its value in the recognition of ventricular failure in man (editorial). *American Journal of Medicine*, **34**, 147-150.
- BRUTSAERT, D. L. (1987) Non-uniformity: a physiologic modulator of contraction and relaxation of the normal heart. *Journal of American College of Cardiology*, **9**, 341-348.
- BRUTSAERT, D.L., HOUSMANS, P.R., GOETHALS, M.A. (1980) Dual control of relaxation. Its role in the ventricular function in the mammalian heart. *Circulation Research*, **47**, 637-652.
- BUJA, L.M. (1995) Basic pathological processes of the heart: relationship to cardiomyopathies. *Physiology and Pathophysiology of the Heart*, **3**, 37-49.
- COLE, H.A., PERRY, S.V. (1975) Phosphorylation of troponin I from cardiac muscle. *Biochemistry Journal*, **149**, 525-533.
- CONSENSUS (1987) Effects of enalapril on mortality in severe congestive heart failure. *New England Journal of Medicine*, **316**, 1429-1435.
- COOKE, R., FRANCK, K., LUCIANI, G.B., PATE, E. (1988) The inhibition of rabbit skeletal muscle contraction by hydrogen ions and phosphate. *Journal of Physiology*, **395**, 77-97.
- COOKE, R., PATE, E. (1985) The effects of ADP and phosphate on the contraction of muscle fibers. *Biophysical Journal*, **48**, 789-798.
- CRANK, J. (1956) Chapter 5. In *The Mathematics of Diffusion*. Oxford University Press.
- CREMO, C.R., GRAMMER, J.C., YOUNT, R.G. (1990) Direct chemical evidence that serine 180 in the glycine-rich loop of myosin binds to ATP. *Journal of Biological Chemistry*, **264**, 6608-6611.
- DE TOMBE, P.P. (1998) Altered Contractile Function in Heart Failure. *Cardiovascular Research*, **40**, 440-443.
- DE TOMBE, P.P., TER KEURS, H.E.D.J. (1991) Lack of effect of isoproterenol on unloaded velocity of sarcomere shortening in rat cardiac trabeculae. *Circulation Research*, **68**, 382-391.
- De WINKEL, M.E.M., BLANGE, T., TREIJTEL, B.W. (1993) The complex Young's modulus of skeletal muscle fibre segments in the high frequency range determined from frequency transients. *Journal of Muscle Research and Cell Motility*, **14**, 302-310.

- DILLMANN, W.H. (1980) Diabetes mellitus induces changes in cardiac myosin of the rat. *Diabetes*, **29**, 579-582.
- DOHET, C., AL-HILLAWI, E., TRAYER, I.P., RÜEGG, J.C. (1995), Reconstitution of skinned cardiac fibres with human recombinant cardiac troponin-I mutants and troponin-C. *FEBS Letters*, **377**, 131-134.
- DONG, W.J., CHANDRA, M., XING, J., SOLARO, R.J., CHEUNG, H. (1997) Fluorescence studies of the N-terminal segment of cardiac troponin I. *Biochemistry*, **36**, 6745-6753.
- DOSREMEDIOS, C.G., MOENS, P.D.J. (1995) Actin and the actomyosin interface - a review. *Biochimica and Biophysica Acta*, **1228**, 99-124.
- DUKE, T. (2000) Cooperativity of myosin molecules through strain-dependent chemistry. *Philosophical Transactions of the Royal Society of London - Series B: Biological Sciences*, **355(1396)**, 529-38.
- EBUS, J.P., STEINEN, G.J.M., ELZINGA, G. (1994) Influence of phosphate and pH on myofibrillar ATPase activity and force in skinned cardiac trabeculae from rat. *Journal of Physiology*, **476**, 501-516.
- EDMAN, K.A.P. (1979) The velocity of unloaded shortening and its relation to sarcomere length and isometric force in vertebrate muscle fibres. *Journal of Physiology*, **291**, 143-159.
- EISENBERG, E., GREENE, L.E. (1980) The relation of muscle biochemistry to muscle physiology. *Annual Reviews in Physiology*, **42**, 293-309.
- ELLIOTT, A.C., SMITH, G.L., EISNER, D.A., ALLEN, D.G. (1992) Metabolic changes during ischaemia and their role in contractile failure I isolated ferret hearts. *Journal of Physiology*, **454**, 467-490.
- ENDO, M., TANAKA, M., OGAWA, Y. (1970) Calcium induced release of calcium from the sarcoplasmic reticulum of skinned skeletal muscle fibres. *Nature*. **228(5266)**, 34-36.
- FABIATO, A. (1983) Calcium-induced release of calcium from the sarcoplasmic reticulum. *American Journal of Physiology*, **245**, C1-C4.
- FABIATO, A., FABIATO, F. (1978) Effects of pH on the myofilaments and the sarcoplasmic reticulum of skinned cells from cardiac and skeletal muscles. *Journal of Physiology*, **276**, 233-255.
- FABIATO, A., FABIATO, F. (1976) Dependence of calcium release, tension generation and restoring forces on sarcomere length in skinned cardiac cells. *European Journal of Cardiology*, **4**, 13-27.
- FARAH, C.S., REINACH, F.C. (1995) The troponin complex and regulation of muscle contraction. *FASEB Journal*, **9**, 755-767.

- FITZSIMONS, D.P., PATEL, J.R., CAMPBELL, K.S., MOSS, R.L. (2001) Co-operative mechanisms in the activation dependence of the rate of force development in rabbit skinned skeletal muscle fibers. *Journal of General Physiology*, **117**(2), 133-48.
- FORISSIER, J.F., CARRIER, L., BONNE, G., BERCOVICI, J., RICHARD, P., HAINQUE, B., TOWNSEND, P., YACCOUB, M.H., FAURE, S., DUBOURG, O., MILLIARE, A., HAGEGE, A.A., DESNOS, M., KOMADJ, M., SCHWATZ, K. (1996) Codon 102 of the cardiac troponin T gene is a putative hot spot for mutations in familial hypertrophic cardiomyopathy. *Circulation*, **94**, 657-675.
- FRANCIS, G.S., COHN J.H. (1990) Heart failure: Mechanisms of cardiac and vascular dysfunction and the rationale for pharmacological intervention. *FASEB Journal*, **4**, 3068-3075.
- FRYER, M.W., NEERING, I.R., STEPHENSON, D.G. (1988) Effects of 2,3-butanedione monoxime on the contractile activation properties of fast- and slow-twitch rat muscle fibre. *Journal of Physiology*, **407**, 53-75.
- FUCHS, F. (1995) Mechanical modulation of the Ca<sup>2+</sup> regulatory protein complex in cardiac muscle. *NIPS*, **70**, 6-12.
- FUCHS, F. (1974) Chemical properties of the Ca-receptor site of troponin as determined from binding studies. *Calcium-binding proteins*, edited by W. Dradikowski, h. Strzelecka-Golaszewska, E. Carafoli, Amsterdam: Elsevier, 1-27.
- GARLICK, P.B., RADDA, G.K., SEELY, P.J. (1979) Studies of acidosis in the ischaemic heart by phosphorus nuclear magnetic resonance. *Biochemical Journal*, **184**, 547-554.
- GASKELL, W.H. (1880) On the tonicity of the heart and blood vessels. *Journal of Physiology*, **3**, 48-75.
- GEEVES, M.A., GOODY, R.S. AND GUTFREUND, H. (1984) Kinetics of Acto-S1 Interaction as a Guide to a Model for the Crossbridge Cycle. *Journal of Muscle Research and Cell Motility*, **5**, 351-361.
- GIBBS, C. (1985) The cytoplasmic phosphorylation potential. Its possible role in the control of myocardial respiration and cardiac contractility. *Journal of Molecular & Cellular Cardiology*, **17**, 727-731.
- GODT, R.E., KENTISH, J.C (1989) Effect of pH on isometric force, MgATPase and tension-cost of skinned skeletal muscle fibers of rabbit and cardiac muscles from rat (Abstract). *Journal of Physiology*, **418**, 68P.
- GODT, R.E., FENDER, K.J., SHIRLEY, G.C., NOSEK, T.M. (1995) Contractile failure with fatigue or hypoxia: studies with skinned skeletal and cardiac muscle fibers. *Biophysical Journal*, **47**, 993a.
- GRANZIER, H.L., IRVING, T.C. (1995) Passive Tension in Cardiac Muscle: Contribution of Collagen, Titin, Microtubules and Intermediate Filaments. *Biophysical Journal*, **68**, 1027-1044.

- GRANZIER, H.L.M., WANG, K. (1993) Passive tension and stiffness of vertebrate skeletal muscle and insect flight muscles: contribution of weak cross-bridges and elastic filaments. *Biophysical Journal*, **65**, 2141-2159.
- GREASER, M.L., GERGELY, J. (1971) Reconstitution of troponin activity from three protein components. *Journal of Biological Chemistry*, **246**, 4226-4233.
- GREAVE S.C., ROCHE A.H.G., MEUTZE J.M., WHITLOCK R.M.L., VEALE A.M.O. (1987) Inheritance of hypertrophic cardiomyopathy: a cross section and M mode echocardiographic study of 50 families. *British Heart Journal*, **58**, 259-266.
- GUILFORD, W.H., DUPUIS, D.E., KENNEDY, G., WU, J.R., PATLACK, J.B., WARSHAW, D.M. (1997) Smooth muscle and skeletal muscle myosins produce similar unitary forces and displacements in the laser trap. *Biophysical Journal*, **72**, 1006-1021.
- GUO, X., WATTANAPERMPHOL, J., PALMITER, K.A., MURPHY, A.M., SOLARO, R.J. (1994) Mutagenesis of cardiac troponin I: role of the unique NH<sub>2</sub>-terminal peptide in myofilament activation. *Journal of Biological Chemistry*, **269**, 15210-15216.
- GUTH, K., WOJCIECHOWSKI, R. (1984) Perfusion cuvette for the simultaneous measurements of mechanical, optical and energetics parameters of skinned muscle fibers. *Pflügers Archives*, **407**, 552-557.
- GWATHMEY, J.K., HAJJAR, R.J., SOLARO, R.J. (1991) Contractile deactivation and uncoupling of crossbridges: effects of 2,3-butanedione monoxime on mammalian myocardium. *Circulation Research*, **69**, 1280-1292.
- HAJJAR, R.J., GWATHMEY, J.K., BRIGGS, G.M., MORGAN, J.P. (1988) Differential Effect of DPI 210-106 on the Sensitivity of the Myofilaments to Ca<sup>2+</sup> in Intact and Skinned Trabeculae from Control and Myopathic Human Hearts. *Journal of Clinical Investigations*, **82**, 1578-1584.
- HARRISON, S.M., LAMONT, C., MILLER, D.J. (1988) Hysteresis and the length dependence of calcium sensitivity in cardiac muscle. *Journal of Physiology* **401**, 117-145.
- HERZIG, J.W., PETERSON, J.W., RÜEGG, J.C., SOLARO, R.J. (1981) Vanadate and phosphate ions reduce tension and increase cross bridges kinetics in chemically skinned heart muscle. *Biochemical Biophysical Acta*, **672**, 191-196.
- HERZIG, J.W., RÜEGG, J.C. (1977) Myocardial cross-bridge activity and its regulation by Ca<sup>2+</sup>, phosphate and stretch. In: Riecher G, Weber A, Goodwin J (eds) Myocardial failure. Springer, Berlin Heidelberg New York, 41-51.
- HIBBERD, M.G., DATZIG, J.A., TRENTHAM, D.R., GOLDMAN, Y.E. (1985) Phosphate release and force generation in skeletal muscle fibers. *Science*, **228**, 1317-1319.
- HIBBERD, M.G., JEWELL, B.R. (1982) Calcium- and length-dependent force production in rat ventricular muscle. *Journal of Physiology (London)*, **329**, 527-540.
- HIROTA, Y. (1980) A clinical study of left ventricular relaxation. *Circulation*, **62**, 756-763.

- HITCHCOCK, S. (1975) Cross-linking of troponin with dimethylamide esters. *Biochemistry*, **14**, 5162-5167.
- HOFMANN, P.A., METZGER, J.M., GREASER, M.L., MOSS, R.L. (1990) Effects of partial extraction of light chain 2 on the Ca<sup>2+</sup> sensitivities of isometric tension, stiffness, and velocity of shortening in skinned skeletal muscle fibers. *Journal of General Physiology*, **95** (3), 477-498.
- HORTER, J.A., LAUER, C., VENTURA-CLAPIER, R., GUERON, M. (1986) Amytal inhibition of respiration does not induce acidosis in isovolumic perfused hearts. A <sup>31</sup>P-NMR study. *Journal of Molecular Cellular Cardiology*, **18**, (suppl) 3, 34.
- HOH, J.F.Y., ROSSMANITH, G.H., KWAN, L.J., HAMILTON, A.M. (1988) Adrenaline Increases the Rate of Cycling of Crossbridges in Rat Cardiac Muscles as Measured by Pseudo-Random Binary Noise-Modulated Perturbation Analysis. *Circulation Research*, **62**, 452-461.
- HOH, J.F.Y., McGRATH, P.A., HALE, P.T. (1978) Electrophoretic analysis of multiple forms of rat cardiac myosin: Effects of hypophysectomy and thyroxine replacement. *Journal of Molecular and Cellular Cardiology*, **10**, 1053-1076.
- HOLROYDE, M.J., ROBERTSON, S.P., JOHNSON, J.D., SOLARO, R.J., POTTER, J.D. (1980) The calcium and magnesium binding sites on cardiac troponin and their role in the regulation of myofibrillar adenosine triphosphatase. *Journal of Biological Chemistry*, **24**, 11688-11693.
- HOSKINS, B.K., LIPSCOMB, S., MULLIGAN, I.P., ASHLEY, C.C. (1999) How do skinned skeletal muscle fibres relax? *Biochemical & Biophysical Research Communications*, **254**, 330-333.
- HOWARD, J. (1997) Molecular motors: structural adaptations to cellular functions. *Nature*, **389** (6651), 561-567.
- HUXLEY, A.F., NIEDERGERKE, R. (1954) Interference microscopy of living muscle fibres. *Nature*, **173**, 971-973.
- HUXLEY, H.E., HANSON, J. (1954) Changes in the cross-striations of muscle during contraction and stretch and their structural interpretation. *Nature*, **173**, 973-976.
- IRVING, M., PIAZZESI, G. (1997) Motions of myosin heads that drive muscle contraction. *News in Physiological Sciences*, **12**, 249-254.
- ISHIJIMA, A., KOJIMA, H., HIGUCHI, H., HARADA, Y., FUNATSU, T., YANAGIDA, T. (1996) Multiple- and single-molecule analysis of the actomyosin motor by nanometre-piconewton manipulation with a microneedle: unitary steps and forces. *Biophysical Journal*, **70**, 383-400.
- IWAMOTO, H. (1995a) Two mechanically distinct types of fast twitch muscle fibres of the frog and their temperature sensitivity, as detected by sinusoidal analysis. *Journal of Muscle Research and Cell Motility*, **16**, 257-265.

- IWAMOTO, H. (1995b) Simple modelling of linear and non-linear mechanical responses to sinusoidal oscillations during muscle contraction. *Journal of Muscle Research and Cell Motility*, **16**, 249-256.
- JACKSON, P., AMPHLETT, G.W., PERRY, S.V. (1975) The structure of troponin T and the interaction with tropomyosin. *Biochemistry Journal*, **151**, 85-97.
- JIN, J.P., RESEK, M.E. (1996) Primary structure of mouse slow skeletal muscle troponin t and developmentally regulated expression. *Molecular Biology of the Cell*, **7**, 537a.
- JANSSEN, P.M.L. (1997) Determinants of contraction and relation in mammalian myocardium: Effects of calcium and sarcomere length. University Utrecht, Ph.D. Thesis.
- JULIAN, F.J., SOLLINS, K.R., SOLLINS, M.R. (1974) A model for the transient and steady-state mechanical behaviour of contracting muscle. *Biophysical Journal*, **14**, 546-562.
- JUNG, D.W.G., BLANGE, T., De GRAAF, H., TREIJTEL, B.W. (1988) Elastic properties of relaxed, activated and rigor muscle fibres measured with microsecond time resolution. *Biophysical Journal*, **54**, 897-908.
- KABSCH, W., MANNHERTZ, H.G., SUCK, D., PAI, E.F., HOLMES, K.C. (1990) Atomic structure of the actin DNAase complex. *Nature*, **347**, 37-44.
- KATZ, A.M., HECHT, H.H. (1969) The early "pump" failure of the ischemic heart. *American Journal of Medicine*, **47**, 497-502.
- KAWAI, M., ZHAO, Y. (1993) Crossbridge Scheme and Force per Crossbridge State in Skinned Rabbit Psoas Muscle Fibres. *Biophysical Journal*, **65**, 638-651.
- KAWAI, M., GUTH, K., WINNIKES, K., HAIST, C., RÜEGG, J.C. (1987) The effect of inorganic phosphate on the ATP hydrolysis rate and the tension transients in chemically skinned rabbit psoas fibers. *Pflügers Archives*, **408**, 1-9.
- KAWAI, M., BRANDT, P.W. (1980) Sinusoidal analysis: a high resolution method for correlating biochemical reactions with physiological processes in activated skeletal muscles of rabbit, frog and crayfish. *Journal of Muscle Research & Cell Motility*, **1**, 279-303.
- KAWAI, M. (1979) Effect of MgATP on cross-bridge kinetics in chemically-skinned rabbit psoas fibers as measured by sinusoidal analysis technique. In *Cross-bridge Mechanism in Muscle Contraction*, edited by Sugi, H. and Pollack, G.H. 149-169.
- KAWASAKI, Y., VAN EERD, J.P. (1972) The effect of Mg<sup>2+</sup> on the conformation of the Ca<sup>2+</sup> binding component of troponin. *Biochemical and Biophysical Research Communication*, **49**, 898-905.
- KENTISH, J.C., MCCLOSKEY, D.T., LAYLAND, J., PALMER, S., LEIDEN, J.M., MARTIN, A.F., SOLARO, R.J. (2001) Phosphorylation of Troponin I by Protein Kinase A Accelerates Relaxation and Crossbridge Cycle Kinetics in Mouse Ventricular Muscle. *Circulation Research*, **88**(10), 1059-1065.

KENTISH, J.C. (1991) Combined inhibitory action of acidosis and phosphate on maximum force production in rat skinned cardiac muscle. *Pflügers Archives*, **419**, 310-318.

KENTISH, J.C., PALMER, S. (1989) Effect of pH on force and stiffness in skinned muscle from rat and guinea-pig ventricle and from rabbit psoas muscle (Abstract). *Journal of Physiology*, **410**, 67P.

KENTISH, J.C. (1986) The effects of inorganic phosphate and creatine phosphate on force production in skinned muscles from rat ventricle. *Journal of Physiology*, **370**, 585-604.

KENTISH, J.C., ALLEN, D.G. (1986) Is force production in the myocardium directly dependent upon the free energy change of ATP hydrolysis? *Journal of Molecular and Cellular Cardiology*, **18**, 879-882.

KENTISH, J.C., MCCLOSKEY, D.T., LAYLAND J., PALMER, S., LEIDEN, J.M., MARTIN, A.F., SOLARO, R.J. (2001) Phosphorylation of troponin I by protein kinase A accelerates relaxation and crossbridge cycle kinetics in mouse ventricular muscle. *Circulation Research*, **88**(10), 1059-65.

KENTISH, J.C., NAYLER, W.G. (1979) The influence of pH on the  $\text{Ca}^{2+}$ -regulated ATPase of cardiac and white skeletal myofibrils. *Journal of Molecular and Cellular Cardiology*, **11**, 611-617.

KENTISH, J.C., NAYLER, W.G. (1978)  $\text{Ca}^{2+}$ -dependent tension generation in chemically "skinned" trabeculae: effect of pH (Abstract). *Journal of Physiology*, **284**, 90-91P.

KERRICK, W.G., POTTER, J.D., HOAR, P.E. (1991) The apparent rate constant for the dissociation of force-generating myosin cross-bridges from actin decreases during  $\text{Ca}^{2+}$  activation of skinned muscle fibres. *Journal of Muscle Research and Cell Motility*, **12**, 53-60.

Kimbal's Biology Pages by Dr. John W. Kimball. Ultramet Web server. URL:

[http://www.ultranet.com/~jkimball/BiologyPages/M/Muscles.html#Anatomy\\_of\\_Skeletal\\_Muscle](http://www.ultranet.com/~jkimball/BiologyPages/M/Muscles.html#Anatomy_of_Skeletal_Muscle)

KOHAMA, K. (1980) Role of the high affinity Ca binding sites of cardiac and fast skeletal troponins. *Journal of Biochemistry*, **88**, 591-599.

KOHLHARDT, M., KUBLER, M. (1975) The influence of metabolic inhibitors upon the transmembrane slow inward current in the mammalian ventricular myocardium. *Naunyn-Schmiedeberg's Archives of Pharmacology*, **290**: 265-274.

KOVANEN, V., SUOMINEN, H., HEIKKINEN, E. (1984) Mechanical properties of fast and slow skeletal muscles with special reference to collagen and endurance training. *Journal of Biomechanics*, **17**, 725-735.

KRUDY, G., KLEEREKOPER, Q., GUO, X., HOWARTH, J.W., SOLARO, R.J., ROSEVEAR, P.R. (1994) NMR studies delineating spatial relationships within the

cardiac troponin I-troponin C complex. *Journal of Biological Chemistry*, **269**, 23731-23735.

LABEIT, S., KOLMERER, B., LINKE, W.A. (1997) The Giant Protein Titin: Emerging Roles in Physiology and Pathophysiology. *Circulation Research*, **80**, 290-294.

LI, P., HOFMANN, P.A., LI, B.S., MALHOTRA, A., CHENG, W., SONNENBLICK, E.H., MEGGS, L.G., ANVERS, P. (1997) Myocardial infarction alters myofilament calcium sensitivity and mechanical behaviour of myocytes. *American Journal of Physiology; Heart Circulation Physiology*, H360-H370.

LI, Z.H., BING, O.H.L., LONG, X.L., ROBINSON, K.G., LAKATTA, E.G. (1997) Increased cardiomyocyte apoptosis during the transition to heart failure in the spontaneously hypertensive rat. *American Journal of Physiology*, **272**, H2313-H2319.

LIN, D., BOBKOVA, A., HOMSHER, E., TOBACMAN, L.S. (1996) Altered cardiac troponin T *in vitro* function in the presence of a mutation implicated in familial hypertrophic cardiomyopathy. *Journal of Clinical Investigation*, **12**, 2842-2848.

LINKE, W.A., POPOV, V.I., POLLACK, G.H. (1994) Passive and active tension in single cardiac myofibrils. *Biophysical Journal*, **67**, 782-792.

LOMPRE, A.M., NADL-GINARD, B., MAHDAVI, V. (1984) Expression of the cardiac ventricular alpha- and beta-myosin heavy chain is developmentally and hormonally regulated. *Journal of Biological Chemistry*, **259**, 6437-6446.

LOMPRE, A., SCHWARTZ, K., d'ALBIS, A., LACOMBE, G., VANTHIEM, N., SWYNGHEDAUW, B. (1979) Myosin isoenzyme redistribution in chronic heart overload. *Nature*, **282**, 105-107.

LORELL, B.H. (1991) Significance of diastolic dysfunction of the heart. *Annual Reviews in Medicine*, **42**, 411-436.

MACHIN, K.E., PRINGLE, J.W.S. (1959) The Physiology of insect flight muscle. II. The mechanical properties of a beetle flight muscle. *Proceedings of the Royal Society, series B*, **151**, 204-225.

MANI, R.S., MCCUBBIN, W.D., KAY, C.M. (1974) Separation and characterisation of the 37 000 Dalton component of the troponin system. *FEBS Letters* **38(3)**, 357-360.

MARBAN, E., KUSUOKA, H. (1987) Maximal Ca<sup>2+</sup>-activated force and myofilament Ca<sup>2+</sup> sensitivity in intact mammalian hearts. *Journal of General Physiology*, **90**, 609-623.

MARIAN A.J., ZHAO G., SETA Y., ROBERTS R., YU Q. (1997) Expression of a mutant (Arg<sup>92</sup>Gln) human cardiac troponin T, known to cause hypertrophic cardiomyopathy. *Circulation Research*, **81**, 76-85.

MARUYAMA, K. (1994) Connectin, an elastic protein of striated muscle. *Biophysical Chemistry*, **50**, 73-85.

MARTYN, D.A., GORDON, A.M. (1992) Force and stiffness in glycerinated rabbit psoas fibers. *Journal of General Physiology*, **99**, 765-816.

- MATSUDA, T., PODOLSKY, R.J. (1986) Ordering of the myofilament lattice in muscle fibers. *Journal of Molecular Biology*, **189**, 361-365.
- McDONALD, K.S., WOLFF, M.R., MOSS, R.L. (1998) Force-velocity and power-load curves in rat skinned cardiac myocytes. *Journal of Physiology*, **511.2**, 519-531.
- McKENNA, W.J., CAMM, A.J. (1989) Sudden death in hypertrophic cardiomyopathy. *Circulation*, **80**, 1489-1492.
- Med Note Web Source URL: <http://www.mednote.co.kr/BOKnote/muscle.html#red>.
- MEHTA, A.D., FIBER, J.T., SPUDICH, J.A. (1997) Detection of single molecule interactions using correlated thermal diffusion. *Proceedings of the National Academy of Sciences USA*, **94**, 7927-7931.
- MEKHFI, H., VENTURA-CLAPIER, R. (1988) Dependence upon high-energy phosphates of the effects of inorganic phosphate on contractile properties in chemically skinned rat cardiac fibres. *Pflügers Archiv - European Journal of Physiology*, **411(4)**, 378-385.
- MEKHFI, H., VEKSLER, V., MATEO, P., MAUPOIL, V., ROCHETTE, L., VENTURA-CLAPIER, R. (1996) Creatine Kinase is the Main Target of Reactive Oxygen Species in Cardiac Myofibrils. *Circulation Research*, **78**, 1016-1027.
- MERCADIER, J.J., BOUVERET, P., GORZA, L., SCHIAFFINO, S., CLARK, W.A., ZAK, R., SWYNGHEDAUW, B., SCHWARTZ, K. (1983) Myosin Isoenzymes in Normal and Hypertrophied Human Ventricular Myocardium. *Circulation Research*, **53**, 52-62.
- MERCADIER, J.J., LOMPRES, A.M., WISNEWSKI, C., SAMUEL, J.L., BERCOVICI, J., SWYNGHEDAUW, B., SCHWARTZ, K. (1981) Myosin isoenzyme changes in several models of rat cardiac hypertrophy. *Circulation Research*, **49**, 525-532.
- METZGER, J.M., MOSS, R.L. (1990) Effects on tension and stiffness due to reduces pH in mammalian fast- and slow-twitch skinned skeletal muscle fibres. *Journal of Physiology*, **428**, 737-750.
- MILLER, C.J., CHEUNG, P., WHITE, P., REISLER, E. (1995) Actins view of actomyosin interface. *Biophysical Journal*, **68**, Suppl. S50-S54.
- MILLER, D. J., ELDER, H. Y., SMITH, G. L. (1985) Ultrastructural and X-ray microprobe analysis of EGTA- and detergent treated heart muscle. *Journal of Muscle Research & Cell Motility*, **6**, 525-540.
- MILLER, D. J., SMITH, G. L. (1984) EGTA purity and the buffering of calcium ions in physiological solutions. *American Journal of Physiology*, **246**, C160-166.
- MILLER, D. J. (1975) Diffusion delays and the rate of contracture development in frog heart muscle. *Pflügers Archives*, **359**, R23
- MOLLOY, J.E., BURNS, J.E., KENDRICK-JONES, J., TREAGER, R.T., WHITE, D.C.S. (1995) Force and movement produced by a single myosin head. *Nature*, **378**, 209-212.

- MOISESCU, D. G. (1976) Kinetics of reaction in calcium activated skinned muscle fibres. *Nature*, **262**, 610-613
- MORKIN, E. (1987) Chronic adaptation in contractile proteins: Genetic regulation. *Annual Review of Physiology*, **49**, 545-554.
- MORIMOTO, S., YANAGA, F., MINAKAMI, R., OHTSUKI, I. (1998)  $Ca^{2+}$  -sensitizing effects of the mutation at Ile<sup>79</sup> and Arg<sup>92</sup> of troponin T in hypertrophic cardiomyopathy. *American Journal of Physiology*, **275**, C200-207.
- MOSS, R.L., FITZSIMONS, D.P. (1998) Strong binding of myosin modulates length-dependent  $Ca^{2+}$  activation of rat ventricular myocytes. *Circulation Research*, **83**, 602-607.
- MOSS, R.L. (1992)  $Ca^{2+}$  regulation of mechanical properties of striated muscle. Mechanistic studies using extraction and replacement of regulatory proteins. *Circulation Research*, **70**(5), 865-884.
- MOSS, R.L., LAUER, M.R., GIULIAN, G.G., GREASER, M.L. (1986) Altered  $Ca^{2+}$ -dependence of tension development in skinned skeletal muscle fibers following modification of troponin by partial substitution with cardiac TnC. *Journal of Biological Chemistry*, **261**, 6096-6099.
- MOSS, R.L., GIULIAN, G.G., GREASER, M.L. (1985) The effects of partial extraction of TnC upon the tension-pCa relationship in rabbit skinned skeletal muscle fibers. *Journal of General Physiology*, **86**, 585-600.
- NADAL-GINARD, B., MAHDAVI, V. (1989) Molecular basis for cardiac performance. Plasticity of the myocardium generated through protein isoform switches. *Journal of Clinical Investigation*, **84**, 1693-1700.
- NASSAR, R., MALOUF, N.N., KELLY, M.B., OAKELY, A.E., ANDERSON, P.A.W. (1991) Force-pCa relation and troponin T isoforms of rabbit myocardium. *Circulation Research*, **69**, 1470-1475.
- NEGELE, J.C., DOTSON, D.G., LIU, W., SSWEENEY, H.L., PUTKEY, J.A. (1992) Mutation of the high affinity calcium binding sites in cardiac troponin C. *Journal of Biological Chemistry*, **267**, 825-831.
- NELSON, R.M., LONG, G.L. (1989) A general method of site-specific mutagenesis using a modification of the thermus aquaticus polymerase chain reaction. *Analytical Biochemistry*, **180**, 147-151.
- NOLAND Jr, T.A., GUO, X., RAYNOR, R.L., JEDEAMA, N.M., AVERYHART-FULLARD, V., SOLARO, R.J., KUO, J.F. (1995) Cardiac troponin I mutants. Phosphorylation by protein kinases C and A and regulation of  $Ca^{2+}$ -stimulated MgATPase of reconstituted actomyosin S-1. *Journal of Biological Chemistry*, **43**, 25445-25454.
- NWASOKWA, O.N. (1993) A model of the time course of myocardial dynamics: use in characterisation of relaxation and evaluation of its indices. *Cardiovascular Research*, **27**, 1510-1521.

- ORCHARD, C.H., KENTISH, J.C. (1990) Effects of changes of pH on the contractile function of cardiac muscle. *American Journal of Physiology*, **258**, C967-C981.
- PAGANI, E.D., ALOUSI, A.A., GRANT, A.M., OLDER, T.M., DZIUBAN, S.W., ALLEN, P.D. (1988) Changes in the myofibrillar content and Mg-ATPase activity in ventricular tissue from patients with heart failure caused by coronary artery disease, cardiomyopathy, or mitral valve insufficiency. *Circulation Research*, **63**, 380-385.
- PALMER, S., KENTISH, J.C. (1998) Roles of Ca<sup>2+</sup> and crossbridge kinetics in determining the maximum rates of Ca<sup>2+</sup> activation and relaxation in rat and guinea pig skinned trabeculae. *Circulation Research*, **83**, 179-186.
- PALMER, S., KENTISH, J.C. (1997) Differential Effects of the Ca<sup>2+</sup> Sensitisers Caffeine and CGP 48506 on the Relaxation Rate of Rat Skinned Cardiac Trabeculae. *Circulation Research*, **80**, 682-687.
- PALMER, S., KENTISH, J.C. (1996) Developmental differences and regional similarities in the responses of rat cardiac skinned muscles to acidosis, inorganic phosphate and caffeine. *Journal of Molecular & Cellular Cardiology*, **28**, 797-805.
- PALMITER K.A., SOLARO R.J. (1997) Molecular mechanisms regulating the myofilament response to Ca<sup>2+</sup>: Implications of mutation causal for familial hypertrophic cardiomyopathy. *Basic Research Cardiology*, **92**, Suppl 1, 63-74.
- PATE, E., COOKE, R. (1989) A model of crossbridge action: the effects of ATP, ADP, and Pi. *Journal of Muscle Research and Cell Motility*, **10**, 181-196.
- PEARLSTONE J.R., SMILLIE L.B. (1977) The binding site of rabbit skeletal alpha-troponin on troponin T. *Canadian Journal of Biochemistry*, **55**, 1032-1038.
- PERRINS, S., GILLILAND, G. (1990) Site-specific mutagenesis using asymmetric polymerase chain reaction and a single mutant primer. *Nucleic Acids Research*, **18**, 7433-7438.
- PERRY, S.V. (1998) Troponin T: genetics, properties and function. *Journal of Muscle Research and Cell Motility*, **19**, 575-602.
- PERRY, S.V., COLE, H.A., HEAD, J.F., WILSON, F.J. (1972) Localisation and mode of action of the inhibitory protein component of the troponin complex. *Cold Spring Harbour Symposia of Quantitative Biology*, **37**, 251-262.
- PETTTT, L. D., POWELL, H. K. J. (1993). International Union of Pure and Applied Chemistry Stability Constants Database (eds. Pettit & Powell). Academic Software, Otley, UK.
- PIANO M.R. (1999) Familial hypertrophic cardiomyopathy. *Journal of Cardiovascular Nursing*, **13**(4), 46-58.
- PODOLSKY, R.J., TEICHHOLZ, L.E. (1970) The relationship between calcium and contraction kinetics in skinned muscle fibres. *Journal of Physiology (London)*, **211**, 19-35.

- POPE, B., HOH, J., WEED, A. (1980) The ATPase activities of rat cardiac myosin isoenzymes. *FEBS Letters*, **118**, 205-208.
- POTTER, J.D., SHENG, Z., PAN, B.S., ZHAO, J. (1995) A direct regulatory role for troponin T and a dual role in the Ca<sup>2+</sup> regulation of muscle contraction. *Journal of Biological Chemistry*, **270**, 2557-2562.
- POTTER, J.D., GERGELY, J. (1974) Troponin, tropomyosin, and actin interactions in the Ca<sup>2+</sup>-regulation of muscle contraction. *Biochemistry*, **13**, 2697-2703.
- POWERS, F.M., SOLARO, R.J. (1995) Caffeine alters cardiac myofilament activity and regulation independently of Ca<sup>2+</sup> binding to troponin-C. *American Journal of Physiology*, **268**, C1348-C1353.
- RACK, P.M.H. (1966) The behaviour of a mammalian muscle during sinusoidal stretching. *Journal of Physiology*, **183**, 1-14.
- RAYMEN, I., RYPNIEWSKI, W.R., SCHMIDT-BASE, K., SMITH, R., TOMCHICK, DR. BENNING, M.M., WINKELMANN, D.A., WESENBERG, G., HOLDEN H.M. (1993) Three-dimensional structure of myosin subfragment-1: a molecular motor. *Science*, **261**(5117), 50-58.
- ROBERTSON, S.P., JOHNSON, J.D., HOLROYDE, M.J., KRANIAS, E.G., POTTER, J.D., SOLARO, R. (1982) The effect of troponin-I phosphorylation on the calcium binding properties of the Ca-regulatory site of bovine cardiac troponin. *Journal of Biological Chemistry*, **257**, 260-263.
- ROSSMANITH, G.H., TJOKORDA, O.B. (1998) Relationships between isometric and isotonic mechanical parameters and cross-bridge kinetics. *Clinical and Experimental Pharmacology and Physiology*, **25**, 522-535.
- ROSSMANITH, G.H. (1986) Tension responses of muscle to n-step pseudo-random length reversals: a frequency domain representation. *Journal of Muscle Research and Cell Motility*, **7**, 299-306.
- ROSSMANITH, G.H., HOH, J.F.Y., KIRMAN, A., KWAN, L.J. (1986) Influence of V1 and V3 isomyosins on the mechanical behaviour of rat papillary muscle as studied by pseudo-random binary noise modulated length perturbations. *Journal of Muscle Research & Cell Motility*, **7**, 307-319.
- SAMBROOK, J., FRITSCH, E.F., MANIATIS, T. (1989) Identification of cDNA clones of interest. In: molecular cloning: a laboratory manual. New York, NY; Cold Spring Harbor. 8.46-8.51.
- SAMUELS, J., RAPPAPORT, L., MERCADIER, J., LOMPRES, A.M., SARTORE, S., TRIBAN, C., SCHIAFFINO, S., SCHWARTZ, K. (1983) Distribution of myosin isozymes within single cardiac cells. *Circulation Research*, **52**, 200-209.
- SANGER, F., NICLEN, S., COULSON, A.R. (1977) DNA sequencing with chain-terminating inhibitors. *Proceedings of the National Academy of Sciences of the United States of America, USA.*, **74**, 5463-5467.

SCHADLER, M. (1967) Proportional aktivierung von ATPase-aktivität und Kontraktionsspannung durch Calcium ionen in isolierten kontraktile Strukturen verschiedener Muskelarten. *Pflügers Archive*, **296**, 70-90.

SCHAUB, M.C., HEFTA, M.A., ZUELLIG, R.A., MORANO, I. (1998) Modulation of contractility in human cardiac hypertrophy by myosin essential light chain isoforms. *Cardiovascular Research*, **37**, 381-404.

SCHEUER, J., BHAN, A.K. (1979) Cardiac contractile proteins. Adenosine triphosphatase activity and physiological function. *Circulation Research*, **45**(1), 1-12.

SCHMIDT-OTT, S.C., BLETZ, C., VHL, C., SAGGAU, W., HAGL, S., RÜEGG, J.C. (1990) Inorganic phosphate inhibits contractility and ATPase activity in skinned fibres from human myocardium. *Basic Research in Cardiology*, **85**, 358-366.

SCHUTT, C.E., MYSLIK, J.C., ROZYCKI, M.D., GOOSNESEKERE, N.C., LINDBERG, U. (1993) The structure of crystalline profilin- $\beta$ -actin. *Nature*, **365**, 810-816.

SCHWARTZ, K., BOHELER, K.R., DE LA BASTIE, D., LOMPRES, A.A., MERCADIER, J.J. (1992) Switches in cardiac muscle gene expression as a result of pressure and volume overload. *American Journal of Physiology*, **262**, R364-R369.

SEIDMAN CE, SEIDMAN JG. (1998) Molecular genetic studies of familial hypertrophic cardiomyopathy. *Basic Research Cardiology*, **93**, Suppl 3, 13-16.

SHENG, Z., STRAUSS, W.L., FRANCOIS, J.M., POTTER, J.D. (1990) Evidence that both  $Ca^{2+}$ -specific sites of skeletal muscle TnC are required for full activity. *Journal of Biological Chemistry*, **265**, 21554-21560.

SILLÉN, L. G., MARTELL, A. E., HOGFELDT, E., SMITH, R. M. (1974). Critical Stability constants. Chemical Society (London). Special publication no. 25 and supplements.

SIMNETT, S.J., JOHNS, E.C., LIPSCOMB, S., MULLIGAN, I.P., ASHLEY, C.C. (1998) Effect of pH, phosphate and ADP on relaxation of myocardium after photolysis of diazo-2. *American Journal of Physiology*, **275**, H951-960.

SLUPSKY, C.M., SYKES, B.D. (1995) NMR solution structure of calcium-saturated skeletal muscle troponin C. *Biochemistry*, **34**(49), 15953-15964.

SMITH, F. H. (1969) Double refracting interference microscope.

SMITH, W.M. (1985) Epidemiology of congestive heart failure. *American Journal of Cardiology*, **55**, 3A-8A.

SMITH, J.P., BARSOTTI, R.J. (1993) A computer-based servo system for controlling isotonic contractions of muscle. *American Journal of Physiology*, **265**, C1424-32.

SMITH, G.L., MILLER, D.J. (1985). Potentiometric measurements of stoichiometric and apparent affinity constants of EGTA for protons and divalent ions including calcium. *Biochimica et Biophysica Acta*, **839**, 287-299.

- SOLARO, R.J., RARICK, H.M. (1998) Troponin and tropomyosin; proteins that switch on and tune in the activity of cardiac myofilaments. *Circulation Research*, **83**, 471-480.
- SOLARO, R.J., VAN EYK, J. (1996) Altered interaction among thin filament proteins modulate cardiac function. *Journal of Molecular Cell Cardiology*, **28**, 217-230.
- SOLARO, R.J., LEE, J., KENTISH, J.C., ALLEN, D.G. (1988) The effects of acidosis on ventricular muscle from adult and neonatal rats. *Circulation Research*, **63**, 779-787.
- SOLARO, R.J., KUMAR, P., BLANCHARD, E.M., MARTIN, A.F. (1986) Differential effects of pH on calcium activation of myofilaments of adult and perinatal dog hearts. *Circulation Research*, **58**, 721-729.
- SOLARO, R.J., WISE, R.M., SHINER, J.S., BRIGGS, F.N. (1974) Calcium requirements for cardiac myofibrillar activation. *Circulation Research*, **34**(4), 525-530.
- SORENSEN, M.M., DA SILVA, A.C.R., GOUVEIRA, C.S., SOUSA, V.P., OSHIMA, W., FERRO, J.A., REINACH, F.C. (1995) Concerted action of the high-affinity calcium binding sites in skeletal muscle troponin C. *Journal of Biological Chemistry*, **270**, 9770-9777.
- SOUFER, R., WOHLGELERNTER, D., VITA, N.A., AMUCHESTEGUI, M., SOSTMAN, H.D., BERGER, H.J., ZARET, B.J. (1985) Intact systolic left ventricular function in clinical congestive heart failure. *American Journal of Cardiology*, **55**, 1032-1036.
- SMITH, G.L., STEELE, D.S. (1994) Effects of pH and inorganic phosphate on rigor tension in chemically skinned rat ventricular trabeculae. *Journal of Physiology*, **478**, 505-512.
- STEELE, D.S., SMITH, G.L. (1992) The effects of caffeine and  $Ca^{2+}$  on rigor tension in triton-treated rat ventricular trabeculae. *Pflügers Archives*, **421**, 343-349.
- STEELE, D.S., MILLER, D.J. (1991) Effects of cAMP and forskolin on caffeine-induced contractures and myofilament Ca-sensitivity in saponin-treated rat ventricular trabeculae. *Journal of Muscle Research and Cell Motility*, **13**, 146-152.
- STEELE, D.S., SMITH, G.L., MILLER, D.J. (1990) The effect of taurine on  $Ca^{2+}$  uptake by the sarcoplasmic reticulum and  $Ca^{2+}$  sensitivity of chemically skinned rat heart. *Journal of Physiology*, **422**, 499-511.
- STEIGER, G.J., RÜEGG, J.C. (1969) Energetics and 'efficiency' in the isolated contractile machinery of insect fibrillar muscle at various frequencies of oscillation. *Pflügers Archives*, **307**, 1-21.
- STULL, J.T. BUSS, J.E. (1978) Calcium binding properties of beef cardiac troponin. *Journal of Biological Chemistry*, **253**, 5932-5938.
- SWIDEREK, K., JAQUET, K., MEYER, H.E., HEILMEYER Jr., L.M.G. (1998) Cardiac troponin I, isolated from bovine heart, contains two adjacent phosphoserines: a first example of phosphoserine determination by derivatization to S-ethylcysteine. *European Journal of Biochemistry*, **176**, 335-342.

SWYNGHEDAUW, B. (1986) Developmental and Functional Adaptation of Contractile Proteins in Cardiac and Skeletal Muscles. *Physiological Reviews*, **66**, 710-771.

TALBOT, J.A., HODGES, R.S. (1981) Comparative studies on the inhibitory region of selected species of troponin-I. *Journal of Biological Chemistry*, **256**, 12374-12378.

TANOKURA, M., TAWADA, Y., ONO, A., OHTSUKI, I. (1983) Chymotryptic subfragments of troponin T from rabbit skeleton muscle. Interaction with tropomyosin, troponin I and troponin C. *Journal of Biochemistry*, **93**, 331-337.

TAYLOR, E.W. (1979) Mechanism of actomyosin ATPase and the problem of muscular contraction. *Critical Reviews in Biochemistry*, **6**, 103-164.

The Physiology and Pharmacology Teaching Web server. URL:

<http://plpk04.plpk.uq.edu.au/GMC/Physiology/ECG99/sld014.htm>.

TOBACMAN, L.S. (1996) Thin filament mediated regulation of cardiac contraction. *Annual Review of Physiology*, **58**, 447-481.

TOBACMAN, L.S (1988) Structure-function studies of the amino-terminal region of bovine cardiac troponin T. *Journal of Biological Chemistry*, **263**, 2668-2672.

TOBACMAN, L.S., LEE, R. (1987) Isolation and functional comparison of bovine cardiac troponin T isoforms. *Journal of Biological Chemistry*, **262**, 4059-4064.

TONOMURA, Y., NAKAMURA, H., KINOSHITA, N., ONISHI, H., SHIGEKAWA, M. (1969) The pre-steady state of the myosin-adenosine triphosphate system. X. The reaction mechanism of the myosin-ATP system and a molecular mechanism of muscle contraction. *Journal of Biochemistry*, **66(5)**, 599-618.

TRAYER, I.P. (1997) How to make your heart beat faster. *TRP3, Q1*, 22-23.

University of New South Wales, Sydney, Oz, Dept of Anatomy, Web Page of Dr. Mark A. Hill URL: <http://anatomy.med.unsw.edu.au/cbl/cbl.htm>.

VAN BUREN, P., HARRIS, D.E., ALPERT, N.R., WARSHAW, D.M. (1995) Cardiac V1 and V3 myosins differ in their hydrolytic and mechanical activities *in vitro*. *Circulation Research*, **77**, 439-444.

VAN EERD, J., KAWASAKI, Y., (1973) Effect of calcium on the interaction between subunits of troponin and tropomyosin. *Biochemistry*, **12**, 4972-4980.

VAN EYK, J.E., HODGES, R.S. (1988) The biological importance of each amino acid residue of the troponin I inhibitory sequence 104-115 in the interaction with troponin C and tropomyosin and actin. *Journal of Biological Chemistry*, **263**, 1726-1732.

VASSEN, R.S., BENJAMIN, E.J., LEVY, D. (1996) Congestive heart failure with normal left ventricular systolic function. *Archives of International Medicine*, **156**, 146-157.

- VENTURA-CLAPIER, R., KUZNETSOV, A., VEKSLER, V., BOEHM, E., ANFLOUS, K. (1998) Functional coupling of creatine kinases in muscles: species and tissue specificity. *Molecular & Cellular Biochemistry*, **184**(1-2), 231-47.
- VENTURA-CLAPIER, R., VASSORT, G. (1980) Electrical and mechanical activities of frog heart during energetic deficiency. *Journal of Muscle Research and Cell Motility*, **1**, 429-444.
- WATKINS, H., MCKNNA, W.J., THEIRFELDER, L., SUK, H.J., ANAN, R., O'DONOGHUE, A., SPIRITO, P., MATSUMORI, A., MORAVEC, C.S., SEIDMAN, J.G., SEIDMAN, C.F. (1995) Mutations in the genes for cardiac troponin T and  $\alpha$ -troponin in hypertrophic cardiomyopathy. *New England Journal of Medicine*, **332**, 1058-1064.
- WATTENAPERMPOOL, J., GUO, X., SOLARO, R.J. (1995) The unique amino-terminal peptide of cardiac troponin I regulates myofibrillar ATPase activity only when it is phosphorylated. *Journal of Molecular Cell Cardiology*, **27**, 1383-1391.
- WENDT, I.R., STEPHENSON, D.G. (1983) Effect of caffeine on calcium activated force production in skinned cardiac and skeletal muscle fibres of the rat. *Pflügers Archives*, **398**, 210-216.
- WESTERBLAD, H., ALLEN, D.G. (1994) Relaxation,  $[Ca^{2+}]_i$  and  $[Mg^{2+}]_i$  during prolonged tetanic stimulation of intact, single fibres from mouse skeletal-muscle. *Journal of Physiology*, **480**, 31-43.
- WHITE, H.D., TAYLOR, E.W. (1976) Energetics and mechanism of actomyosin ATPase. *Biochemistry Journal*, **15**, 5818-5826.
- WHITE, D.C.S., THORSON, J. (1973) The kinetics of muscle contraction. *Progress in Biophysics and Molecular Biology*, **27**, 173-255.
- WHITE, S.P., COHEN, C., PHILLIPS, G.N. JR. (1987) Structures of co-crystals of tropomyosin and troponin. *Nature*, **325**, 826-828.
- WILLADSEN K.A., BUTTERS C.A., HILL L.E., TOBACMAN L.S. (1992) Effects of the amino-terminal regions of tropomyosin T on the thin filament assembly. *Journal of Biological Chemistry*, **267**, 23746-23752.
- WOLFF, M.R., BUCK, S.H., STROKER, S.W., GREASER, M.L., MENTZER, R.M. (1996) Myofibrillar calcium sensitivity of isometric tension is increased in human dilated cardiomyopathies. *Journal of Clinical Investigation*, **98**, 167-176.
- WOLSKA, B.M., KITADA, Y., PALMITER, K.A., WESTFALL, M.V., JOHNSON, M.D., SOLARO, R.J. (1996) CGP-48506 increases contractility of ventricular myocytes and myofilament by effects on actin-myosin reaction. *American Journal of Physiology*, **39**, H24-H32.
- XIANG, J.Z., KENTISH, J.C. (1995) Effects of inorganic phosphate and ADP on calcium handling by the sarcoplasmic reticulum in rat skinned cardiac muscles. *Cardiovascular Research*, **29** (3), 391-400.